DE-FC07-96ID13438

VOC CONTROL IN KRAFT MILLS –

TASK A: PREDICTIVE MODEL

By

Junyong (J.Y.) Zhu, Xinsheng Chai
Louis L. Edwards, Yongxiang Gu
Amyn S. Teja
Adrianna G. Kirkman

September, 2001

Work Performed Under Contract No: DE-FC07-96ID13438

For

U.S. Department of Energy
Office of Industrial Technologies
Washington, D.C. 20585

By

Institute of Paper Science and Technology, Atlanta, GA
University of Idaho, Moscow, ID
Georgia Institute of Technology, Atlanta, GA
North Carolina State University, Raleigh, NC

TABLE OF CONTENTS

PREFACE AND ACKNOWLEDGEMENTS

A joint research effort was carried out in this program to develop a comprehensive understanding for the control of the air emission of volatile organic compounds (VOCs) in kraft mills. The program was selected by the Office of Industry Technologies of the US Department of Energy and American Forest and Paper Association (AF&PA) as a successful story project in 1998. This report summaries the contribution of Task A of the program. The main contribution of Task A is the development of VOC formation and vapor liquid equilibrium database and a computational model for the prediction of VOC air emission in kraft mill fiber lines.

This task of the research can be divided into three parts: the VOC database development, VOC air emission predictive model development, and predictive model validation through mill site liquid and air sampling. The database work was carried out experimentally at the Institute of Paper Science and Technology, Georgia Institute of Technology, and the North Carolina State University. The predictive model development was carried out at the University of Idaho with assistance from the Institute of Paper Science and Technology. The model validation through mill sampling was conducted by the Institute of Paper Science and Technology, the University of Idaho, National Council for Air and Stream Improvement (NCASI) in the Pulp and Paper Industry, and the North Carolina State University.

We would like to acknowledge the contributions by those who made the success of this program possible. We are especially indebted to NCASI for providing financial support and technical effort through the expertise and contribution of Mr. Ashok Jain (Manager) and his team, in the southeastern region of NCASI, for their continued participation of this program and providing mill samplings of VOC air emission. We would also like to acknowledge Georgia Pacific Corporation and Boise-Cascade Corporation for their participation of the program by letting us conduct VOC air emission measurements in their mills and providing technical assistance while we were at their mills. Many past and present postdoctoral research fellows, graduate students, and technical staff at our organizations have contributed to the program. Many of them are coauthors of the publications listed under the heading of “LIST OF RELEVANT PUBLICATIONS” in this report.

LIST OF RELEVANT PUBLICATIONS

- **Book Chapter**

  Chai, X.-S. and Zhu, J.Y. (2001), "Application of Headspace Gas Chromatography in the Pulp and Paper Industry," in *Recent Research Development in Analytical Chemistry*, Transworld Research Network, ISBN:81-86846-95-6, 1, p61.

- **Refereed Publications**

1. Chai, X.-S., Luo, Q., and Zhu, J.Y., (2001), "A Multiple Headspace Extraction Gas Chromatographic Method for the Study of Process Kinetics," Submitted to *J. Chromatography - A*.
2. Teja, A.S., Gupta, A.K., Bullock, K. R., Chai, X.-S., and Zhu, J.Y., (2001), "Henry's Constants of Methanol in Aqueous Systems Containing Salts," *Fluid Phase Equilibria*, **185**, p265.
3. Gu, Y., Edwards, L.L., (2001), "Cluster Rule Simulation: Part 1 of 4: Mill Applications," *TAPPI J.*, **84**(4), p62.
4. Gu, Y., Edwards, L.L., Zhu, J.Y., and Chai, X.S., (2001), "Cluster Rule Simulation: Part 2 of 4: Kraft Mill Methanol Generation Models," *TAPPI J.*, **84**(4), p62.
5. Gu, Y., Edwards, L.L., Zhu, J.Y., Liu, P.H., and Chai, X.S., (2001), "Cluster Rule Simulation: Part 3 of 4: Kraft Mill Methanol Equilibrium Calculations," *TAPPI J.*, **84**(4), p62.
6. Gu, Y., Edwards, L.L., (2001), "Cluster Rule Simulation: Part 4 of 4: Mill Validated Air Emission Models," *TAPPI J.*, **84**(4), p62.
7. Chai, X.S., Yoon, S.-H., Zhu, J.Y., Li, J., (2001), "The Fate of Hexenuronic Acid Groups during Alkaline Pulping of Loblolly Pine," *J. Pulp Paper Sci*., **27**(12) (in press).
8. Chai, X.S., Luo, Q., Yoon, S.-H., Zhu, J.Y., (2001), "The Fate of Hexenuronic Acid Groups during Kraft Pulping of Hardwoods," *J. Pulp Paper Sci.*, **27**(12) (in press).
9. Chai, X.S., Zhu, J.Y., and Li, J., (2001), "A Simple and Rapid Method to Determine Hexenuronic Acid Groups in Chemical Pulps," *J. Pulp Paper Sci.*, **27**(5), p165.
10. Chai, X.-S., Q. Luo, and Zhu, J.Y. (2001), "Analysis of Non-volatile Species in a Complex Matrix by Headspace Gas Chromatography," *J. Chromatography A.*, **909**(2), p65.
11. Yoon, S.-H., Chai, X.S., Zhu, J.Y., Li, J., and Malcolm, E.W., (2001), "In-Digester Odor Reduction in Kraft Pulping," *Advances Environ Res.*, **5**(1), p91
12. Chai, X.S., Luo, Q., Zhu, J.Y., (2000), "A Simple and Practical Kappa Test Method for Process Control in Pulp production," *Process Control and Quality*, **11**(5), p407.
13. Chai, X.S., Liu, P.H., and Zhu, J.Y., (2000), "Analysis of Volatile Organic Sulfur Compounds in Kraft Liquors by Full Evaporation Headspace Gas Chromatography," *J. Pulp Paper Sci.*, **26**(5), p167

14. Zhu, J.Y., Yoon, S.-H., Liu, P.-H., and Chai, X.-S., (2000), "Methanol Formation in Alkaline Wood Pulping," *TAPPI J.*, **83**(7), p65.

15. Gupta, A.K., Teja, A., Zhu, J.Y., Chai, X.S., (2000), "Henry's Constants of n-Alkanols in Water at Temperatures between 40 C and 90 C.," *Fluid Phase Equilibria*, **170**, p183.

16. Zhu, J.Y., Liu, P.H., and Chai, X.S., Bullock, K.R., Teja, A.S., (2000), "Henry's Law Constant of Methanol in Pulping Spent Liquor," *Environ Sci. Techno.*, **34**(9), p1742

17. Chai, X.S., and Zhu, J.Y., (1999), "Direct and Rapid Pulp Kappa Number Determination Using Spectrophotometry," *J. Pulp Paper Sci.*, **25**(11), p387

18. Zhu, J.Y., Chai, X.S., (1999), "Automation in Determining Solute Concentration and Henry's Constant by Multiple Headspace Extraction Gas Chromatography," *Invited Paper*, *American Lab. News*, **31**(8), p28C

19. Zhu, J.Y., Chai, X.S., and Dhasmana, B., (1999), "The Formation of Volatile Organic Compounds (VOCs) during Pulping," *J. Pulp Paper Sci.*, **25**(7), p256.

20. Zhu, J.Y. and Chai, X-S, (1999), "Vapor-Liquid Equilibrium Partitioning of Methanol in Black Liquors," *TAPPI J.*, **82**(2) p123.

21. Chai, X.S. and Zhu, J.Y., (1998), "Simultaneous Measurements of Solute Content and Henry's constant by Multiple Extraction Headspace Gas Chromatography," *Analytical Chemistry*, **70**(16) p3481.

22. Chai, X.S. and Zhu, J.Y., (1998), "An Indirect Headspace Gas Chromatographic Method for Vapor-Liquid Equilibrium Study," *J. Chromatography A* , **799**, p207.

23. Zhu, J.Y., Chai, X.S., and Dhasmana, B., (1998), "Development of a Database for Volatile Organic Compound (VOC) Emission Prediction in Kraft Mills Using Headspace Gas Chromatography," *Innovative Advances in the Forest Products Industries, AIChE Symposium Series*, **94**(318), p165.

24. Chai, X.S., Dhasmana, B., and Zhu, J.Y., (1998), "Determination of Liquid VOC Contents in Kraft-Mill Streams Using Headspace Gas Chromatography," *J. Pulp Paper Sci.*, **24**(2), p50.

EXECUTIVE SUMMARY

The formation of volatile organic compounds (VOCs), such as methanol, in kraft mills has been an environmental concern. Methanol is soluble in water and can increase the biochemical oxygen demand. Furthermore, it can also be released into atmosphere at the process temperatures of kraft mill-streams. The Cluster Rule of the EPA now requires the control of the release of methanol in pulp and paper mills. This research program was conducted to develop a computer simulation tool for mills to predict VOC air emissions.

To achieve the objective of the research program, much effort was made in the development of analytical techniques for the analysis of VOC and determination of vapor liquid partitioning coefficient of VOCs in kraft mill-streams using headspace gas chromatography. With the developed analytical tool, methanol formation in alkaline pulping was studied in laboratory to provide benchmark data of the amount of methanol formation in pulping in kraft mills and for the validation of VOC formation and vapor-liquid equilibrium submodels. Several millwide air and liquid samplings were conducted using the analytical tools developed to validate the simulation tool.

The VOC predictive simulation model was developed based on the basic chemical engineering concepts, i.e., reaction kinetics, vapor liquid equilibrium, combined with computerized mass and energy balances. Four kraft mill case studies (a continuous digester, two brownstock washing lines, and a pre-evaporator system) are presented and compared with mill measurements. These case studies provide valuable, technical information for issues related to MACT I and MACT II compliance, such as condensate collection and Clean-Condensate-Alternatives (CCA)[*].

[*] Rather than collecting brown stock washer vents, the Cluster Rules offers the alternative condensates for washing to accomplish the equivalent reduction.

INTRODUCTION

With the increasingly restrictive environmental regulations posed by the federal agencies, maintaining environmentally sound and technologically competitive practices in kraft mill operations is key to the success of the U.S. pulp and paper industry. The EPA's Cluster Rule requires control of volatile organic compounds (VOCs) released from kraft mills. VOC air emission is a very complicated problem and it varies significantly from mill to mill. Recently, the National Council for Air and Stream Improvement (NCASI) initiated a project on onsite sampling of VOC air emissions at various mills, however the data is not very conclusive. There is a lack of comprehensive understanding of the VOC air emission problem, which caused difficulties in adopting necessary and effective measures in many kraft mills to tackle the problem.

VOCs are primary formed in the pulping process. The release of VOC's in kraft mills is determined by several factors: (1) the concentrations of VOCs in mill streams that are primarily determined by the amount of VOC formed in the pulping and other processes, (2) the fundamental thermodynamic vapor-liquid equilibrium (VLE) behavior of the VOCs in mill streams, (3) mass transfer associated with specific mill processes, and (4) the mill operation conditions, such as wood species, pulping and bleaching chemicals, water reuse in operation, etc. The overall objective of Task A of the present research is to develop a computer simulation tool for the prediction of VOC air emission. The tool can be used by mill engineers to achieve VOC air emission compliance through process optimization and design improvement. The development of the predictive tool relies heavily on the fundamental understanding of the sources and pathways of VOCs in kraft mills. Therefore, one key focus of the present research is to develop databases of VOC formation in pulping, VOC concentrations in various mill streams, and the VLE partitioning coefficients of VOCs in kraft mill streams. The effect of mass transfer on VOC pathways are mill process specific and can be accounted for by using many existing mass transfer correlations. Another focus of the project is to develop the computational models for each operational process for the prediction of VOC air emission. The models are then

integrated for the development of a design tool to predict VOC air emission in the entire fiber line. The design tool is finally validated through mill-wide liquid and air sampling.

A significant amount of effort in the research was devoted on the development of techniques for the analysis of VOC content in various kraft mill streams and the determination of VLE partitioning coefficient. This is because most existing techniques are not suitable for the analysis of VOCs in kraft mill streams due to the complex sample matrix and corrosive nature of the streams. Most VLE data of VOCs in the literature are obtained from aqueous solutions of VOC and therefore not valid for VLE of VOCs in kraft mill streams that often contain dissolved organic materials, such as lignin and hemicellulose, and inorganic salts, such as sodium carbonate. Laboratory pulping experiments were conducted for the study of VOC in pulping, the primary sources of VOC in kraft mill fiber line. The research effort on the development of VOC predictive tool was built on the University of Idaho's 30+ years of experience on computational process simulation.

Methanol accounts for 90% of the VOCs in kraft mills. Methanol was adopted as the surrogate of other VOCs by EPA. Therefore, this research was focused on methanol. The overall objective of the present research is to develop a computer simulation model for the prediction of methanol air emission in the fiber line of a kraft mill. Specific objectives are (1) development of measurement methods to determine VOC/methanol concentration and Henry's constants in various kraft mill streams, (2) determine methanol concentration and Henry's constants in various streams, (3) develop a database of methanol formation during pulping, (4) develop and validate a VOC simulation model as a process design tool for mill VOC air emission compliance.

CHAPTER 1: DEVELOPMENT OF MEASUREMENT METHODS

Kraft mill streams have complex matrices and consists of organic and inorganic materials. Headspace gas chromatography (HSGC) is a powerful technique for volatile species analysis. It relies on the vapor liquid equilibrium of a volatile species in a nonvolatile matrix within a closed container (a sample vial). The volume of the space unoccupied by the nonvolatile matrix is called the headspace (vapor or gas phase space). The basic principle of HSGC and many useful methods can be found in textbooks [1-3] and review articles [4, 5]. Because direct liquid phase probing is not necessary, HSGC eliminates the sample matrix effect on measurements and therefore suitable for VOC analysis in the present research involving complex sample matrices. With the advances in chromatographic technology, many commercial HSGC systems are available, making HSGC in industrial applications convenient and practical. We will discuss several methods and procedures that we developed for determination of VOC concentrations and Henry's constants in krfat mill streams in this chapter.

1.1 Instrumentation – Headspace Gas Chromatograph

1.1.1 Headspace Operating Principle

A commercial HSGC, i.e., HP-7694 Automatic Headspace Sampler and Model HP-6890 capillary gas chromatograph (Hewlett-Packard, now Agilent Technologies, Palo Alto, CA, USA) was used in this work. The basic operating principle is similar to most other commercial HSGC systems. Figure 1.1 shows a picture of an HP commercial headspace gas chromatographic system. Fig. 1.2 shows a schematic diagram of an HP Headspace Sampler. The operation of the sampler is simple. A sample is first placed in a vial, which is then sealed by a septum, and placed in the sample vial tray of the headspace sampler. The unfilled space in the vial is called the headspace. The sample vial is then transported to an oven (a well-controlled temperature environment) to achieve vapor-liquid phase equilibrium within the vial. When valve S1 is open and S2 is closed and positions 4 and 5, and 1 and 6 of the injection valve are connected, the

sample vial is pressurized by a gas (helium, nitrogen, or air) through a hypodermic needle to create a pressure head for sampling. The vapor phase in the headspace to be analyzed is transferred into the sample loop when valve S1 is closed and S2 is open. The vapor in the sample loop is then injected into the GC column by a carrier gas flow when the positions of 1 and 2, and 3 and 4 of the injection valve are connected. If multiple headspace extraction (MHE) operation is desirable, the procedures described above are repeated on the sample vial. The entire operation is controlled by a personal computer and is fully automated.

1.1.2 Headspace Operating Conditions

It is important to operate the headspace at a proper set of conditions for accurate measurements. Most of the HSGC techniques rely on the VLE of the analyte in the headspace. Therefore, it is critical to achieve analyte equilibrium in the vial static headspace. We conducted equilibrium tests at 70^{o}C using an aqueous methanol solution to obtain the desired vial equilibrium time through HSGC analysis of the headspace vapor. Vial gentle shaking mode was selected in the tests. As shown in Fig. 1.3, the signal peak area of the GC flame ionization detector (FID) increases with equilibrium time and then reaches a constant value, indicating that VLE of methanol has been established. Figure 1.3 also shows that a large sample size requires a longer equilibrium time as expected. Figure 1.4 shows the effect of sample size on equilibrium time for an aqueous methanol solution. Although the equilibrium time also varies with the sample matrix, the data presented in Fig. 1.4 can be used as a guideline for methanol analysis in kraft mill streams.

Vial pressurization is used in most commercial headspace samplers to create a pressure head within the vial for sampling. Vial pressurization reduces the analyte concentration in the headspace, raising the issue of analyte dilution, which will be discussed in the next paragraph. Different headspace sampler, may use different control techniques for pressurization. Pressurization time is used for pressurization control with a constant pressure head in the HP-7694 sampler. We tested the effect of vial pressurization time on measured GC FID signal peak area using an aqueous methanol solution. Because pressurization dilutes the analyte concentration within the headspace, the measured signal decreases with pressurization time initially as shown in Fig. 1.5 and then reaches a constant level because a fixed pressure head is

used. Although pressurization time can affect GC signal, it should not affect the accuracy of absolute measurements through calibration as long as the same pressurization time is used for both the calibration and testing experiments. Several HSGC techniques use the ratio, r_A, of the GC signal peak areas obtained from two separate measurements using two different sample sizes. We plotted r_A in Fig. 1.5 and found that r_A is not affected by the vial pressurization time. A pressurization time of 0.2 min is used in most of our experiments.

The sample-loop in most commercial headspace samplers is filled through venting the pressurized vial to atmosphere. The venting time is used to control the sample-loop filling process. We studied the effect of sample-loop fill time on measured FID signal peak area using a methanol-water solution. As shown in Fig. 1.6, the measured FID signal peak area reaches a constant level at about a loop fill time of 0.2 min for the two sample sizes tested. A constant ratio of the two signals is also achieved with a loop fill time of 0.2 min. A longer loop fill time, e.g., 0.2 min, can also lead to an atmosphere pressure within the sample vial, important in multiple headspace extraction (MHE) HSGC measurements.

1.2 Quantitative Analysis

The difficulties in analysis of VOC in kraft mill streams is mainly due to the fact that samples often have complex matrices. A typical example is spent pulping liquor, which is called black liquor because of its color. Black liquor contains dissolved organic solids such as lignin, hemicellulose, organic and inorganic salts, hydroxide, and sulfide. The volatile organic compounds (VOCs) in black liquor were primary formed during the pulping process and the concentrations of VOCs in the liquor are on the order of ppm (mg/L) level. NCASI [6] developed a method for the measurement of liquid methanol concentration in weak black liquors. The method requires the addition of chemicals to precipitate the solids in weak black liquors. It has several disadvantages: (1) the amount of chemicals added (mass ratio of chemical to black liquor = 30:1) significantly dilutes the VOC concentration in the sample and reduces the measurement accuracy; (2) the method is only suitable for the analysis of weak black liquors because the solids precipitation method cannot be used for other mill streams; and (3) the method is tedious and time-consuming. In the following section, we will describe a standard addition

HSGC method for the analysis of methanol in black liquors that is demonstrated in the present research. The method can be easily applied to measure other VOCs in other kraft mill streams.

1.2.1 Methodology – The Standard Addition Method

The standard addition HSGC technique was initially developed by Drozd and Novak [7]. It is based on the thermodynamic VLE and mass balance of the analyte. We demonstrated that the method is effective for volatile species analysis in kraft mill streams, including in black liquor [8].

Figure 1.7 schematically describes the standard addition method. Two sample vials both filled with the same volume of sample solution were used. A known very small amount of concentrated methanol solution was then added to one of the vials. The volume of the solution added is very small compared to the volume of the original solution and, therefore, can be ignored. After phase equilibrium was established within each vial, headspace GC analysis of each sample was conducted.

It can be assumed that the analyte concentrations in these two sample vials are very low or the analyte is under infinite dilution (which is valid for most VOCs in pulp and paper mill streams even after the standard addition). Therefore, the analyte VLE partitioning in these two vials follows Henry's law. According to Henry's law, the concentration of a solute dissolved in a dilute solution at equilibrium is proportional to the partial pressure of the gas, that is,

$$P_i = HC_i \qquad \text{or} \qquad H = \frac{P_i}{C_i}. \tag{1.1}$$

where P_i is the partial vapor pressure, and C_i is the solute mole concentration in the solution of species i under equilibrium. When a liquid sample of volume V_L^0 containing a solute is introduced into a closed system with a headspace, some of the solute may be transported from the liquid phase through the liquid-gas interface into the gas phase to become vapor, while some of the vapor may diffuse into the solution at the interface. These two mass transport processes will reach a dynamic equilibrium between the vapor and liquid phases after some time. At equilibrium, the partial pressure of the solute in the vapor phase is proportional to the

concentration of the solute in the liquid. The proportionality coefficient is the Henry's constant of the solute in the solution.

By mass conservation, the amount of solute in the vapor phase in a vapor-liquid system under equilibrium can be described as:

$$n_1 = C_0 V_L^0 - \alpha C_1 V_L^0 = \frac{P_1 V_G^0}{RT}, \tag{1.2}$$

where n_1, C_1, and P_1 are the total moles of solute in the vapor phase, the concentration of the mole solute in the liquid phase, and the solute partial vapor pressure, respectively, under equilibrium state 1. C_0 is the solute concentration in the original sample. V_L^0 is the volume of the sample solution. α is the solution volume expansion factor due to temperature change between state 0 and state 1. V_G^0 is the volume of the headspace. We assumed that the vapor phase solute in the headspace follows the ideal gas law. R is the universal gas constant, and T is the temperature of the vapor.

If a certain volume V_S of concentrated solution with a known solute concentration of C_S is added into this system, the existing equilibrium will be disturbed and a new equilibrium state will be reached after a while. The amount of solute in the vapor phase under the new equilibrium state can be expressed as:

$$n_2 = C_0 V_L^0 + C_S V_S - \alpha C_2 V_L^0 = \frac{P_2 V_G^0}{RT}, \tag{1.3}$$

where we assume that the total volume of the solution remains the same as long as the volume of the concentrated solution added is negligible compared to the initial volume of the solution, i.e., $V_L^0 >> V_S$. Subscript 2 denotes the new equilibrium state. From Eqns. (1.2) and (1.3), we can obtain the concentrations of the solute in the liquid phase under the two equilibrium states,

$$C_1 = \frac{C_0 V_L^0 RT - P_1 V_G^0}{\alpha V_L^0 RT}, \text{ and} \tag{1.4}$$

$$C_2 = \frac{C_0 V_L^0 RT + C_S V_S RT - P_2 V_G^0}{\alpha V_L^0 RT}, \tag{1.5}$$

Under infinite dilution, the Henry's constant is not dependent on the solute concentration in the solution. Therefore, we have

$$H = \frac{P_1}{C_1} = \frac{P_2}{C_2}. \tag{1.6}$$

Then, the initial solute concentration in the sample solution can be calculated from Eqns. (1.4) to (1.6) as,

$$C_0 = \frac{C_S V_S}{(P_2 / P_1 - 1) V_L^0}, \tag{1.7}$$

where the solute vapor partial pressure P_1 and P_2 in the vapor phase can be measured using a headspace GC system.

If gas chromatography is used for the headspace analysis, the GC response is measured as the peak area A_i of the species detected, which is proportional to the sample loop volume V_{loop} of the GC system and the solute partial pressure P_i, i.e.,

$$A_i = f' V_{loop} P_i. \tag{1.8}$$

Substituting Eqn. (1.8) into Eqn. (1.7), we can find the concentration of the solute in the sample solution through headspace GC measurements,

$$C_0 = \frac{C_S V_S}{(A_2 / A_1 - 1) V_L^0}. \tag{1.9}$$

Eqn. (1.9) is the mathematical expression of the present method for measurements of liquid concentration of VOCs in sample streams.

1.2.2 Experimental

1.2.2.1 Chemicals

Methanol, methyl ethyl ketone (MEK), and acetone were mixed with deionized water to make standard solutions of methanol-water, MEK-water, and acetone-water to validate the present method. The ranges of the concentration of these three standard solutions were 100-2000, 10-100, and 1-10 ppm, respectively, and were selected to match their liquid contents in typical kraft mill streams. The combination of these three concentration ranges covers trace species concentrations over three orders of magnitude within the infinite dilution assumption limit.

Four pulping black liquor samples from two kraft mills (mills A and B) were used for comparison studies of the measured methanol concentration in liquid using the present method and the method developed by NCASI. Measurements of methanol and MEK were also conducted in various kraft mill streams from Mill C.

1.2.2.2 Apparatus and Operation

Measurements were carried out using an Model HP-7694 Automatic Headspace Sampler and Model HP-6890 capillary gas chromatograph as discussed previously. The GC is equipped with a flame ionization detector (FID). GC conditions: HP-5 capillary column at 30°C; carrier gas helium flow: 3.8 mL/min. A flame ionization detector (FID) was employed with hydrogen and air flows of 35 and 400 mL/min, respectively. Headspace operating conditions: 25 minutes gentle shaking for equilibration of the sample, vial pressurization time: 0.2 min, and sample loop fill time: 1.0 min., loop equilibration time: 0.05 min. Most of the experiments were conducted at a headspace sampler temperature of 70°C to avoid water vaporization and obtain a good sensitivity as sufficient methanol will be present in the vapor phase at this temperature.

The sample preparation and measurement procedures were as follows: pipette duplicate 10 mL of sample solution into two 20 mL vials: add 10 μL of pure methanol solvent by microsyringe into one of the vials; then, close the vials and place it into the headspace sample tray for measurement.

1.2.3 Results and Discussions

1.2.3.1 The Method of Standard Addition

We applied the method of standard addition to develop a technique for VOC concentration measurements in sample solutions. The method of standard addition (or the known increment method) is widely used in analytical techniques, such as potentiometry, polarography, and atomic spectroscopy [8]. In this method, a certain volume of solution with a known concentration of the solute is added into the sample solution (called "standard addition"). By measuring the signal changes before and after this "standard addition," the concentration of the solute in the sample can be calculated. The main advantage of this method is that it can measure solute concentration in the samples having a high but unknown total ionic strength or for samples with highly variable solution components. Unlike the traditional standard addition method, the present method takes the approach of analyzing the solute in the vapor phase rather than in the liquid phase before and after the standard addition to indirectly determine the concentration of the solute concentration in the original sample solution. In addition, it does not require calibration as can be seen in Eqn. (1.9) that does not contain any calibration constants.

1.2.3.2 Experimental Technique Validation

The repeatability of the method was demonstrated by using a standard methanol-water solution (methanol = 800 mg/L). A relative standard deviation (RSD) of measured methanol concentration in solution was less than 3% for the five samples tested, indicating that the repeatability of the technique is excellent.

The experimental technique was validated using a set of standard VOC-water (methanol-water, MEK-water, and acetone-water) solutions with known concentrations. The present method measures the VOC concentration of the standard solution according to Eqn. (1.9), where the GC peak areas A_1 and A_2 were obtained from the measurements of the vapor sample in the headspace taken before and after the standard addition of each solution. For a combined VOC concentration range of 1-2000 ppm described previously, the comparison between the standard and the measured data was excellent. An excellent correlation between the standard and the measured concentrations is shown in Fig. 1.8. The errors for all the measurements were less than 5.0%.

1.2.3.3 Chromatographic Separation of Various Compounds in Black Liquor Vapor

Many kraft mill streams consist of various compounds that will be present in their vapor phases. Accurate measurement of methanol vapor concentration in mill streams requires the elimination of interference from other substances during chromatography. Black liquor is one of the most difficult mill streams for GC analysis as it contains many hydrocarbons and sulfur compounds. Fig. 1.9 shows a GC chromatogram of the vapor phase of a softwood black liquor using a FID detector. The GC/mass spectroscopy was used to identify the various compounds contained in the vapor phase as shown in Fig. 1.9. Through optimisation by choosing a low column temperature of 30^{o}C and moderate gas carrier gas flow rate of 3.8 mL/min as mentioned previously, methanol can be measured under the GC conditions for the present study.

1.2.3.4 Comparison with NCASI Method

Table 1.I shows the methanol concentrations in different black liquors. It can be seen that the data obtained by the present method show a good agreement with the results obtained using the method developed by NCASI. The differences in measuring methanol content between these two methods are within the error margins of the methods. Experimental repeatability test indicated that the relative standard deviation (RSD) of the data obtained using the NCASI method was about 10%. While the RSD of the data obtained using the present headspace method was about 5%.

1.2.3.5 VOC Concentration in Various Mill Streams

To demonstrate the present method for VOC analysis in various mill streams, we conducted measurements of the methanol and MEK contents in various kraft mill streams from Mill C using the present method, the results are shown in Table 1.II. Mill C is an unbleached kraft paper mill. For this particular mill, the data indicate: (1) the weak wash sample in the recovery cycle did not contain methanol, but some MEK; (2) the shower water and filtrate sample in the washers had a significant concentration of methanol and MEK; (3) the blow tank condensate sample from the digester also had a high content of methanol and MEK as indicated by the measurement of the sample from the hot water tank; (4) the weak black liquor sample had significant methanol and MEK contents; and (5) the white water sample from the paper machine head tank of the present unbleached mill contained some methanol, but no MEK.

VOCs are primary formed in the pulping process. Therefore, their concentrations in various streams of the fiber line are primary determined by dilution through washing and water reuse in the fiber line and by the vapor-liquid equilibrium in various processes. We conducted three mill-wide VOC sampling in mill liquid streams. The detailed characterization of VOC concentration of will be presented in the next Chapter.

1.2.4 The Full Evaporation HSGC Method

We also developed a full evaporation (FE) HSGC method for volatile organic sulfur compounds analysis in black liquor and other kraft mill streams. Because this research does not deal with sulfur compound, the method will not be discussed in this report. Interested readers should refer to the work that we published [10, 11] for detail.

1.3 VLE Determination

The complex sample matrix of many streams from pulp and paper mills also makes VLE determination of solute difficult. In this section, we will discuss three HSGC methods for VLE analysis of methanol in various pulp and paper mill streams. Because the concentrations of methanol and many other VOCs in mill streams are low and can be treated under infinite dilution, determination of Henry's law constant is the main objective of VLE analysis.

Henry's law constant is defined according to the following equation as mentioned previously:

$$H_i = \lim_{x \to 0} \frac{P_i^v}{x_i} = \lim_{x \to 0} \frac{y_i \cdot P}{x_i} \tag{1.10}$$

where x_i and y_i are the mole fraction of the species i in the liquid and vapor phase, respectively. For a system at equilibrium in a static headspace, the vapor phase can be assumed to follow the ideal gas law,

$$y_i \cdot P = P_i^v = C_{Gi} \cdot RT \tag{1.11}$$

where C_{Gi} is the solute mole concentration in the headspace (vapor phase) and R is the universal gas constant. In a system in which all solutes are at infinite dilution, the mole fraction of solute i in the liquid phase can be approximated as

$$x_i \approx \frac{n_i}{n_j} = \frac{C_{Li}}{\rho_j / M_j} = C_{Li} \cdot v_j \qquad (1.12)$$

where C_{Li} is the solute concentration in the liquid phase at equilibrium, and ρ_j, M_j, and v_j are the density, molecular weight, and the molar volume of the solvent, respectively. Equation (1.12) is still a good approximation even for spent pulping liquors with total solids content around 20%.

Combining Eqs. (1.11), (1.12), and (1.10) leads to a relationship between the Henry's constant of species i and its partition coefficient $K_i = C_{Li}/C_{Gi}$ in a static headspace:

$$H_i = \frac{RT}{v_j K_i} = \frac{\rho_j RT}{M_j \cdot K_i} \qquad (1.13)$$

1.3.1 The Direct HSGC Method

The direct HSGC method for VLE analysis was demonstrated by Kolb et al. [12]. We will not discuss in grate detail in this report. The method simply measures the equilibrium solute concentrations in the liquid and vapor phase separately and directly for the calculation of K_i and H_i. With headspace measurement, the equilibrium solute concentration in the vapor phase can be easily expressed in terms of the measured GC detector peak area A, i.e,

$$C_{Gi} = f \cdot A \qquad (1.14)$$

Because the equilibrium solute concentration in the liquid phase can be calculated from the initial solute concentration in the original sample based on material balance, we have,

$$K_i = \frac{C_{Li}}{C_{Gi}} = \frac{C_0 - \beta C_{Gi}}{f \cdot A_i} \qquad (1.15)$$

where f is the GC response factor and $\beta = V_G/V_L$ is the phase ratio.

Equation (1.15) is valid for determination of the VLE partitioning coefficient, K_i, in any systems. We applied Eq. (1.15) to determine Henry's law constant of methanol in black liquors in this research [13]. The volume of the sample vial was 20 mL and the liquor sample size was 10 mL for all the experiments conducted, which gave the headspace volume of 10 mL and the phase ratio $\beta = 1$. Therefore, if K_i is much greater than 1, i.e., $K_i > 10$, $C_{Gi} << C_{Li}$ ($< C_0$) can be ignored in Eq. (1.15), and, hence,

$$K_i \approx \frac{C_0}{f \cdot A_i} \tag{1.16}$$

We adopted an external calibration standard to obtain the GC response factor f by using a standard aqueous methanol solution with known methanol concentration of C_{s0} = 800 mg/L and methanol VLE partition coefficient K_{si}, (e.g., K_{si} = 570 at 70°C [14]), and, hence,

$$K_i = \frac{A_{si}}{A_i} \cdot \frac{C_o}{C_{so}} \cdot K_{si} \tag{1.17}$$

where A_{si} is the FID signal peak area recorded in measuring the headspace vapor of the standard solution at the temperature corresponding to K_{si}.

Equation (1.17) is especially suitable for VLE analysis in black liquor. We have used Eq. (1.17) to obtain a semiempirical correlation for the prediction of Henry's constant of methanol in black liquor [13] and will be discussed in detail later this report.

1.3.2 The Modified Method of Equilibrium Partitioning in Closed Systems (EPICS)

The EPICS method was initially developed by Lincoff and Gossett [15, 16]; it determines Henry's law constant indirectly based on the VLE of the solute in a closed system and on solute mass conservation. In the method, two sample vials were used, and the volume ratio of the two testing solutions was arbitrarily taken as 10 [15] and 4 [16]. The mass of the solute in the two solutions was equal [15], or the mass ratio was measured [16]; therefore, the solute concentrations in the two vials were different. It was assumed that the solute in two solutions was under infinite dilution; therefore, the VLE partitioning coefficients of the solute in these two solutions are equal at a given temperature. The advantages of the EPICS method are

that no special apparatus is required and calibration is not necessary. Henry's constant can be obtained by measuring the vapor concentration ratios from a pair of sealed vials with different solution volumes and solute concentrations through headspace gas chromatography.

Later Kolb et al. [17] took a similar approach but conducted several headspace measurements. They used several vials filled with the same solution but with different volumes, instead of using two vials filled with solutions of different solute concentrations. They derived the VLE partitioning coefficient as a function of the vapor phase concentration measured by the HSGC, solute concentration in the original sample, and a volume ratio (sample volume over headspace volume) parameter called the phase ratio, β, a known constant. They called the method of phase ratio variation (PRV).

In principle, the PRV and EPICS method, are not much different. Both are based on solute VLE in static headspace and mass conservation. The main problem of these two methods is that their accuracy is poor in applied to systems with a large partitioning coefficient, for example K>10 as shown by Gosett in his error analysis [16] and K>144 as indicated by Ettre et al. [17].

From a mathematical point of view, it is sufficient and necessary to solve a VLE problem with two and only two equations (two independent measurements). Therefore, it is not necessary to conduct more than two headspace measurements as required in the PRV method [17]. From a physical point of view, the VLE partitioning coefficient K changes with solute concentration except within the range of infinite dilution in which K can be approximated as a constant. Therefore, it is not appropriate to determine K or even Henry's constant on a very strict basis (the concept of infinite dilution is not well-defined physically and mathematically) using two solutions with different concentrations as adopted in the EPICS method [15, 16]. Based on the above reasoning, we propose to conduct two headspace measurements and only two in two vials filled with the same solution but with different sample volume to further develop the EPICS and PRV method [14].

1.3.2.1 Methodology

Figure 1.10 shows the schematic diagram that described our proposed modified EPICS method. We used two sample vials both filled with the same sample solution of different

volumes rather than two different solutions as in the EPICS method. We conducted a headspace analysis of each sample after a phase equilibrium was established within each vial. The solute of the two systems has the same VLE partitioning coefficient *K* as the two systems are identical, which can be used to connect the two independent headspace measurements to determine *K*. The following is the derivation of the present indirect HSGC method.

When a sample solution of volume V_L with a solute concentration of C_L^0 is introduced into a closed vial, the total moles *M* of the solute in the vial can be expressed as:

$$M = C_L^0 V_L = C_L V_L + C_G V_G = C_G (V_L \cdot K) + C_G V_G = C_G [(V_L \cdot K) + V_G], \qquad (1.18)$$

where C_G and V_G are the concentration and volume of the solute in the vapor phase, respectively.

Therefore, the total moles of the solutes in two separate vials can be written as:

$$M_1 = C_L^0 V_L^1 = C_G^1 [(V_L^1 \cdot K) + V_G^1], \qquad (1.19)$$

$$M_2 = C_L^0 V_L^2 = C_G^2 [(V_L^2 \cdot K) + V_G^2], \qquad (1.20)$$

respectively.

The VLE partitioning coefficient *K* can be derived from Eqns. (1.19) and (1.20),

$$\frac{1}{K} = \frac{V_L^1 (1 - C_G^1 / C_G^2)}{C_G^1 / C_G^2 (V_T - V_L^1) - V_L^1 / V_L^2 (V_T - V_L^2)}. \qquad (1.21)$$

The solute concentration in the vapor phase C_G is proportional to the peak area from GC measurement. Thus, we have

$$C_G^1 / C_G^2 = A_1 / A_2. \qquad (1.22)$$

Substitute Eqn. (1.22) into (1.21), the VLE partitioning coefficient *K* or its inverse *H** , the dimensionless Henry's constant, can be determined

$$H^* = \frac{1}{K} = \frac{V_L^1(1 - A_1 / A_2)}{A_1 / A_2 (V_T - V_L^1) - V_L^1 / V_L^2 (V_T - V_L^2)} = \frac{V_L^1(1 - r)}{r(V_T - V_L^1) - x(V_T - V_L^2)}, \quad (1.23)$$

where $r = A_1 / A_2$, and $x = V_L^1 / V_L^2$. In this study, we take $V_L^1 > V_L^2$, or x>1. Therefore, r >1. When the solute is under infinite dilution, Eqn. (1.23) gives the Henry's constant of the solute.

1.3.2.2 Experimental

Methanol and deionized water were used to make solutions of methanol-water for the present study. The methanol concentration was about 800 mg/L. The experimental conditions of the HSGC system were the same as those described in section 1.2.2.

The measurement procedure was as follows: Pipette 10 (V_L^1) and 0.05 (V_L^2) mL of the sample solution into two 20 mL vials ($x = V_L^1 / V_L^2$=200), respectively. Then close the vials and put into the oven of the Headspace Sampler. The vial is gently shaken to achieve equilibrium. The vial is then pressurized by helium to create a pressure head to fill the sample loop. The vapor in the sample loop is finally analyzed by the GC.

1.3.2.3 Precision Analysis of the Method

We conducted a mathematical precision analysis of Eqn. (1.23) based on the following variance estimation equation:

$$s^2(H^*) = \left(\frac{\partial H^*}{\partial V_L^1}\right)^2 s^2(V_L^1) + \left(\frac{\partial H^*}{\partial r}\right)^2 s^2(r) + \left(\frac{\partial H^*}{\partial x}\right)^2 s^2(x) + \left(\frac{\partial H^*}{\partial V_L^2}\right)^2 s^2(V_L^2) + \left(\frac{\partial H^*}{\partial V_T}\right)^2 s^2(V_T)$$

(1.24)

where the variance of r can be calculated from the variances of the peak areas A_1 and A_2 similar to that of H^*,

$$s^2(r) = \frac{1}{A_2^2} s^2(A_1) + \frac{A_1^2}{A_2^4} s^2(A_2). \quad (1.25)$$

We conducted replica HSGC measurements in nine (9) testing vials filled with 10 μL (much less than the smallest volume of the smaller sample, i.e., V_L^2=40 μL, used in this study) aqueous methanol solution to determine the variance of GC peak area A. We found that the relative standard deviation (RSD) of nine (9) replica measurements was 2.1% as listed in Table 1.III. Based on this experiment, it is assumed that $\sigma^2(A_1) = \sigma^2(A_2) = 2.5\%A_1 > 2.5\%A_2$ ($A_1 > A_2$ in this study). Therefore, $\sigma^2(r)=0.625\text{X}10^{-3}(r^2+1)$ from Eqn. (1.25). The variances of other independent variables were also determined experimentally. It was found that the main contribution to the variance of *H* or K* is the *r* term. By neglecting the contribution from other measurement variables, we have

$$\frac{\sigma^2(H^*)}{(H^*)^2} \approx \frac{(1-x)^2}{(1-r)^4} \cdot \left(\frac{V_T}{V_L^1}\right)^2 \cdot (H^*)^2 \cdot \sigma^2(r). \qquad (1.26)$$

It can be seen from Eqn. (1.26) that the relative variance of the measured partitioning coefficient *K (H*)* is a complex function of the experimental variables, *x*, *K (H*)*, and V_L^1 (or V_L^2). Mathematical calculations were carried out to study the precision of the developed method for solution volume ratio *x* from 2 to 1000, VLE partitioning coefficient *K* ranging from 2 to 1000, and V_L^1 = 10, 1, 0.1, and 0.05 mL. We found that the volume ratio *x* of the two testing solutions can affect the precision of the method significantly. The calculated results indicate that the relative measurement error increases with *x* rapidly initially and then reaches an asymptotic value as shown in Fig. 1.11 where the volume of the large sample V_L^1 was 10 mL. The predicted experimental errors of Henry's constant of methanol (*H**=0.0017; or *K*=588) in aqueous solutions agree with those obtained experimentally through several replica measurements as shown in Fig. 1.11. Fig. 1.11 also indicates that a very large solution volume ratio (x >100) is required to obtain a good measurement of VLE partitioning coefficient *K* when it is large (*K*>200). This is because the two separate HSGC measurements of the vapor in the two headspaces will not be significantly different or the ratio of the peak areas *r* is not sufficiently larger than unity (*r* can be derived from Eqn. (1.23)) to obtain good accuracy when a small difference between the two sample volumes or small *x* is used. This precision behavior was also observed by Ettre et al. [17] in their study. Unfortunately, little was done to resolve the problem

in their study. The authors proposed to reduce the solute concentration, meaning to alter the measurement system.

Our analysis also indicates that by significantly reducing the sample volumes of both samples, good accuracy can be obtained with a small x in measuring large K's as shown in Fig. 1.12a where the larger sample volume V_L^1 was varied. To obtain good VLE analysis of a system with a very large K (~1000) of the solute, we can design an experiment using a very large x = 1000 with V_L^1 = 10 mL (or V_L^2 = 10 μL), or design one using a small x = 4 with V_L^1 = 100 μL (or V_L^2 = 25 μL) as shown in Figs. 1.11 and 1.12a, respectively. The advantage of using small sample sizes and a small solution volume ratio x is that the equilibrium time can be reduced significantly as we discussed previously. Our experimental data indicate that the sensitivity of the GC measurements will not deteriorate by using small sample sizes to measure very large K's. Table 1.IV shows the effect of sample size on the measured GC signal (peak area) of the methanol-water solution. The GC peak area was only reduced by three times when the sample size was decreased by three (3) orders of magnitude. A signal level of peak area A=190 obtained using the smallest sample size of 10 μL is well in the range of good signal-to-noise ratio as the GC linear response range was A=0-2000. The GC signal will drop much faster with the decrease of sample size for systems with smaller K's. However, we found that it is not suitable to measure small K's using small sample sizes and a small solution volume ratio as shown in Fig. 1.12b. Small K's can be easily and accurately measured with large sample sizes in both of the testing vials using the present, EPICS, and PRV methods.

1.3.2.4 Comparison with Literature Data

Determination of large values of VLE partitioning coefficient (K>200), such as the Henry's constant of methanol H^* ($=1/K$) in water for temperatures ranging from 295 to 350K, is difficult. Indirect techniques are ideal for this type of application because they can eliminate most of the systematic and calibration errors. We conducted two sets of experiments to demonstrate that the present indirect HSGC method can be applied with good precision. We used two completely different sets of experimental parameters V_L^1=10 mL and V_L^2=50 μL (or $x=V_L^1/V_L^2$=200) and V_L^1=100 μL and V_L^2=40 μL (or $x=V_L^1/V_L^2$=2.5), respectively, to measure the

same quantity of the Henry's constant of methanol H^* in water. Good agreement of the results measured by these two methods were obtained as shown in Table 1.V, indicating the validity of our mathematical precision analysis of the method. We averaged the measurements of the Henry's constants of methanol from the two sets of experiments correspondingly to compare with literature data. The data obtained using the present indirect HSGC method show excellent agreement with those in the literature [18-22] as shown in Fig. 1.13. A linear regression analysis shows that the logarithm of all the data fit to a straight line with the inverse of temperature very well, demonstrating the validity and the accuracy of the present method.

1.3.3 Multiple Headspace Extraction (MHE) Method

MHE HSGC was developed to achieve analysis automation. It is similar to dynamic gas extraction (or purge-trap), but is carried out in steps. The mathematical model of the MHE method was developed by McAuliffe [23, 24] and Suzuki et al. [25]. The method was further developed by Kolb and Ettre [26-28]. MHE HSGC has been successfully applied in many industries for quantitative analysis [29, 30]. Kolb and Ettre [28, 3] developed an MHE technique for VLE determination; however, they have never demonstrated the technique experimentally. In this research, we developed and experimentally demonstrated an MHE HSGC technique that can simultaneously determine solute concentration and Henry's constant [31]. The method is rapid, automated, and accurate. We also found through experiments that the MHE technique proposed by Kolb and Ettre [28, 3] is inaccurate and produces large uncertainties for VLE determination. The method is particularly useful for determination vapor-liquid equilibrium of analyte in mill condensates and filtrates.

1.3.3.1 Methodology

For a given sample solution of volume V_L with a solute mass of m_0 introduced into a closed vial of volume V_T, vapor-liquid phase equilibrium can be established within the vial with an equilibrium headspace pressure of P_o. The equilibrium concentration of the solute in the vapor phase C_G is proportional to the concentration in the liquid phase C_L. For infinitely diluted solutions, the proportionality coefficient is the dimensionless Henry's constant H^* of the solute, i.e.,

$$H^* = C_G / C_L , \tag{1.27}$$

where C_G and C_L are volumetric mass concentration, i.e., mg/L.

As discussed previously, pressurization of the sample vial to a pressure of P_h using inert gas is a common practice in headspace measurements to create a pressure head for sampling. It is assumed that the pressurization time is very short so that the equilibrium remains unchanged. It should be pointed out that the solute volumetric concentration C_G within the headspace is a constant before and after pressurization. After pressurization, the headspace vapor is vented out to fill the sample loop. The sample is then injected into the GC column to complete the first headpsace measurement. Further venting is often necessary to reduce the headspace pressure close to its initial equilibrium pressure P_o. The headspace measurement disturbed the equilibrium in the vial. According to Kolb and Ettre [28], a new VLE can be reestablished within the vial and the VLE conditions are exactly repeated. A second headspace measurement is then conducted. This procedure can be repeated several times. We label each equilibrium state as *1, 2, …, i, …, n*, correspondingly, in the following derivation.

The initial mass of the solute m_1 (or the solute mass at the first equilibrium state) in the sample vial can be expressed as:

$$m_1 = C_{G1}V_G + C_{L1}V_L , \tag{1.28}$$

where V_G and V_L are the volumes of vapor and liquid phases in the vial, respectively.

The amount of solute vapor extracted out of the headspace of the sample vial can be expressed as a certain fraction of the solute vapor in the headspace before venting, i.e.,

$$m_{EX,\,solute} = \beta C_G V_G, \tag{1.29}$$

where β is called the sample volumetric flow fraction. Therefore, the total mass of the solute within the vial after the first headspace extraction can be written as m_2,

$$m_2 = (C_{G2}V_G + C_{L2}V_L) = m_1 - \beta_1 C_{G1}V_G , \tag{1.30}$$

We can express the mass of vapor mixture within the headspace after each extraction as follows,

$$m_3 = (C_{G3}V_G + C_{L3}V_L) = m_2 - \boldsymbol{j}_2 C_{G2}V_G = m_1 - V_G(\boldsymbol{j}_1 C_{G1} + \boldsymbol{j}_2 C_{G2}), \tag{1.31a}$$

$$\vdots$$

$$m_n = (C_{Gn}V_G + C_{Ln}V_L) = m_1 - V_G(\boldsymbol{j}_1 C_{G1} + \boldsymbol{j}_2 C_{G2} + \cdots + \boldsymbol{j}_{n-1} C_{G(n-1)}) = m_1 - V_G \sum_1^{n-1} \boldsymbol{j}_i C_{Gi} \tag{1.31b}$$

.

We neglected the change of solute volume V_L due to heating and headspace extraction in the above derivation. Furthermore, we assume that the headspace operating conditions remained unchanged for each headspace extraction, which is valid according to Kolb and Ettre [28, 3]. Therefore, the sample volumetric flow fractions are a constant, i.e., $\boldsymbol{j}_1 = \boldsymbol{j}_2 = \ldots = \boldsymbol{j}_i = \ldots = \boldsymbol{j}_{n-1} = \boldsymbol{j}$, though the absolute solute mass extracted out is reduced due to the reduced solute concentrations of the liquid and vapor phases within the vial. Above mass conservation derivations are schematically shown in Fig. 1. 14.

For infinitely diluted solutions,

$$H^* = \frac{C_{G1}}{C_{L1}} = \frac{C_{G2}}{C_{L2}} = \frac{C_{G3}}{C_{L3}} = \cdots = \frac{C_{Gn}}{C_{Ln}}. \tag{1.32}$$

Substituting Eqns. (1.32) into Eqn. (1.31b), we have

$$C_{Gn}\left(V_G + \frac{V_L}{H_c}\right) = m_1 - \boldsymbol{j} V_G \sum_1^{n-1} C_{Gi} \quad . \tag{1.33}$$

where the solute concentration in the headspace C_G is proportional to the measured GC peak area A, i.e., $A = fC_G$. We can then express Eqn. (1.33) as a first-order linear equation,

$$\sum_1^{n-1} A_i = a + bA_n, \tag{1.34}$$

with

$$a = \frac{f \cdot m_1}{\beta V_G}, \tag{1.35a}$$

and

$$b = -\frac{1}{\beta}\left(1 + \frac{1}{H^*} \cdot \frac{V_L}{V_G}\right) = -\frac{1}{\beta}\left(1 + \frac{1}{\beta \cdot H^*}\right), \tag{1.35b}$$

where $\beta = V_G / V_L$ is the phase ratio according to Kolb and Ettre [28].

$\sum_{1}^{n-1} A_i$ and A_n can be obtained through MHE GC measurements. A linear regression analysis can be applied to obtain the intercept *a* and the slope *b* of Eqn. (1.34). The concentration and the Henry's constant of the solute can be calculated from *a* and *b* using Eqns. (1.35a) and (1.35b), i.e.,

$$C_0 = \frac{m_1}{V_L} = \frac{a\beta}{f} \cdot \frac{V_G}{V_L} = \frac{a\beta}{f}\beta, \tag{1.36}$$

or simply as Kolb and Ettre [3],

$$C_0 = f_{MHE} \cdot \sum_{1}^{n} A_i = f_{MHE} \cdot [a + (b+1)A_n], \tag{1.37}$$

and

$$H^* = -\frac{1}{(1+\beta b)\beta}, \text{ or } K = \frac{1}{H^*} = -(1+\beta b)\beta \tag{1.38}$$

where *f* and β are two unknown constants and can be calibrated.

We would like to point out that the present derivation did not assume that each headspace extraction is an identical isothermal expansion and the vapor mixture in the headspace follows ideal gas law that are required in the MHE method (Eqn. 1.41) by Kolb and Ettre [28, 3]. Therefore, the present MHE method to measure Henry's constant is more universal from both theoretical and practical points of view. Furthermore, with the assumption of isothermal

expansion headspace extraction and ideal gas law, the sample volumetric flow fraction $\boldsymbol{j}$ in Eqn. (1.38) can be related to the pressure ratio $\boldsymbol{r}$ used by Kolb and Ettre [28, 3].

The amount of solute vapor extracted out of the headspace is simply the product of the total vapor mixture extracted out of the headspace, $m_{EX} = V_G (P_h - P_o)/(RT)$ (from ideal gas law), and the solute mass fraction $C_G / \boldsymbol{r}_{Ph}$ in the headspace before venting (ρ_{Ph} is the headspace mixture gas density before venting), i.e.,

$$m_{EX,solute} = m_{EX} \cdot C_G / \boldsymbol{r} = C_G V_G \cdot (P_h - P)/P_h = C_G V_G \cdot (1 - P_o / P_h) . \qquad (1.39)$$

Substituting Eqn. (1.29) into Eqn. (1.39), we have

$$\boldsymbol{j} = 1 - P_o / P_h = 1 - \boldsymbol{r} , \qquad \text{or} \quad \boldsymbol{r} = 1 - \boldsymbol{j} . \qquad (1.40)$$

The MHE method of Kolb and Ettre [3] can be expressed as

$$K = \frac{1}{H^*} = \frac{\boldsymbol{r} - Q'}{Q' - 1} \cdot \boldsymbol{b} = \frac{(1 - \boldsymbol{j} - Q')}{Q' - 1} \cdot \boldsymbol{b} , \qquad (1.41)$$

Therefore, both the present MHE method (Eqn. (1.38)) and that of Kolb and Ettre [3] (Eqn. (1.41)) can determine VLE partitioning coefficient K or H^* with or without calibration depending on whether the headspace pressure ratio ρ is known or not. Neither method is better than the other from an application point of view. However, without the assumptions of ideal gas law and isothermal headspace venting, Eqn. (1.38) is still valid, but Eqn. (1.41) is not.

1.3.3.2 Experimental

Chemicals

Methanol, ethanol, and isopropanol of analytical grade were used as solutes and de-ionized water as solvent to prepare methanol-, ethanol-, and isopropanol-water solutions. The methanol-water solution was used as the standard solution for calibration to obtain f and φ with a known methanol concentration of 800 mg/L and Henry's constant at a temperature range of 25-80^{o}C according to the literature [18-22] and our previous study [14].

Apparatus and Operation

Again, measurements were carried out using an HP-7694 Automatic Headspace Sampler and an HP-6890 capillary gas chromatograph equipped with an HP ChemStation for data acquisition and analysis. The basic operating principles and procedures of the headspace sampler for multiple headspace extraction are very similar to that described by Kolb and Ettre [28], except that the venting process was combined with the sample transfer process in the present headspace sampler. More specifically, the sample loop is open to the atmosphere during sample transfer. The duration of the sample transfer process (sample loop fill time) controls the pressure inside the sample vial. Headspace operating conditions were the same as those described previously.

The measurement procedure was as follows: pipette 50 µL of sample solution into a 20-mL vial, which gives a phase ratio β=399. The sample size (or β) can be varied as necessary. The Headspace Sampler then heats the sample in the vial to a desired temperature with strong shaking for three minutes to achieve vapor-liquid equilibrium within the vial. At equilibrium, the vial is pressurized by compressed air, and the headspace is partially withdrawn to fill the sample loop and vent to the atmosphere to reduce the vial pressure to close to its initial vial pressure. The sample is injected into the GC column for analysis. The GC signal as peak area A is recorded. This procedure is repeated 10 times automatically for multiple headspace extraction analysis and can be programmed by the HP ChemStation.

Method Calibration

Most commercial headspace systems control the headspace pressure P_h by the pressurization time. Therefore, the pressure ratio r, or the sample volumetric flow fraction j, varies with the headspace temperature and the headspace volume V_G (or phase ratio β), so does the proportional coefficient f between the GC peak area and the vapor phase solute concentration. We calibrated j and f as a function of temperature at β = 399 (used in this reserach) by conducting multiple headspace extraction measurements in a methanol-water solution of concentration 800 mg/L at headspace temperatures of 40, 50, 60, 70, and 80°C. At a given temperature, we conducted ten-headspace-extraction GC measurements of the methanol-water sample. We established the following procedure for calibration:

1. Prepare a solute (methanol)-water sample solution with known solute concentration (C_0 = 800 mg/L) and solute VLE partitioning coefficient K at a given temperature range.

2. Pipette 50 μL of sample solution into a 20-mL vial, which gives a phase ratio β=399. The phase ratio can be varied as necessary.

3. Put the sample vial into the headspace sampler tray. The headspace GC system is so programmed that it will (1) automatically heat the sample in the vial to a desired temperature (e.g., 40°C) with strong shaking for three minutes to achieve vapor-liquid equilibrium, (2) pressurize the vial by the compressed air, (3) partially withdrawn the vial headspace vapor to fill the sample loop and vent to the atmosphere to return to its initial pressure, (4) the vapor sample is transferred to the GC for analysis and the GC peak area A is recorded.

4. Program the HP Station so that the above procedure is automatically repeated 10 times for multiple headspace extraction analysis.

5. Conduct linear regression analysis using the 10 GC peak areas A_i recorded to obtain the slope b and the intercept a through Eqn (1.34) with n = 10. Fig. 1.15 shows the results of a typical regression analysis of the GC peak areas A_i from multiple (10) headspace extractions, where $a = 2387.8$ and $b = 10.862$.

6. Calculate the calibration constants f and $\boldsymbol{j}$ from Eqns. (1.35a) and (1.35b) using the literature-given methanol VLE partitioning coefficients [18-22, 14] and known methanol concentration (C_0 = 800mg/L) with the slope b and intercept a obtained, respectively.

7. Repeat procedures (3) to (6), but at a different headspace temperature.

Table 1.VI lists the calibration results. We correlated $\boldsymbol{j}$ and f with temperature T in °C as follows,

$$\boldsymbol{j}(\boldsymbol{b}=399) = 0.3777 - 0.00574 \cdot T + 7.7614 \times 10^{-5} \cdot T^2 \tag{1.42}$$

$$f(\boldsymbol{b}=399) = 437 + 3.1 \cdot T - 0.06 \cdot T^2 \tag{1.43}$$

Equations (1.42) and (1.43) are valid for any solute-solvent systems under headspace GC conditions used in the present study. The effect of phase ratio β on *f* can be directly calculated using Eqn. (1.36). The effect of β on φ can also be accounted for without recalibration. Assuming that headspace operating conditions (temperature and the pressurization pressure; therefore, the total volumetric flow into the headspace) remain the same, we have

$$\varphi(\beta_{cal}) \cdot V_G(\beta_{cal}) = \varphi(\beta) \cdot V_G(\beta) \tag{1.44}$$

Since $V_G = V_T \cdot \beta/(\beta+1)$, we can obtain the following equation to correct the effect of β on the sample volumetric flow fraction φ.

$$\varphi(\beta) = \frac{\beta_{cal}}{\beta_{cal}+1}\frac{\beta+1}{\beta}\varphi(\beta_{cal}) = \frac{399}{400}\cdot\frac{\beta+1}{\beta}\cdot\varphi(\beta=399) \tag{1.45}$$

1.3.3.3 Results and Discussions

Precision Analysis

We conducted a mathematical precision analysis of the present MHE GC method for simultaneous determination of the concentration and the Henry's constant of a solute by Eqns. (1.36) and (1.38) using the following variance estimation Equations, respectively:

$$\sigma^2(C_0) = \left(\frac{\partial C_0}{\partial a}\right)^2 \sigma^2(a) + \left(\frac{\partial C_0}{\partial f}\right)^2 \sigma^2(f) + \left(\frac{\partial C_0}{\partial \varphi}\right)^2 \sigma^2(\varphi) + \left(\frac{\partial C_0}{\partial \beta}\right)^2 \sigma^2(\beta) \tag{1.46}$$

$$\sigma^2(H^*) = \left(\frac{\partial H^*}{\partial b}\right)^2 \sigma^2(b) + \left(\frac{\partial H^*}{\partial \varphi}\right)^2 \sigma^2(\varphi) + \left(\frac{\partial H^*}{\partial \beta}\right)^2 \sigma^2(\beta) \tag{1.47}$$

where the variances $\sigma^2(f)$=2.0%f^2, $\sigma^2(\varphi)$=2.0%φ^2, σ^2(a)=2.0%a^2, and $\sigma^2(b)$=2.0%b^2 are determined based on experimentally measured relative standard deviations of *f*(1.3%), φ(1.8%), *a*(1.0%), and *b*(1.7%), respectively, during calibration. The variance of phase ratio $\sigma^2(\beta)$=2.0x10$^{-4}\beta^2$ is calculated from the variances of the phase volumes $\sigma^2(V_G)$ and $\sigma^2(V_L)$ similar to Eqns. (1.46) or (1.47), with $\sigma^2(V_G)$=1.0%V_G^2 and $\sigma^2(V_L)$=1.0%V_L^2 based on experiments.

From mathematical calculations using Eqns. (1.46) and (1.47), we found that the phase ratio β is a key parameter that controls the accuracy of the present MHE method. The results indicate that a β value of greater than 2 is required to obtain good measurements of solute concentration with uncertainties less than 10% as shown in Fig. 1.16. We used Eqn. (1.45) to account for the effect of β on the volumetric flow fraction j in calculating the effect of j on the measurement uncertainty of the solute Henry's constant. We found that the measurement uncertainty is also affected by the solute Henry's constant itself as shown in Fig. 1.16. Figure 1.16 also indicates that there is an optimum β at which the uncertainty is minimum for a given solute-solvent system or a given solute Henry's constant. The minimum uncertainty also varies with the Henry's constant from less than 0.8% at H^* = 0.001 to 10% at H^* = 1.0. Furthermore, the optimum phase ratio, β_{opt}, correlates very well with the Henry's constant to the following relationship as shown in Fig. 1.17,

$$H^* \cdot \beta_{Opt} = 1.0 . \tag{1.48}$$

This relationship agrees with the recommendation of Ioffe and Vitenberg [2] in designing MHE experiments. As noticed by Kolb and Ettre [3], this recommendation (Eqn. (1.48)) to chose β is difficult to follow, in particular, in measuring very small Henry's constant. Moreover, as shown in Fig. 1.16, the slopes or the derivatives of the uncertainty curve with respect to β are very high in the vicinity of β_{opt}, indicating the difficulties to achieve good precision in experiments because β_{opt} cannot be determined using Eqn. (1.48) before the Henry's constant is being measured. Fortunately, Fig. 1.16 shows that the uncertainties will be less than 10% as long as $\beta < 2\beta_{opt}$ such as $\beta \approx 4$ can give good measurements of solute Henry's constant in a wide range (H^*<1.0, or K>1.0) using the present MHE method. The present method however is not suitable to measure solute Henry's constant >1.0. The analysis also indicate that increasing the volume of the sample vial V_T does not affect the above uncertainty characteristics, but shifts the optimum phase ratio β to a greater value.

For comparison purposes, we conducted a precision analysis of the MHE method by Kolb and Ettre [3] (Eqn. (1.41)) using a similar variance estimation equation,

$$\sigma^2(K) = \left(\frac{\partial K}{\partial Q'}\right)^2 \sigma^2(Q') + \left(\frac{\partial K}{\partial \phi}\right)^2 \sigma^2(\phi) + \left(\frac{\partial K}{\partial \beta}\right)^2 \sigma^2(\beta). \quad (1.49)$$

We used same variances of ϕ and β for the analysis of the present MHE method and variance of the ratio of the GC peak areas, $\sigma^2(Q') = 1.25\times10^{-3}(Q')^2$, by assuming $\sigma^2(A_1) = \sigma^2(A_2) = \ldots = \sigma^2(A_i) = \ldots \sigma^2(A_n) = 2.5\%A$ based on experimentally determined relative standard deviation of A(2.3%). The analysis indicates that the first term in Eqn.(23) is the major contributor to the method uncertainty. Figure 1.17 plots the optimum phase ratio β_{opt} and the measurement uncertainties at β_{opt} for measuring Henry's constant in a range of 0.001 - 100 using the present and the Kolb and Ettre [3]'s MHE GC method. The results show that the β_{opt} for both of these methods correlates with Henry's constant well to Eqn. (1.48). Figure 1.17 clearly indicates that the minimum uncertainties of Eqn. (1.41) are about 20-30%. The precision of the present MHE method is as much or more than an order of magnitude better than that of the method by Kolb and Ettre [3] for $H^* < 0.2$, a significant progress in the development of MHE GC method for VLE studies. From a mathematical point of view, the poor precision of the Kolb and Ettre [3] method is caused by the close-to-zero term, *Q'-1*, in the denominator in Eqn. (1.41) that amplifies a small measurement error in the peak areas A or the peak area ratio Q' to a large error in K or H^*, the fundamental problem of the method. More specifically, the amplification for $\sigma^2(Q')$ is $(\partial K/\partial Q')^2 = [(\rho - 1)\beta]^2/(Q'-1)^4$ that is inversely proportional to the fourth power of $(Q'-1)$. For a typical value of $Q'=0.85$, $1/(Q'-1)^4$ is about 2000. Physically, Eqn. (1.41) did not take full advantage of multiple headspace extraction techniques; it only uses two headspace extraction measurements.

Method Validation

According to the derivation by Kolb and Ettre [28], the Logarithmic peak area obtained from the ith headspace extraction $Log(A_i)$ should be linearly proportional to $(i-1)$ or simply i if the VLE conditions for each headspace extraction can be exactly repeated in MHE measurements. We plotted the GC signal of peak area A_i of methanol measured in a methanol–water solution of concentration 800 mg/L at 60°C. We obtained a near perfect linear correlation with a correlation coefficient of 0.9987 between the Logarithmic peak area A_i and the extraction number i as shown in Fig. 1.18, indicating the validity of the basic assumption that the VLE

conditions were exactly repeated for each headspace measurement in this study. We then carried out a linear regression analysis according to Eqn. (1.34) to test the validity of our derivation and the accuracy of the experiment. Again, we obtained a near perfect regression as shown in Fig. 1.15 with a correlation coefficient of 0.9997 and the relative fitting errors of the slope and the intercept are 0.9 and 1.5%, respectively. With such a good regression, we are confident that the concentration and the Henry's constant derived from the intercept *a* and the slope *b* of the regression analysis, respectively, will be accurate. It should be pointed out that a minimum of three extractions is required to use the present MHE method through Eqn. (1.34).

The basic principle for solute concentration measurement of the present MHE method (Eqn. (1.36)) is not much different from that of Kolb and Ettre [3, 28] (Eqn. (1.37)) in measuring solute concentration; therefore, we expect that the measurement accuracy will be the same. We conducted nine replica measurements of a methanol-water solution of 800 mg/L using the present method. The average measured concentration was 797 mg/L. The standard deviation was 2.7%, within our precision prediction limit as shown in Fig. 1.16. To further validate the present method, we conducted comparison measurements of methanol concentrations in nine filtrate samples collected from a fiber line kraft pulp mill using both the present MHE method and an indirect HSGC method [7, 8]. For methanol concentration ranging from 50 – 1000 mg/L, the relative differences in measured methanol concentrations using these two methods are within $\pm$ 4.5% as listed in Table 1.VII except one sample for an unknown reason. The 4.5% difference is within the measurement uncertainties of these two methods obtained from several replica measurements. These measurements demonstrate the validity of the present method for solute concentration measurements in any solution.

Henry's Constant Measurement

We measured the Henry's constants of isopropanol and ethanol in water solutions at a temperature range of 40-80^{o}C using the present MHE GC method (Eqn. (1.38)). We compared our measurements to those obtained by Kolb et al. [12] using a direct headspace GC method. Linear regression shows that the Logarithm of the Henry's constants fits very well to the inverse of the temperature in Kelvin as shown in Fig. 1.19. Correlation coefficients are 0.9999 and 0.9984 as obtained from the fitting of the isopropanol and ethanol data both reported by Kolb et

al. [18] and those measured by the present MHE method. The relative errors of the slopes and the intercepts are 1.2 and 1.9% and 6.2 and 4.0% for the isopropanol and ethanol linear lines, respectively. The linear relationship obtained agrees with the van't Hoff Equation in basic thermodynamic theory for solute, i.e., the Henry's constant is proportional to the partial molar excess enthalpy, a function of temperature. Because Kolb et al. [12] did not provide the standard deviations of their measurements, we compared our data with the fitted equations to both sets of data as shown in Fig. 1.19. We found that the residual sums of squares of the fits are 1.1×10^{-4} and 1.37×10^{-3} for isopropanol and ethanol, respectively. We also plotted $\pm$ 10% relative error bars of our data based on our replica measurements and uncertainty predictions for H^* = 0.001 – 0.01 as shown in Fig. 1.16, most of the data points fall onto the two fitted lines within the $\pm$ 10% error bars.

We calculated the Henry's constants of isopropanol and ethanol at the temperature range stated above with present experimental data using Eqn. (1.41) to experimentally verify the measurement uncertainty of the MHE method by Kolb and Ettre [3]. The pressure ratio is calculated using Eqn. (1.40), i.e., $\rho=(1 - j)$ with j =0.313 calculated from Eqn (1.42). The peak area ratios Q' are calculated from the measured peak areas. Table 1.VIII lists two sample calculations of Henry's constants of isopropanol and ethanol in water solutions at 60^{o}C. It was found that the relative standard deviations of Q' in the two experiments are only about 4.3 and 2.3 % (close to those used in precision analysis), respectively. However, the relative standard deviations in measured Henry's constants are 36 and 23% for isopropanol and ethanol, respectively, which agree with our mathematical predictions as shown in Fig. 1.16. This is an indication of the poor precision of the MHE method by Kolb and Ettre [3] due to the error amplification effect of the (Q'-1) term in Eqn. (1.41) as discussed previously.

1.4 Summary

We developed and demonstrated several headspace gas chromatographic methods for species concentrations and Henry's constants measurements of volatile organic compounds (VOCs) in various kraft mill streams. The standard addition HSGC method was used for analysis of VOC concentrations throughout this research. The direct HSGC VLE method was used for determination of VOC Henry's constant in black liquors. The indirect and MHE HSGC

VLE methods were used for the determination of Henry's constant in mill filtrates. In the next two chapters, we will discuss the mill-wide liquid sampling results using these methods.

REFERENCES

1. Hachenberg, H. and Schmidt, A.P., *Gas Chromatographic Headspace Analysis,* Heyden and Son, London, 1977.
2. Ioffe, B.V. and Vitenbery, A.G., *Headspace Analysis and Related Methods in Gas Chromatography*, John Wiley and Sons, New York, 1984.
3. Kolb, B. and Ettre, L.S., 1997, *Static Headspace-Gas Chromatography: Theory and Practice*, Wiley-VCH, New York.
4. Drozd, J. and Novak, J., *J. Chromatogr.*, **165**:141, 1979.
5. Namiesnik, J., Gorecki, T., and Biziuk, M., *Analytica Chimica Acta,* **237**:1, 1990
6. Gunshefki, M. and Cloutier, S., "NCASI procedures for collection and analysis of black liquor samples," *NCASI Technical Memo*, 1994.
7. Drozd, J. and Novak, J., *J. Chromatogr.*, **136**:27, 1977
8. Chai, X.-S., Dhasmana, B., and Zhu, J.Y., *J. Pulp and Paper Sci.*, **24(**2):50, 1998
9. Davis, D.G. in *Instrumental Analysis*, Eds: H.H. Bauer, G.D. Christlan, J.E. O'Reilly, Allyn Bacon, Boston, 1978, p.102.
10. Chai, X.S., Liu, P.H., and Zhu, J.Y., *J. Pulp Paper Sci.*, **26**(5):167, 2000
11. Chai, X.S. and Zhu, J.Y., 2001, in "Recent Research and Development in Analytical Chemistry," Transworld Research Network, Kerala, India
12. Kolb, B., Welter, C., and Bichler, C., *Chromatographia*, **34**:235, 1992.
13. Zhu, J.Y., Liu, P.-H., and Chai, X.-S., *Environ. Sci. Technol.*, **34**:1742, 2000
14. Chai, X.-S. and Zhu, J.Y., *J. Chromatogra. A.*, **799**:207, 1998.
15. Lincoff, A.H. and Gossett, J.M., 1984, in *Gas Transfer at Water Surfaces,* Eds: Brutsaert and Jirka, Reidel, Dordrecht, p. 17.
16. Gossett, J.M., *Environ. Sci. Technol.*, **21**:202, 1987.
17. Ettre, L.S., Welter, C., and Kolb, B., *Chromatographia*, **35**:73, 1993.
18. M.T. Hofstee, A. Kwantes, and C.W.A. Rijnders, *Symp. Dist. Brighton*, 105, 1960.
19. K.A. Pividal, A. Birtigh, and S.I. Sandler, *J. Chem. Eng. Data*, **37**:484, 1992.
20. A.J. Dallas, Ph.D. Dissertation, University of Minnesota, Minneapolis, MN, 1993.

21. Z.S. Kooner, R.C. Phutela, and D.V. Fenby, *Aust. J. Chem.,* **33**:9, 1980.

22. A. Lebert and D.J. Richon, *J. Agric. Food Chem.* **32**:1156, 1984.

23. McAuliffe, C., *Chem. Technolo.*, 46, 1971.

24. McAuliffe, C., U.S. Patent 3, 759,086, 1973.

25. Suzuki, M., Tsuge, S., Takeuchi, T., *Anal. Chem.,* **12**:1, 1970.

26. Kolb, B., *Chromatographia,* **15**:587, 1982.

27. Ettre, L.S., Jones, E., Todd, B.S., *Chromatogr. Newsl.*, **12**:1, 1984.

28. Kolb, B. and Ettre, L.S., *Chromatographia,* **21**:505, 1991.

29. Hughes, M.M. and DeLassus, P.T., *ANTEC*, 1340, 1991.

30. Snyder, J.M. and Mounts, T.L., *JAOCS*, **67**(11):800, 1990.

31. Chai, X.-S., and Zhu, J.Y., *Anal Chem.,* **70**:3481, 1998.

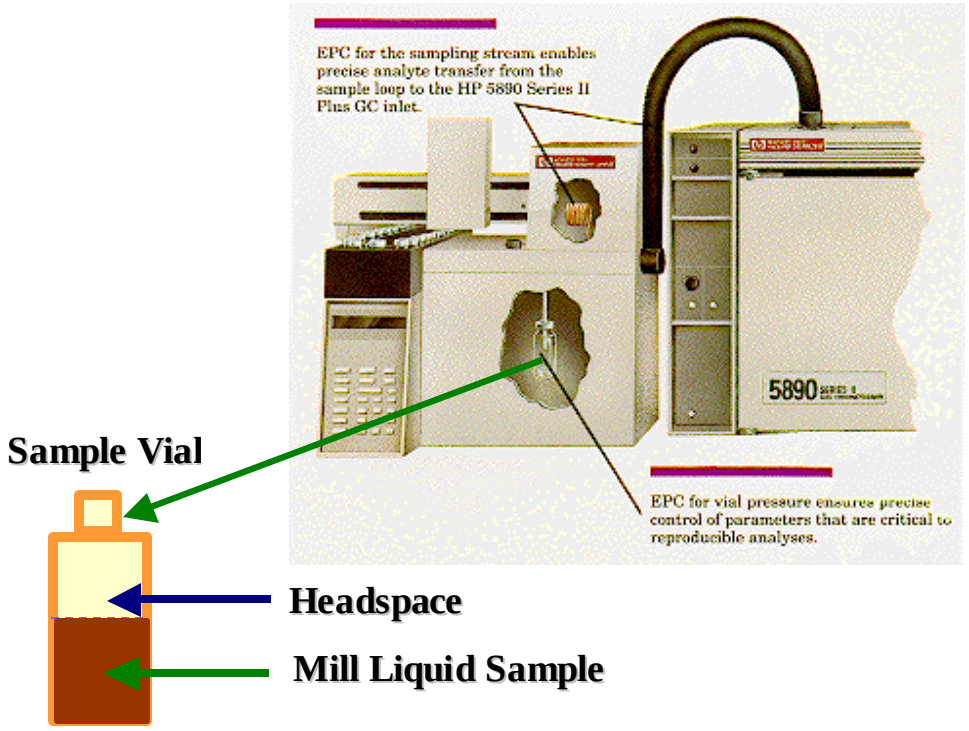

Fig. 1.1. A picture shows a commercial headspace gas chromatographic system.

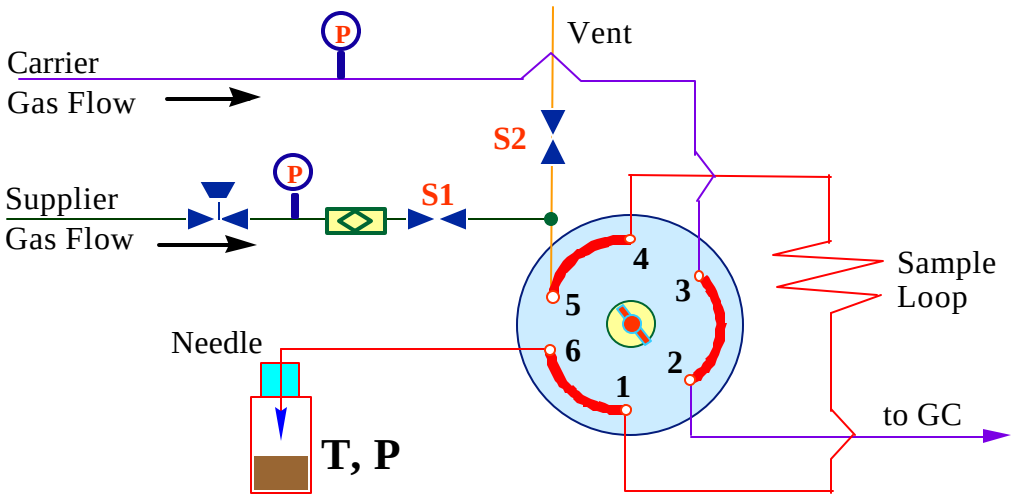

Fig. 1.2. A schematic diagram of a headspace injection system.

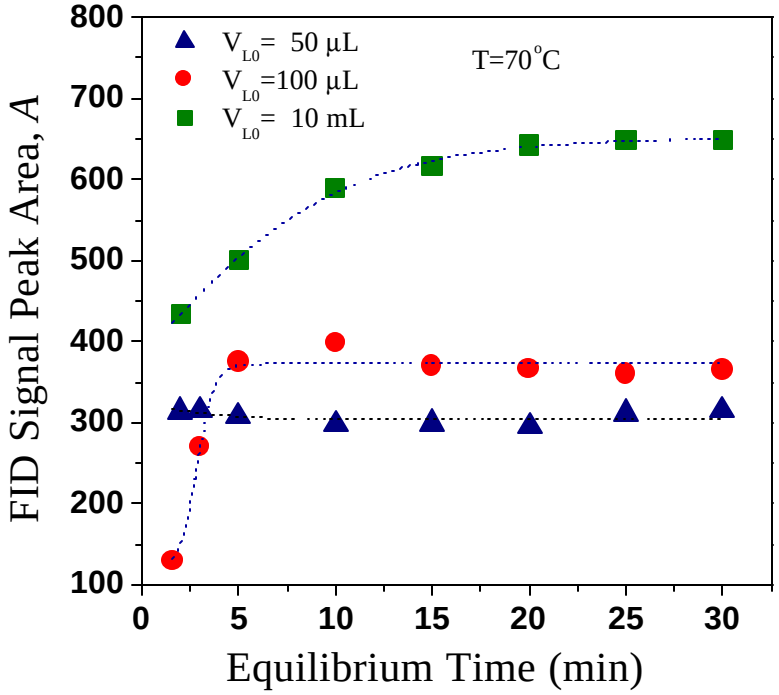

Fig. 1.3. The effect of vial equilibrium time on measured GC FID signal peak area.

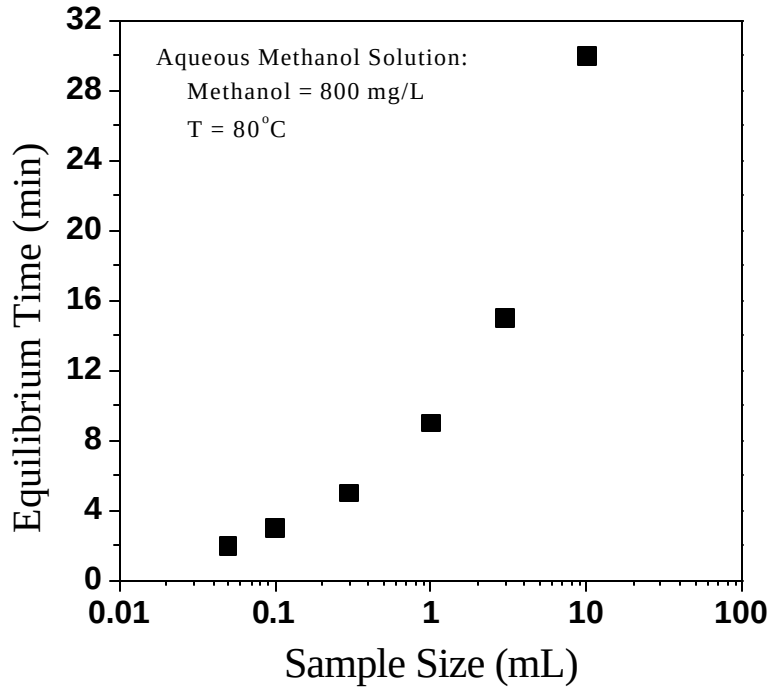

Fig. 1.4. The effect of sample size on vial equilibrium time.

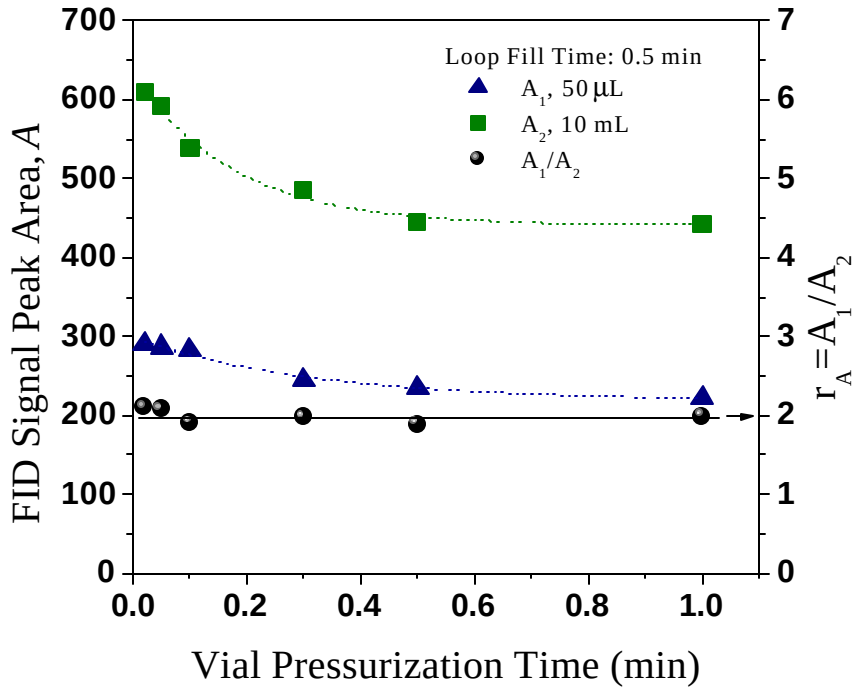

Fig. 1.5. The effect of vial pressurization time on measured FID signal peak area.

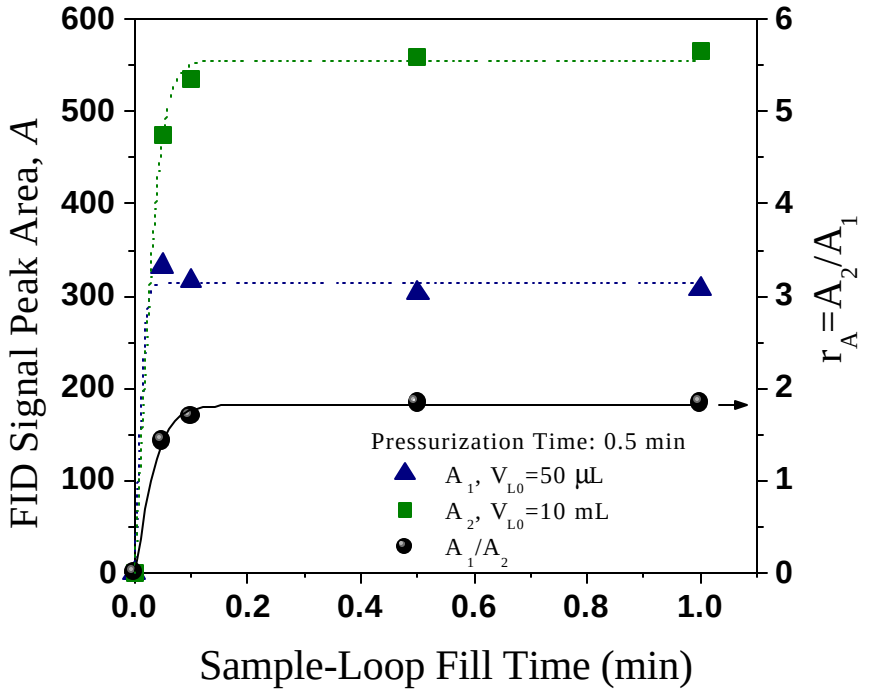

Fig. 1.6. The effect of sample-loop fill time on measured FID signal peak area.

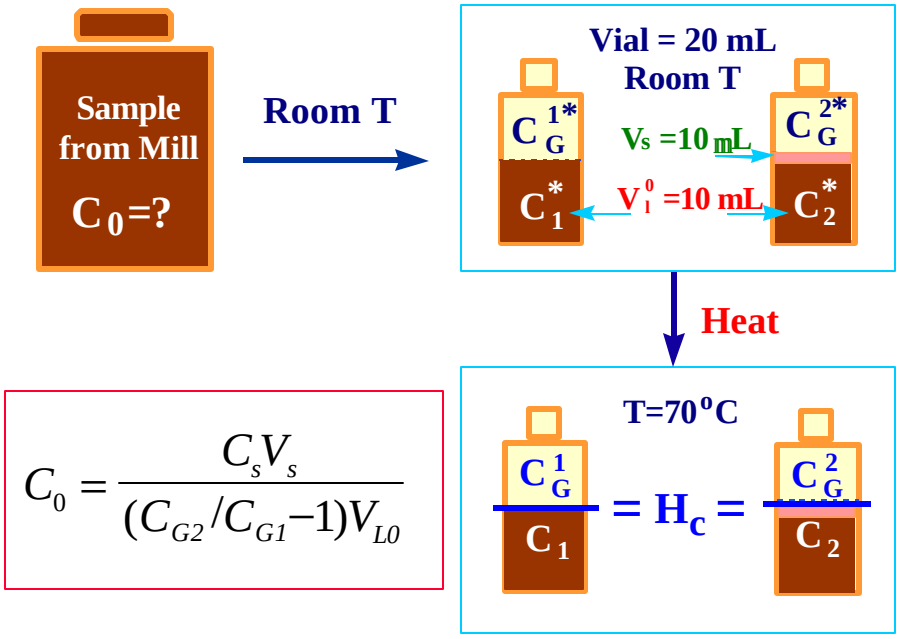

Fig. 1.7. Schematic diagram describing the indirect HSGC method for analysis of VOCs.

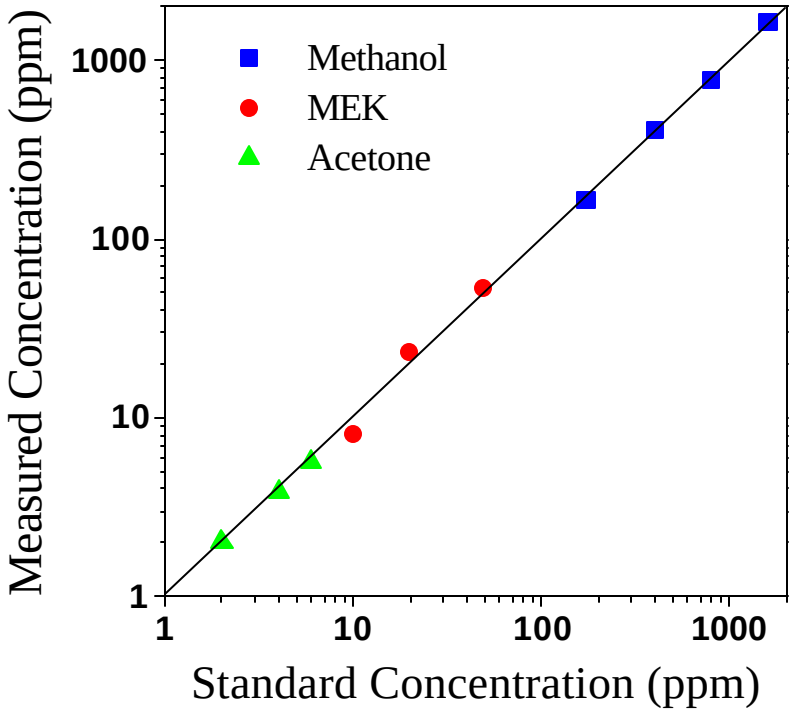

Fig. 1.8. Comparison between measured and known VOC concentrations in standard VOC-water solutions.

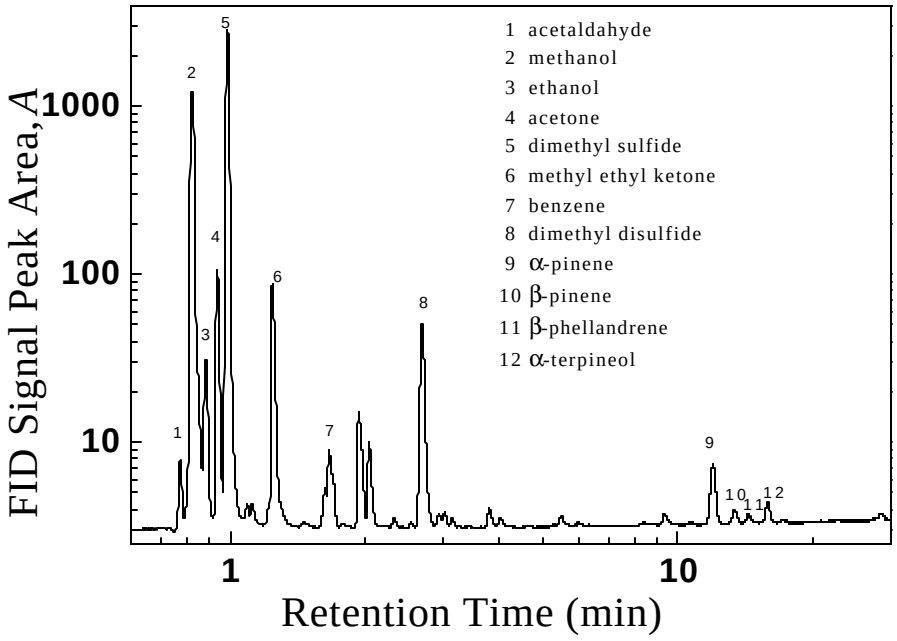

Fig. 1.9. A typical chromatogram of a softwood kraft black liquor vapor obtained from HSGC analysis with FID.

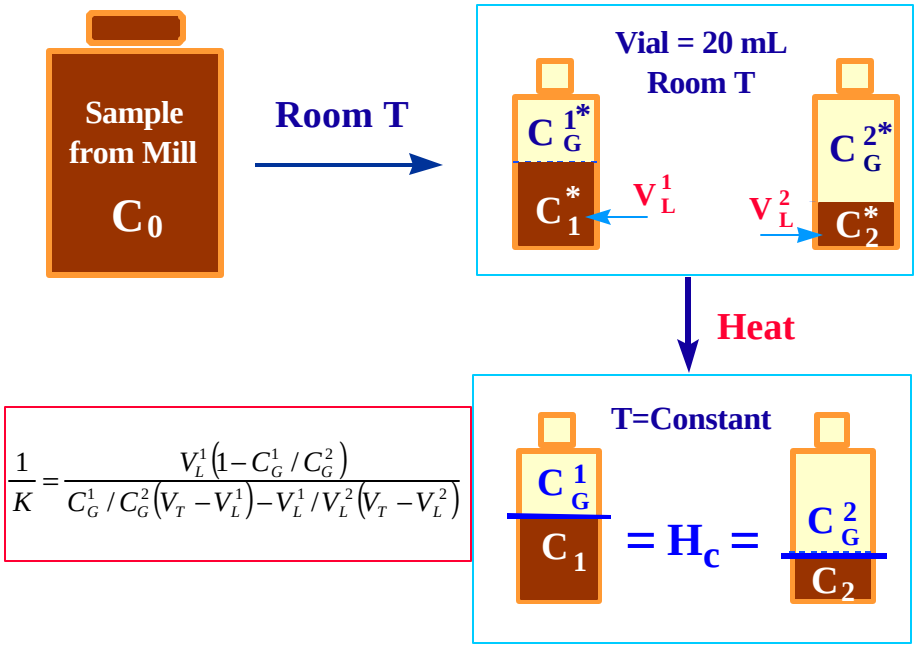

Fig. 1.10. A schematic diagram that describes the modified EPICS method.

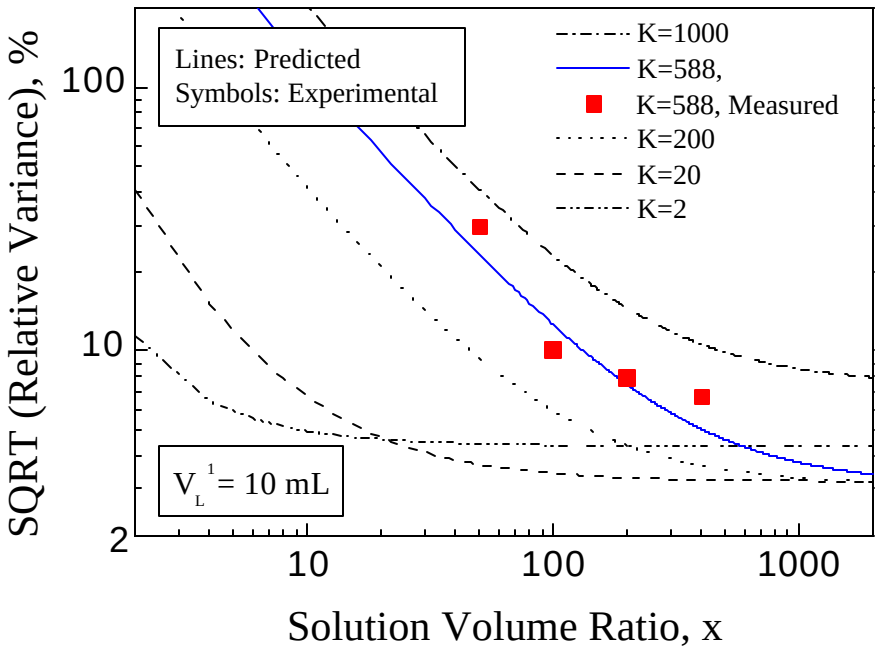

Fig. 1.11. Effect of sample volume ratio on the accuracy of the refined EPICS method.

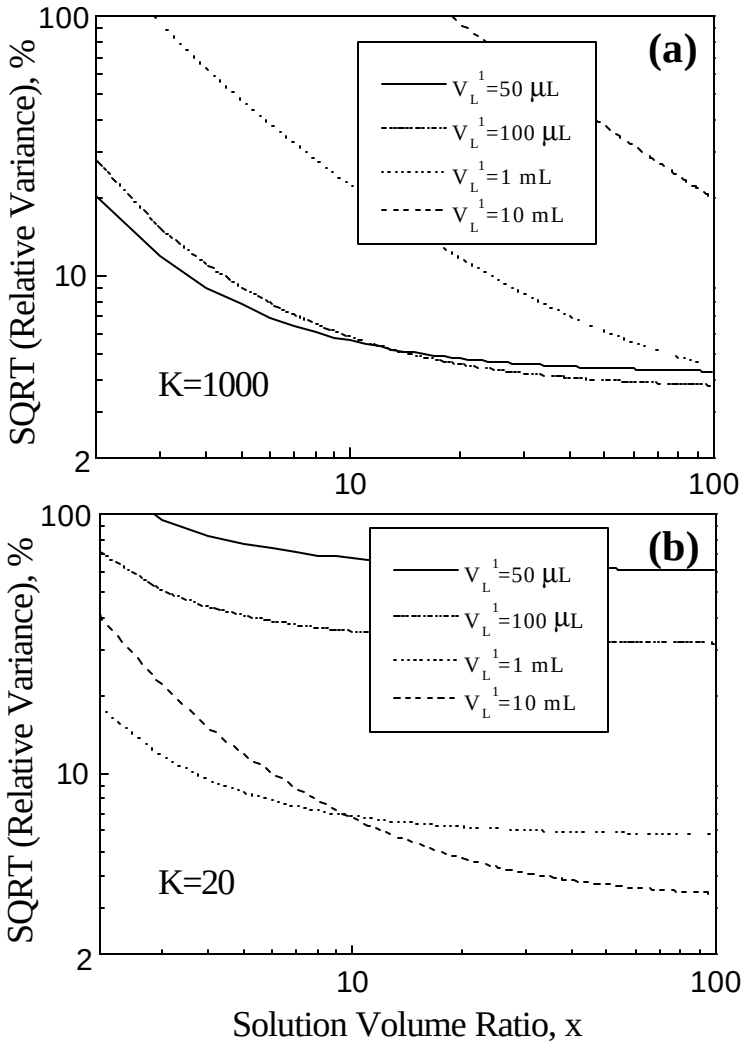

Fig. 1.12. The effect of the sample volume V_L^1 on the relative measurement error at different solution volume ratio *x*'s. (a) K = 1000 and (b) K = 20.

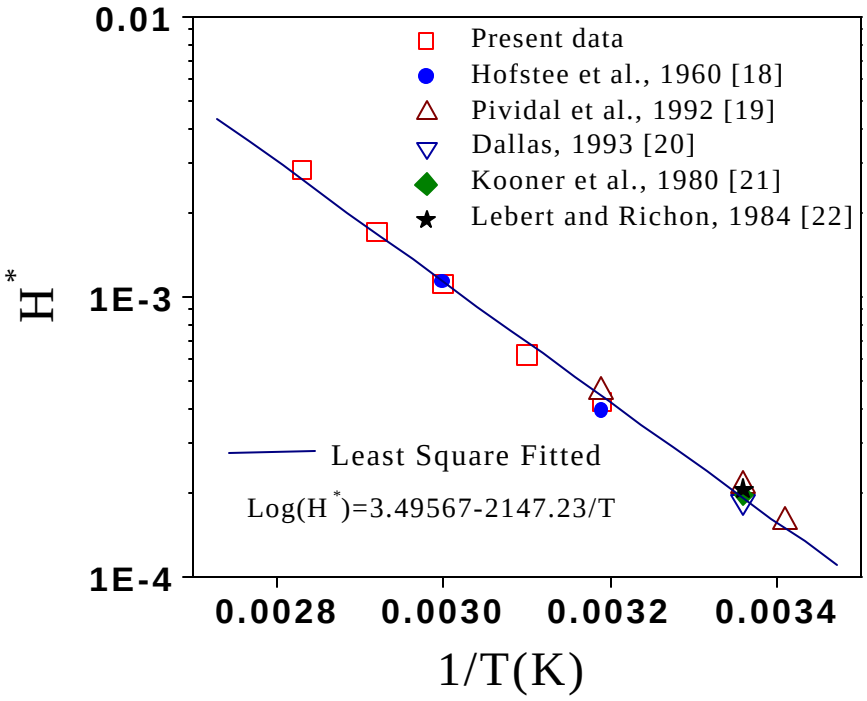

Fig. 1.13. Effect of temperature methanol Henry's constant and a comparison with literature data.

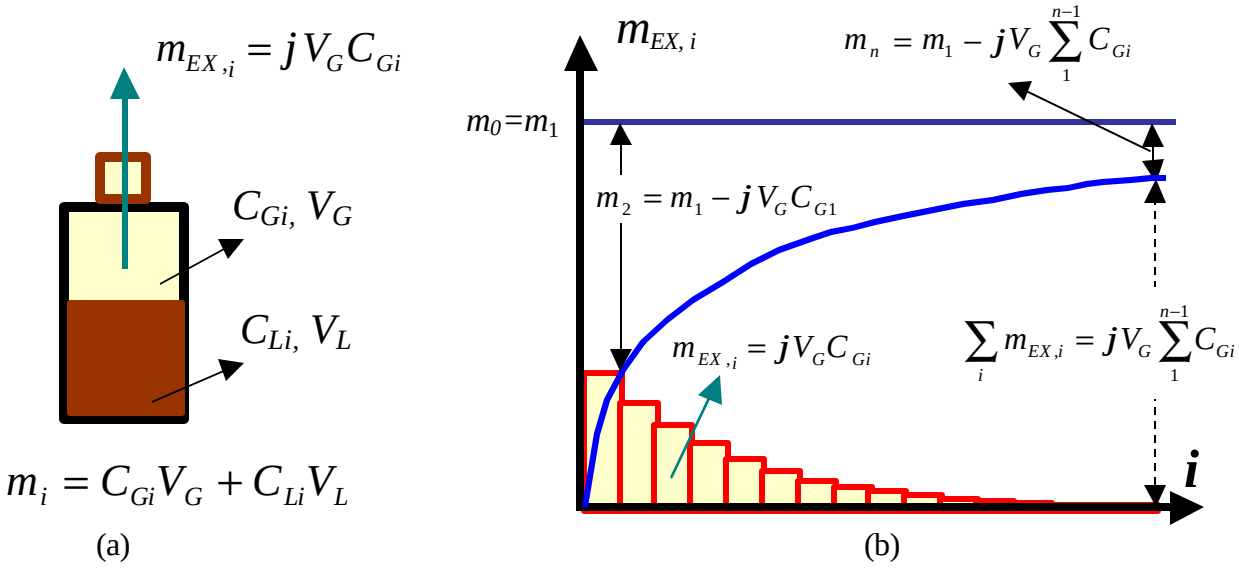

Fig. 1.14. A schematic diagram that shows the principle of MHE GC technique.

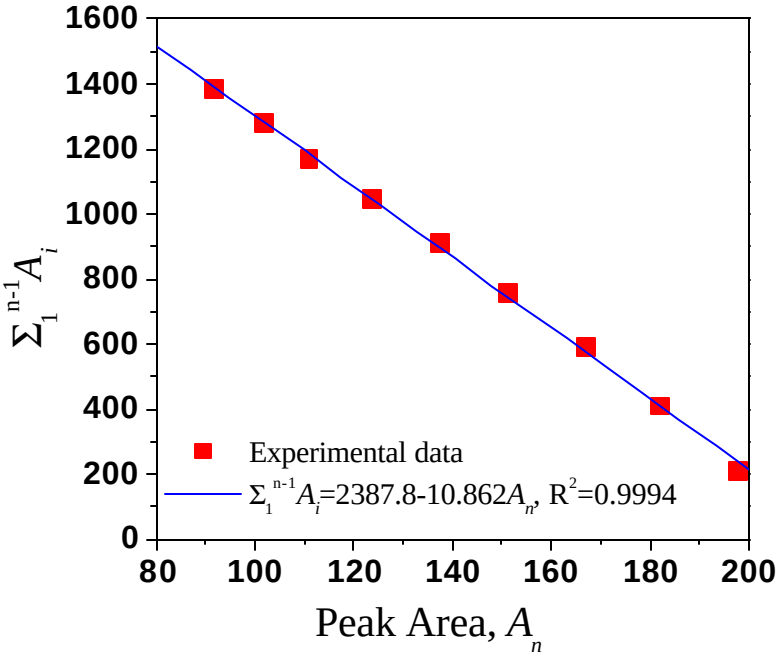

Fig. 1.15. Typical linear correlation (Eqn. 1.34) between the sum of the GC signals (peak areas) of the first (n-1)th headspace measurements and the signal of the nth measurement.

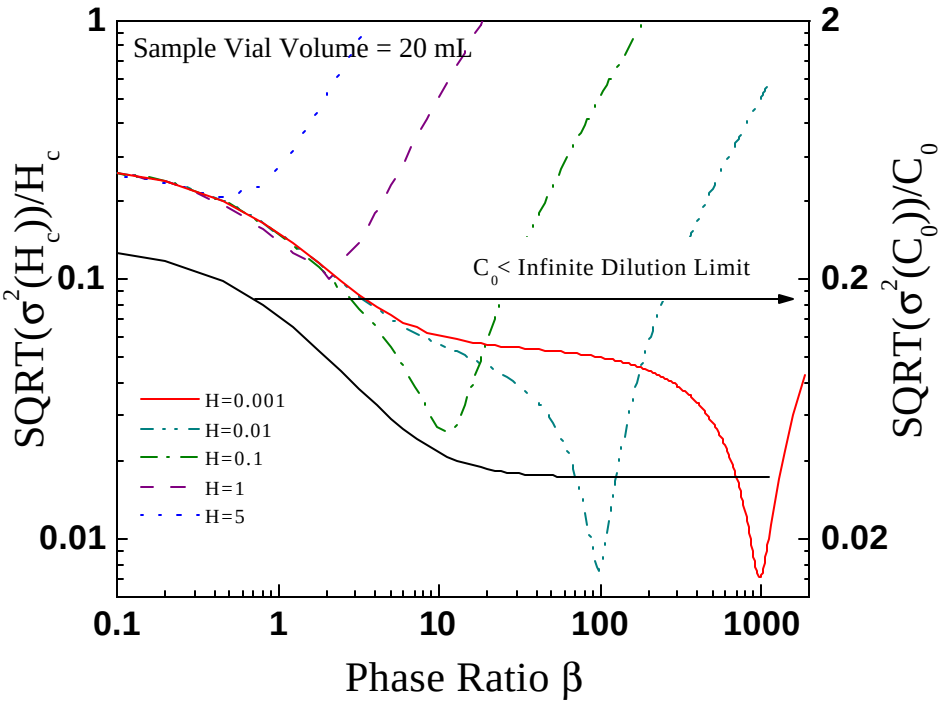

Fig. 1.16. The calculated effect of phase ratio on the measurement uncertainty of solute concentration and Henry's constants using the present multiple headspace extraction method.

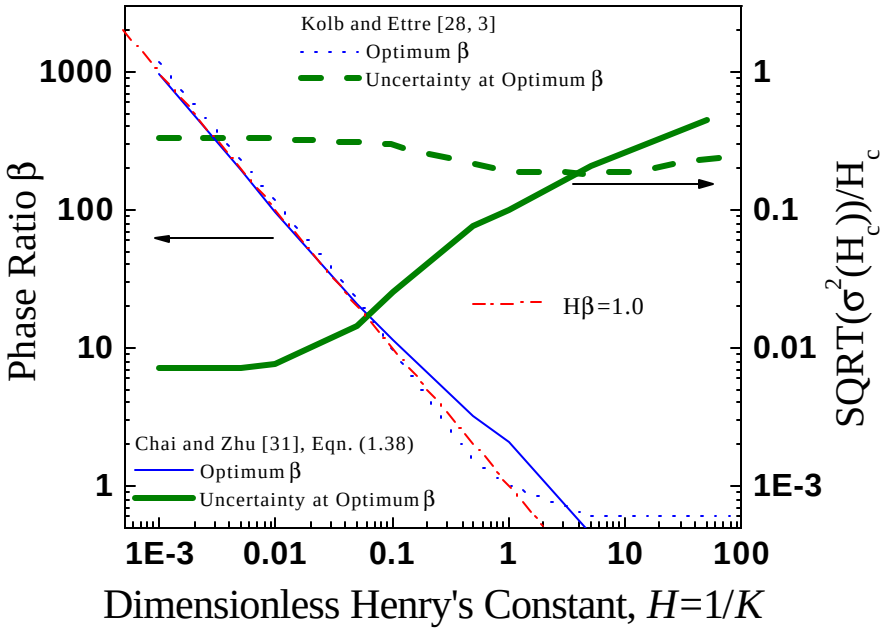

Fig. 1.17. Comparison of the measurement uncertainties of Henry's constants at the optimum phase ratios between the present MHE method and that of Kolb and Ettre [3].

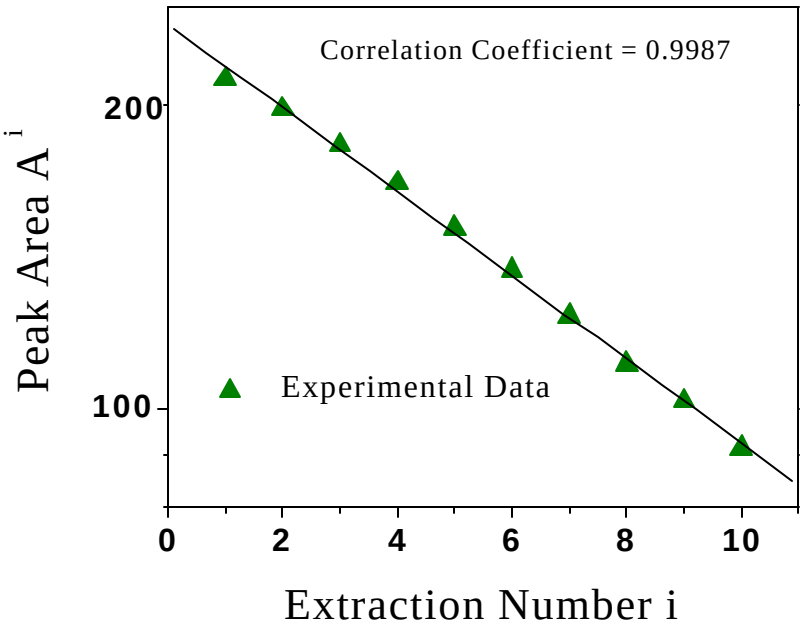

Fig. 1.18. A typical correlation between the gas chromatographic signals (peak areas) and the headspace extraction number in multiple headspace measurements.

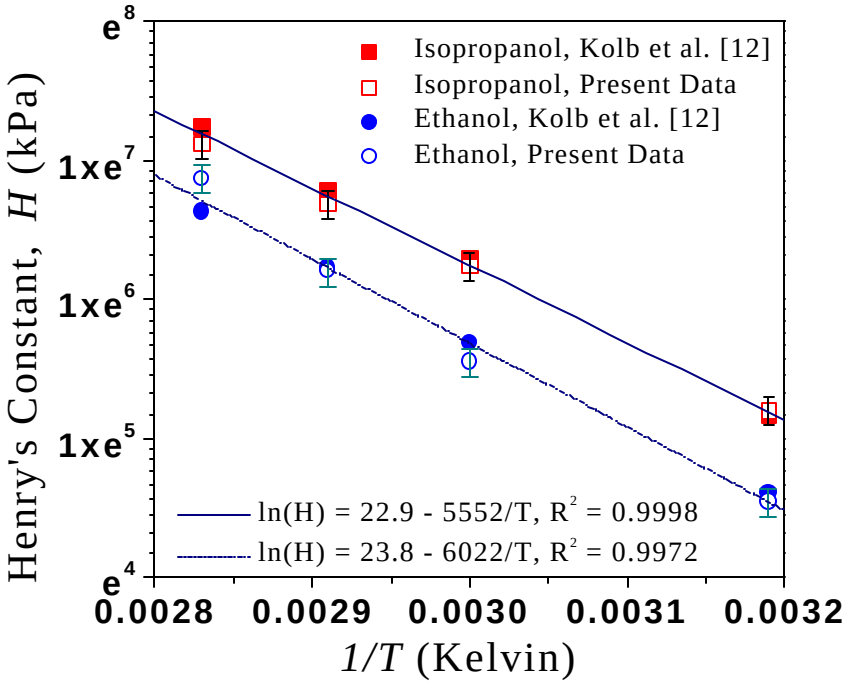

Fig. 1.19. Comparisons of measured Henry's constants of isopropanol and ethanol in water solutions with literature data, respectively, at various temperatures.

Table 1.I. Comparisons of measured methanol concentrations in four black liquors using the NCASI method and the present method.

SAMPLE	Solids Content (%)	Methanol Concentration (ppm)		
		NCASI method	Present method	Difference (%)
Softwood. Mill A	15.2	775	736	5.0
Hardwood, Mill A	17.1	961	906	5.7
Softwood, Mill B	11.5	434	419	3.5
Hardwood, Mill B	10.8	527	560	-6.3

Table 1.II. Methanol and MEK concentrations in various mill streams measured using the present method.

Sample Number	Sample Location Description	Methanol (ppm)	MEK (ppb)
1	weak wash liquor from recovery cycle	<1	74.5
2	white water from paper machine head tank	40	0
3	pulp wash shower water first stage (digester 1)	277	165
4	filtrate stream from first washing stage (digester 1)	251	433
5	filtrate stream from second washing stage (digester 1)	238	316
6	filtrate stream from first washing stage (digester 2)	201	583
7	filtrate stream from second washing stage (digester 2)	172	481
8	condensate from blow tank steam in hot water tank	315	251
9	weak black liquor to evaporator	272	307

Table 1.III. List of measurements to determine the variance of GC peak area.

Sample No.	Measured GC Peak Area
1	188.2
2	189.3
3	193.2
4	185.4
5	188.9
6	195.7
7	193.0
8	196.3
9	196.5
MEAN	**191.8**
RSD	**2.1%**

Table 1.IV. Effect of sample size on the measured GC signal (peak area) of methanol in water of concentration of 800 mg/L.

Sample Size (mL)	Measured GC Peak Area
10,000	600.1
5,000	598.7
1,000	588.6
500	576.4
100	494.4
50	419.8
40	390.3
30	349.4
20	288.9
10	190.2

Table 1.V. Comparison of the Henry's constant of methanol in water measured using the present method with two different sets of experimental parameters.

Experiment	**Experimental Parameters**			**Measured Henry's Constant** H^*				
	V_L^1 (ml)	V_L^2 (ml)	$x = V_L^1 / V_L^2$	T=40°C	T=50°C	T=60°C	T=70°C	T=80°C
I	10	0.05	200	0.00042	0.00062	0.00111	0.00171	0.00284
II	0.1	0.04	2.5	0.00052	0.00067	0.00105	0.00169	0.00250

Table 1.VI. List of calibration experimental results of j and f at several temperatures using a methanol-water solution of concentration 800 mg/L.

Temperature (°C)	Henry's Constant H^* (Literature)	b (Regression Obtained)	j (Calibrated)	a (Regression Obtained)	f (Calibrated)
40	0.00044	-23.12± 0.41	0.271	3205± 36	468
50	0.00071	-14.92± 0.12	0.286	2815± 14	433
60	0.00112	-9.83± 0.13	0.313	2496± 15	420
70	0.00170	-6.61± 0.12	0.354	1849± 18	353
80	0.00260	-4.55± 0.06	0.416	1352± 10	303
Relative Standard Deviation (RSTD)	N/A	1.4%	N/A	0.8%	N/A

Table 1.VII. Comparisons of measured methanol concentrations in several environmental samples from a kraft pulp mill between the present MHE method and an indirect headspace gas chromatographic method.

No.	Methanol Concentration (mg/L)		Relative Difference (%)
	Previous method [7, 8]	**Present MHE method**	
1	53	52	-1.9
2	94	91	-3.2
3	183	183	0.0
4	311	331	6.4
5	402	390	-2.3
6	613	605	-1.0
7	678	700	3.2
8	775	808	4.3
9	969	992	2.4

Table 1.VIII. Sample calculations of Henry's constants of isopropanol and ethanol in water solutions at temperature 60^{o}C using the MHE method of Kolb and Ettre [3] with the raw data measured in this study.

Headspace Extraction Number, i	**Isopropanol**			**Ethanol**		
	Peak Area A_i	**$Q'=A_i/A_{i-1}$**	***H****	**Peak Area A_i**	**$Q'=A_i/A_{i-1}$**	***H****
1	593.2	-	-	396.5	-	-
2	546.7	0.9216	0.00084	352.3	0.8885	0.00139
3	464.2	0.8491	0.00233	328.6	0.9327	0.00069
4	398.7	0.8589	0.00206	288.4	0.8777	0.00161
5	319.8	0.8021	0.00431	253.8	0.8800	0.00156
6	263.7	0.8246	0.00320	222.0	0.8747	0.00167
7	218.8	0.8297	0.00299	193.3	0.8707	0.00176
8	178.6	0.8163	0.00356	169.4	0.8764	0.00164
9	146.8	0.8219	0.00331	147.6	0.8713	0.00175
10	118.9	0.8099	0.00387	127.9	0.8665	0.00186
Mean	**N/A**	**0.8371**	**0.00294**	**N/A**	**0.8820**	**0.00155**
Relative STD	**N/A**	**0.043**	**0.359**	**N/A**	**0.023**	**0.227**

* Calculated from Eq. (1.41)

CHAPTER 2 VOCs IN KRAFT MILL STREAMS

VOCs are formed primarily in the pulping process in kraft mills. The continuing process in pulp and paper manufacturing transports VOCs into various downstream process streams. We report mill-wide liquid sampling results in this chapter to provide benchmark data. The HSGC measurement method described in Chapter 1 was used for sample analysis.

2.1 Mill Liquid Sampling Process

A simple liquid sampling process was developed to conduct mill-wide liquid sampling. Process streams were connected to a cooling coil submerged in an ice-water bucket of about 10 gallons. Process streams can be cooled down to about 30-40^{o}C from 60-70^{o}C after the cooling coil. Both the process temperature and the cooled sample temperature were taken using a thermocouple. A 100 mL sample bottle was used to collect the sample from the sample coil directly. The bottle was completely filled without headspace and tightly sealed and labeled. The samples were further cooled down in an ice chest and shipped to our laboratory at the Institute of Paper Science and Technology for analysis.

2.2 Mill I Sampling Results

A 3-day mill wide VOC sampling was conducted. Each location was sampled three times, except for a few locations where there were difficulties in sampling. The samples are labeled to reflect the sample information. The first letter indicates whether the sample is a liquid sample (L) or an air sample (A). The next two digits identify sample location. The next 4 digits are the date (day and month) of sample collected. The last two digits are the sample number. For pulp suspensions, e.g., vat and mat samples, pulp samples were collected and then squeezed to get liquid samples. Table 2.I shows the pulp consistency from the first run. Other samples were collected as it was for sample analysis. All the raw VOC data along with sample process

temperature and pH are listed in Table 2.II, 2.III, and 2.IV for the three runs. Table 2.V lists the dimensionless Henry's constant of methanol in various mill streams at different temperatures. More studies on VLE partitioning of methanol in mill streams will be presented in Chapter 3.

2.3 Mill II Sampling Results

A 3-day mill-wide VOC sampling was conducted. Each location was sampled three times, except for a few locations where there were difficulties in sampling. The samples are labeled to reflect the sample information. The first digit of the sample ID is the sample number. The letters are the abbreviation of the sample location. The digits in the middle or at end of the sample ID are the machine number or line number. For pulp suspensions, pulp samples were again collected and then squeezed to get liquid samples. All the raw VOC data along with sample process temperature and pH are listed in Table 2.VI.

2.4 Mill III Sampling Results

A 3-day mill-wide VOC sampling was conducted. The mill has a little line (small production rate and flow rate) and a big line (large production and flow rate). Each location was sampled three times, except for a few locations where there were difficulties in sampling. For pulp suspensions, pulp samples were again collected and then squeezed to get liquid samples. The three runs were then averaged and presented in Table 2. VII and 2.VIII, respectively. The air emission data were presented in Table 2. IX.

Table 2.I. Pulp Sample Consistency Results from First Run.

Date	Location	Sample Label	pH	Temperature (K)	Consistency (%)
9/18/97	BRN ATU Diff.	C01091801	11.4	345.7	12.5
9/18/97	BRN ATU Diff.	C01091802		345.4	11.9
9/18/97	BRN ATU Diff.	C01091803		344.6	11.3
9/16/97	BSW Mat	C03091601	10.79	341.8	14.5
9/16/97	BSW Mat	C03091602		354.5	16.4
9/16/97	BSW Mat	C03091603		353.1	14.0
9/16/97	O_2 Blow Line	C05091601	10.66	344.2	3.2
9/16/97	O_2 Blow Line	C05091602		347.0	5.9
9/16/97	O_2 Blow Line	C05091603		344.2	4.3
9/16/97	O_2 ATU Diff D1 Stage	C07091601	10.79	349.8	12.9
9/16/97	O_2 ATU Diff D1 Stage	C07091602		349.5	12.3
9/16/97	O_2 ATU Diff D1 Stage	C07091603		349.0	13.5
9/17/97	D_o Mat	C15091701	2.44	340.8	1.8
9/17/97	D_o Mat	C15091702		340.8	1.9
9/17/97	D_o Mat	C15091703		341.3	1.8
9/17/97	D_o Mat	C16091701	7.22	347.5	13.6
9/17/97	D_o Mat	C16091702		347.0	12.3
9/17/97	D_o Mat	C16091703		341.8	12.6
9/17/97	Eop Vat	C21091701	11.38	352.2	2.0
9/17/97	Eop Vat	C21091702		351.0	2.1
9/17/97	Eop Vat	C21091703		352.3	3.0
9/17/97	Eop Mat	C22091701	4.06	345.9	14.8
9/17/97	Eop Mat	C22091702		345.4	13.3
9/17/97	Eop Mat	C22091703		344.5	13.4

Table 2.II: Samples from the First Run Methanol Content and Dimensionless Henry's Constant in the Liquid Sample at 343 K (70^{o}C).

Date	Location	Sample Label	pH	MeOH/liquid (ppm)	H_c 343K	T (K)
9/18/97	BRN ATU Diff. Squeeze	L01091801	11.4	612	0.00161	345.7
9/18/97	BRN ATU Diff. Filtrate	L02091801	11.72	936	0.00169	323.9
9/16/97	BSW Mat Squeeze	L03091601	10.79	775	0.00176	341.8
9/18/97	BRN ATU Diff Shower	L04091801	10.92	703	0.00191	347.7
9/16/97	O_2 Blow Line	L05091601	10.66	969	0.00179	344.2
9/16/97	O_2 ATU Diff Filt	L06091601a	10.81	678	0.00197	352.5
9/16/97	O_2 ATU Diff Filt	L06091601b	10.73	883	0.00173	350.6
9/16/97	O_2 ATU Diff D1 Stage Sqz	L07091601	10.79	516	0.00187	349.8
9/18/97	Strip-Cona (Dlorswiz)	L08091801	9.90	458	0.00169	339.4
9/16/97	O_2 ATU Diff Shower	L11091601	10.89	459	0.00168	347.3
9/18/97	Drain Filtrate	L11091801*	10.37	603	0.00174	342.2
9/18/97	D_o Feed	L13091801	2.83	402	0.00170	328.1
9/17/97	D_o Vat Liquor	L15091701	2.44	320	0.00202	340.8
9/18/97	D_o Vat Liquor	L15091801*	2.32	403	0.00153	337.5
9/17/97	D_o Mat Sqz	L16091701	7.22	138	0.00155	347.5
9/17/97	D_o Filtrate	L17091701	2.52	311	0.00166	332.0
9/17/97	E_2 Filtrate	L19091701	12.03	53	0.00184	346.7
9/17/97	D_1 Filtrate	L20091701	3.53	151	0.00164	347.0
9/17/97	Eop Vat Liquor	L21091701	11.38	183	0.00229	352.2
9/17/97	Eop Mat Sqz	L22091701	4.06	94	0.00140	345.9
9/17/97	Eop Filtrate	L23091701	11.30	183	0.00179	349.4

Table 2.III. Samples from the Second Run Methanol Content and Dimensionless Methanol Henry's Constant in the Liquid Sample at 343 K (70°C).

Date	Location	Number	pH	MeOH/liquid ppm	H_c 343K	T (K)
9/18/97	BRN ATU Diff. Squeeze	L01091802	11.23	672	0.00169	345.4
9/18/97	BRN ATU Diff. Filtrate	L02091802	12.13	828	0.00152	345.9
9/16/97	BSW Mat Squeeze	L03091602	10.69	803	0.00180	354.3
9/18/97	BRN ATU Diff Shower	L04091802	11.04	750	0.00152	348.6
9/16/97	O_2 Blow Line	L05091602	10.73	913	0.00192	347.0
9/16/97	O_2 ATU Diff Filt	L06091602a	10.69	696	0.00152	357.6
9/16/97	O_2 ATU Diff Filt	L06091602b	10.73	935	0.00145	352.0
9/16/97	O_2 ATU Diff D1 Stage Sqz	L07091602	10.80	649	0.00145	349.8
9/18/97	Strip-Cona (Dlorswiz)	L08091802	9.51	545	0.00162	338.8
9/16/97	O_2 ATU Diff Shower	L11091602	10.83	576	0.00164	345.9
9/18/97	Drain Filtrate	L11091802*	10.48	583	0.00220	346.5
9/18/97	D_o Feed	L13091802	3.38	346	0.00208	329.3
9/17/97	D_o Mat Liquor	L15091702	2.38	313	0.00211	340.8
9/18/97	D_o Mat Liquor	L15091802*	2.27	332	0.00196	337.5
9/17/97	D_o Mat Sqz	L16091702	7.10	151	0.00180	347.0
9/17/97	D_o Filtrate	L17091702	2.46	309	0.00147	328.8
9/17/97	E_2 Filtrate	L19091702	12.15	40	0.00190	348.7
9/17/97	D_1 Filtrate	L20091702	3.36	110	0.00175	346.5
9/17/97	Eop Vat Liquor	L21091702	11.27	179	0.00207	351.0
9/17/97	Eop Mat Sqz	L22091702	3.93	99	0.00204	345.4
9/17/97	Eop Filtrate	L23091702	10.77	196	0.00186	350.0

Table 2.IV. Samples from the Third Run Methanol Content and Dimensionless Methanol Henry's Constant in the Liquid Sample at 343 K (70^{o}C).

Date	Location	Number	pH	MeOH/liquid ppm	H_c 343K	T (K)
9/18/97	BRN ATU Diff. Squeeze	L01091803	11.25	695	0.00152	344.6
9/18/97	BRN ATU Diff. Filtrate	L02091803	11.98	698	0.00179	348.4
9/16/97	BSW Mat Squeeze	L03091603	10.67	708	0.00164	353.1
9/18/97	BRN ATU Diff Shower	L04091803	11.05	725	0.00139	348.6
9/16/97	O_2 Blow Line	L05091603	10.56	1046	0.00159	344.2
9/16/97	O_2 ATU Diff Filt	L06091603a	10.70	593	0.00171	350.4
9/16/97	O_2 ATU Diff Filt	L06091603b	10.60	770	0.00173	353.1
9/16/97	O_2 ATU Diff D1 Stage Sqz	L07091603	10.69	501	0.00180	348.7
9/18/97	Strip-Cona (Dlorswiz)	L08091803	9.63	417	0.00187	336.1
9/16/97	O_2 ATU Diff Shower	L11091603	10.50	576	0.00191	346.5
9/18/97	Drain Filtrate	L11091803*	10.76	437	0.00199	346.6
9/18/97	D_o Feed	L13091803	2.07	370	0.00199	335.3
9/17/97	D_o Mat Liquor	L15091703	2.33	351	0.00194	342.8
9/18/97	D_o Mat Liquor	L15091803*	2.15	258	0.00217	337.9
9/17/97	D_o Mat Sqz	L16091703	7.16	126	0.00210	341.5
9/17/97	D_o Filtrate	L17091703	2.40	331	0.00201	332.6
9/17/97	E_2 Filtrate	L19091703	12.03	37	0.00199	353.8
9/17/97	D_1 Filtrate	L20091703	3.13	122	0.00152	348.0
9/17/97	Eop Vat Liquor	L21091703	11.08	184	0.00165	352.2
9/17/97	Eop Mat Sqz	L22091703	3.87	104	0.00140	344.5
9/17/97	Eop Filtrate	L23091703	11.86	198	0.00141	352.0
9/18/97	ClO2	L12091801	1.98	515	0.00170	282.5

Table 2.V Dimensionless Henry's constant of Methanol in Mill streams (first run samples) at different Temperatures

Date	Location	Number	pH	Temperature, ^{o}C			
				50	60	70	80
9/18/97	BRN ATU Diff. Squeeze	L01091801	11.4	0.00074	0.00102	0.00161	0.00254
9/18/97	BRN ATU Diff. Filtrate	L02091801	11.72	0.00067	0.00095	0.00169	0.00191
9/16/97	BSW Mat Squeeze	L03091601	10.79	0.00077	0.00092	0.00176	0.00171
9/18/97	BRN ATU Diff Shower	L04091801	10.92	0.00083	0.00104	0.00191	0.00167
9/16/97	O_2 Blow Line	L05091601	10.66	0.00075	0.00112	0.00179	0.00253
9/16/97	O_2 ATU Diff Filt	L06091601a	10.81	0.00078	0.00123	0.00197	0.00175
9/16/97	O_2 ATU Diff Filt	L06091601b	10.73	0.00078	0.00129	0.00173	0.00211
9/16/97	O_2 ATU Diff D1 Stage Sqz	L07091601	10.79	0.00082	0.00125	0.00187	0.00207
9/18/97	Strip-Cona(Dlorswiz)	L08091801	9.90	0.00075	0.00100	0.00169	0.00265
9/16/97	O_2 ATU Diff Shower	L11091801	10.89	0.00079	0.00118	0.00168	0.00217
9/18/97	Drain Filtrate	L11091801*	10.37	0.00082	0.00136	0.00174	0.00223
9/18/97	Do Feed	L13091801	2.83	0.00071	0.00112	0.00170	0.00299
9/17/97	D_o Mat Liquor	L15091701	2.44	0.00073	0.00114	0.00202	0.00245
9/18/97	D_o Mat Liquor	L15091801*	2.32	0.00081	0.00117	0.00153	0.00254
9/17/97	D_o Mat Sqz	L16091701	7.22	0.00065	0.00107	0.00155	0.00250
9/17/97	D_o Filtrate	L17091701	2.52	0.00092	0.00122	0.00166	0.00260
9/17/97	E_2 Filtrate	L19091701	12.03	0.00083	0.00109	0.00184	0.00187
9/17/97	D_1 Filtrate	L20091701	3.53	0.00077	0.00101	0.00164	0.00256
9/17/97	Eop Vat Liquor	L21091701	11.38	0.00075	0.00139	0.00229	0.00247
9/17/97	Eop Mat Sqz	L22091701	4.06	0.00084	0.00096	0.00140	0.00237
9/17/97	Eop Filtrate	L23091701	11.30	0.00081	0.00114	0.00179	0.00443

Table 2.VI. Raw Data of Mill-Wide Sampling at Mill II

Sample ID (washer)	Sample ID Description	T:Process (°C)	pH	MeOH (ppm)	DMS (ppb)	MEK (ppb)	Benzene (ppb)	Toluene (ppb)
1BSWV11	Brown stock washer vat, line #1, stage #1	72.9	12.62	366.8	8889.6	928.2	35.9	1
1BSWV12	Brown stock washer vat, line #1, stage #2	58.2	12.49	111.4	430.7	671.5	18.1	0.1
1BSWV21	Brown stock washer vat, line #2, stage #1	72.6	12.68	342.6	9642.5	1001.9	67.1	1
1BSWV22	Brown stock washer vat, line #2, stage #2	61.7	12.52	153	785.6	220	19.4	-
1BSWV31	Brown stock washer vat, line #3, stage #1	73.7	12.78	390.8	9712.5	967.8	8.9	1.1
1BSWV32	Brown stock washer vat, line #3, stage #2	60.9	12.47	147.9	880	161.6	73.4	0.2
1BSWM11	Brown stock washer mat, line #1, stage #1	57.1	12.28	158.3	53.9	92.6	14.4	-
1BSWM12	Brown stock washer mat, line #1, stage #2	53.1	11.93	38.7	10	-	26.3	-
1BSWM21	Brown stock washer mat, line #2, stage #1	56.8	12.49	236.2	380.6	277.7	38.3	-
1BSWM22	Brown stock washer mat, line #2, stage #2	56.7	11.95	52.5	62.4	47.1	33.4	-
1BSWM31	Brown stock washer mat, line #3, stage #1	60	12.02	194.9	166.4	198.9	27.8	-
1BSWM32	Brown stock washer mat, line #3, stage #2	53.9	11.72	51.9	15.3	47.1	12.3	-
1BSWF11	Brown stock washer filtrate, line #1, stage #1	72.2	12.77	410.2	10078.3	1063.6	29.5	1.2
1BSWF12	Brown stock washer filtrate, line #1, stage #2	58.9	12.52	130.2	473.7	262.3	65	0.2
1BSWF21	Brown stock washer filtrate, line #2, stage #1		12.74	335.4	9011.6	945.1	63.7	1.2
1BSWF22	Brown stock washer filtrate, line #2, stage #2		12.62	159.7	1224.6	181.9	42.4	0.2
1BSWF31	Brown stock washer filtrate, line #3, stage #1	72.2	12.97	394.5	10056.5	960.5	89.6	1.1
1BSWF32	Brown stock washer filtrate, line #3, stage #2	61.1	12.52	161.4	1276	218.4	28	0.2
1BSW1FWS	Brown stock washer #1 fresh water shower	54.2	7.43	3.9	-	-	23.9	-
1BSW2FWS	Brown stock washer #2 fresh water shower	54.5	7.05	1.5	-	-	2.5	-
1BSW3FWS	Brown stock washer #3 fresh water shower	55.7	7.37	2.3	-	-	22.3	0.1
1BSWFT	Brown stock washer foam tank	55.2	12.41	399.2	6387.7	914.2	65.6	1.1
1FECC	Flash evaporators clean condensate	52.5	11.54	1159.3	43.7	690.1	-	-
1MEESC	Multiple effect evaporators stripped condensate	37.1	11.55	179.3	27.5	352.4	20.4	0.1
1MEECC	Multiple effect evaporators stripped condensate	52.1	11.38	550	155.3	686.1	7	0.2

1PM2LVB4	Paper machine #2 low vacuum bottom line	46.4	6.73	26.3	60.8	-	14.2	-
1PM2LVT3	Paper machine #2 low vacuum top line	29.1	6.87	23.3	15	-	33.5	-
1PM1BHX	Paper machine #1 bottom headbox	60.1	6.22	23.5	20	-	35.2	-
1PM1THX	Paper machine #1 top headbox	57.9	6.1	22.6	16.1	-	37.4	-
1PM2BHX	Paper machine #2 bottom headbox	56.2	6.98	21.2	18.6	-	4.8	-
1PM2THX	Paper machine #2 top headbox	55.5	6.3	24.9	25.3	-	30	-
1PMTEFF	Paper machine total effluent	46	4.47	18.8	12.3	-	36.5	-
1BLOXOUT	Oxidized black liquor outlet	78.7	-	54.1	253.3	576.7	3.7	1.1
2BSWV11	Brown stock washer vat, line #1, stage #1	73	12.57	372.9	8317.1	1252.8	49	1.1
2BSWV12	Brown stock washer vat, line #1, stage #2	58	12.3	99.7	259.9	145.3	28.9	0.2
2BSWV21	Brown stock washer vat, line #2, stage #1	73.5	12.5	345.5	8485.9	1148.1	22.5	1
2BSWV22	Brown stock washer vat, line #2, stage #2	57.7	12.3	137.8	517.3	212.7	80.5	0.1
2BSWV31	Brown stock washer vat, line #3, stage #1	74.4	12.55	445.6	9704.1	1134.3	8.8	2.4
2BSWV32	Brown stock washer vat, line #3, stage #2	61.8	12.34	180	659.2	198.1	46.1	0.1
2BSWM11	Brown stock washer mat, line #1, stage #1	57.9	12.07	173.5	45.1	124.2	43.2	-
2BSWM12	Brown stock washer mat, line #1, stage #2	54.5	11.42	29.7	-	-	29.2	-
2BSWM21	Brown stock washer mat, line #2, stage #1	63.5	12.27	268	1238.8	397.8	12.3	0.2
2BSWM22	Brown stock washer mat, line #2, stage #2	55.7	11.32	21.5	-	-	16.6	-
2BSWM31	Brown stock washer mat, line #3, stage #1	59.2	12.23	264.8	630.3	338.6	29.6	0.2
2BSWM32	Brown stock washer mat, line #3, stage #2	53.2	11.7	42.8	10.8	-	30.4	-
2BSWF11	Brown stock washer filtrate, line #1, stage #1	71.9	12.52	408.3	8813.9	1024.7	23.2	1.2
2BSWF12	Brown stock washer filtrate, line #1, stage #2	57.4	12.23	111.5	198.3	169.7	31.9	0.1
2BSWF21	Brown stock washer filtrate, line #2, stage #1	72.4	12.61	368	9130.9	1102.6	54.3	1
2BSWF22	Brown stock washer filtrate, line #2, stage #2	61.6	12.32	162.6	751	229.8	43	0.2
2BSWF31	Brown stock washer filtrate, line #3, stage #1	72.9	12.34	439.9	10589.2	1175.7	61.5	0.9
2BSWF32	Brown stock washer filtrate, line #3, stage #2	60.9	12.3	166.7	675.9	224.1	82.3	0.3
2BSW1FWS	Brown stock washer #1 fresh water shower	44.4	7.42	2	-	-	11.3	-
2BSW2FWS	Brown stock washer #2 fresh water shower	55.1	7.01	-	-	-	1.8	-

2BSW3FWS	Brown stock washer #3 fresh water shower	55.8	7.29	2.1	-	-	27.5	-
2BSWFT	Brown stock washer foam tank	53.5	12.6	435.9	6818.4	1019	18.9	1.4
2FECC	Flash evaporators clean condensate	55.3	9.56	1351.6	206.4	664.2	14.1	-
2MEESC	Multiple effect evaporators stripped condensate	38.9	11.68	172.5	90.3	470.1	17.8	0.2
2MEECC	Multiple effect evaporators stripped condensate	70.2	9.26	556.5	61.6	630.1	18.5	-
2PM2LVB4	Paper machine #2 low vacuum bottom line	44.1	6.7	21.9	59.6	-	20.5	-
2PM2LVT3	Paper machine #2 low vacuum top line	39.1	6.38	20.5	10.5	-	16.7	-
2PM1BHX	Paper machine #1 bottom headbox	59.8	6.83	24.8	19.1	2484.5	-	-
2PM1THX	Paper machine #1 top headbox	58.1	5.75	24.4	12.1	2013.6	-	-
2PM2BHX	Paper machine #2 bottom headbox	59.6	6.38	25.8	21.2	1133.5	-	-
2PM2THX	Paper machine #2 top headbox	58.2	6.15	25.9	15.7	2240.9	-	-
2PMTEFF	Paper machine total effluent	47.3	4.73	17.6	15	47.1	25.4	-
3BSWV11	Brown stock washer vat, line #1, stage #1	72.5	12.71	376.9	7440.3	1015.7	85.2	0.9
3BSWV12	Brown stock washer vat, line #1, stage #2	56.7	12.34	103.4	312.6	134	38.4	0.2
3BSWV21	Brown stock washer vat, line #2, stage #1	70.8	12.75	333	8341.5	1087.2	12.9	1
3BSWV22	Brown stock washer vat, line #2, stage #2	62.3	12.34	174.1	1311.9	315.8	39.8	0.3
3BSWV31	Brown stock washer vat, line #3, stage #1	73.1	12.57	425.7	9094.4	993.8	83.9	1.3
3BSWV32	Brown stock washer vat, line #3, stage #2	58.9	12.22	156.8	543	183.9	20.7	0.2
3BSWM11	Brown stock washer mat, line #1, stage #1	57.5	12.07	150.1	77.9	136.4	48.1	0.1
3BSWM12	Brown stock washer mat, line #1, stage #2	54.7	11.97	44.2	19.8	54.4	33.1	0.1
3BSWM21	Brown stock washer mat, line #2, stage #1	61.5	12.48	239.2	901.3	416.5	53.6	0.2
3BSWM22	Brown stock washer mat, line #2, stage #2	56.5	12.12	71.5	80.7	68.2	13.4	-
3BSWM31	Brown stock washer mat, line #3, stage #1	61.9	12.32	178.7	233.8	216.8	32.9	0.2
3BSWM32	Brown stock washer mat, line #3, stage #2	55.5	11.97	54.6	14.4	49.5	22.9	-
3BSWF11	Brown stock washer filtrate, line #1, stage #1	72	12.53	451.2	8223.4	1196.8	14.8	1.3
3BSWF12	Brown stock washer filtrate, line #1, stage #2	57.7	12.16	100.3	224.6	148.6	20.2	0.2
3BSWF21	Brown stock washer filtrate, line #2, stage #1	69.5	12.66	356.4	6925.6	1086.4	13.6	1
3BSWF22	Brown stock washer filtrate, line #2, stage #2	61.7	12.31	165.5	1002.1	306.1	25.6	0.7

3BSWF31	Brown stock washer filtrate, line #3, stage #1	72.2	12.66	428.9	8514.1	988.1	44.1	1.1
3BSWF32	Brown stock washer filtrate, line #3, stage #2	60.1	12.34	156.6	428.8	289	56.8	0.2
3BSW1FWS	Brown stock washer #1 fresh water shower	54.1	7.44	2.4	5.1	-	29.8	-
3BSW2FWS	Brown stock washer #2 fresh water shower	55.5	6.9	2	-	-	25.3	-
3BSW3FWS	Brown stock washer #3 fresh water shower	56	7.15	2.6	-	-	1.6	-
3BSWFT	Brown stock washer foam tank	53.5	12.54	331	6591.1	1294.2	49	1.5
3FECC	Flash evaporators clean condensate	52.9	9.61	1339.2	274.7	542.4	6.8	-
3MEESC	Multiple effect evaporators stripped condensate	34.4	11.23	166	18.1	258.2	2.6	-
3MEECC	Multiple effect evaporators stripped condensate	63.2	9.22	565.2	73	430.3	21.9	-
3PM2LVB4	Paper machine #2 low vacuum bottom line	44.1	6.72	23.6	44	-	4.6	-
3PM1BHX	Paper machine #1 bottom headbox	60.1	6.07	25.5	18.8	-	27.8	-
3PM1THX	Paper machine #1 top headbox	68.1	6.01	24.4	13.6	55.2	15	1.7
3PM2BHX	Paper machine #2 bottom headbox	59.6	6.28	28.3	25	-	41.7	0.2
3PM2THX	Paper machine #2 top headbox	58.2	6.37	27.6	31.4	-	35.3	-
3PMTEFF	Paper machine total effluent	45.3	4.82	18.9	11	-	39.3	-
MEEPROD	Multiple effect evaporators product		-	26.7	22	319.2	9.5	0.2
BSWFTCL	Brown stock washer foam tank vapor condensate from the left side	114	8.95	671.7	7157.3	1347	8.4	-

Table 2.VII. VOC Concentrations[1] in Brownstock Washing Liquor Samples of Little Line (June 28 – July 1, 1999)

Little Line Brownstock Washing													
Sample	**ID**	**Temperature**		**Methanol**		**Acetone**		**MEK**		**Benzene**		**Toluene**	
		Case A [2]	Case B [2]	Case A [2]	Case B [2]	Case A [2]	Case B [2]	Case A [2]	Case B [2]	Case A [2]	Case B [2]	Case A [2]	Case B [2]
		°F	°F	mg/L	mg/L	mg/L	mg/L	mg/L	mg/L	mg/L	mg/L	mg/L	mg/L
Knotter Accept	LKN	*196*	*196*	332	307	1.6	2.1	0.59	0.71	0.044	0.050	0.037	0.039
No.1 Vat	LV1	185	181	301	276	1.7	2.2	0.53	0.58	0.044	0.064	0.031	0.023
No.1 Filtrate	LF1	181	181	305	280	1.8	2.3	0.58	0.62	0.040	0.051	0.038	0.019
No.1 Mat CO	LM1	158	156	238	176	2.2	3.3	0.33	0.23	0.111	0.033	0.033	0.020
No.2 Vat	LV2	154	142	237	146	1.8	3.1	0.34	0.21	0.068	0.043	0.034	0.020
No.2 Filtrate	LF2	150	143	229	156	1.9	3.6	0.33	0.21	0.056	0.051	0.023	0.013
No.2 Mat CO	LM2	138	134	211	104	2.8	2.0	0.17	0.09	0.032	0.029	0.026	0.016
No.3 Vat	LV3	137	134	218	93	2.8	1.5	0.19	0.07	0.031	0.034	0.026	0.020
No.3 Filtrate	LF3	135	134	214	98	2.7	1.5	0.19	0.07	0.030	0.032	0.023	0.014
No.3 Mat CO	LM3	139	137	225	69	1.4	0.7	0.21	0.05	0.043	0.037	0.026	0.015
Pressure Sceen Feed	LPS	137	*134*	219	79	1.4	0.6	0.20	0.07	0.039	0.040	0.035	0.036
Decker Vat	LV4	148	142	224	72	1.4	0.6	0.21	0.05	0.038	0.033	0.027	0.016
Decker Filtrate	LFD	133	133	220	75	1.3	0.6	0.20	0.04	0.040	0.023	0.026	0.011
Decker Mat CO	LM4	144	142	326	94	1.4	0.5	0.32	0.06	0.031	0.031	0.024	0.015
Decker Shower	LS6	146	147	347	116	1.6	0.4	0.39	0.07	0.043	0.018	0.026	0.013
Foam Tank Cond.	LTS	151	170	448	274	7.4	2.3	1.75	0.62	0.024	0.073	0.021	0.020

Table 2.VIII. VOC Concentrations[1] in Brownstock Washing Liquor Samples of Big Line (Mill III, June 28 – July 1, 1999).

Big Line Brownstock Washing											
Sample	**ID**	**Temperature**		**Methanol**		**Acetone**		**MEK**		**Benzene**	
		Case A [2]	**Case B** [2]	**Case A** [2]	**Case B** [2]	**Case A** [2]	**Case B** [2]	**Case A** [2]	**Case B** [2]	**Case A** [2]	**Case B** [2]
		°F	°F	mg/L	mg/L	mg/L	mg/L	mg/L	mg/L	mg/L	mg/L
Hot Refiner Stock	BRH	201	201	273	283	1.9	1.9	0.56	0.59	0.028	0.018
No.1 Vat	BV1	187	188	253	254	1.9	1.8	0.52	0.50	0.009	0.009
No.1 Filtrate	BF1	181	189	241	251	1.9	1.8	0.53	0.53	0.047	0.034
No.1 Mat CO	BM1	166	175	177	181	1.5	1.6	0.31	0.37	0.015	0.013
No.2 Vat	BV2	151	158	160	156	1.5	1.6	0.29	0.34	0.073	0.008
No.2 Filtrate	BF2	151	158	164	160	1.5	1.6	0.28	0.35	0.043	0.013
No.2 Mat CO	BM2	144	156	155	137	2.3	1.8	0.22	0.26	0.014	0.018
No.3 Vat	BV3	138	146	128	116	1.8	1.8	0.20	0.24	0.024	0.007
No.3 Filtrate	BF3	140	146	135	120	1.7	1.9	0.20	0.25	0.023	0.016
No.3 Mat CO	BM3	140	140	128	114	2.3	2.6	0.16	0.16	0.005	0.006
Cold Refineer Stock	BRC	144	145	119	100	1.6	2.6	0.05	0.16	0.019	0.004
No.4 Vat	BV4	141	144	118	88	1.5	1.8	0.18	0.16	0.017	0.007
No.4 Filtrate	BF4	140	144	119	88	1.5	1.8	0.19	0.17	0.012	0.007
No.4 Mat CO	BM4	138	138	141	90	1.4	1.4	0.22	0.17	0.008	0.007
No.4 Shower	BS4	140	146	153	111	1.4	1.1	0.30	0.22	0.020	0.004
BHE Clean Cond.	BS6	155	154	369	131	1.5	0.3	0.35	0.05	0.013	0.015
MEE Comb. Cond.	BS5	160	161	164	160	2.3	2.2	0.52	0.49	0.018	0.015
Foam Tank Cond.	BT1	138	126	424	636	5.3	13.5	0.94	1.19	0.011	0.045

1. Analyzed by IPST
2. Case A = High methanol in Decker/No.4 washer shower. (June 28 for Big Line, July 1 for Little Line).
   Case B = Low methanol in Decker/No.4 washer shower. (June 29 for Big Line, June 30 for Little Line).

Table 2.IX. Measured Air Emission Data in Brownstock Washer Vents (Mill III, June 28 – July 1, 1999).

		Little Line Washers		Big Line Washers [1]	
		Case A [2]	Case B [2]	Case A [2]	Case B [2]
Stage 1 [1,4]					
Methanol	ppm	196	88	33	37
Stack Flow	DSCFM	1529	1568	25649	25099
Stack Temperature	F	131.3	122.0	108.0	115.0
Moisture	%	14.2	11.3	7.6	9.3
Emission	lb/hr	1.5	0.7	4.3	4.7
Stage 2 [1,4]					
Methanol	ppm	102	**27**	31	23
Stack Flow	DSCFM	1406	1601	31076	31065
Stack Temperature	F	118.3	106.7	104.0	104.0
Moisture	%	9.3	7.5	6.9	7.0
Emission	lb/hr	0.7	**0.2**	4.8	3.6
Stage 3 [1,4]					
Methanol	ppm	160	42	12	6
Stack Flow	DSCFM	1261	1370	23811	23837
Stack Temperature	F	122.3	119.3	93.7	94.0
Moisture	%	11.8	11.2	4.5	4.5
Emission	lb/hr	1.0	0.3	1.5	0.7
Foam Tank [5]					
Methanol	ppm	291	428	503	591
Stack Flow	DSCFM	634	983	1155	981
Stack Temperature	F	115.0	142.7	142.0	142.0
Moisture	%	9.9	20.7	20.0	20.0
Emission	lb/hr	0.9	2.1	2.9	2.9

1. Four vacuum drum washers with a shared hood which has 3 stacks.

2. Case A = High methanol in last washer shower.
Case B = Low methanol in last washer shower.

3. Air samples were collected and analyzed by NCASI.

4. Corresponding to No.1~3 washer hood.

5. Combined vents for No.1~3 washer seal tanks for both big and little line.

CHAPTER 3: HENRY'S CONSTANTS OF VOCs

Henry's law constant directly relates the partial vapor pressure to the infinite dilution activity coefficient of a dissolved species in a given solution as defined in Chapter 1 by Eq. (1.10). The dimensionless Henry's constant H* is the inverse of partitioning coefficient K and can be related to the infinite dilution activity coefficient as follows:

$$g_i^{\infty} = H_i^{*} \frac{RT}{v_j p_i^{sat}} \qquad (3.1)$$

where γ_i^{∞} is the infinite dilution activity coefficient of the solute *i* in water, P_i^{sat} is the vapor pressure of a solute at given temperature, and v_j, *R*, and *T* have been described earlier. In environmental science, the partial vapor pressure of a volatile pollutant species can be used to predict the air emission of the pollutant in many industrial sites. In this research, obtaining the Henry's constants of VOCs is the key for the development of a computer simulation model for the prediction of VOC air emission in kraft mills. Mill streams, especially spent pulping liquor, contain inorganic salts. Knowledge of the partitioning behavior of methanol in aqueous solutions containing salts is therefore essential for estimating VOC emissions from pulp and paper mills. As discussed in the introduction of this report, the focus of the study is methanol. This chapter presents the experimental data of Henry's constant of methanol in aqueous solutions and in kraft pulping spent liquors. The study of Henry's constant of methanol in aqueous solutions lays a foundation for the study in kraft mill streams, including spent pulping liquor that has the most complex sample matrix.

3.1 Experimental

The carrier gas (helium) flow rate in the HP-7694 Automatic Headspace Sampler was set at 3.9 mL/min, and the sample was allowed to attain equilibrium with gentle shaking for 30 min. The other parameters such as vial pressurization time, sample-loop fill time and loop equilibration time were maintained at 0.2, 1.0, and 0.05 min, respectively. The pressure source for pressurization of the vial was maintained at 18 psig. A flame ionization detector (FID) was employed with hydrogen and airflow rates of 35 and 400 mL/min, respectively. The HP-5

capillary column temperature was maintained at 30°C in all experiments, except for samples consisting of pentanol and hexanol. In these cases, the column temperature was raised to 150°C in order to detect a signal. In order to determine the time required for the headspace samples to reach equilibrium, the signal peak area counts on chromatograms were plotted versus time for 10 mL of dilute solutions of several alkanols at 40°C. Fig. 3.1 shows the results of the equilibration tests. As can be seen, the signal count increases with time and approaches a constant value in less than 30 min. This implies that equilibrium is reached inside the vial in less than 30 minutes and also supports the findings of Chai and Zhu [1] who used an equilibration time of 25 minutes for methanol in water.

3.1.1 Materials

Methanol (purity >99.4%), ethanol (>99%), 1-propanol (>99.4%), 1-butanol (>99.4%), 1-pentanol (>98%), and 1-hexanol (>98%) were all purchased from Fisher in the highest purity grade available. Anhydrous sodium carbonate and anhydrous sodium sulfate (both >99.5% pure) were also purchased from Fisher and used as received. Deionized water was obtained from Fisher and used for preparing solutions. Microliter syringes obtained from Supelco Inc. were used to measure volumes. Clear glass vials with a volume 21.75 ± 0.10 mL were purchased from Supelco Inc. and made airtight with 20-mm aluminum seals with PTFE/grey butyl molded septa (also purchased from Supelco Inc.).

Pulping spent liquor, also called black liquor from its color, is an aqueous solution containing dissolved organic and inorganic solids. It is a byproduct of the wood delignification process in pulp manufacturing. The dissolved organic materials are complex substances derived from cellulose, hemicellulose, lignin, and other extractives in the wood. The soluble inorganic solids are mainly sodium salts with minimal quantities of potassium salts. The total solids content of pulping spent liquor or weak (unconcentrated) black liquor is around 5-20% with the organic-to-inorganic ratio around 0.45. Black liquor is caustic with a pH value of greater than 13. It also contains many volatile organic compounds (VOCs), such as methanol, methyl ethyl ketone (MEK), and dimethylsulfide (DMS), formed during pulping. The concentrations of these VOCs are very low and can be assumed to be at infinite dilution from a thermodynamic point of view.

Weak black liquors derived from various wood species and collected from both kraft pulp mills and laboratory pulping processes were used in this study. Four softwoods of Douglas-fir, white spruce, western hemlock, and southern pine, and six hardwoods of aspen, basswood, birch, maple, oak, and sweet gum were used in laboratory pulping experiments. The total dissolved solids contents of all the liquors were less than 25% and the black liquors were therefore treated as aqueous solutions. Analytical-grade sulfonated lignin, mixed-wood kraft lignin, sodium carbonate, sodium sulfate, sodium chloride, sodium hydroxide, dimethylsulfide (DMS), dimethyldisulfide (DMDS), methyl ethyl ketone (MEK), and α-pinene were added to standard water-methanol solutions to study the effects of these minor constituents of black liquors on the Henry's constant of methanol.

3.1.2 Experimental Conditions

To achieve good signal-to-noise ratio in GC measurements, GC conditions were set as follows: HP-5 capillary column at 30°C; carrier gas helium flow: 3.8 mL/min. A flame ionization detector (FID) was employed with hydrogen and air flows of 35 and 400 mL/min, respectively. Headspace operating conditions: gentle shaking for equilibration of the sample for 25 minutes, vial pressurization time of 0.2 min to create a pressure head in the headspace for sample transfer to the sample loop, sample-loop fill time of 1.0 min, and loop equilibration time of 0.05 min. The sample loop is heated to avoid condensation. In instrument evaluation tests, we found that the GC signal peak area did not vary with the sample-loop filling time and loop equilibrium time in certain operating ranges, respectively, indicating that the sample in the loop is a good representative of the sampled vapor phase.

3.1.3 Sample Preparation

Stock solutions of each n-alkanol in water were prepared in 250-mL flasks with a solute concentration of 5000 μg of alkanol/liter of water at room temperature. Stock solutions of sodium carbonate and sodium sulfate were prepared gravimetrically. The stock solutions were stirred for 24 hours, and then used to prepare solutions with alkanol concentrations ranging from 40 μg/liter to 1000 μg/liter, depending on the validity of Henry's constant region for the alkanol, and salt concentrations ranging from 0 to 1.5 mol/kg. Precise alkanol concentrations are not

required in the method of Chai and Zhu [1] since the dimensionless Henry's constant is determined from the ratio of two areas obtained from chromatographic analysis of the headspace in two vials.

The two vials contained 10 mL or 50-100 μL of the solution. 10 mL of the dilute solution was pipetted into the first vial in order to maintain minimum headspace volume as suggested by the manufacturer. 50 μL of the methanol or ethanol solution was added to the second vial using a microsyringe. In the case of the other alkanols, 100 μL of the solution was added to the second vial. In order to minimize errors, three sets of vials were prepared containing slightly different concentrations of alkanol. Special care was taken during the transfer of liquid into the glass vials, and the vials were sealed immediately after addition of the solution. Thus, for each measurement of Henry's constant, a total of eighteen samples were analyzed at constant temperature (three samples × two different liquid volumes × three concentrations). The samples were used to verify that a linear response of the GC detector would be obtained over a larger concentration range than used in the actual experiments.

3.2 Measurements in Aqueous n-Alkanol Solutions

3.2.1 Henry's Constants

Henry's constants of methanol and ethanol in water were measured at 40, 50, 60, and 70°C, which are below the normal boiling temperatures of these alkanols. In the case of the remaining alkanols, data were obtained at 40, 50, 60, 70, 80, and 90°C. The data are plotted in Figs. 3.2 and 3.3. Using an analysis similar to that performed by Chai and Zhu [1] we estimate the error in the measurements of Henry's constants to be less than ±10%.

Most of the literature data on Henry's constants of alkanols in water have been reported at temperatures close to 25°C and therefore cannot be compared directly with our measurements. However, comparisons of extrapolated data with literature values are discussed below.

Our data were correlated using the van't Hoff equation:

$$\ln(H) = a - b/T \qquad (3.2)$$

The results of the regression for the n-alkanols are given in Table 3.I. In general, *a* and *b* increase as the carbon number increases. Henry's constants of alkanols in water at 25°C were calculated using Eq. (3.2) and are compared with literature data in Table 3.II. The agreement between calculated and literature values (2-4%) is excellent, except in the case of hexanol. Even here, however, the agreement is probably within experimental error. The experimental data were also compared with Henry's constants calculated using group contribution [2], bond contribution [2], and QSAR [3] methods. These comparisons are also shown in Table 3.II. The QSAR method predicted the data better than the other methods.

A multiple linear regression analysis was performed on the data in order to correlate the natural logarithm of Henry's constants with temperature and carbon number. The following relationship was obtained:

$$\ln(H) = c - d/T + e*Cn \qquad (3.3)$$

where *Cn* represents the number of carbon atoms in the alkanol, and $c = 11.512$, $d = 6164$, $e = 0.329$ and $R^2 = 0.985$. The maximum deviation between calculated and experimental values was found to be 0.28 and the average deviation was ± 0.09.

3.2.2 Infinite Dilution Activity Coefficients

In order to further check the consistency of the experimental data, Henry's constants were converted to infinite dilution activity coefficients using Eq. (3.1). The natural logarithm of infinite dilution activity coefficient versus the inverse temperature is plotted in Figs. 3.4-3.7. Literature values from a review paper [4] are also shown along with the values calculated using the UNIFAC and ASOG methods. A linear fit to these data will yield partial molar excess enthalpy at infinite dilution, according to the following relation:

$$\left|\frac{d(\ln g_i^{\infty}}{d(1/T)}\right|_{P,x} = \frac{\bar{h}_i^{ex\infty}}{R} \qquad (3.4)$$

The partial molar excess enthalpy at infinite dilution obtained from the slopes of the lines can also be compared with the values obtained by calorimetric measurements.

In the case of methanol, results of this study are in good agreement with the literature, especially with results obtained using a differential static cell [5]. Moreover, the measurements of dilute mixture VLE data by Christensen [6] using a recirculating still are in good agreement with the results of this study. On the other hand, values reported by Bergmann and Eckert [7] using differential ebulliometry appear to be too low and those reported by Pecsar and Martin [8] using gas liquid chromatography show a trend that is opposite to the expected trend based on calorimetric measurements. The empirical correlation developed by Pierotti et al. [9] and the UNIFAC and ASOG methods seem to underpredict the data.

In the case of ethanol, the results of this study are also in good agreement with literature values, especially with those obtained by differential ebulliometry [10] and by gas stripping methods [11, 12]. One interesting feature of all literature values is that data obtained by different methods show good agreement at approximately 60^{o}C, but not at other temperatures. The Pierotti et al. [9] correlation underpredicts infinite dilution activity coefficients, whereas the Pecsar and Martin [8] data show a trend that is opposite to that expected.

Few literature data are available for comparison in the case of propanol (Fig. 3.6). At high temperature, the gas stripping methods [11, 13] yield results that are of the same order of magnitude. However, the slope is very different. The Pecsar and Martin [8] data again show an increase in magnitude of $\gamma\infty$ values with decrease in the temperature that is opposite to that expected. The Pierotti et al. [9] correlation and the UNIFAC and ASOG methods predict values that are lower than experimental values.

Butanol results are presented in Fig 3.7. Results obtained by differential ebulliometry [14] and the UNIFAC method show a positive slope on plotting ln ($\gamma\infty$) versus T-1. This is opposite to that expected based on partial molar excess enthalpy at infinite dilution obtained from calorimetric measurements [15, 16]. Results from the present study appear to be high compared with literature values and the values predicted by the UNIFAC method.

Table 3.III lists the partial molar excess enthalpies at infinite dilution obtained from the slopes of the linear plots together with literature values. The partial molar excess enthalpies of methanol and ethanol obtained in this work compare well with calorimetric measurements. For

propanol and butanol, results from this study are lower by a factor of three. No literature values are available for comparison in the case of pentanol and hexanol.

3.3 Measurements and Prediction of Henry's Constants of Methanol in Aqueous Solutions Containing Salts

In this study, we report new data for partition coefficients of methanol in aqueous solutions containing sodium carbonate and sodium sulfate. The data show a linear dependence of partition coefficients of methanol with salt concentration. This linear dependence extends also to black liquor solutions from pulp and paper mills. Furthermore, the data can be extrapolated in temperature and salt concentration using an extension of the relationship proposed by Harvey [17].

From Eq. (3.3), the Henry's constant of aqueous methanol solution can be expressed as

$$\ln(H) = 8.969 - \frac{5206.8}{T} \tag{3.5}$$

The average deviation for this correlation is about 0.3% with an R^2 value of 0.9981. We estimate the experimental error to be $\pm$ 10%. Data for methanol in aqueous Na_2CO_3 and aqueous Na_2SO_4 solutions at temperatures between 40-65 C were measured in this work and are presented in Table 3.IV. Figures 3.8 and 3.9 show these data in the form of ln(H) plotted vs. 1/*T*. A salting-out behavior of methanol is observed with the addition of either salt. At a fixed temperature, Henry's constants of methanol in these salt solutions were found to vary linearly with the mass concentration of the salt. This is shown in Figure 3.10, where the data for both salts fall on a single straight line, within experimental error. Thus, the anion apparently plays no role in the salting-out behavior of methanol. This relationship can also be used to predict partitioning in black liquor solutions, as shown by the data from Zhu et al. [18] also plotted in Figure 3.10. Apparently, the partitioning of methanol in black liquor can be estimated from knowledge of the total sodium salt concentration of the black liquor.

The relationship shown in Figure 3.10 applies at a particular temperature (or, in other words, different lines are obtained at different temperatures). The data, however, can be generalized using a relationship reported by Harvey [17]. This relationship was based on an

expansion of the Helmholtz energy about the critical point of the solvent [19] and was of the form:

$$T \ln\left(\frac{H_{ij}}{f_j}\right) = A + B(\rho - \rho_j^c) \qquad (3.6)$$

where f_j is the fugacity of the solvent and ρ and $\rho_j{}^c$ are its saturated density and critical density, respectively. The constants A and B in this equation can be obtained by fitting, but they are also meaningful thermodynamic quantities [17]. From a practical point of view, however, Eq. (3.6) has several disadvantages. First, it is an asymptotic relationship valid near the critical point of the solvent. Second, the fugacity and density of the solvent are rarely available in practice. Harvey [17] overcame these limitations by replacing the fugacity with the vapor pressure, replacing the density behavior with a scaling relationship in terms of temperature, and adding an empirical term to account for the temperature dependence away from the critical point. The resulting equation is given by:

$$\ln(H) = \ln(p_1^s) + \frac{A}{T_r} + B\frac{(1-T_r)^{0.355}}{T_r} + C\exp\left(\frac{1-T_r}{T_r^{0.41}}\right) \qquad (1.7)$$

An important advantage of Eq. (3.7) is that it allows the extrapolation of low-temperature data to high temperatures, since it is constrained to yield the correct asymptotic behavior as the critical point of the solvent is approached.

We have developed an extension of this correlation to include a dependence on salt concentration as follows:

$$\ln(H) = \ln(p_1^S) + \frac{A}{T_r} + \frac{B(1-T_r)^{0.355}}{T_r} + C\cdot\exp\left(\frac{1-T_r}{T_r^{0.41}}\right) + D\cdot x_S \qquad (3.8)$$

where a single value of parameter D is used for all salt concentrations. Our results for sodium salts (Figure 3.10) also indicate that the parameter D is likely to be the same for salts with a common cation. Equation (3.8) therefore represents an extremely powerful model for extrapolating Henry's constant data both in temperature and salt concentration (for salts with a common cation).

We have tested Eq. (3.8) using data for benzene-water compiled by Tsonopolous and Wilson [20]. The constants *A*, *B*, and *C* were determined from this data and used to correlate Henry's constants of benzene in seawater at various salt concentrations. Figures 3.11 and 3.12 show these results. It is quite remarkable that one additional parameter (*D*) is able to correlate Henry's constant data in salt solutions over an extended range of temperatures [21].

These calculations were repeated for the systems studied in the present work. Parameters *A*, *B*, and *C* were again determined from binary solution data (without salt), and parameter *D* was determined from data at a single salt concentration. Once again, the agreement with measurement is excellent as shown in Fig. 3.13.

3.4 Measurements and Prediction of Henry's Constants of Methanol in Black Liquor

3.4.1 Effect of Temperature

Twenty-two black liquor samples were collected from both kraft mills and our laboratory pulping processes of various wood species. Because the operating process temperature of weak black liquor in kraft mills varies significantly, we measured the Henry's constants of the 22 black liquors in a temperature range of 50 to 80^{o}C. Our measurements indicate that the Henry's constant of methanol in all black liquors follows the van't Hoff relationship with temperature as shown by Eq. (3.2). Table 3.V lists the linear regression results along with the correlation coefficients for the liquors tested. Only the results from 4 black liquor samples are shown in Fig. 3.14.

For comparison, we have also plotted Henry's constants of methanol in water in Fig. 3.14. The results as listed in Table 3.V show that the slopes for the 22 black liquor samples were very close to the slope of the aqueous methanol solution. The relative standard deviations of the slopes for black liquors (22 data sets) and all the samples (23 data sets including water-methanol mixture) were 6.4 and 6.9%, respectively. Also, the slopes of all the black liquor samples were slightly smaller than that of the aqueous methanol solution, indicating that the partial molar

excess enthalpy of methanol in black liquor (a multicomponent system) is only slightly smaller than that in water (a two-component system).

Figure 3.14 indicates that there are significant variations in measured methanol Henry's constants among various black liquors. The variations in the compositions of the black liquors due to inorganic and organic solids content, pH, and the presence of other species are a possible cause of these differences.

3.4.2 Effect of Lignin

Black liquor contains significant amounts of dissolved organic materials such as lignin. To understand the effect of lignin on Henry's constants of methanol, we measured methanol Henry's constants in several model solutions containing water, methanol, and sulfonated lignin. We found that the methanol Henry's constant is not affected by the presence of sulfonated lignin. Figure 3.15 shows the normalized Henry's constants of methanol measured in such solutions at two temperatures, 343 and 353 K, and various sulfonated lignin concentrations. Similar experiments were also conducted using mixed-wood lignin in a slightly caustic solution (mixed-wood lignin can only be dissolved in caustic solutions) yielded from kraft pulping of softwood to linerboard-grade pulps (Westvaco Corp., SC). It was found that Henry's constant of methanol is only a weak function (increases with the increase) of mixed-wood lignin mass concentration ranging from 0 to 13%.

3.4.3 Effect of pH

We took a similar approach to study the effect of pH on the Henry's constant of methanol in black liquors. Black liquor is a caustic solution with a nominal pH value of about 13. Different amounts of sodium hydroxide were added to methanol-water solutions. Henry's constants in these solutions were measured. As shown in Fig. 3.16, our results indicate that the Henry's constant of methanol is proportional to the hydroxide concentration to the power of 0.2, which means that the effect of pH is not significant. It should be noted that the sodium ion concentration also contributes to the variations shown in Fig. 3.16. The effect of ionic strength, or more specifically, sodium salt concentration, on methanol Henry's constant is discussed in the next section.

3.4.4 Effect of Inorganic Salt

Black liquor contains significant amounts of inorganic solids. These inorganic solids are mainly sodium carbonate (Na_2CO_3) and sodium sulfate (Na_2SO_4) plus minimal amounts of sodium thiosulfate ($Na_2 S_2O_3$), sodium chloride (NaCl), and potassium salts. To understand the effect of inorganic solids on methanol Henry's constant, we measured the Henry's constant in water-methanol solutions containing Na_2CO_3 , Na_2SO_4 , $Na_2 S_2O_3$, and NaCl, respectively. We found that the logarithm of Henry's constant of methanol increases linearly with the sodium salt mass concentration at a given temperature but not dependent on the type of salt, as shown in Fig. 3.17. The measured Henry's constants of methanol in actual black liquors are also shown in Fig. 3.17. The total mass concentrations of the inorganic materials (more than 95% are sodium salts) in the 22 black liquor samples studied were obtained by subtracting the lignin content (organic solids measured by UV absorption) from the measured total solids content. We used the following equation to express this relation [22]:

$$\ln(H) = c \cdot S_{Salt} + d \qquad (3.9)$$

where S_{salt} is the total sodium salt mass concentration of the liquor.

3.4.5 Effects of dimethylsulfide, dimethyldisulfide, methyl ethyl ketone, α-pinene, β-pinene, fatty acids, resin acids

Many other chemical species, such as dimethylsulfide (DMS), dimethyldisulfide (DMDS), methyl ethyl ketone (MEK), α-pinene, β-pinene, fatty acids, and resin acids present in weak black liquors can affect the methanol Henry's constant. To determine the effect of these compounds, we prepared methanol-water solutions, each containing one of these compounds, to study their individual effects on Henry's constant of methanol. The results indicate that the effect of these compounds on methanol Henry's constant is insignificant at the concentration levels present in weak black liquor. Figures 3.18–3.21 show the effects of α-pinene, DMS, MEK, and DMDS.

3.4.6 Empirical Correlation

The results presented in this work show that temperature and inorganic solids (salts) content are the two main variables that affect Henry's constants of methanol in black liquors. The effects of pH, lignin concentration, and other organic compounds are not significant and can be neglected. Because the ratio of the inorganic to organic solids (wood lignin) in black liquors does not vary significantly and the total solids content can be easily determined with very good accuracy, the total solids content *S* can be used to account for the effect of inorganic salts on Henry's constant of methanol. Furthermore, the slight effect of wood lignin on methanol Henry's constant can be accounted for by using the total solids content. To demonstrate the validity of this assumption, we plotted the measured methanol Henry's constants in the 22 black liquors against the total solids content. As shown in Fig. 3.22, we found that the logarithm of Henry's constant of methanol is linearly related to total solids content at four different temperatures tested, indicating that the minor effect of wood lignin on methanol Henry's constant is well accounted for by using the total solids content. The scatter in the data can be attributed to experimental errors, the effects of minor variables such as pH, the presence of other components, and the small variations of inorganic/organic ratio from liquor to liquor. This is demonstrated by the fact that the measured Henry's constants of methanol in a given black liquor sample at the 4 temperatures (50, 60, 70, and 80^{o}C) are very consistent; i.e., all the measured data points are either lower or higher than the expected (regression) value.

The experimental data can be correlated using the following expression, based on the work of Stumm and Morgan [23] and Schwarzenbach et al. [22]:

$$\ln(H) = -\frac{A}{T} + B \cdot S + C \qquad (3.10a)$$

or

$$H = m\left[\exp(-\frac{A}{T} + B \cdot S)\right]. \qquad (3.10b)$$

with $m = 3.77 \times 10^{12}$, $A = 5620$, $B = 1.63$, and H in *Pa*. Figure 3.23 plots the direct comparison of the methanol Henry's constants of 22 black liquors measured at 4 temperatures with those

predicted using Eq. (3.10). We found that the model-predicted methanol Henry's constants agree very well with those measured experimentally.

3.4.7 Measurement Uncertainty

Although black liquor can be treated as an aqueous solution, the distribution of various dissolved solids in the liquor can be inhomogeneous, which makes it difficult to obtain uniform and representative samples during experiments. Therefore, liquor sampling can contribute to measurement uncertainty. Sampling of the liquid phase and the vapor phase can also contribute to measurement uncertainty. We conducted 11 replicate measurements (repeatability test) using black liquor collected from a kraft mill to estimate the actual measurement uncertainty. We found that the maximum error of the 11 individual measurements relative to the average value of the 11 measurements was 15%. However, the relative standard deviation of the 11 measurements was 8.8%. We conducted triplicate experiments and averaged the results; therefore, the actual measurement uncertainty of the data presented in this study is less than the relative standard deviation of the single measurement of 8.8%.

3.5 Conclusions

Dimensionless Henry's constants of n-alkanols, methanol through hexanol, in water were measured between 40^{o}C and 90^{o}C using a headspace gas chromatographic technique recently developed by Chai and Zhu [1]. The data were consistent and in good agreement with literature data when available. The temperature dependence of dimensionless Henry's constants was modeled with the classical van't Hoff equation. An empirical correlation was established for the dimensionless Henry's constants of n-alkanols in water as a function of temperature and number of carbon atoms in the n-alkanol.

Henry's constants were also converted to infinite dilution activity coefficients and compared with literature data. In addition, partial molar excess enthalpies at infinite dilution for n-alkanols in water were obtained and found to be in agreement with the negative partial molar excess enthalpies at infinite dilution from calorimetric measurements. Infinite dilution activity coefficients were also in good agreement with other experimental values. The UNIFAC and

ASOG models generally underpredicted infinite dilution activity coefficients of alkanols with three or more carbon atoms.

Henry's constants for methanol in water, water + salt, and black liquor solutions have been measured and their consistency verified. At a fixed temperature, Henry's constants of methanol in aqueous salt solutions vary linearly with salt mass concentration. This relationship can be used to predict partitioning in black liquor solutions.

Henry's constant data can also be correlated over an extended temperature range based on the model of Harvey. An extension of this model to salt solutions has been presented in this work. The extended model requires one additional parameter for solutions containing salts with a common cation and can be used to extrapolate data over a wide range of temperatures.

Henry's constant of methanol in weak black liquor can be correlated using two parameters, temperature and inorganic solid contents. The effect of other variables, such as pH, lignin content, and the presence of other organic materials, is insignificant. A two-parameter empirical model can be used for the prediction of methanol Henry's constants in weak black liquors.

REFERENCES

1. Chai, X. S. and Zhu, J. Y. *J. of Chromatography A.*, **799**:207, 1998
2. Hine, J. and Mookerjee, P. K., *Journal of Organic Chemistry*, **40**:292, 1975.
3. Nirmalakhandan, N. N. and Speece, R. E., *Environ. Sci. & Techno.*, **22**:1349, 1988.
4. Kojima, K., Zhang, S., and Hiaki, T. *Fluid Phase Equilibria.* **131**:145, 1997.
5. Pividal, K. A., Birtigh, A., and Sandler, S. I. *J. Chem. Eng. Data.* **37**:484, 1992.
6. Christensen, S. P. *Fluid Phase Equilibria*, **150-151**:763, 1998
7. Bergmann, D. L. and Eckert, C. A. *Fluid Phase Equilibria.* **63**:141, 1991.
8. Pecsar, R. E. and Martin, J. J. *Anal. Chem.* **38**:1661, 1996.
9. Pierotti, G. J., Deal, C. H., and Derr, E. L. *Industrial & Engineering Chemistry.* **51**:95, 1959.
10. Prausnitz, J. M., Private communication with Brandani et al. (1990) (Brandani, S.; Brandani, V., and Giacomo, G. D., *Ind. Eng. Chem. Res.*, **31**:420, 1992.

11. Lee, H. J. *Journal of Korean Institute of Chemical Engineering*, **1983,** 21, 317. Cited in Activity Coefficients at Infinite Dilution. DECHEMA Chemistry Data Series, Vol. IX, Part 4, DECHEMA, Frankfurt, Germany, 1994.

12. Richon, D., Sorrentino, F., and Voilley, A. *Industrial & Engineering Chemistry Process Design Development.* **24**:1160, 1985

13. Lebert, A. and Richon, D., *J. Agricultural & Food Chemistry*, **32**:1156, 1984.

14. Tochigi, K. and Kojima, K., *J. Chemical Engineering of Japan*, **9**:267, 1976.

15. Trampe, D. M. and Eckert, C. A., *J. Chemical and Engineering Data,* **36**:112, 1991.

16. Korolev, V. P., Batov, D. V., and Krestov, G. A. *Russian J. Physical Chemistry*, **59**:212, 1985.

17. Harvey, A. H., *Ind. Eng. Chem. Res.*, 37 (1998) 3080-3088.

18. Zhu, J. Y., Liu, P. H., Chai, X. S., Bullock, K. R., and Teja, A. S. *Envon. Sci. & Techno.*, **34** :1742, 2000.

19. Harvey, A. H., Levelt Sengers, J. M. H. and Tanger, J. C. IV., *J. Phys. Chem.*, **95**:932, 1991.

20. Tsonopoulous. C. and Wilson, G. M., *AIChE J.*, **29**:990, 1983.

21. Dewulf, J., Drijvers, D., and Van Langenhove, *J. Atmospheric Environment*, **29**:323, 1995.

22. Schwarzenbach, R. P., Gachwend, P. M., and Imboden, D. M. *Environmental Organic Chemistry*; Wiley: New York, pp 109-123, 1993.

23. Stumm, W. and Morgan, J. J. *Aquatic Chemistry: An Introduction Emphasizing Chemical Equilibria in Natural Waters*; Wiley: New York, pp 38-55, 1981.

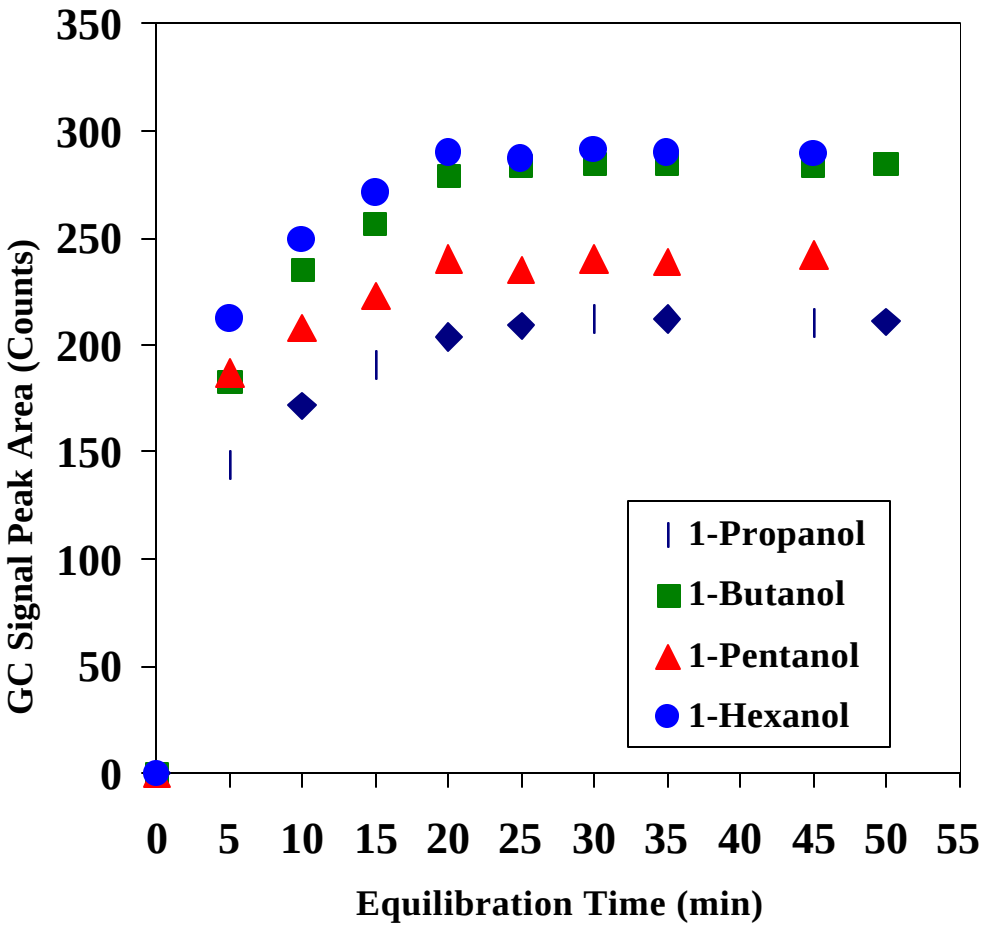

Fig. 3.1. Equilibration test of GC headspace system

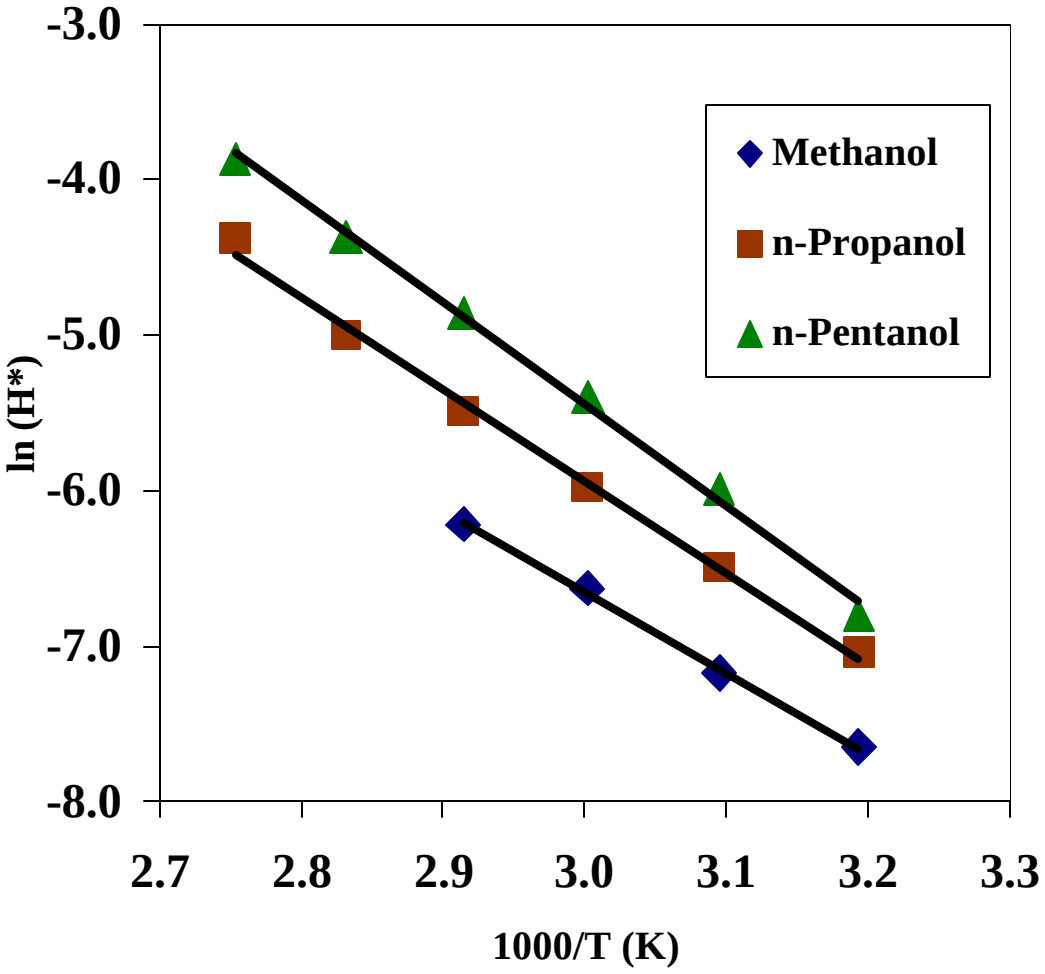

Fig. 3.2. Dimensionless Henry's constants of methanol, n-propanol, and n-pentanol in water

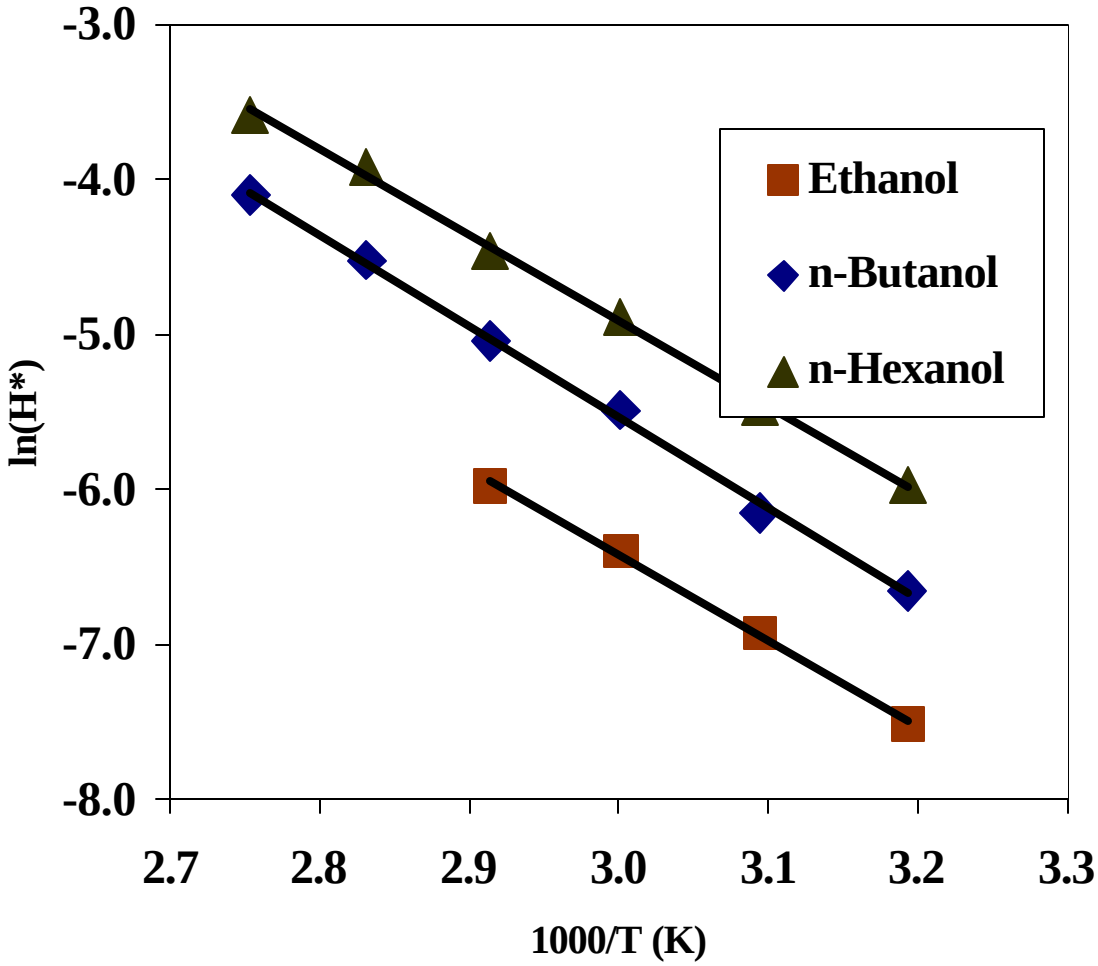

Fig. 3.3. Henry's constants of ethanol, n-butanol, and n-hexanol in water

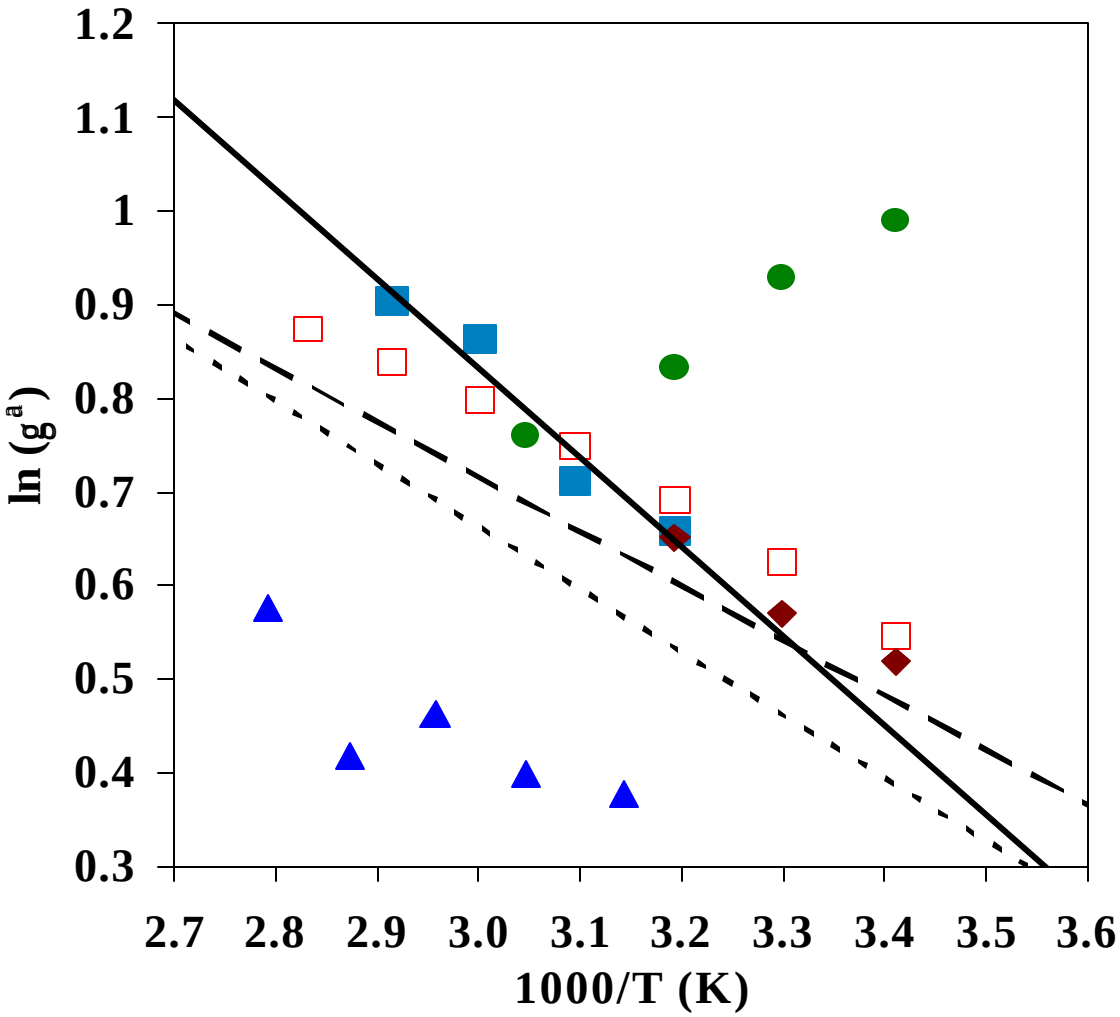

Fig. 3.4. Infinite dilution activity coefficients of methanol in water. Data of this work (■); Christensen [6] (□); Bergmann and Eckert [7] (▲); Pecsar and Martin [8] (●); Pividal et al. [5] (◆). The lines were calculated using UNIFAC (------); Pierotti et al. [9] (……); this work (——).

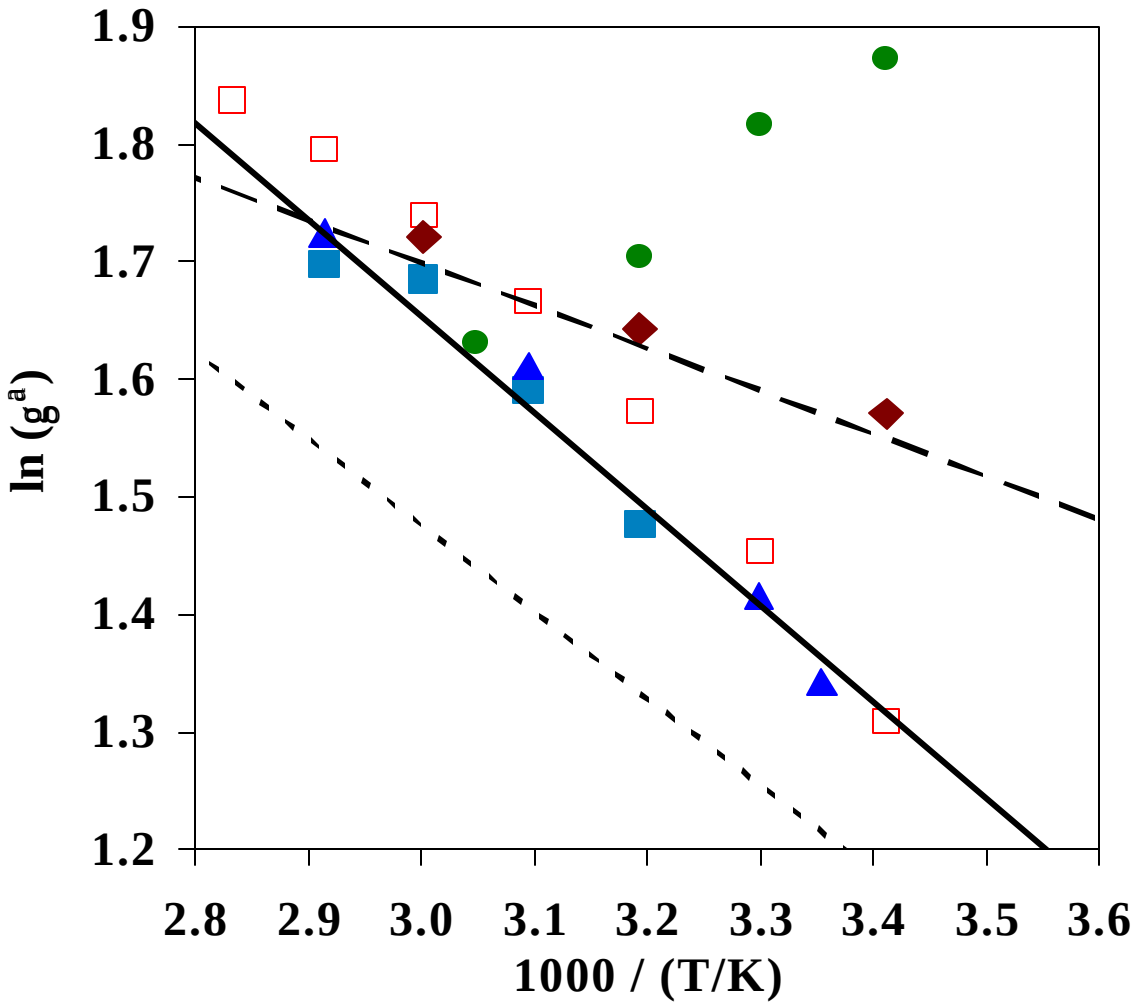

Fig. 3.5. Infinite dilution activity coefficients of ethanol in water. Data of this work (■); Christensen [6] (□); Pransnitz [10] (▲); Pecsar and Martin [8] (●); Pividal et al. [5] (◆). The lines were calculated using UNIFAC (------); Pierotti et al. [9] (……); this work (——).

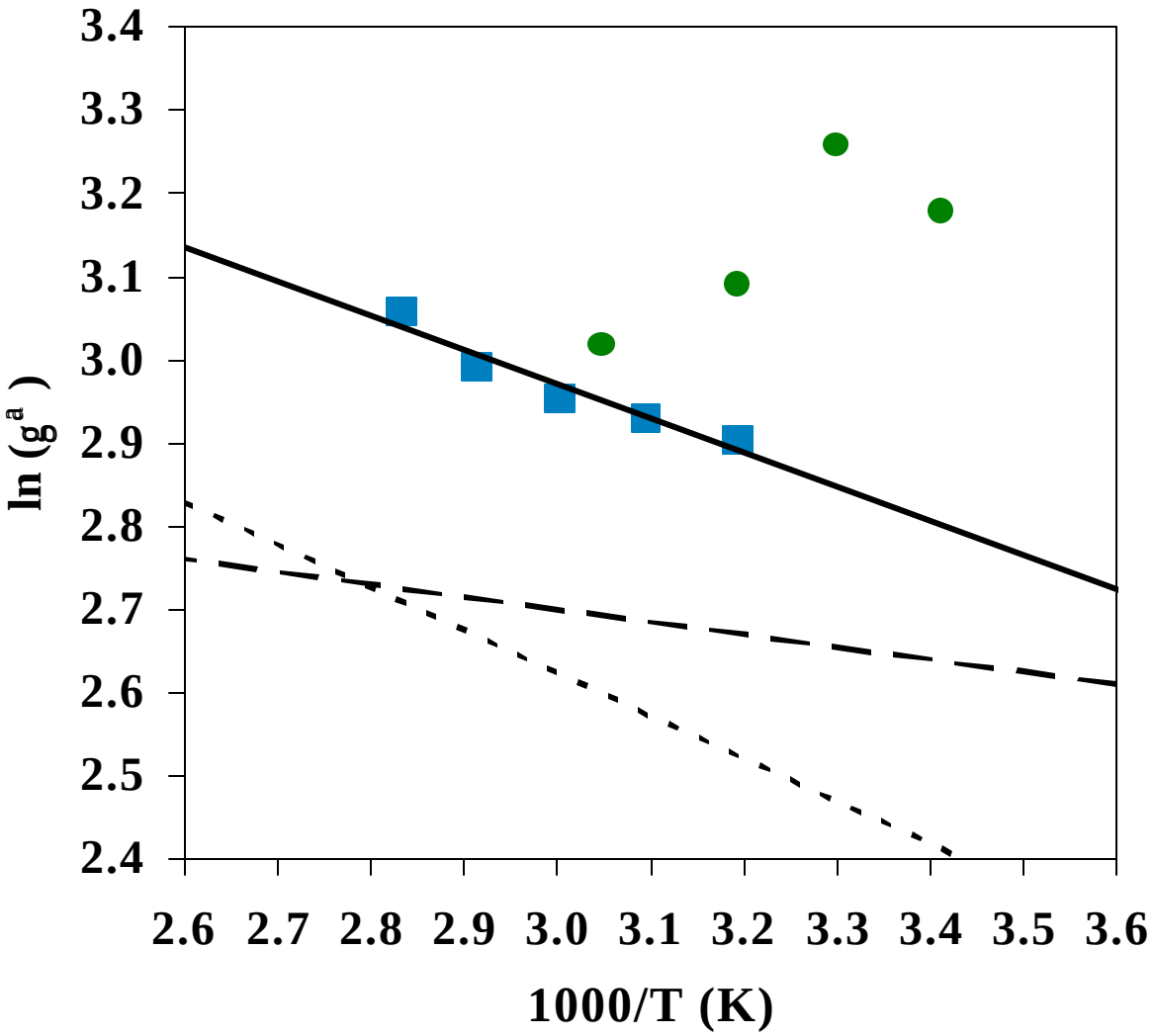

Fig. 3.6. Infinite dilution activity coefficients of propanol in water. Data of this work (■); Pecsar and Martin [8] (●). The lines were calculated using UNIFAC (------); Pierotti et al. [9] (……); this work (——).

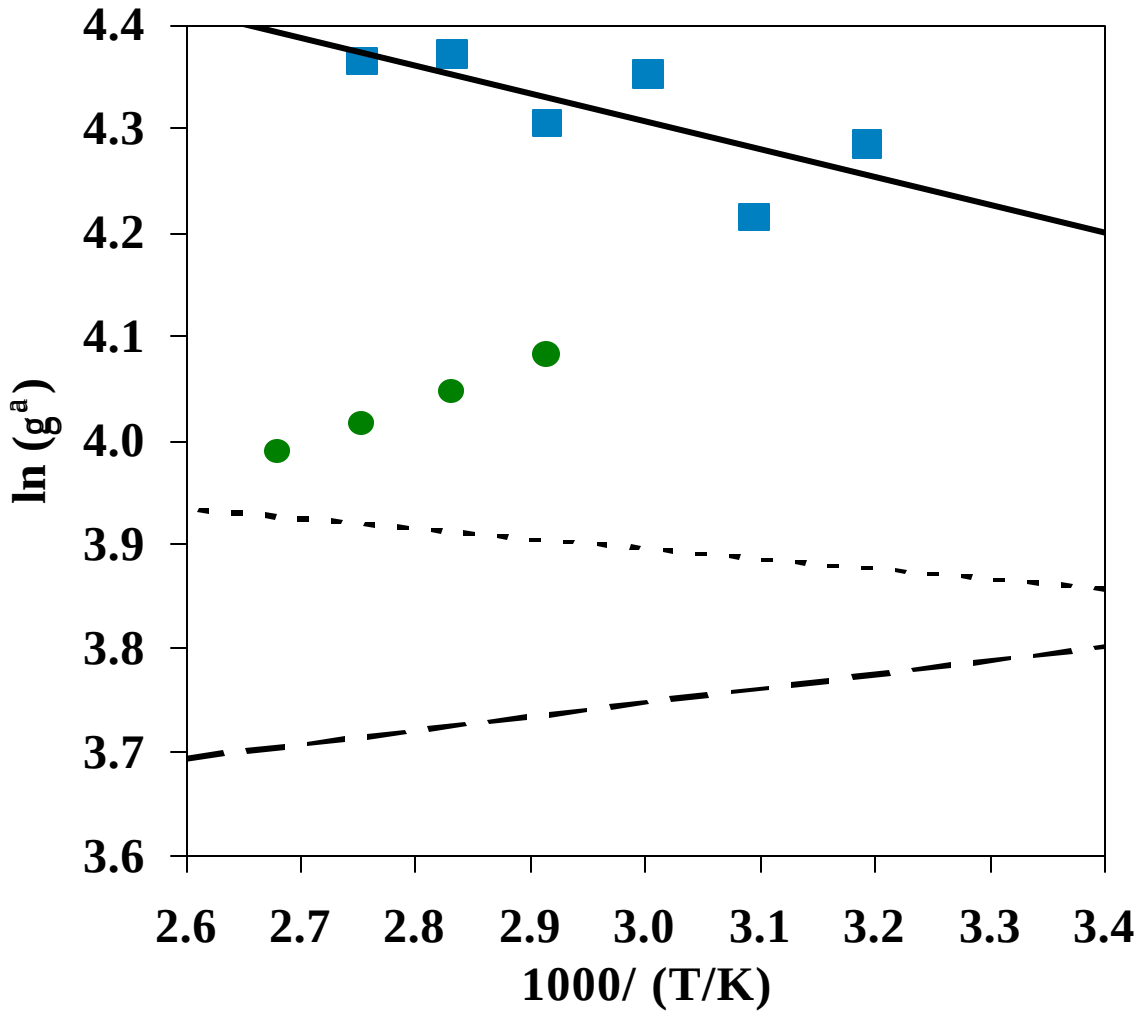

Fig. 3.7. Infinite dilution activity coefficients of butanol in water. Data of this work (■); Tochigi and Kojima [20] (●). The lines were calculated using UNIFAC (------); Pierotti et al. [9] (……); this work (——).

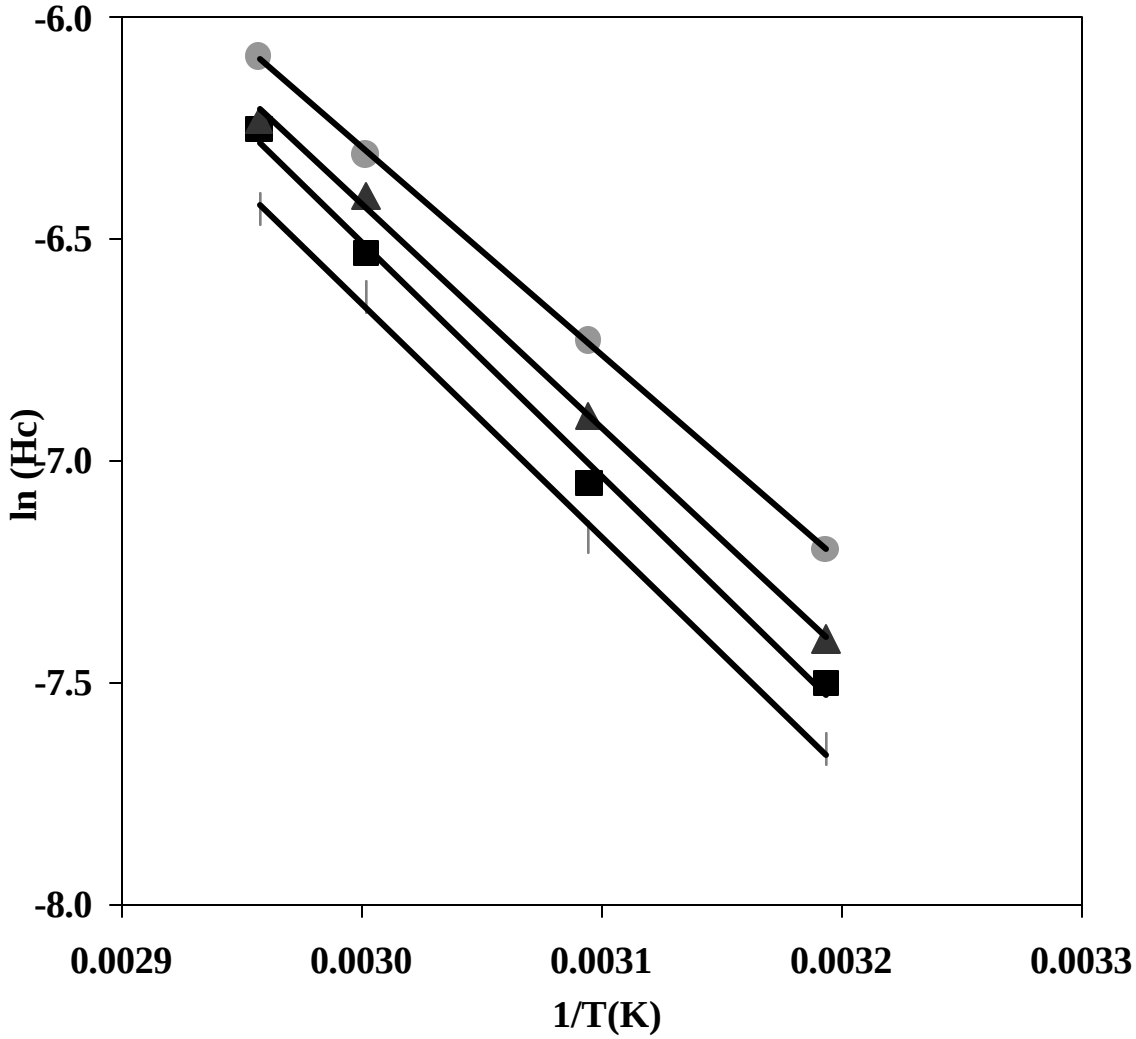

Fig. 3.8. Dimensionless Henry's constants of methanol in aqueous Na_2CO_3.
◆ 0 mol/kg ■ 0.5 mol/kg ▲ 1.0 mol/kg ● 1.5 mol/kg

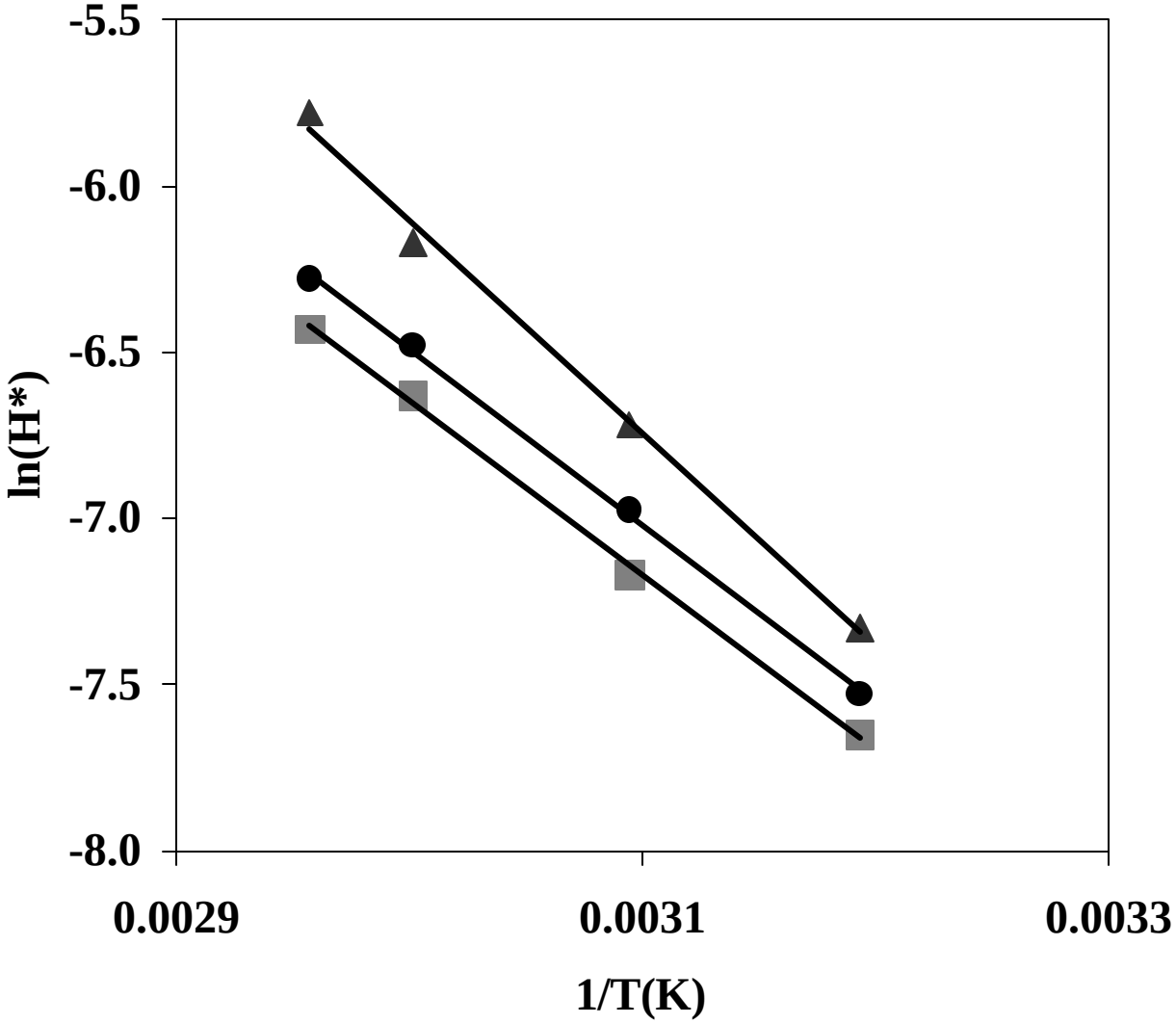

Fig. 3.9. Dimensionless Henry's constants of methanol in aqueous Na_2SO_4.
■ 0 mol/kg ● 0.4 mol/kg ▲ 0.8 mol/kg.

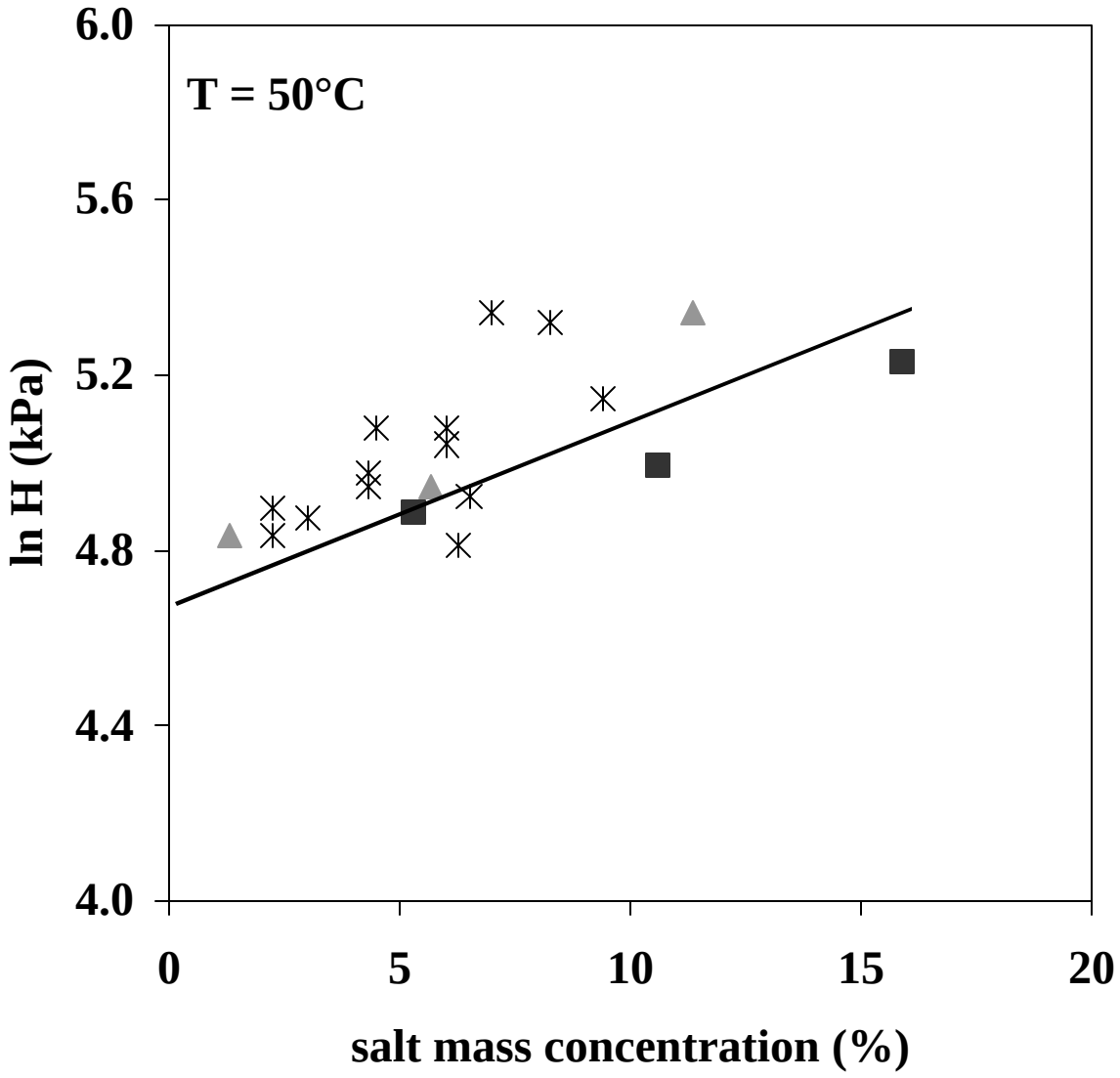

Fig. 3.10. Dimensionless Henry's constants of methanol in aqueous systems.
▲ Na_2SO_4 ■ Na_2CO_3 ● Black liquors.

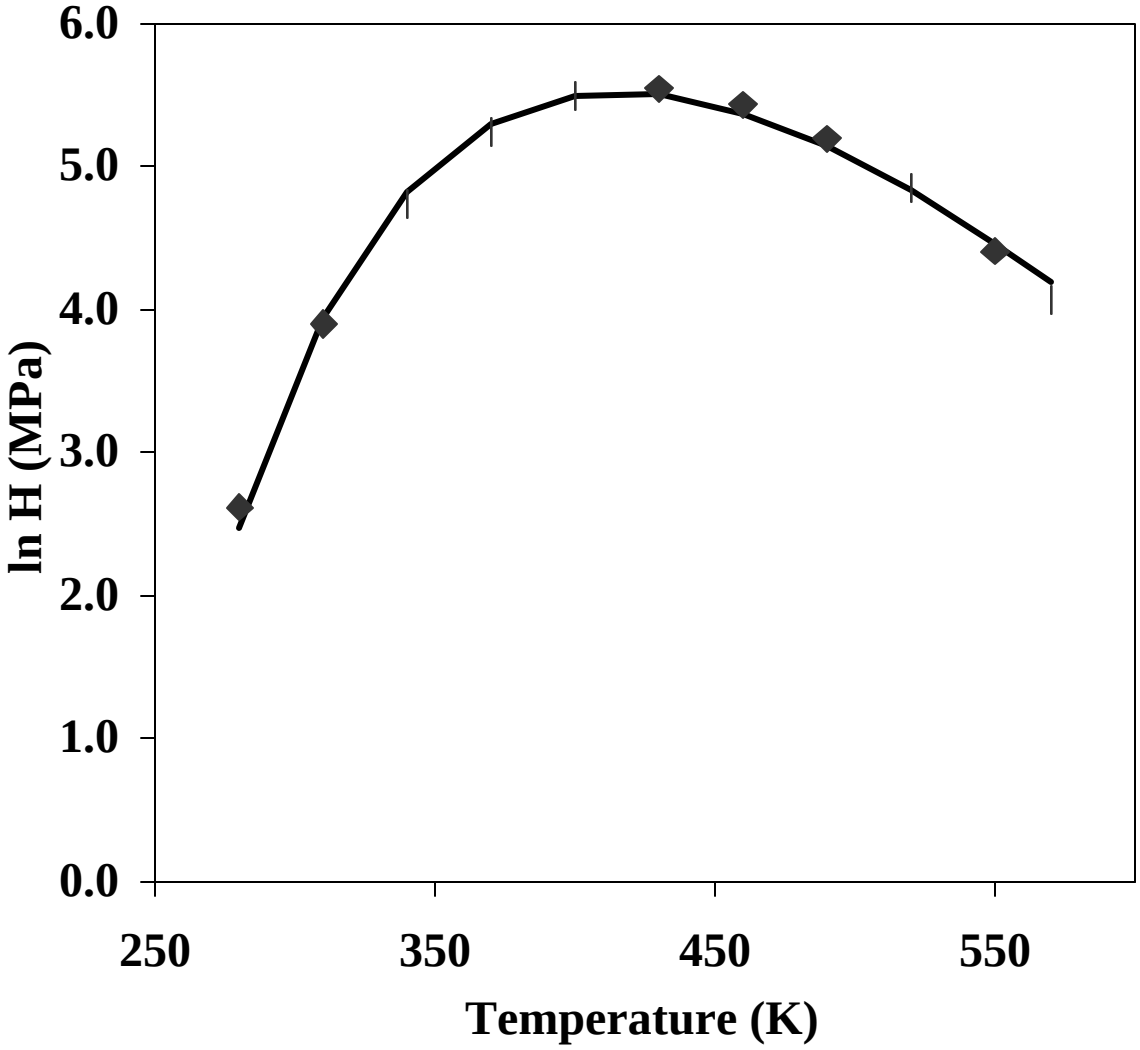

Fig. 3.11. Henry's constant of benzene in water.
◆ Data of Tsonopoulos and Wilson [20]; — Eq. (3.7)

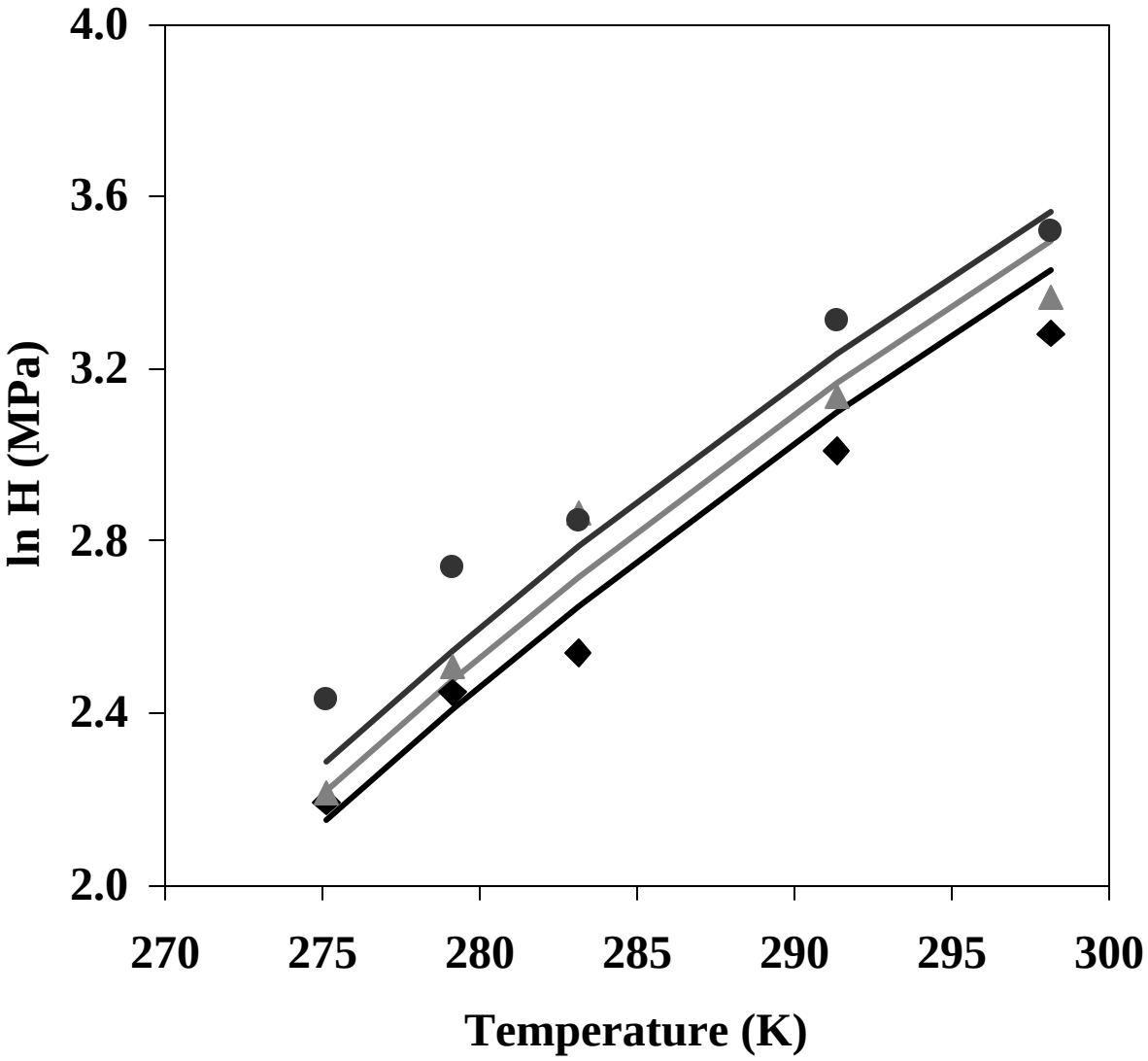

Fig. 3.12. Henry's constant of benzene in seawater with salt concentration
◆ 0 ppt ▲ 17.5 ppt ● 35 ppt.
Data are from Dewulf et al. [21] and the solid line is Eq. (3.8).

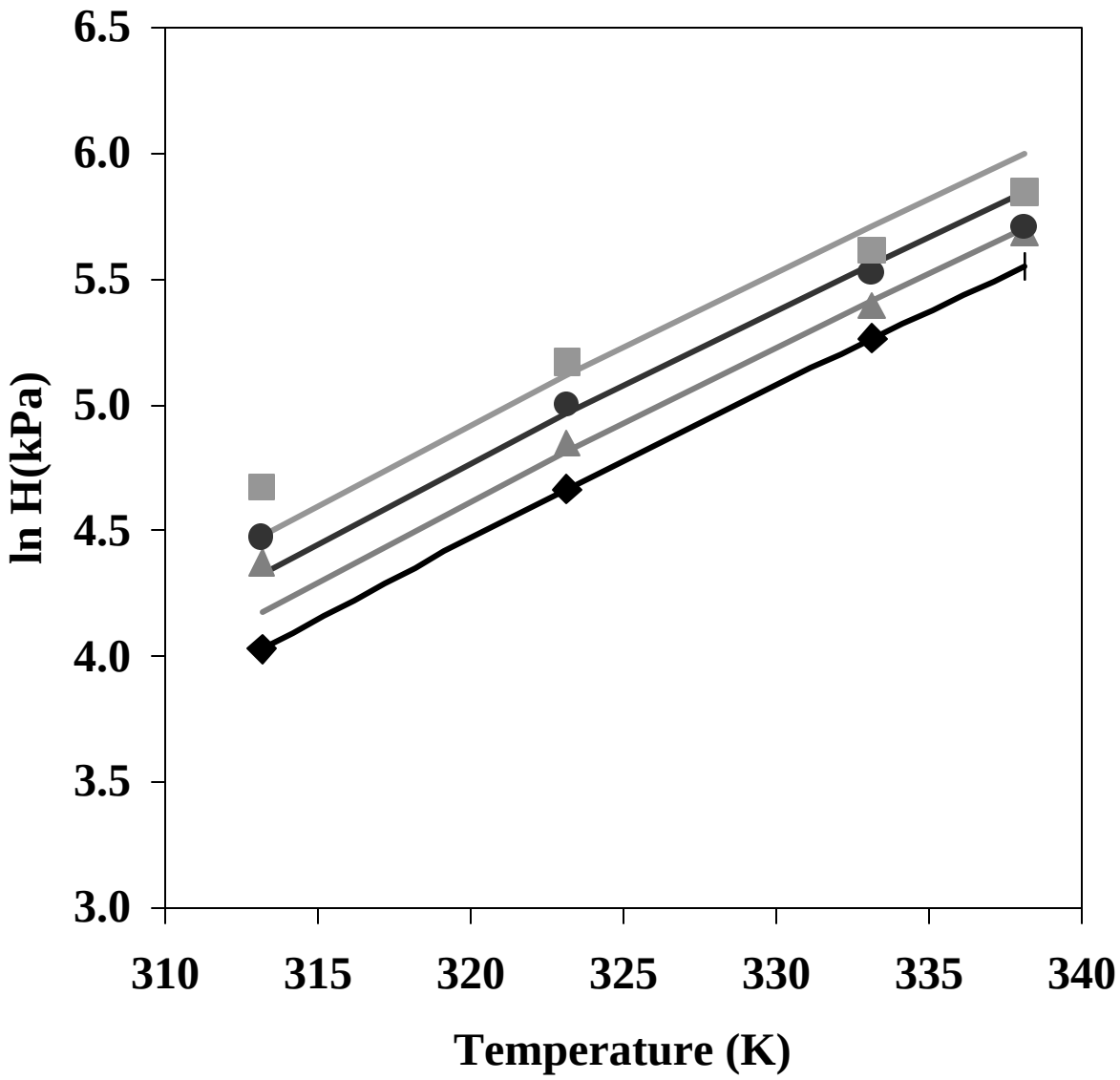

Fig. 3.13. Henry's constant of methanol in aqueous Na_2CO_3 at salt concentration of ◆ 0 mol/kg ▲ 0.5 mol/kg ● 1.0 mol/kg ■ 1.5 mol/kg. The solid line is Eq. (3.8).

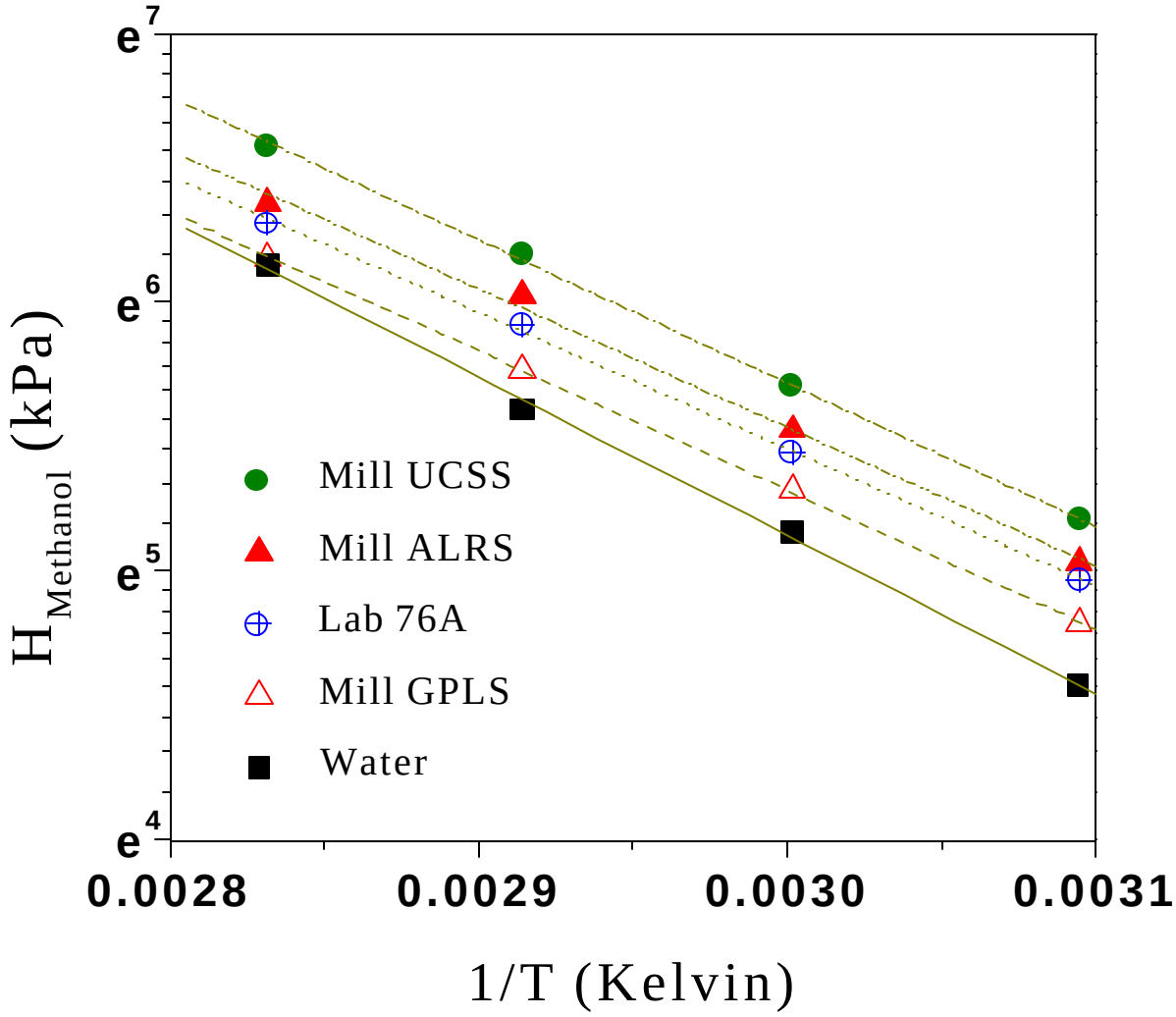

Fig. 3.14. Effect of temperature on methanol Henry's constants in black liquors.

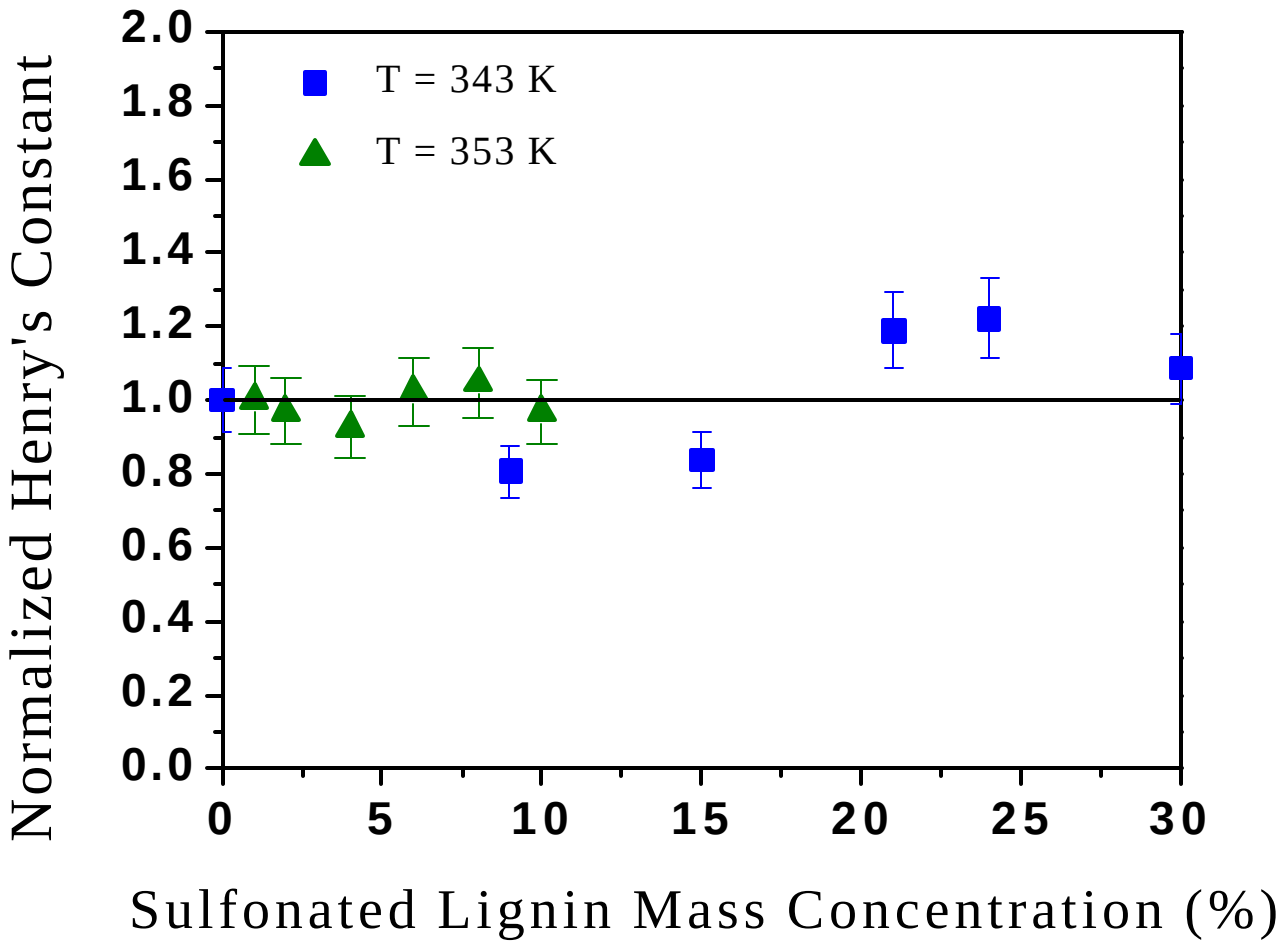

Fig. 3.15. Effect of spiked sulfonated lignin concentration on methanol Henry's constants in methanol-water mixtures.

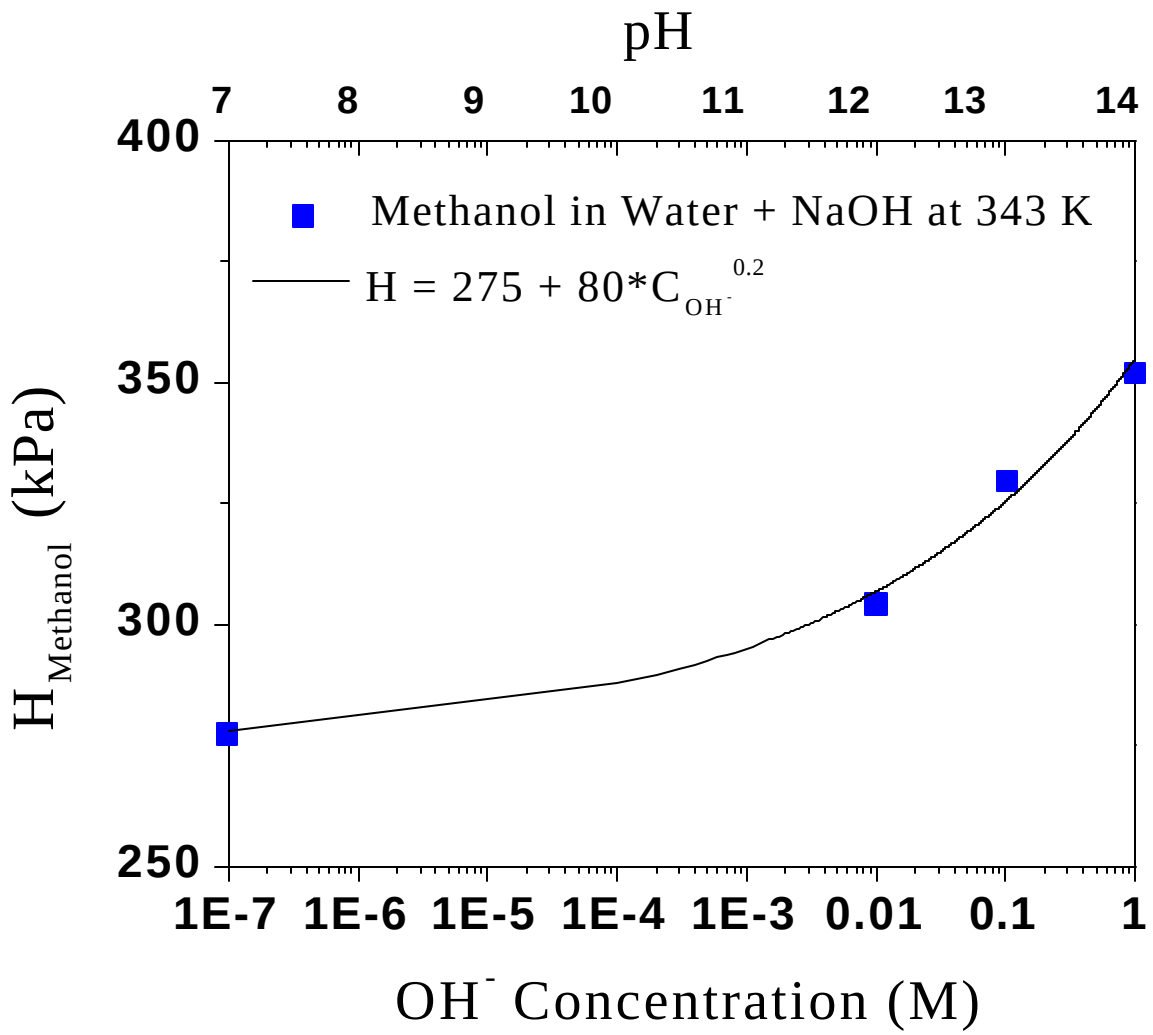

Fig. 3.16. Effect of spiked OH^- concentration (pH) on methanol Henry's constants in methanol-water mixtures.

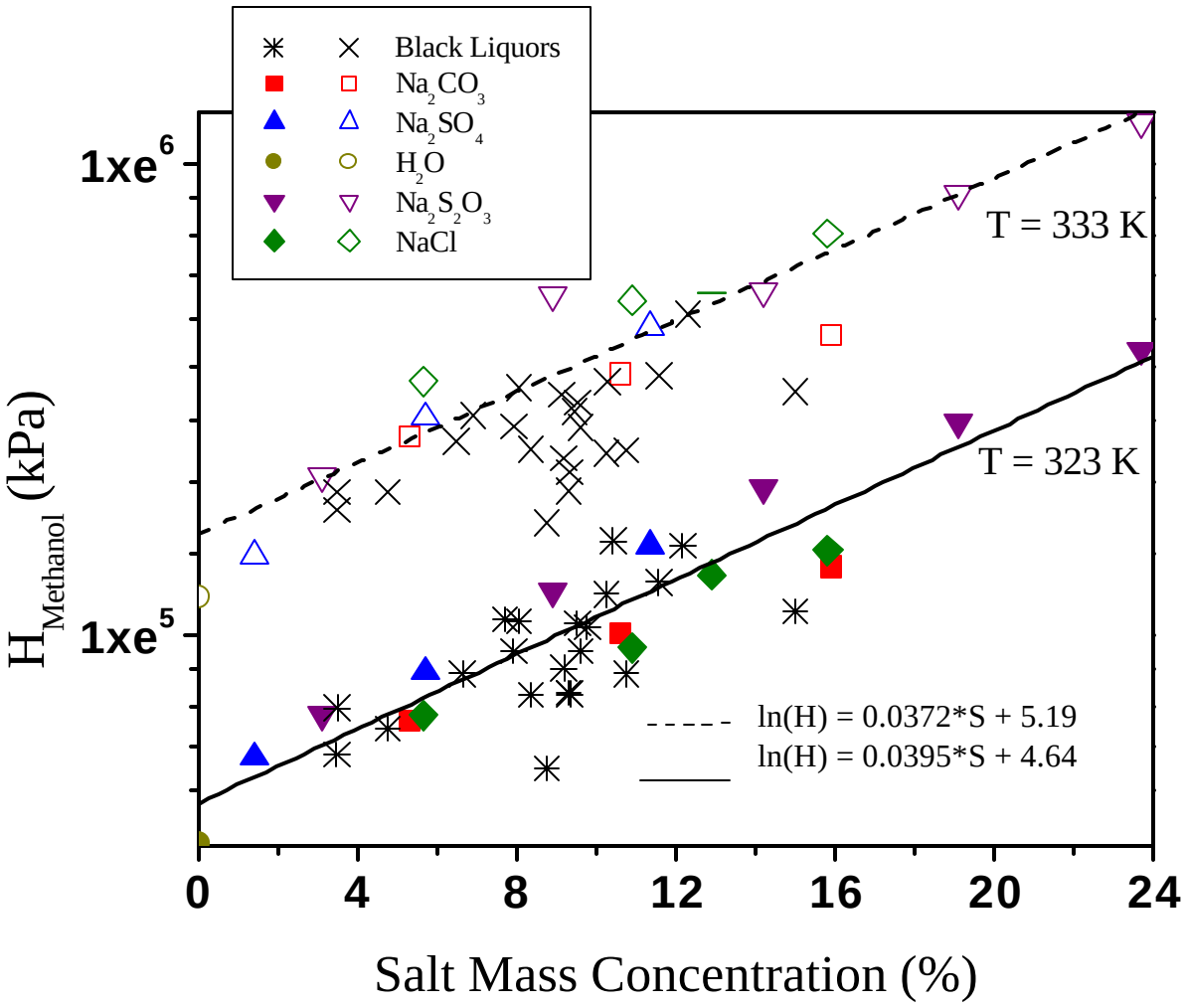

Fig. 3.17. Effect of sodium salt mass concentration on methanol Henry's constants in methanol-water mixtures and black liquors.

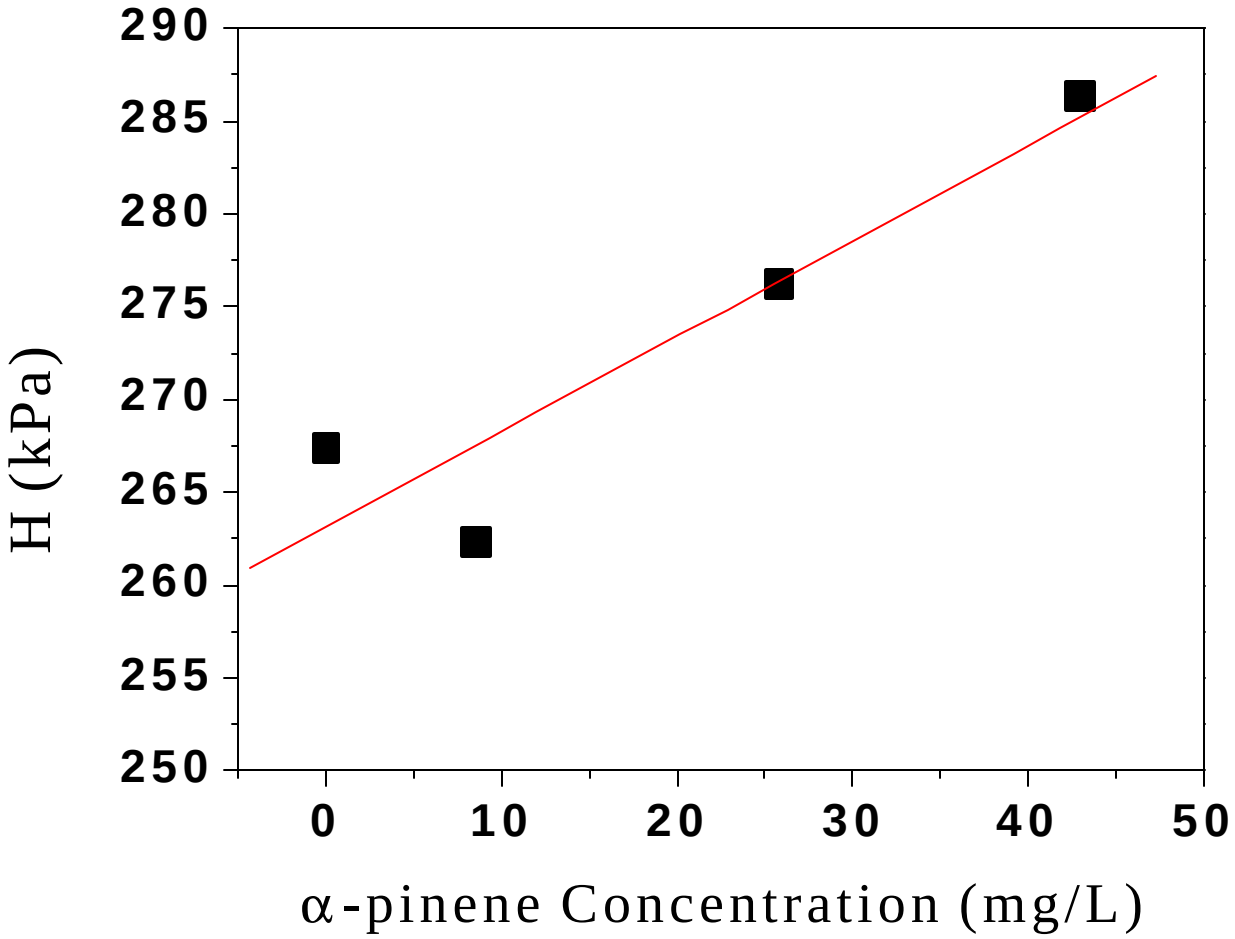

Fig. 3.18. Effect of spiked α-pinene concentration on methanol Henry's constants in methanol-water mixtures.

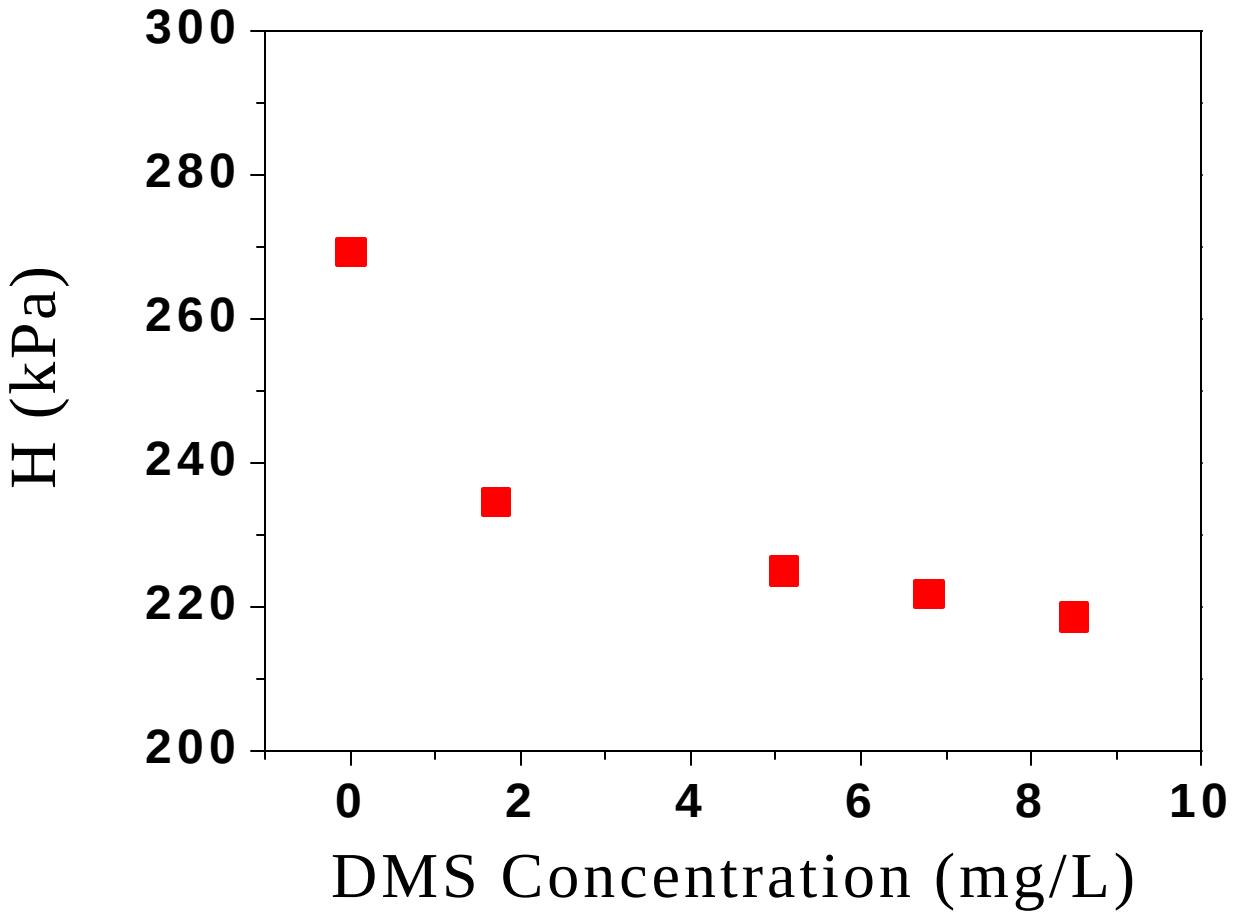

Fig. 3.19. Effect of spiked dimethylsulfide concentration (DMS) on methanol Henry's constants in methanol-water mixtures.

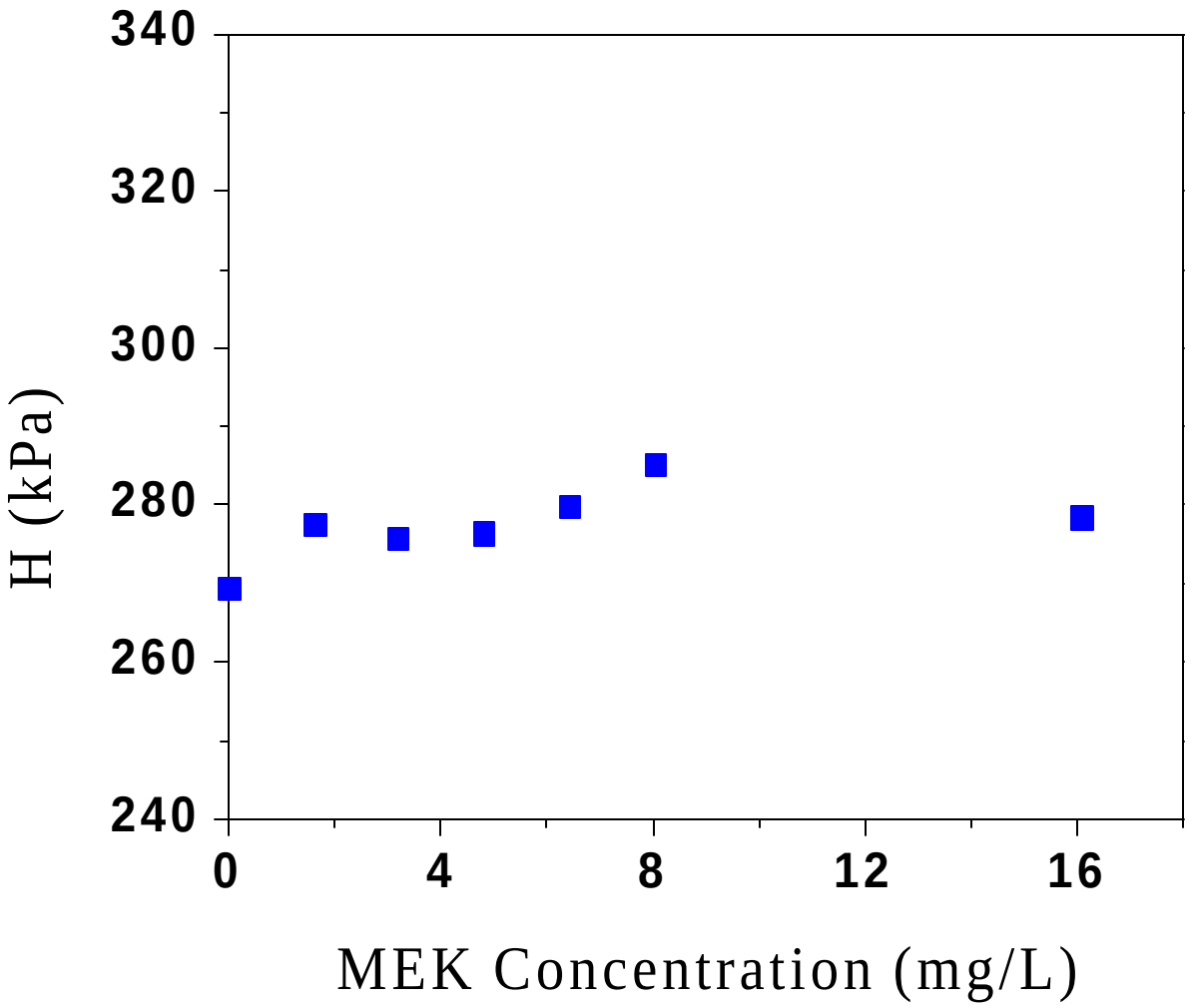

Fig. 3.20. Effect of spiked methyl ethyl ketone (MEK) concentration on methanol Henry's constants in methanol-water mixtures and black liquors.

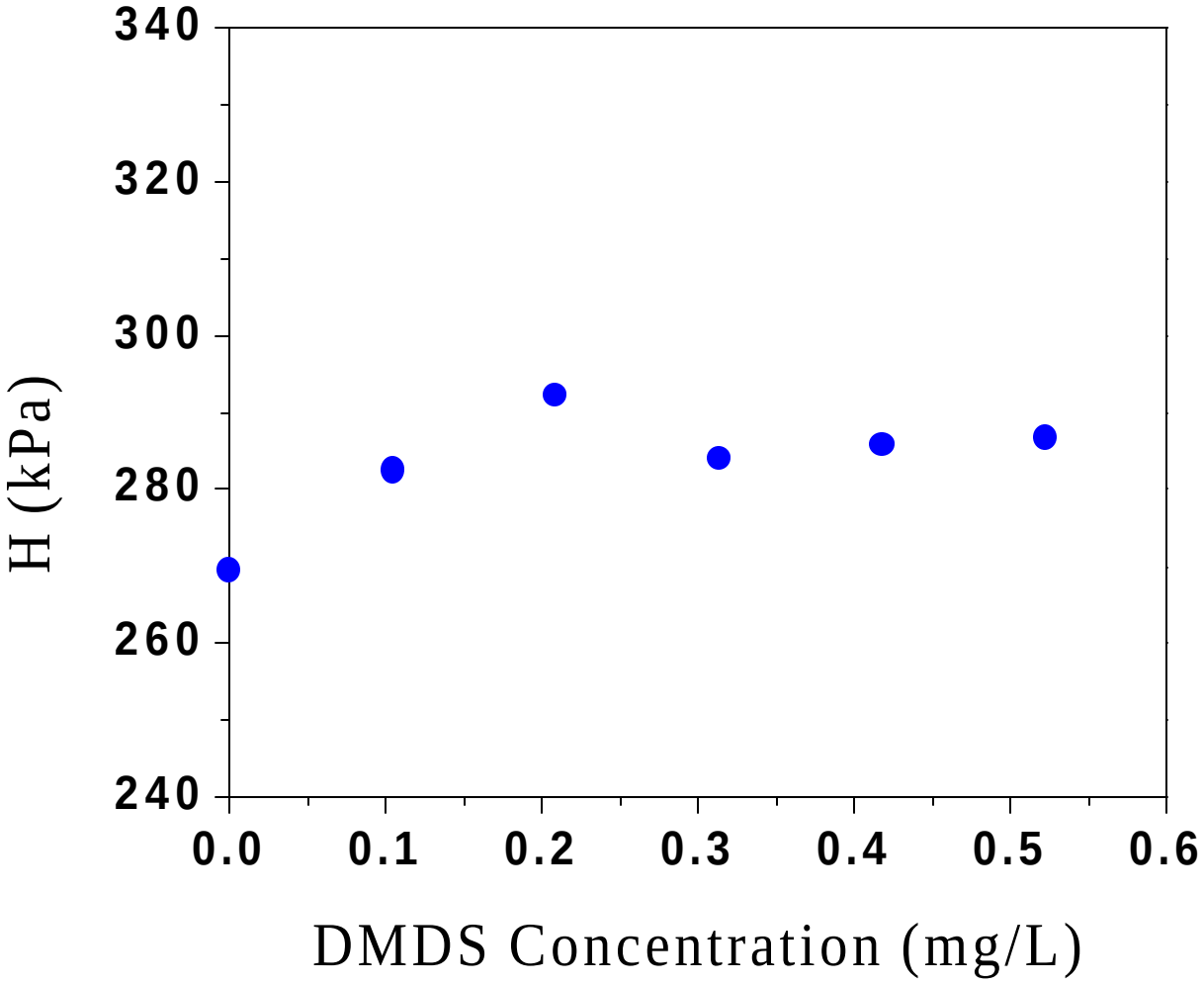

Fig. 3.21. Effect of spiked dimethyldisulfide concentration (DMDS) on methanol Henry's constants in methanol-water mixtures.

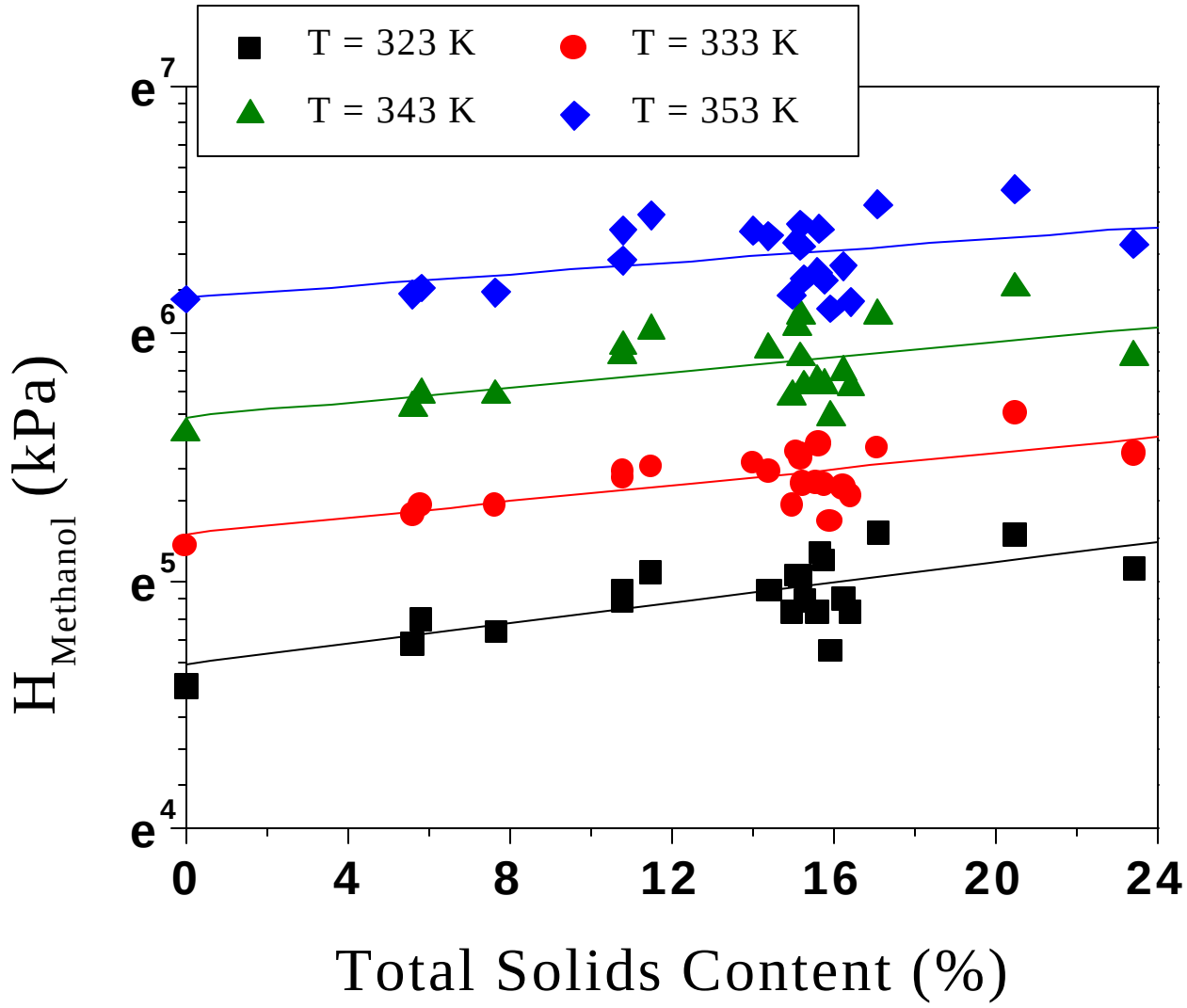

Fig. 3.22. Correlation of measured methanol Henry's constants with total solids content in black liquors.

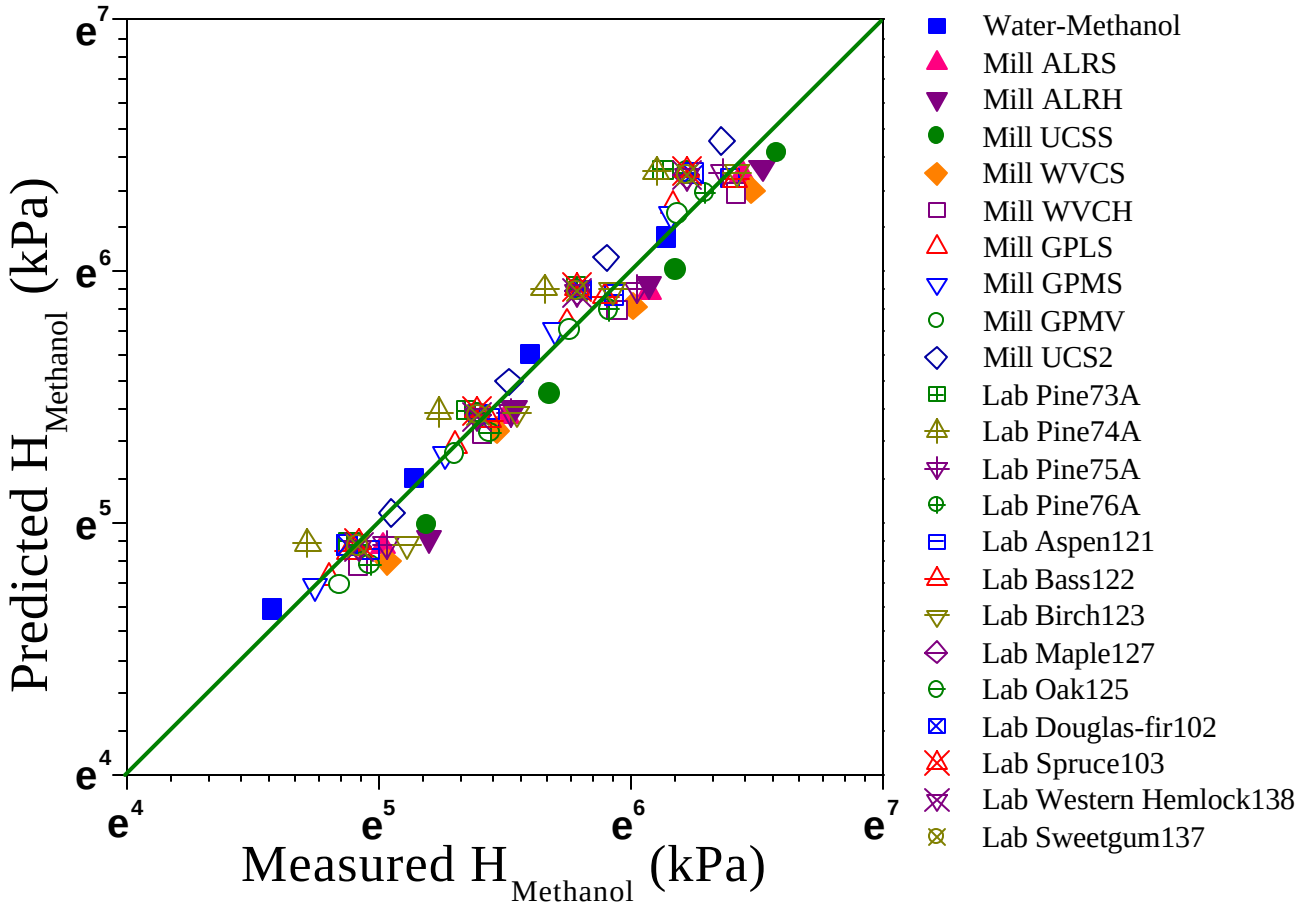

Fig. 3.23. Comparison of measured methanol Henry's constants in black liquors with those predicted by the semiempirical correlation.

Table 3.I. Parameters of the van't Hoff equation for n-alkanols in water

n-Alkanols	***a***	***b***	R^2
Methanol	8.969	5206.8	0.9981
Ethanol	10.173	5531.6	0.9979
Propanol	11.830	5923.2	0.9959
Butanol	12.141	5892.0	0.9982
Pentanol	14.233	6559.6	0.9967
Hexanol	11.705	5538.7	0.9982

Table 3.II. Comparison of log(H^*) at 25^{o}C

	Methanol	**Ethanol**	**Propanol**	**Butanol**	**Pentanol**	**Hexanol**
This Work	-3.69	3.64	-3.49	-3.31	-3.31	-2.98
Exp. Data: Hine & Mookerjee (1975)	-3.72	-3.59	-3.56	-3.46	-3.46	-3.20
Exp. Data: Abraham (1987)	-3.74	-3.67	-3.56	-3.46	-3.46	-3.23
Exp. Data: Li & Carr (1993)	-3.74	-3.66	-3.54	-3.45	-3.45	-3.20
Group Contribution: Hine & Mookerjee (1975)	-3.83	-3.70	-3.55	-3.41	-3.41	-3.12
Bond Contribution: Hine & Mookerjee (1975)	-3.89	-3.72	-3.54	-3.37	-3.37	-3.02
QSAR: Nirmala-Khandan & Speece (1988)	-3.65	-3.59	-3.49	-3.39	-3.39	-3.19

Table 3.III. Partial molar excess enthalpy at infinite dilution for n-alkanols

Unit in J/mol	**Methanol**	**Ethanol**	**Propanol**	**Butanol**	**Pentanol**	**Hexanol**
This Work	-7,916	-9,069	-3,419	-2,217	-1,756	7,344
Calorimetric Values Trampe and Eckert, 1991	-7,000	-10,020	-9,900	-8,740		
Calorimetric Values Korolev et al., 1985	-7,050	-9,750	-9,810	-9,315		
From γ^{∞} data Pividal et al., 1992	-5,100	-2,750				
From γ^{∞} data Bergmann, 1990	-4,000					

Table 3. IV. Dimensionless methanol Henry's constants, H*, in aqueous salt solutions measured in this research

	Salt Concentration (mol/kg)	40°C	50°C	60°C	70°C
H2O	0	0.000476	0.000769	0.00132	0.00161
Na_2CO_3	0.5	0.000553	0.000867	0.00146	0.00193
	1.0	0.000611	0.00101	0.00166	0.00197
	1.5	0.000747	0.00119	0.00182	0.00227
Na_2SO_4	0.4	0.000537	0.000921	0.00153	0.00187
	0.8	0.000656	0.00121	0.00209	0.00309

Table 3.V. A list of fitting parameters of Eq. (3.1) for a water-methanol mixture and black liquors.

Sample	a	b	Correlation Coefficient
Water-Methanol	-5878	22.766	0.9992
Mill ALRS	-5337	21.708	0.9996
Mill ALRH	-5164	21.024	0.9981
Mill UCSS	-5092	20.729	0.9996
Mill WVCS	-5179	20.835	0.9999
Mill WVCH	-5525	22.118	0.9980
Mill GPLS	-5119	20.988	0.9947
Mill GPMS	-5553	22.187	0.9983
Mill GPMV	-5734	22.648	0.9996
Mill UCS2	-5325	21.233	0.9997
Lab Pine73A	-5101	20.623	0.9999
Lab Pine74A	-4930	20.305	0.9991
Lab Pine75A	-4793	19.723	0.9991
Lab Pine76A	-5120	20.857	0.9996
Lab Aspen121	-5452	21.825	0.9997
Lab Bass122	-5767	22.733	0.9996
Lab Birch123	-4907	20.281	0.9976
Lab Oak125	-4305	18.366	0.9947
Lab Maple127	-5010	20.527	0.9996
Lab Douglas-fir102	-5175	20.903	0.9995
Lab Spruce103	-5128	20.787	0.9997
Lab Western Hemlock138	-4872	19.947	0.9998
Lab Sweetgum137	-4912	20.124	0.9996
Mean	**-5190**	**21.01**	**0.9989**
RSD	**6.9%**	**5.0%**	**0.15%**

CHAPTER 4: VOC FORMATION IN KRAFT PULPING

As we discussed previously, methanol has been identified as the major alcohol in pulp mill process streams [1-4]. Methanol is soluble in water and can increase the biochemical oxygen demand (BOD) [5]. Furthermore, it can also be released into the atmosphere at the process temperatures of kraft mill streams. Methanol is primarily produced through the pulping process in digesters. Its formation during pulping depends on the pulping time, temperature, hydroxide concentration or alkalinity, and wood species [5]. Two different mechanisms of methanol formation in pulping processes are generally accepted [6-8]: the rapid alkali-catalyzed elimination of methanol from the 4-O-methylglucuronic acid residues in hemicellulose [6] to form hexenuronic acid groups and methanol, and the demethylation of lignin [7, 8]. However, the amount of demethylated methoxyl groups in lignin in an alkaline pulping process is small according to Sarkanen et al. [8]. Therefore, it is reasonable to assume that a substantial amount of methanol is formed through the demethylation of xylan [6, 8]. Because most of the methoxyl groups in lignin have not been demethylated during pulping [8], they can be hydrolyzed to form methanol in the downstream processes, such as bleaching and chemical recovery, whenever a set of favorable reaction conditions exists.

In this part of the study, we validated methanol formation through alkali-catalyzed elimination of methanol from hemicellulose during wood pulping by measuring the hexenuronic acid groups in pulps and methanol in the pulping spent liquors. The study also investigated the effect of four pulping processes, i.e., soda, kraft, polysulfide kraft, and multistage kraft, and pulping conditions, i.e., different alkali charges, sulfidities, and catalyst anthraquinone (AQ), on methanol formation. The effects of kappa number and wood species (both hardwood and softwood) on methanol formation were also studied. The results indicated that the alkali-catalyzed reactions of xylan contribute to about 40% of the total methanol formation in kraft pulping of southern pine to bleachable grade. For a given active alkali (AA) charge and kappa number, soda pulping produced more methanol than kraft and polysulfide kraft pulping processes did; furthermore, both the increase in sulfidity and the addition of catalyst AQ reduced methanol formation.

4.1 Experimental

4.1.1 Pulping

Three sets of pulping experiments were conducted. The first two sets of experiments were conducted at the Institute of Paper Science and Technology. The third set was conducted at the North Carolina State University (NCSU).

The first set of pulping experiments was conducted using eight rotating bomb digesters to study the effect of kappa number and wood species on methanol formation in pulping. The volume of each bomb digester was 500 mL. Fifty grams of oven-dry wood chips of four softwoods (Douglas-fir, white spruce, western hemlock, and loblolly pine) and six hardwoods (aspen, bass, birch, maple, oak, and sweetgum) were used in each cook. For the pulping of southern pine, the cooking liquor-to-wood-chip ratio was 4.0 L/kg. Conventional kraft, soda, polysulfide kraft, and multistage kraft pulping processes to simulate RDH processes were conducted. The active alkali charge AA (as Na_2O) was maintained at 18% on wood for all the pulping processes except the multistage pulping. Three sulfidities of S=10, 20, and 30% and four AQ concentrations of 0, 0.025, 0.05, and 0.1% on wood were used in kraft pulping. A polysulfide concentration of 1.5% on wood and a sulfidity of S=18% were used in polysulfide kraft pulping. The multistage pulping processes were designed as follows: Stage 1 used black liquor with AA=9 g/L (as Na_2O) and Na_2S=12 g/L and lasted 20 minutes when pulping temperature was raised from 100 to 130^{o}C, Stage 2 used black liquor with AA=15 g/L and Na_2S=12 g/L and lasted 20 minutes when pulping temperature was raised from 130 to 160^{o}C, and Stage 3 used white liquor with AA=18% and sulfidity S=30% and lasted to the end of the cook and varied for different cooks. Therefore, some of the cookings may only have experienced Stage 1 or 2, depending on the total cooking time used to achieve the desired kappa number. For the pulping of the rest of the wood species, the pulping liquor-to-wood ratio was 3.7, sulfidity was 31%, and the active alkali charge was 17% for softwoods and 16% for all hardwoods. For each set of pulping conditions selected, cooking temperature was first linearly ramped from a room temperature of 23^{o}C to 170^{o}C in 70 minutes or at a rate of 2.1^{o}C per minute, then maintained at 170^{o}C to continue delignification. The pulping processes in different digesters were terminated at different pulping times to obtain the rates of formation of methanol and hexenuronic acid. By this approach, the effect of kappa number on methanol formation was

obtained. The pulp kappa numbers were measured using the standard TAPPI Test Method (T236 cm-85) [9].

The second set of experiments was conducted in a laboratory batch digester (ME&K) to mainly study the time-dependent formation characteristics of various VOCs in conventional pulping processes. The load of each batch cooking was 800 grams of oven-dried (o.d.) chips. Both southern pine (softwood) and birch (hardwood) were used. Southern pine and birch were pulped separately by both kraft and soda processes, with and without a catalyst, anthraquinone (AQ). The EA charge was 18% and sulfidity was 25% for kraft pulping. After the addition of the chips and cooking liquor, the temperature of the digester was raised from room temperature to 100^{o}C in 20 minutes. Then it was brought to 170^{o}C in an hour, and maintained at 170^{o}C for two hours. After the completion of the cooking, the digester was cooled to room temperature by draining the black liquor. The pulp was thoroughly washed before the handsheets were made for kappa number and viscosity analysis. During each cooking process, a small amount (15 mL) of cooking liquor was collected at about 15-20 minute intervals after the temperature reached 100^{o}C.

The third set of experiments was conducted at NCSU to study the effect of alkali charge, sulfidity, and cooking temperature on methanol formation. Three hundred grams of wood chips at a liquor-to-wood ratio of 4:1 were pulped in 3-liter reactors in a rotating autoclave. At the end of a cook, each reactor was cooled in an ice bath to ensure condensation of the volatiles before opening the reactor. The black liquor was stored in sealed vials and kept in a refrigerator until tested for methanol content. The yield and kappa number were determined for the pulp by TAPPI standard methods.

4.1.2 Analyses of Methanol and Hexenuronic Acid Groups (HexA)

The analytical method [3] described in Chapter 1 of this report was used for methanol analysis in black liquor in the first sets of experiments. The EPA Method 1624 using a 5890 Gas Chromatograph with purge and trap capability was employed at NCSU for methanol analysis in weak black liquor. The GC capillary column was an HP-INNOwax (crosslinked polyethylene glycol) and the trap column was a VOCARB 3000 (CarbopackB/Carboxen 1000 and 1001). A 5-mL black liquor sample size was used with a cyclopentanol internal standard. One drop of defoamer was added to reduce foaming of the black liquor during the purge and trap procedure.

The UV-spectrophotometric HexA analysis method that we developed [10] uses a low absorptive mercuric chloride hydrolysis agent together with a spectral compensation technique to directly and rapidly (each measurement only takes 30 minutes) determine HexA concentration in chemical pulps obtained in the second set of pulping experiments. In this method, 22 mM (0.6%) mercuric chloride and 0.7% sodium acetate, of analytical grade from commercial sources, are used to make a hydrolysis solution. Then approximately 0.05 gram of air-dried pulp handsheet with a known moisture content is accurately weighed and put into a 20-mL vial with 10 mL of hydrolysis solution. The mixture is sealed in the vial by a septum. To obtain good mixing of the pulp with the hydrolysis solution, we shake the vial and then heat the mixture for 30 minutes in a water bath with a temperature range of 60-70°C. After the solution is cooled to room temperature, UV absorption measurements of the filtered solution are conducted in a 10-mm path length silica cell using a commercial spectrophotometer (UV-8453, Hewlett-Packard, now Agilent Technologies) at a wavelength range of 260 to 290 nm.

4.2 Results and Discussion

4.2.1 The First Set of Experiments

4.2.1.1 Understanding Methanol Formation During Pulping

Figure 4.1 shows the time-dependent methanol and pulp kappa data of three replicate experiments of conventional kraft pulping of southern pine obtained in the second set of experiments. The methanol data are presented as kilogram per metric ton of oven-dry pulp based on measured pulp yields and methanol concentrations in the pulping spent liquors. The time-dependent methanol data show similar characteristics to those obtained in the first set of experiments [11] using a different batch digester (ME&K), i.e., methanol formation is slow initially due to low cooking temperature, then increases rapidly as the temperature reaches 170^{o}C, and finally levels out. A certain amount of methanol was formed instantly at the beginning of the pulping process. Although these three sets of experiments were conducted in a six-month period, the results show remarkable repeatability. We measured the amount of HexA in the pulp samples obtained in the kraft conventional pulping processes of southern pine with sulfidity S=30% and active alkali charge AA=18% to validate the mechanism of methanol

formation through rapid alkali-catalyzed elimination of methanol from 4-O-methylglucuronic acid residues in hemicellulose [6]. According to the alkali-catalyzed methanol formation reaction of 4-O-methylglucuronic acid residues [6], the production of one mole of HexA will be accompanied by the formation of one mole of methanol. Figure 4.2 shows the correlation of the measured methanol in the pulping spent liquors and the measured HUA in the corresponding pulps. Because the methanol formation is not linearly dependent on cooking time, as shown in Fig. 4.1, the pulping temperature is not a linear function of methanol formation in Fig. 4.2. The data indicate that the amounts of methanol measured in the pulping spent liquors are linearly proportional to the amounts of HexA found in the pulps up to a methanol level of 53 mol/oven dried ton (ODT)-wood or 1.66 kg/ODT-wood (R^2=0.9938) when the pulping temperature reaches 160^{o}C. Furthermore, the slope of the linear relationship is close to unity (0.90, to be exact, from least-squares fitting of the first three data points, corresponding to pulping time of 65 minutes and temperature 160^{o}C.) Therefore, the amount of HexA dissolution and the amount of methanol formation from lignin demethylation in the pulping liquor are negligible. This validates the 1:1 relationship of the amounts of methanol and HUA formed through the xylan degradation reaction. The slightly lower-than-unity (10%) slope of the linear relationship is perhaps due to the fact that some of the HexA formed associated with methanol formation is no longer with the pulp and is dissolved into the pulping spent liquors. It is noticed that the methanol-HexA linear line does not pass through the origin of the coordinate with a positive methanol intercept of 32 mol/ODT-wood (or 1.0 kg/ODT-wood) when HexA (measured) = 0. This is perhaps due to the fact that some of methanol was released instantly at the beginning of cooking by the degradation reactions. We conducted cooking of southern pine wood chips using pure water heated up to 170^{o}C to verify this argument. From the measurements in the final cooking solution, about 28 mol/ODT-wood (or 0.875 kg/ODT-wood, very close to the intercept of 1.0 kg/ODT-wood shown in Fig.4.2) of methanol was obtained.

From the experimentally obtained unity slope of the methanol and HexA relationship, we can conclude that except for the methanol that is released instantly at the beginning of the pulping process, the elimination of methanol from xylan is the only methanol formation mechanism during the initial pulping process and lignin demethylation does not contribute to methanol formation below pulping temperature 160^{o}C (corresponding to a kappa number of 140). Figure 4.2 also shows that the methanol-HexA data deviate from the linear relationship as

delignification continues after pulping temperature reaches 160^{o}C. However, this deviation is not significant until the kappa number reaches about 120, indicating that lignin demethylation may start to contribute to methanol formation. With the completion of the methanol elimination reaction from xylan and further HexA dissolution into the solution, the HexA content measured in pulp decreases as pulping continues. One can extrapolate the maximum measurable amount of HexA content in wood (about 46 mol/ODT-wood) from the data presented in Fig. 4.2. Based on the extrapolation, the contribution of methanol elimination from the xylan to methanol formation can be estimated to be about 51 (=83-32, calculated from the least-square fitted equation shown in Fig. 2) mol/ODT-wood (or 1.59 kg/ODT-wood). The remaining 42 (=125-51-32, the total formation is 125) mol/ODT-wood (or 1.31 kg/ODT-wood) is the contribution from lignin demethylation. Based on this calculation, we can conclude that for bleachable-grade pulping of southern pine, methanol formation from xylan is the major factor contributing to methanol formation in pulping processes, accounting for about 40% of the total methanol formed (as measured from the final cooking spent liquor). Lignin demethylation accounts for about 35%.

4.2.1.2 Effect of Sulfidity

Figure 4.3 shows the effect of sulfidity on methanol formation during kraft pulping of southern pine. The results plotted as methanol versus pulp kappa numbers clearly show that increasing sulfidity reduces methanol formation at a given pulp kappa number. There are two factors that might explain this phenomenon. A longer cooking time is required in a lower-sulfidity pulping process to achieve the same kappa number than that required in a higher-sulfidity pulping process; a longer cooking time will increase methanol formation. Secondly, a lower sulfidity means a higher effective alkali concentration in the pulping liquor because the active alkali was maintained at 18% for all the pulping processes; an increase in effective alkali (or HO^{-} concentration) leads to an increase in methanol formation. The HexA data obtained in our previous study [12] of alkaline pulping of southern pine (not presented in the present paper) indicate that the amount of HexA in pulp decreased with the increase of sulfidity at the same kappa number, which verifies the second argument. More results on effect of sulfidity on methanol formation were obtained in the third set of experiments, presented later in this chapter.

4.2.1.3 Effect of Catalyst Anthraquinone (AQ)

Figure 4.4 shows the effect of AQ addition on methanol formation in conventional kraft pulping. Although the data show some scattering, the results clearly indicate that AQ can reduce methanol formation. This reduction is not very significant at a low-dosage application (a single curve was drawn for the two data sets of no AQ and 0.025% AQ addition in Fig. 4.4). However, at a high-dosage application, i.e., 0.1%, the reduction of methanol formation is very significant. This phenomenon can be explained by the accelerated delignification due to the catalyst AQ, which reduces the cooking time to achieve the same kappa number. A dosage of 0.1% AQ may not be permitted in many mills; however, the results indicate that AQ can be used in mills not only to facilitate delignification but also to reduce methanol formation.

4.2.1.4 Effect of Pulping Processes

Figure 4.5 shows the effect of pulping processes on methanol formation as a function of pulp kappa number. Data with a kappa number greater than 130 were excluded in Fig. 4.5. The data clearly show the difference in methanol formation among various pulping processes. Soda cooking produces much more methanol than kraft cooking at a given kappa number. There are two factors that contribute to the higher methanol formation in soda pulping. Firstly, the delignification rate is lower in soda pulping than in kraft pulping. A longer pulping time is required to achieve the same kappa number in soda pulping than that required in kraft pulping. Secondly, the effective alkali is higher in soda pulping than in kraft pulping because the active alkali was maintained at 18% for both the soda and kraft pulping processes; an increase in effective alkali (or HO^- concentration) results in more methanol formation.

The results in Fig. 4.5 also show that polysulfide kraft pulping processes consistently produce less methanol than conventional kraft pulping processes. Polysulfide can reduce the degradation of hemicellulose through the peeling-off reactions of oxidation of end groups to carbolic acid groups to reduce methanol formation. The methanol formation in RDH pulping processes is slightly less than that in kraft pulping. This may be explained by the lower effective alkali used in the first and second stages in an RDH pulping process.

4.2.1.5 Effect of Wood Species

Conventional kraft pulping experiments of various wood species were carried out to investigate the effect of wood species on methanol formation as shown in Figs. 4.6 and 4.7. The data are averaged over 2-5 replicate experiments. The specific number of replicate experiments varies with wood species. Figure 4.6 shows the results obtained from the pulping of softwoods. Four softwoods of Douglas-fir, white spruce, western hemlock, and southern pine were used. Both bleachable (kappa number around 30) and linerboard (kappa number around 60) pulps were produced. Figure 4.6 shows that western hemlock and southern pine produce the least (7.3 kg/ODT pulp) and most (9.3 kg/ODT pulp) amounts of methanol in bleachable-grade pulping of softwoods, respectively. Figure 6 also shows that Douglas-fir and southern pine produce the least (5.6 kg/ODT pulp) and most (7.3 kg/ODT pulp) amounts of methanol in linerboard-grade pulping, respectively. Furthermore, the difference in methanol formation between bleachable and linerboard pulping processes is the smallest (1.3 kg/ODT pulp) for western hemlock and largest (2.7 kg/ODT pulp) for Douglas-fir.

Figure 4.7 shows the methanol formation data during pulping of six hardwoods: aspen, bass, birch, maple, oak, and sweetgum. Bleachable (kappa number around 14), liner-board (kappa number around 50, a little lower than the anticipated value of 60), and an intermediate kappa (kappa number around 25) grades of pulps were produced. For bleachable-grade pulp, the methanol formation is highest (15.0 kg/ODT pulp) and lowest (9.6 kg/ODT pulp) when pulping sweetgum and aspen, respectively. The variation in methanol formation in linerboard-grade pulping of various hardwoods is not very significant, ranging from 4.3 to 5.4 kg/ODT pulp. However, the results show that the difference in methanol formation between bleachable and linerboard pulping is about 75-300%.

Overall, the results in Figs. 4.6 and 4.7 indicate that hardwoods produce more methanol than softwoods when producing an equivalent grade of pulp, which agrees with the results obtained in the second set of experiments [11] to be discussed later. The total methanol formation varies from wood to wood mainly due to the differences in structure between softwood xylan and hardwood xylan and the variations of methoxyl group content in xylan and lignin of the woods.

4.2.2 The Second Set of Experiments: The Formation of Ketones

Figures 4.8 and 4.9 show the concentration profiles of VOC's during kraft and soda pulping of softwood and hardwood. We found that the methanol concentration profiles are almost identical for both except that more methanol is produced in hardwood cooking than in softwood cooking. More methanol formation was also reported by Wilson et al. [13]. Hardwood has a higher content of 4-O-methyl-D-glucuronoxylans in hemicellulose than softwood does, and hardwood lignin has more methoxyl groups than softwood lignin does [14]. Softwoods contain only coniferyl alcohol, while hardwoods contain both coniferyl (50-75%) and sinapyl alcohols (25-50%). Sinapyl alcohol contains more methoxyl groups than coniferyl alcohol as shown in Fig. 4.10. Furthermore, the peak methanol formation rate in hardwood pulping is higher than that in softwood pulping. Ninety percent of the methanol was formed within the first 75 minutes in the hardwood pulping processes. It took about 90 minutes to achieve 90% of the methanol in softwood pulping.

According to Wilson and Hrutfiord [1], all of the ketones found in pulping, as methyl ketones, are formed through the air oxidation of extractives followed by decomposition of the extractive hydroperoxide, which undergoes a reverse alcohol condensation at a high temperature in the digester. We found in this study that the major ketone species generated in all the pulping processes were acetone and MEK. The concentration profiles of these ketones during the pulping were quite different from those of methanol as shown in Figs. 4.8b and 4.9b. In the cookings of the softwood, the profiles of acetone and MEK measured in the kraft pulping process are similar to those measured in the soda pulping, i.e., the concentrations of acetone and MEK reached a maximum at 50 minutes and then decreased after the cooking temperature reached 170^{o}C. This behavior could be explained as a result of hemiacetals, or hemiketals, reactions between methanol and ketones [15]. Either acetals or ketals can react with methanol to form hemiacetals or hemiketals under certain conditions as follows:

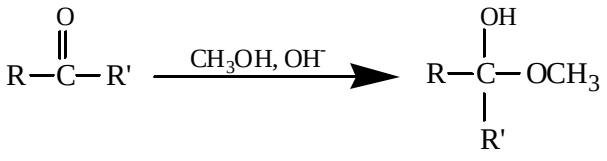

Aldehyde or ketone — Hemiacetal or hemiketal (14)

which leads to a decrease in ketone concentration as cooking continues. However, some other researchers believe that the equilibrium between acetal/ketal and the corresponding aldehyde/ketone is unaffected by hydroxide [16], which contradicts the above explanation. The results also show that the acetone and MEK concentrations in the kraft hardwood pulping process did not decrease until very late in the cooking process for unknown reasons as shown in Fig. 4.9b. Further study is needed to understand the reaction mechanism. Figs. 4.8b and 4.9b also show that more acetone than MEK is formed in both kraft and soda pulping of a hardwood and a softwood.

4.2.3 The Third Set of Experiments

Statistical analysis of the data was done using Statistical Analysis System, SAS [17]. Tables 4.A1 and 4.A2 and Figs. 4.1A and 4.2A in the appendix of this chapter show the raw data collected from the softwood and hardwood cooks. The cooks for both species types were replicated, but the data from the first set of softwood cooks were lost due to procedural errors.

4.2.3.1 Softwood Results

Figure 4.11 shows the methanol data from the softwood cooks plotted as a function of kappa number. As expected, the methanol increases with decreasing kappa number, in agreement with the results obtained in the first set of experiments at IPST [18]. The data range from about 10 to 22 lb methanol/ODT pulp for a kappa number range of 78 to 18. Due to the nature of the experimental design, however, it is difficult to determine from a graph like Figure 4.11 the exact relationship between each of the four cooking variables and the methanol generated.

Nonlinear statistical analysis of the kappa number data resulted in the following model:

*Kappa # = 150.5-6.6388*AA*(1-exp(-Hfactor/655))-26.4405*(1-exp(-S/12.8809))*

with R^2=0.92; AA=active alkali, and S=sulfidity, as previously defined.

Figure 4.12 shows the plot of predicted kappa number from the model against the actual value. Good agreement is achieved with this model.

Linear regression was used for analysis of the methanol generation as a function of cooking conditions. The model for methanol prediction is shown below.

$$Methanol\ (lb/ODT) = 559.1169 - 33.106*AA - 0.00465*AA*Kappa\# + 0.2034*AA*T - 3.33*T$$

The R^2 for the model is 0.61 and predicted versus actual methanol is shown in Figure 4.13. Note that sulfidity is not a significant variable in the methanol generation equation except through its contribution to kappa number, in agreement with the conclusion drawn from the first set of experiments conducted at IPST [18]. Figure 4.14 shows predicted methanol generated versus kappa number at AA=18%, sulfidity=30%, temperature = 170°C; the H-factor was varied for different kappa numbers. Also shown are reference data points reported in the first set of experiments [18] (also shown in Fig. 4.5 in this report). The prediction agrees reasonably well with the reference data, although there seems to be some spread in both the reference and predicted data below a kappa number of 30.

Figures 4.15 and 4.16 show predicted methanol generation versus predicted kappa number for selected active alkali of 18% and temperature of 170°C for three levels of sulfidity. As shown in Figure 4.15, with increasing H-factor the kappa number decreases and the methanol increases at each level of sulfidity. Increasing the sulfidity at a given H-factor causes a slight increase in methanol generated. However, as shown in Figure 4.16, the effect of sulfidity on methanol is linear with respect to kappa number.

More significant results are seen in the effects of alkali and temperature. Figure 4.17 shows methanol as a function of H-factor at two temperature and three active alkali levels. At a constant temperature, H-factor is representative of time in the cook. The points were derived by varying the H-factor to achieve constant kappa numbers. Taken in sequence starting from the left, the kappa numbers in each series are 68.1, 53.5, 44.2, 38.4, 34.7, and 33.0. As expected, as kappa number decreases methanol generation increases. At 170° C, as active alkali increases, methanol generation increases. At 160° C, however, as active alkali increases, methanol generation decreases. This might be the result of the fact that at low temperature and low alkali, the cook must be longer to reach a given kappa number. Thus, for 160° C, the 15% active alkali condition gives a higher methanol than the 19% alkali due to a longer cooking time. On the other hand, at 170°C, the 15% alkali gives a lower methanol than the 19% alkali, in spite of being a longer cook. Clearly, the interaction of cooking variables in determining the methanol generation is no simple matter.

Figure 4.18 further demonstrates this point in a plot of points at the same kappa number, taken from Figure 4.17. In this representation, the increasing methanol with decreasing active alkali at low temperature is shown for kappa numbers of 68.1 and 34.7. The reverse true for the higher temperature – increasing alkali produces increasing methanol. The behavior is consistent over the kappa number range of this study. Since each circle of points represents the same kappa number, clearly some combinations are preferred over others for minimizing the amount of methanol produced in a cook. Thus, it can be concluded that high active alkali/high temperature and low active alkali/low temperatures will produce higher levels of methanol.

4.2.3.2 Hardwood Results

Figure 4.19 shows the methanol data from the hardwood cooks plotted as a function of kappa number. The data range from about 18 to 77 lb methanol/ODT pulp for a kappa number range of 37 to 11. For the conditions used, the majority of the data is clustered in the kappa number range of 10 to 20 with the methanol mostly between 20 to 40 lb/ODT. As expected, the methanol generated from hardwood is significantly higher than that from the softwood cooks [1,13, 18].

Nonlinear statistical analysis of the kappa number data using the same form as the softwood model resulted in the following equation:

$$Kappa\ \# = 40.7886 - 1.294*AA*(1-\exp(-Hfactor/432.8)) - 7.2018*(1-\exp(-S/23.5738))$$

with R^2=0.23; AA=active alkali, and S=sulfidity, as previously defined.

Figure 4.20 shows the plot of predicted kappa number from the model against the actual value. The prediction at higher kappa numbers is not very good and the remainder of the analysis will focus on kappa numbers of about 20 or below, which is also the predominant range of the experimental data.

Linear regression analysis resulted in the following model:

$$Methanol,\ lb/ODT = -175.34 + 0.73*AA + 5.99*S + 36.06*Hfactor^{0.1} - 0.016*AA*T - 0.33*AA*S$$

The R^2 for the model is 0.61 and predicted versus actual methanol is shown in Figure 4.21. Note that, unlike the softwood model, for hardwoods sulfidity is a significant variable in the methanol generation equation, and H-factor appears in the equation instead of kappa number. Figure 4.22

shows predicted methanol values at AA=18%, sulfidity=30%, temperature=170°C, and variable H-factor to generate different kappa numbers. As kappa number decreases, the methanol increases. Also shown in the figure are reference data points obtained from the first set of experiments [18]. Since the chips used in this study consisted of a mixture of hardwoods, it is not unexpected that the methanol prediction is intermediate to the points for the single species in the first set of experiments [18].

Figure 4.23 shows the methanol generated as a function of kappa number at three levels of sulfidity. As sulfidity increases, the methanol increases. This result indicates a greater dependence on sulfidity for hardwood than that indicated for softwood, as shown in Figure 4.16.

Figures 4.24 and 4.25 show the effects of alkali and temperature at a sulfidity of 25%. As discussed in the softwood section for Figures 4.17 and 4.18, the H-factor was varied in order to keep the kappa numbers constant between the sets of conditions. The kappa numbers are 21.5, 19.1, 17.9, 17.3, 17.0, and 14.6, reading from left to right on Figure 4.24. The figure shows that methanol increases as AA decreases at both low and high temperatures. At a constant AA, methanol is higher at the lower temperature, and that holds true at all three AA levels. Figure 4.25 shows conditions to achieve kappa numbers of 21.5 and 17 and clearly shows that the high alkali and high temperature result in the lowest methanol generation, with alkali being more significant than the temperature. Similar results were found at sulfidity of 40%. However, as shown in Figure 4.26, at 15% sulfidity, it was found that increasing alkali increased methanol generation at both levels of temperature. Increasing the temperature at constant alkali still resulted in lower methanol, as was seen at the other sulfidity levels. There appears to be some minimum sulfidity, below which the response to increased alkali changes from decreasing to increasing the methanol generation.

4.3 Conclusions

We conducted laboratory pulping experiments using various wood species under various pulping conditions in bomb-type rotating batch digesters. We validated the methanol formation mechanism through alkali-catalyzed methanol elimination from 4-O-methylglucuronic acid groups in hemicellulose [7] of wood xylan by the direct measurements of hexenuronic acid

groups in pulps. The results obtained from the pulping of bleachable grades from southern pine indicate that methanol formation from hemicellulose contributes to about 40% of the total methanol formed. About 25% of the methanol naturally present in wood is released instantly at the beginning of pulping. The remaining 35% of the methanol may be formed as a result of lignin demethylation reactions.

The results also indicate that increasing sulfidity reduces methanol formation for a given active alkali charge in kraft pulping. AQ addition in pulping can reduce methanol formation through increased delignification that results in a short reaction time. Soda pulping produces more methanol than kraft pulping at a given pulp kappa number and active alkali charge. Polysulfide kraft pulping produces less methanol than kraft pulping, possibly due to reduced hemicellulose degradation. Wood species can have a significant effect on total methanol formation. The study further confirms our previous work [10] that hardwoods produce more methanol than softwoods do.

The following conclusions were drawn from the third set of experiments:

The statistical experimental design and analysis resulted in regression models for predicting kappa number and methanol generation as a function of cooking conditions.

Sulfidity played only a small role in the methanol generation in softwoods. There was a small increase in methanol with increasing sulfidity at a given kappa number. On the other hand, sulfidity plays a significant role in hardwood methanol generation, again with increased generation with increasing sulfidity.

For softwood cooks, the interactions between active alkali, temperature, and H-factor/cooking time are complex. To reach a given kappa number, low alkali and low temperature will result in more methanol generation, probably because of the long cooking time required. However, for that same kappa number at high cooking temperature, high alkali results in higher methanol generation.

For hardwood cooks at a given kappa number and moderate to high sulfidity, methanol generation is higher at low alkali and low temperature, again suggesting a cooking time effect, perhaps. However, at low sulfidity, the trend is reversed, with high alkali producing high

methanol at low temperature. A more thorough study of the nature of the sulfidity effect would be necessary to better explain this result.

REFERENCES

1. Wilson, D.F. and Hrutfiord, B.F., *TAPPI J*, **54**(7):1094, 1971.
2. NCASI, "Volatile Organic Emissions from Pulp and Paper Mill Sources, Part IV – Kraft Brownstock Washing, Screening and Rejects Refining Sources," *NCASI Technical Bulletin* No. 678, 1994.
3. Chai, X.S., Dhasmana, B., and Zhu, J.Y, *J. Pulp & Paper Sci*., **24**(2):50, 1998.
4. Bethge, P.O. and Ehrenborg, L., *Svensk Papperstidning,* **70**(10):347, 1967.
5. Ronnholm, A.A.R., *Paperi ja Puu,* No. 11:72, 1977.
6. Clayton, D.W., *Svensk Papperstidning,* **66**(4):115, 1963.
7. Blackwell, B. R., MacKay, W. B., and Murray, F.E., *TAPPI J.,* **62**(10):33, 1979.
8. Sarkanen, K.V., Chirkin, G., and Hrutfiord, B.F., *TAPPI J.,* **46**(6):375, 1963.
9. "Kappa Number of Pulp," TAPPI Test Method T236 cm-85, 1996.
10. Chai, X.S., Zhu, J.Y., and Li, J., *J. Pulp & Paper Sci.*, **27**(5):165, 2001.
11. Zhu, J.Y., Chai, X.S., and Dhasmana, B., *J. Pulp & Paper Sci.,* **25**(7):256, 1999.
12. Chai, X.S., Yoon, S.-H., Zhu, J.,Y., and Li, J. "The Fate of Hexenuronic Acid Groups in Alkaline Pulping of Loblolloy Pine," *J. Pulp and Paper Sci.,* **27**(12), 2000 (in press).
13. Wilson, D.F., Johanson, L.N., and Hrutfiord, B., *TAPPI J.*, **55**(8):1244, 1972.
14. Biermann, C.J., "*Handbook of Pulping and Papermaking,*" 2nd Ed. Academic Press, San Diego, CA, 1996.
15. Wingrove, A.S. and Caret, R.L., "*Organic Chemistry*," Harper & Row, New York, 1981.
16. March, J., "*Advanced Organic Chemistry: Reactions, Mechanisms, and Structure,*" McGraw-Hill, New York, 1968.
17. SAS/STAT User's Guide: Version 6, SAS Institute, Cary, NC, 1990.
18. Zhu, J.Y., Yoon, S.-H., Liu, P.-H., and Chai, X.-S., *TAPPI J.,* **83**(7):65, 2000.

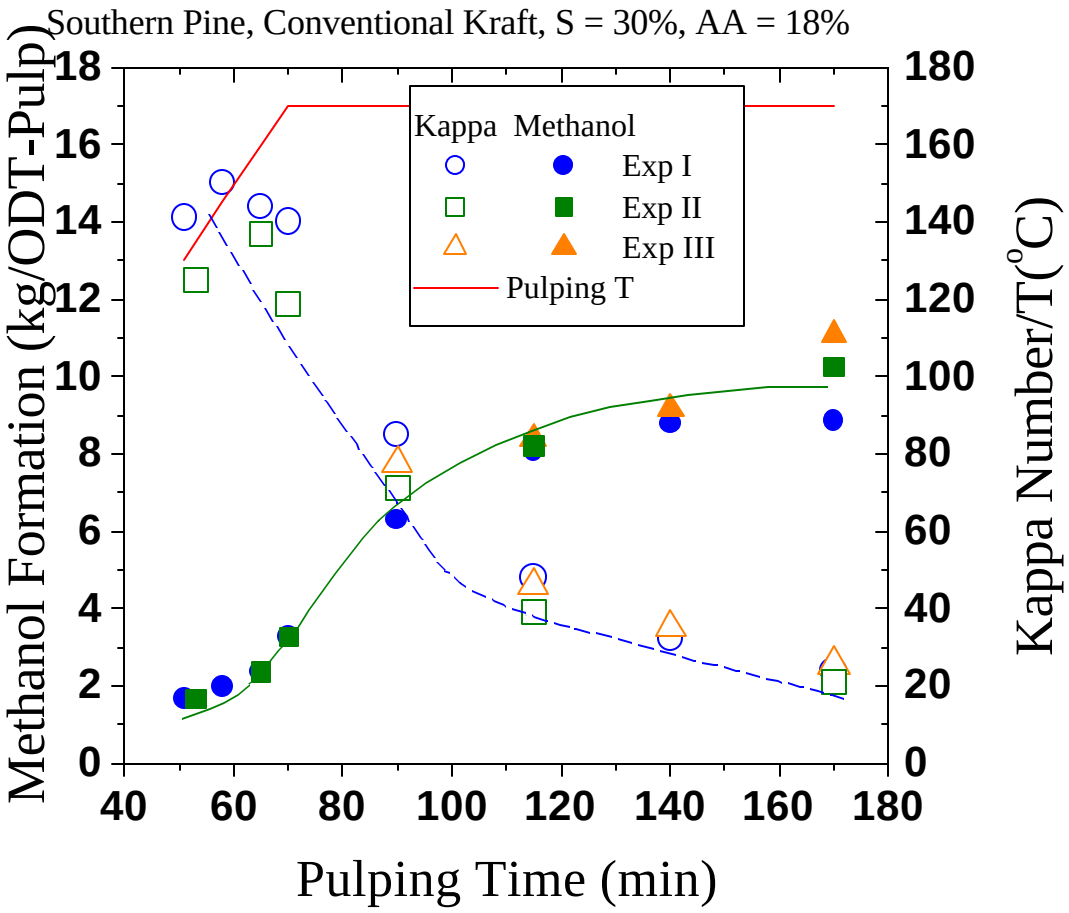

Fig. 4.1. Time-dependent methanol formation during conventional kraft pulping processes.

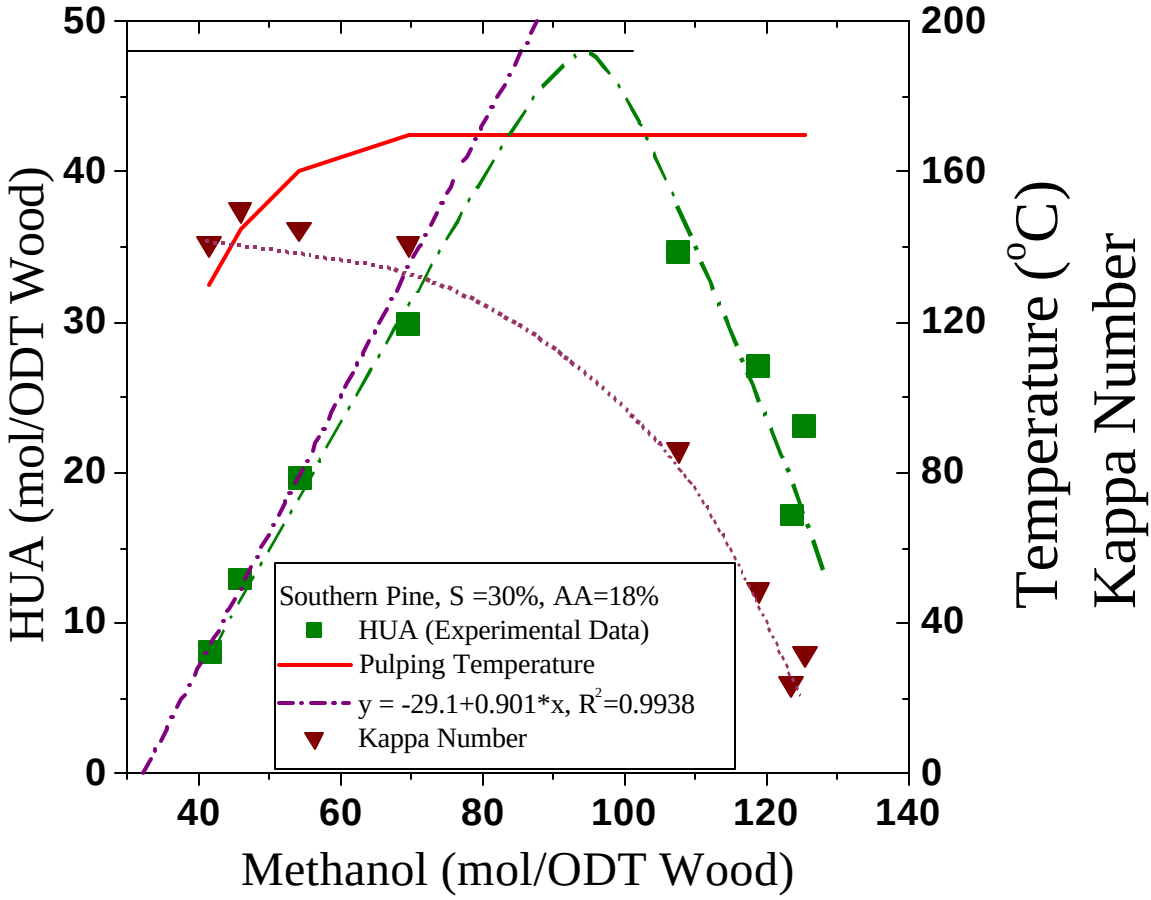

Fig. 4.2. The relationship of measured methanol in pulping liquors and hexenuronic acid groups in pulps in a set of conventional kraft pulping processes.

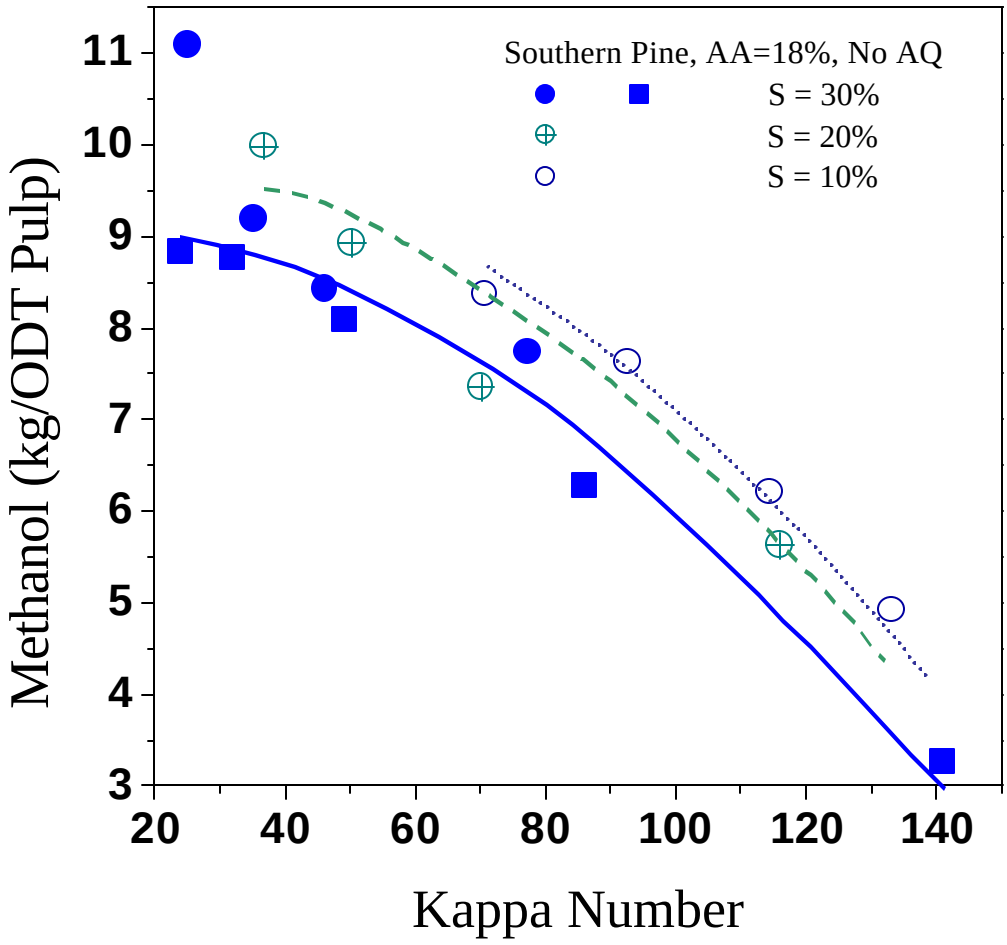

Fig. 4.3. The effect of sulfidity on methanol in conventional kraft pulping of southern pine.

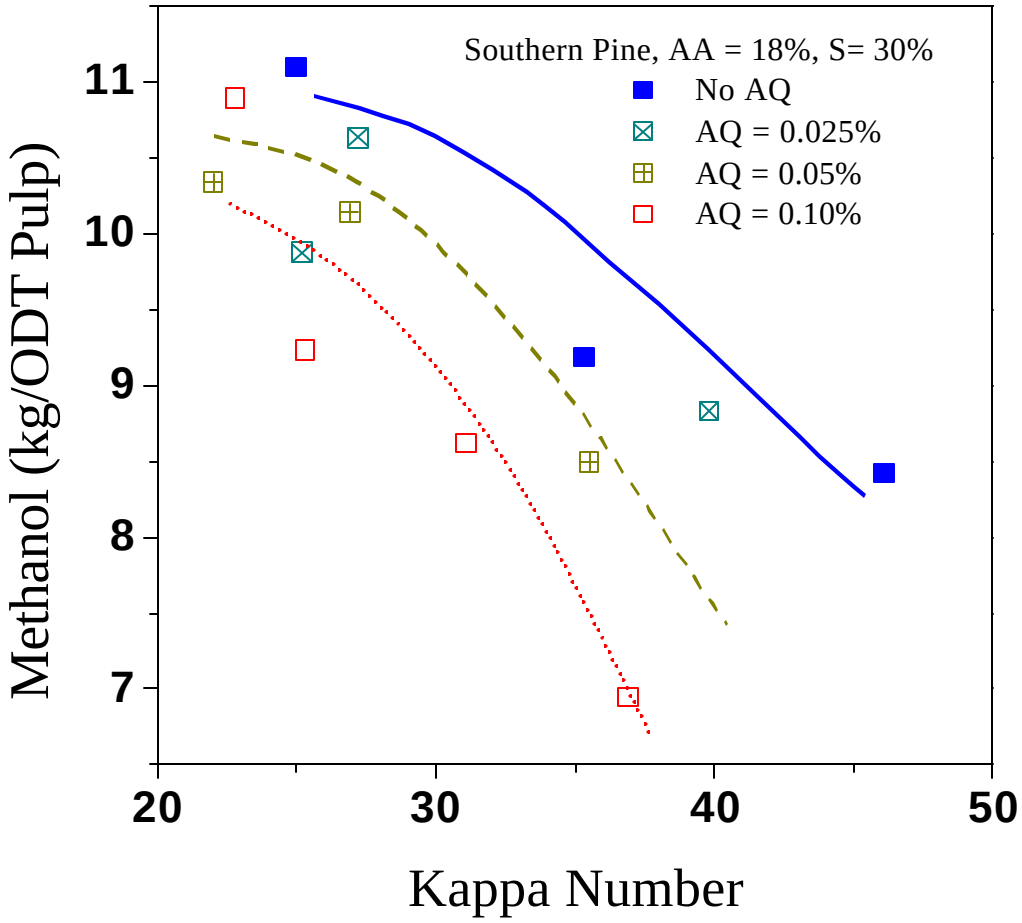

Fig. 4.4. The effect of catalyst AQ on methanol in conventional kraft pulping of southern pine.

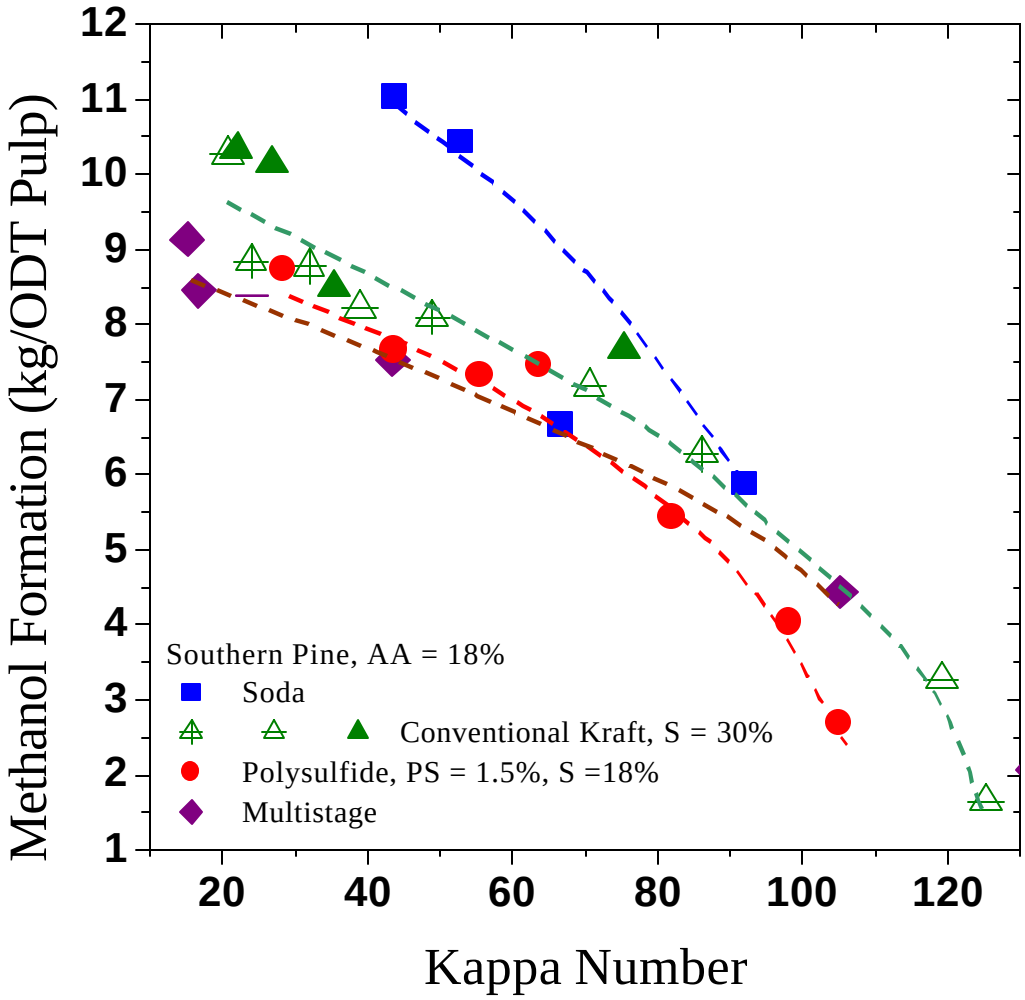

Fig. 4.5. The effect of pulping processes on methanol formation.

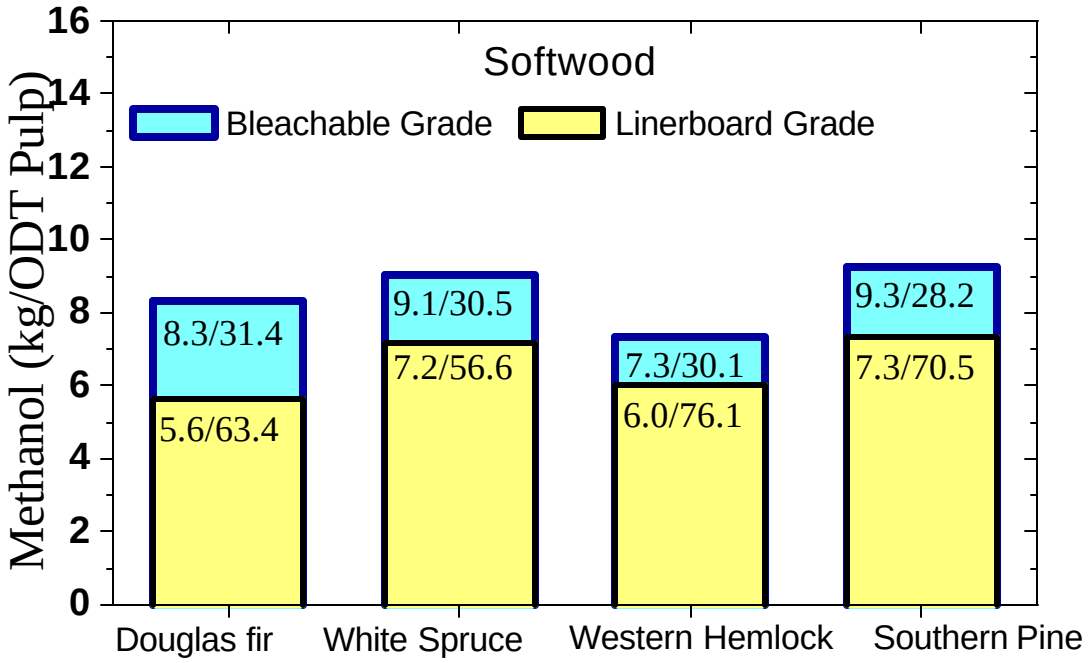

Fig. 4.6. The measured methanol formation data in conventional kraft pulping of four softwoods (the first number in the bar is the methanol formation, and the second number after the slash is the pulp kappa number).

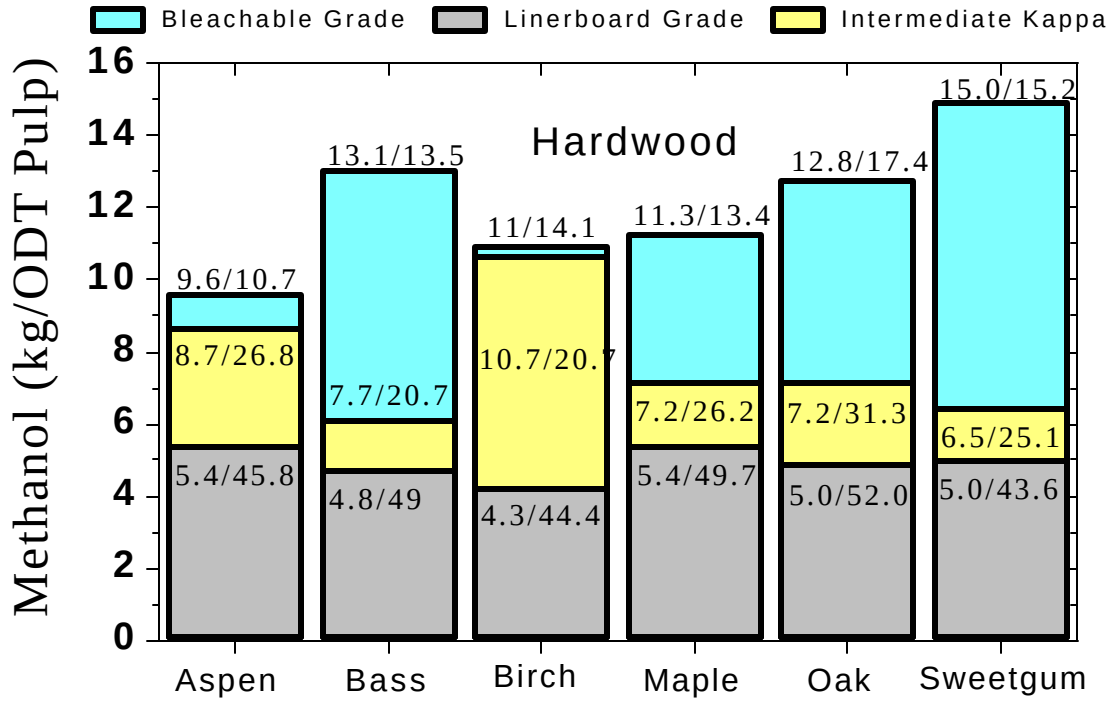

Fig. 4.7. The measured methanol formation data in conventional kraft pulping of six hardwoods (the first number in the bar is the methanol amount, and the second number after the slash is the pulp kappa number).

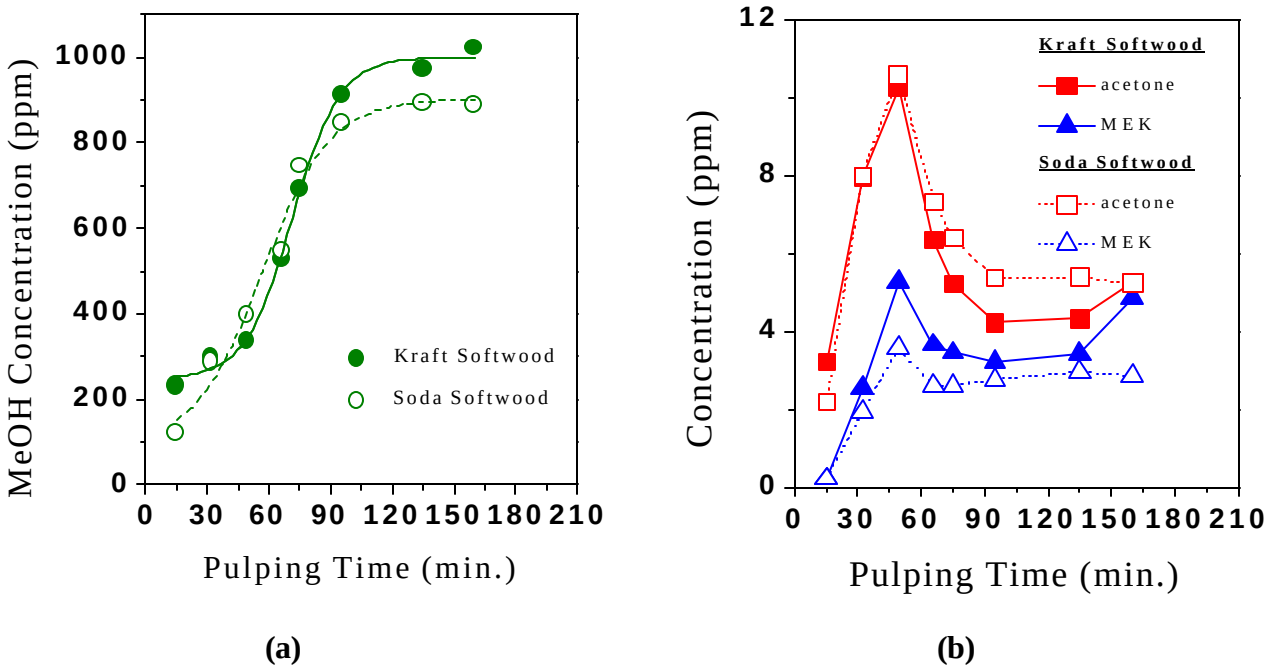

Fig. 4.8. Time-dependent concentration profiles in a softwood pulping process. (a) methanol; (b) acetone and MEK.

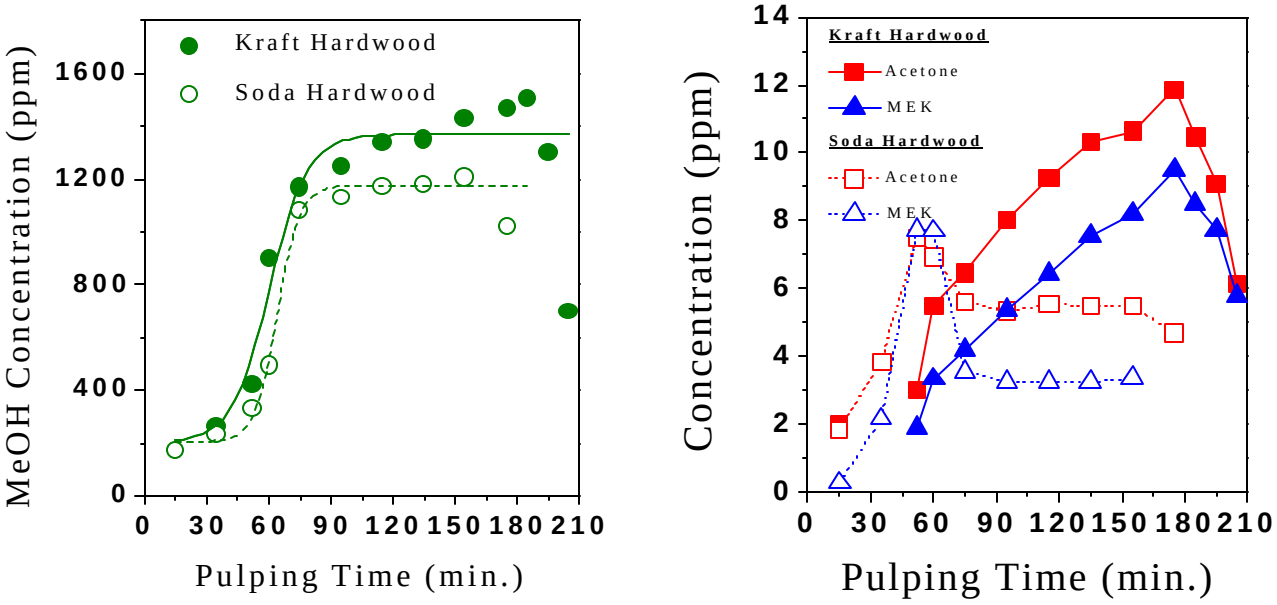

Fig. 4.9. Time-dependent concentration profiles in a hardwood pulping process. (a) methanol; (b) acetone and MEK.

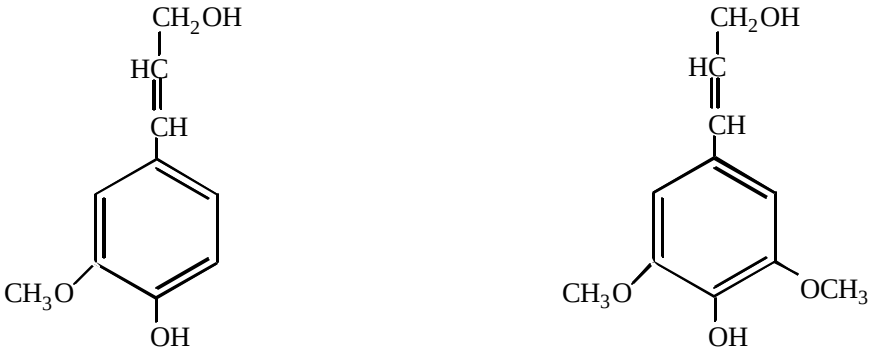

Coniferyl alcohol Sinapyl alcohol

Fig. 4.10. Schematic diagrams of two alcohol structures in wood lignin.

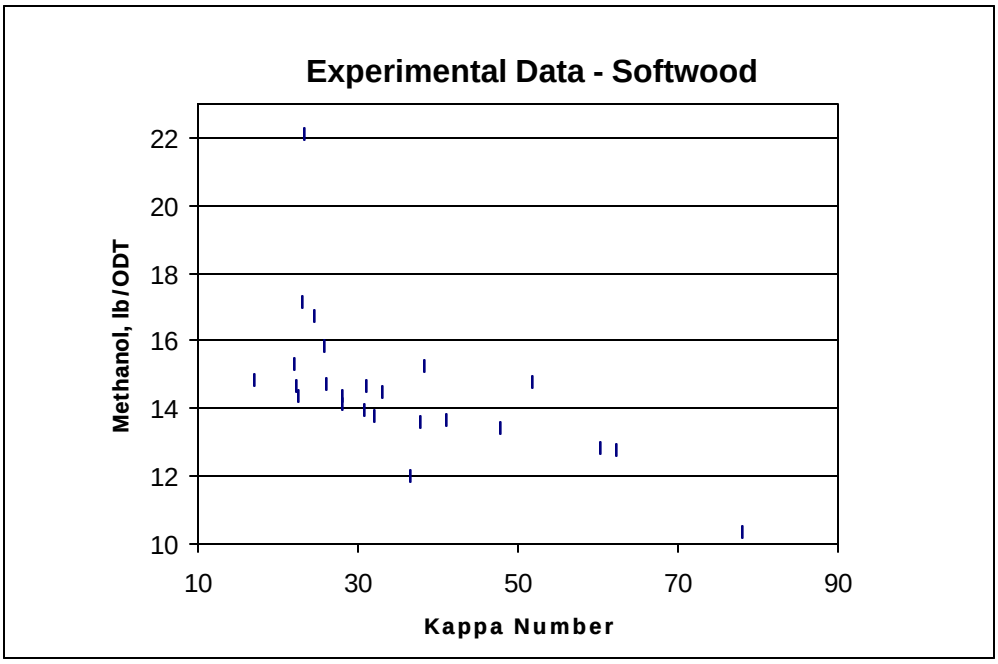

Fig. 4.11. Experimental softwood methanol generation as a function of kappa number.

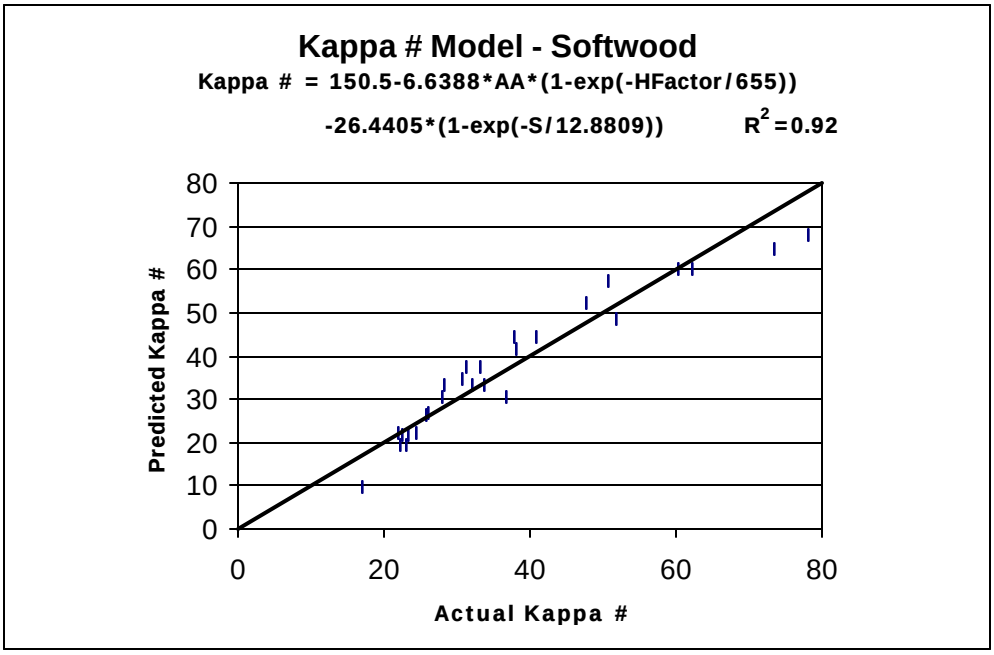

Fig. 4.12. Actual versus predicted kappa number for softwood.

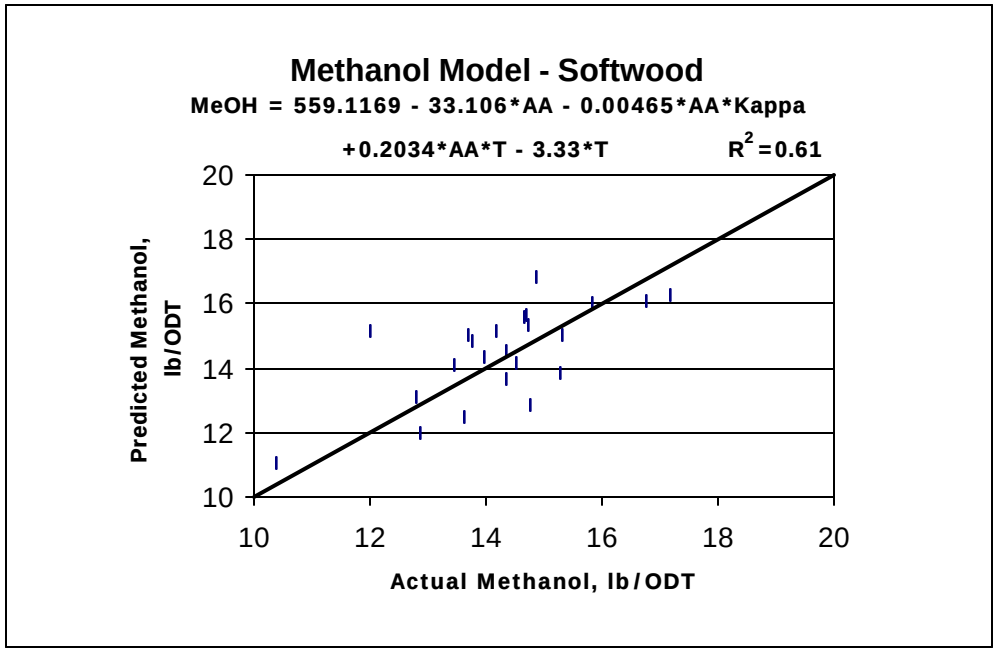

Fig. 4.13. Actual versus predicted methanol generation for softwood.

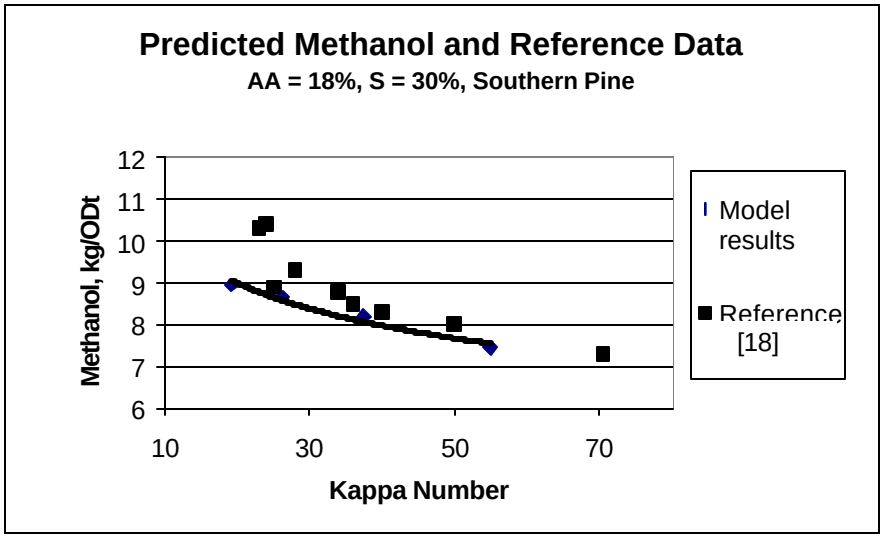

Fig. 4.14. Methanol model results compared to reference data for softwood.

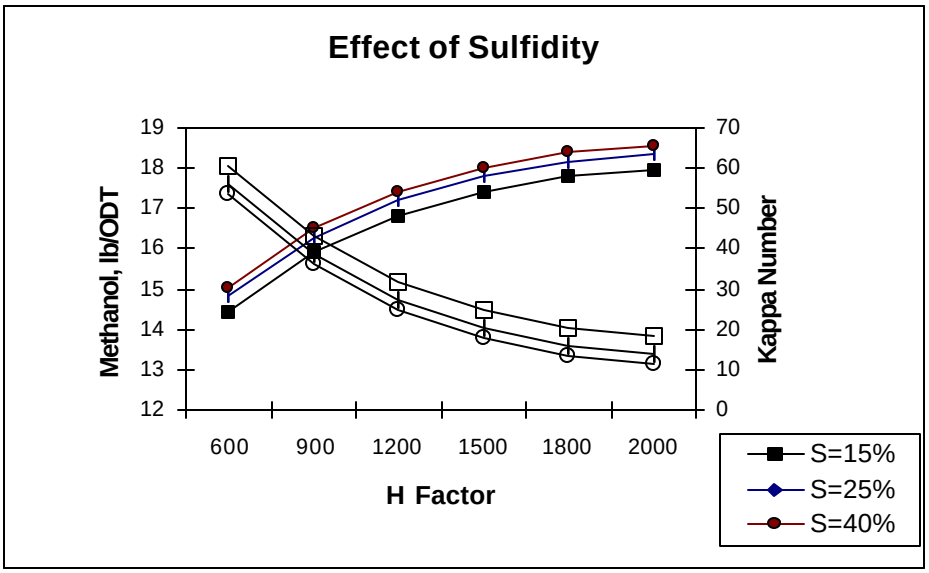

Fig. 4.15. Effect of sulfidity on kappa number and methanol generation in softwood cooks.

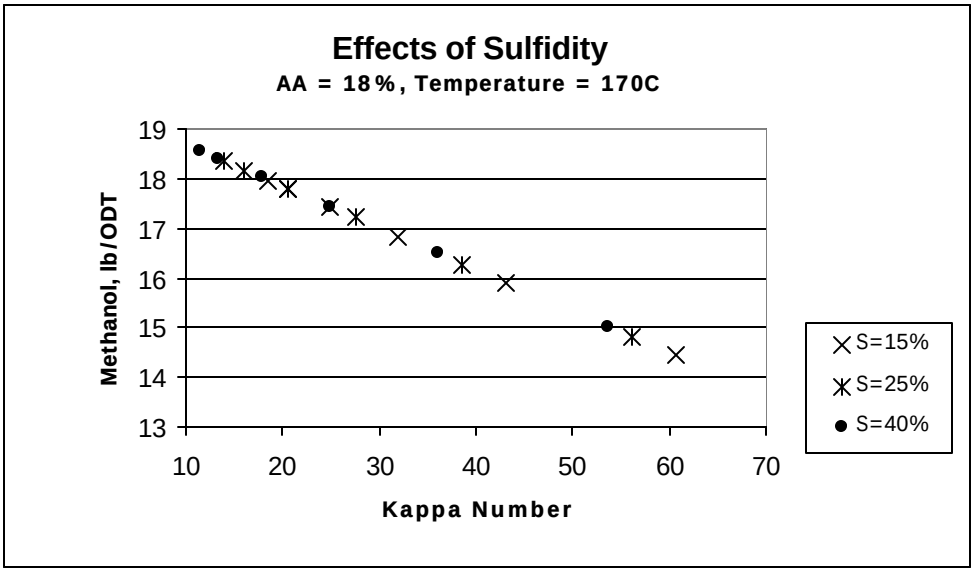

Fig. 4.16. Effect of sulfidity on methanol generation as a function of kappa number.

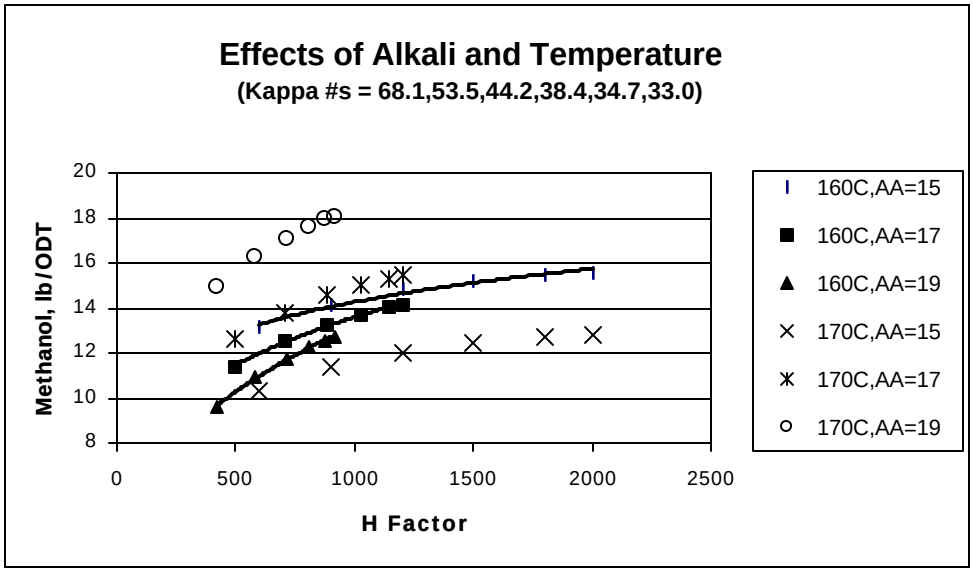

Fig. 4.17. Effect of alkali and temperature on softwood methanol generation as a function of H Factor at constant kappa numbers (Kappa numbers are shown above in sequence in each series, reading from leftmost point to right).

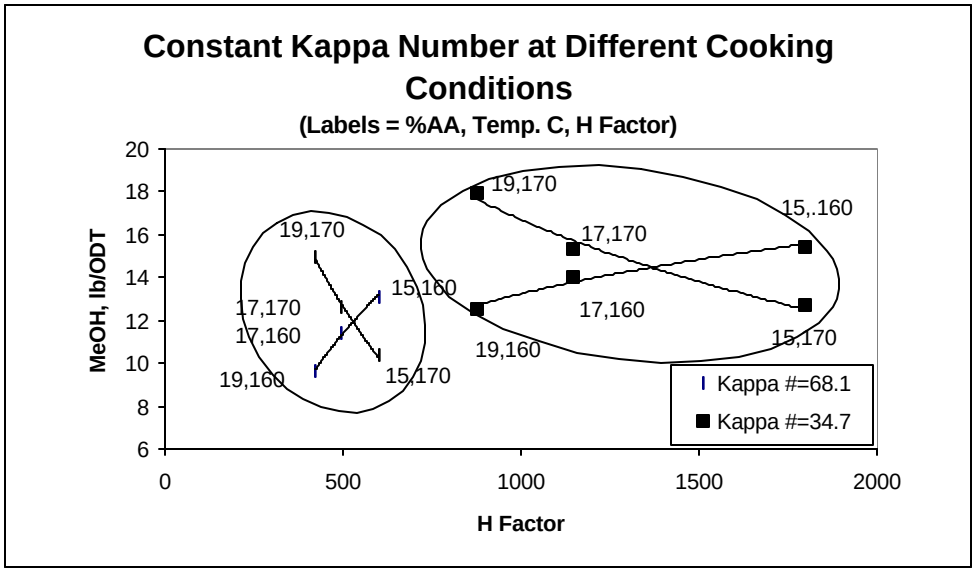

Fig. 4.18. Methanol generation as a function of softwood cooking conditions for a target kappa number.

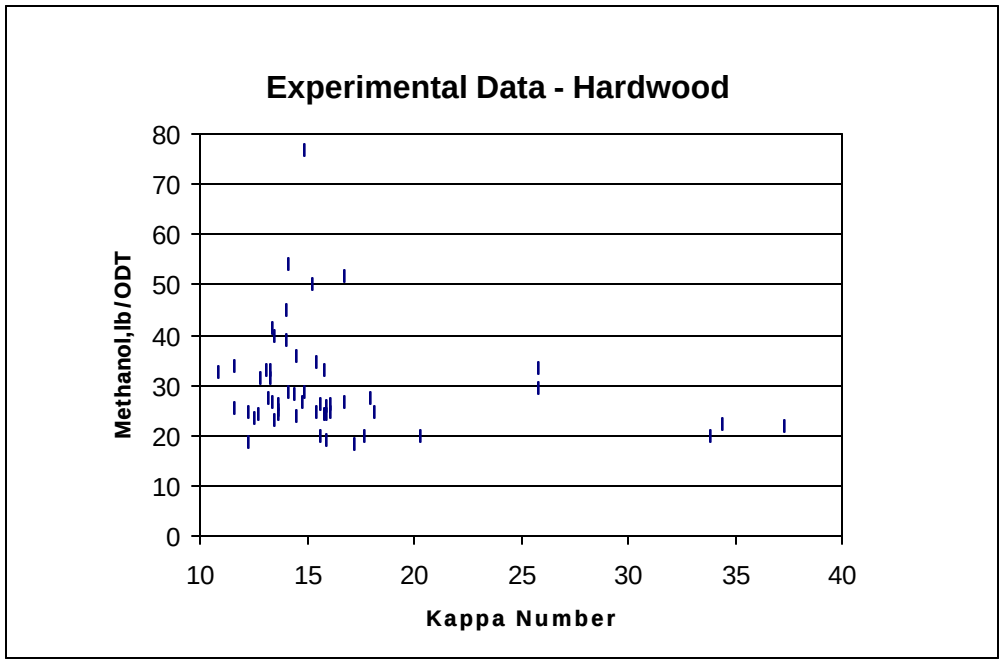

Fig. 4.19. Experimental hardwood methanol generation as a function of kappa number.

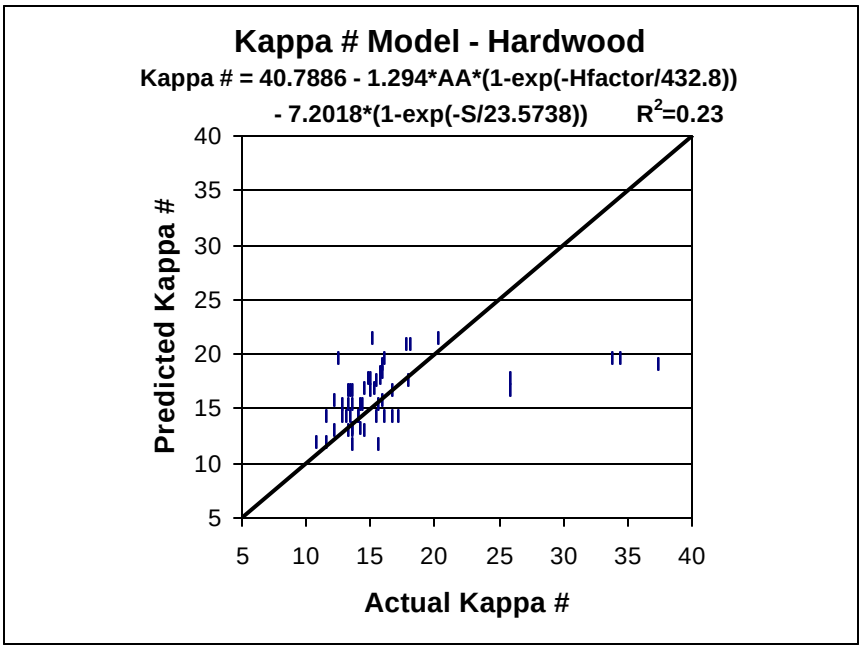

Fig. 4.20. Actual versus predicted kappa number for hardwood.

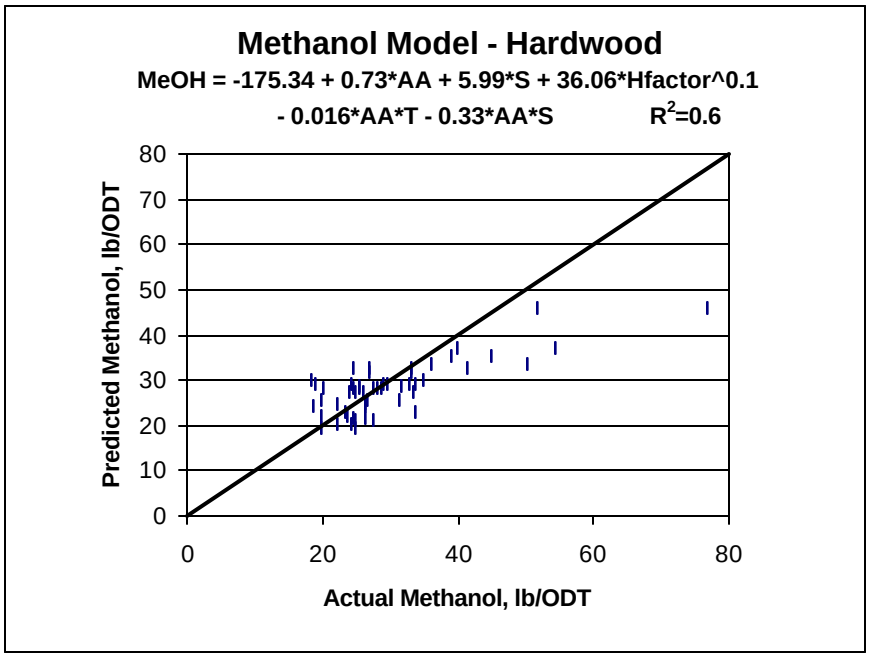

Fig. 4.21. Actual versus predicted methanol generation for hardwood.

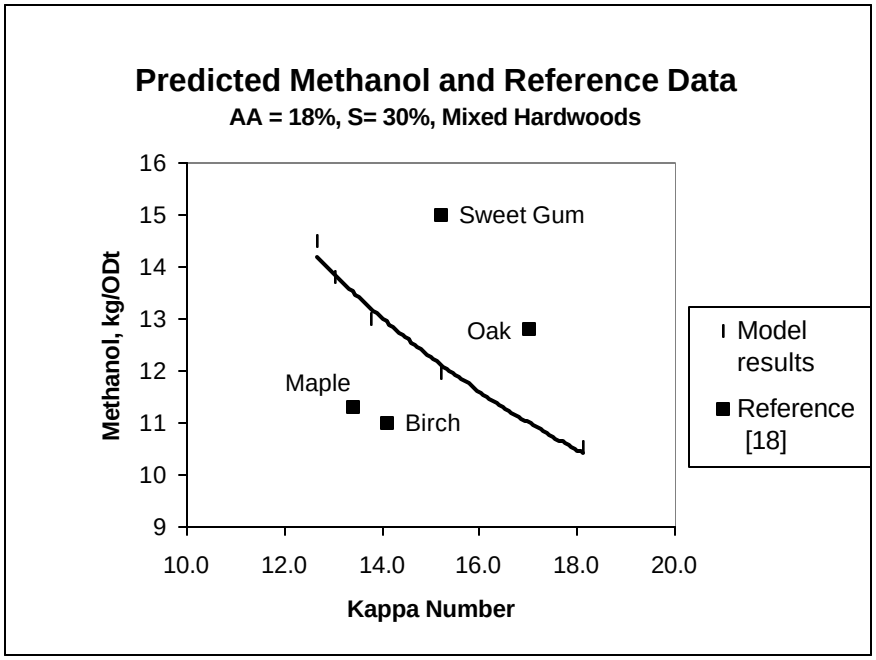

Fig. 4.22. Methanol model results compared to reference data for hardwood.

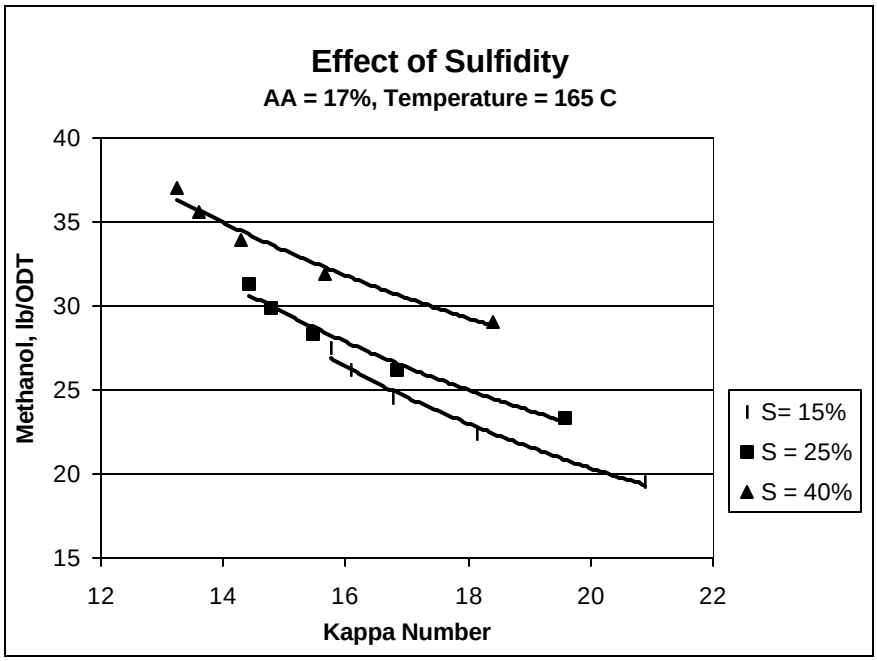

Fig. 4.23. Effect for sulfidity on methanol generation as a function of kappa number in hardwood.

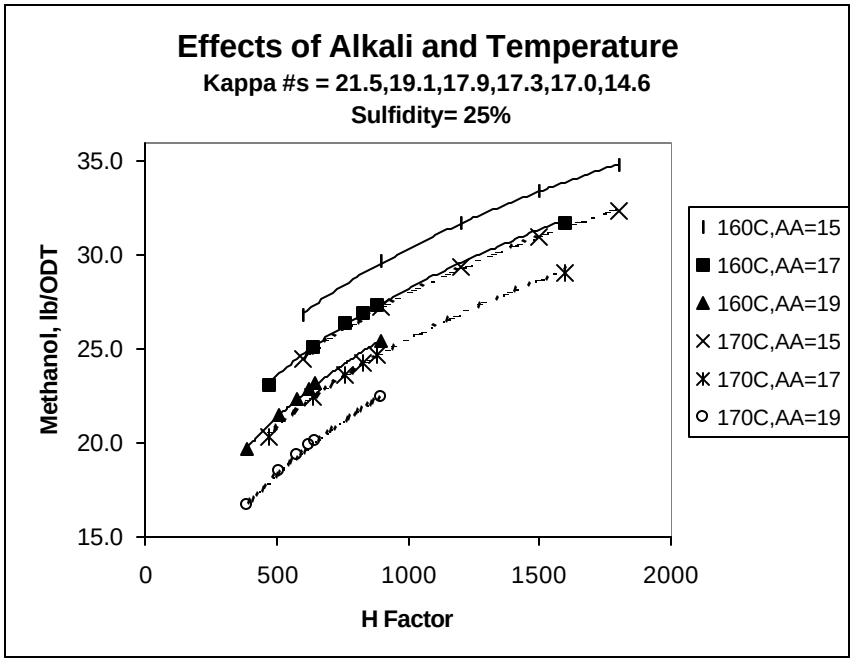

Fig. 4.24. Effect of alkali and temperature on hardwood methanol generation as a function of H Factor at constant kappa numbers and moderate sulfidity (Kappa numbers are shown above, in sequence in each series, reading from leftmost point to right).

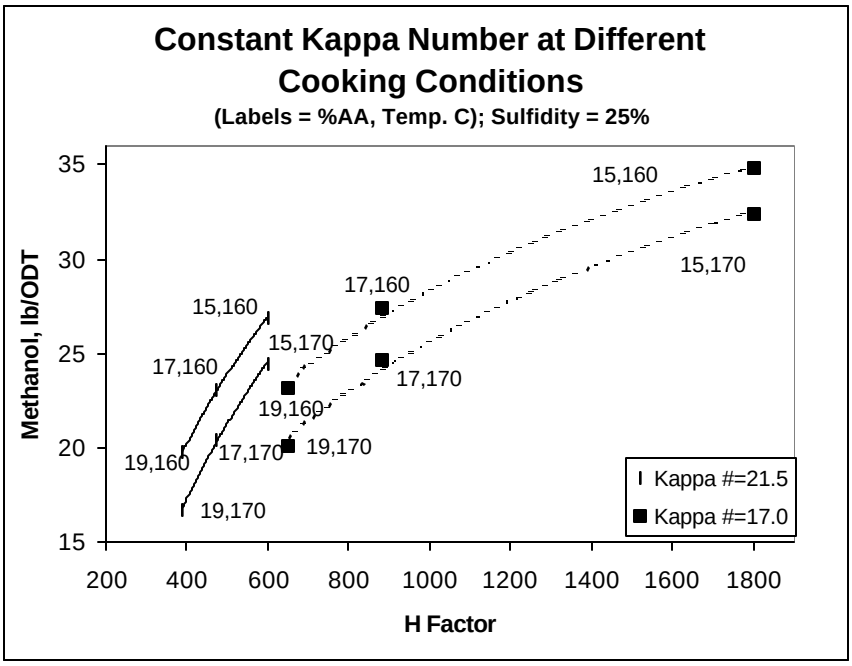

Fig. 4.25. Methanol generation as a function of hardwood cooking conditions for a target kappa number and moderate sulfidity.

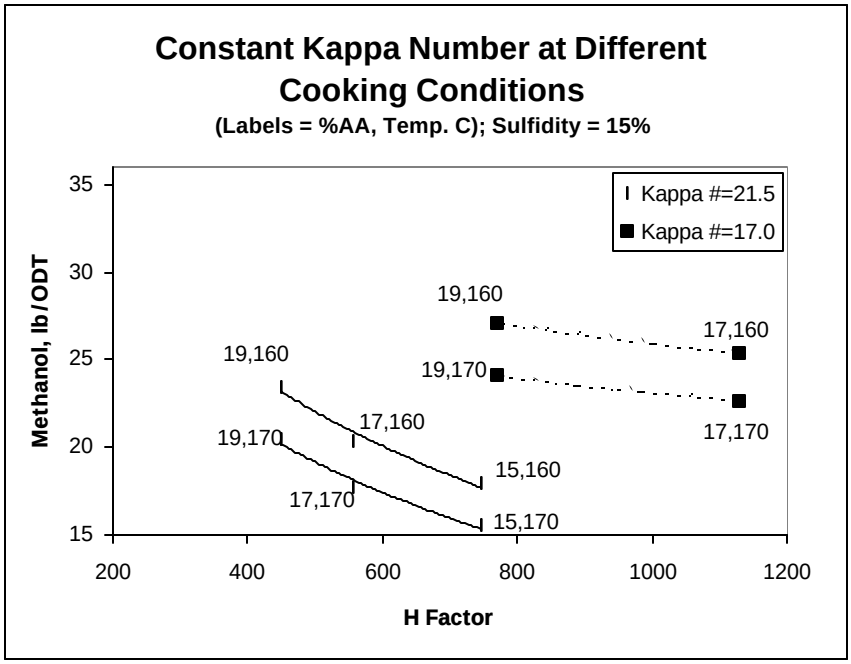

Fig. 4.26. Methanol generation as a function of hardwood cooking conditions for a target kappa number and low sulfidity.

APPENDIX

Table 4.AI. Raw data for Softwood Cooks and Methanol Analysis

Species Type	Active Alkali % on wood	Sulfidity % on AA	Temp °C	H-Factor	Methanol ppm	Kappa Number	Screened Yield %	Total Yield %	Methanol lb/ODT
1 SW	15	15	165	1200	789	51.7	40.4	42.8	14.8
2 SW	19	15	165	1200	769	25.7	38.2	38.9	15.8
3 SW	15	40	165	1200	801	38.2	40.7	42.0	15.3
4 SW	19	40	165	1200	836	23.0	37.7	39.0	17.2
5 SW	17	25	170	600	703	62.3	40.3	44.0	12.8
6 SW	17	25	170	1800	812	24.4	36.8	38.8	16.8
7 SW	17	25	160	600	707	60.2	39.7	44.0	12.9
8 SW	19	25	160	1200	699	22.4	39.0	39.0	14.3
9 SW	17	25	160	1800	744	21.9	38.9	38.9	15.3
10 SW	17	15	165	600	703	73.4	33.4		
11 SW	17	40	165	600	676	50.8	37.5		
12 SW	17	25	165	1200	730	33.6	39.0		
13 SW	17	25	165	1200	683	32.0	38.7	39.7	13.8
14 SW	17	15	165	1800	718	26.1	38.1	39.0	14.7
15 SW	17	40	165	1800	723	22.2	38.5	39.4	14.7
16 SW	15	25	170	1200	711	37.8	37.8	41.8	13.6
17 SW	19	25	170	1200	1053	23.2	37.0	38.1	22.1
18 SW	17	15	170	1200	720	31.1	37.4	39.3	14.7
19 SW	15	25	165	1800	700	30.7	39.3	40.1	14.0
20 SW	19	25	165	1800	685	17.0	36.8	36.9	14.9
21 SW	17	25	165	1200	700	28.1	39.2	39.6	14.2
22 SW	15	25	165	600	599	78.0	36.6	46.2	10.4
23 SW	19	25	165	600	697	47.8	39.6	41.5	13.5
24 SW	15	25	160	1200	712	40.9	39.8	41.7	13.7
25 SW	17	15	160	1200	722	33.1	38.9	39.8	14.5
26 SW	17	40	160	1200	726	27.9	39.6	40.5	14.4
27 SW	17	40	170	1200	613	36.6	36.5	40.9	12.0

Table 4.AII. Raw Data for Hardwood Cooks and Methanol Analysis (Wood 1)

	Species Type	Active Alkali % on wood	Sulfidity % on AA	Temp °C	H-Factor	Methanol ppm	Kappa Number	Screened Yield %	Total Yield %	Methanol lb/ODT
1	HW2-1	15	15	165	1200	1413	15.9	44.3	46.6	24.3
2	HW2-2	19	15	165	1200	1391	11.6	43.3	43.7	25.5
3	HW2-3	15	40	165	1200	4551	14.9	43.9	47.4	76.9
4	HW2-4	19	40	165	1200	1502	15.6	45.1	45.8	26.3
5	HW2-5	17	25	170	600	1365	12.5	42.9	46.3	23.6
6	HW2-6	17	25	170	1800	1963	15.4	44.1	45.2	34.8
7	HW2-7	17	25	160	600	1540	16.1	44.6	46.8	26.3
8	HW2-8	19	25	160	1200	1871	13.3	44.6	45.1	33.2
9	HW2-9	17	25	160	1800	1887	13.1	45.1	45.5	33.2
10	HW2-10	17	15	165	600	1442	18.1	41.9	46.5	24.8
11	HW2-11	17	40	165	600	1118	15.9	42.7	47.1	19.0
12	HW2-12	17	25	165	1200	1606	14.4	44.8	45.7	28.1
13	HW2-13	17	25	165	1200	1586	13.2	45.1	46.2	27.5
15	HW2-15	17	40	165	1800	3117	14.1	45.2	46.0	54.3
16	HW2-16	15	25	170	1200	1860	14.9	48.0	51.7	28.8
17	HW2-17	19	25	170	1200	1141	12.2	47.9	49.3	18.5
18	HW2-18	17	15	170	1200	1477	13.5	47.9	51.0	23.2
19	HW2-19	15	25	165	1800	2052	14.5	44.8	45.8	35.9
20	HW2-20	19	25	165	1800	1755	10.8	42.5	42.8	32.8
21	HW2-21	17	25	165	1200	1435	13.6	44.2	45.5	25.3
22	HW2-22	15	25	165	600	1197	20.3	41.2	48.3	19.8
23	HW2-23	19	25	165	600	1455	15.4	45.1	46.9	24.8
24	HW2-24	15	25	160	1200	1881	15.8	44.1	45.7	33.0
25	HW2-25	17	15	160	1200	1468	13.4	44.0	44.4	26.5
26	HW2-26	17	40	160	1200	2556	14	45.1	45.7	44.8
27	HW2-27	17	40	170	1200	2667	13.4	49.6	51.5	41.5

Table 4.AII continued - Raw Data for Hardwood Cooks and Methanol Analysis (Wood 2)

	Species Type	Active Alkali % on wood	Sulfidity % on AA	Temp °C	H-Factor	Methanol ppm	Kappa Number	Screened Yield %	Total Yield %	Methanol lb/ODT
1	HW1-1	15	15	165	1200	1370	37.3	26.2	49.8	22.0
2	HW1-2	19	15	165	1200	1674	12.8	42.0	42.5	31.5
3	HW1-3	15	40	165	1200	3053	16.7	45.1	47.4	51.6
4	HW1-4	19	40	165	1200	1624	13.6	53.0	53.2	24.4
5	HW1-5	17	25	170	600	1199	33.8	41.9	48.3	19.9
6	HW1-6	17	25	170	1800	1041	17.2	42.6	45.7	18.2
7	HW1-7	17	25	160	600	1298	34.4	43.6	46.8	22.2
8	HW1-8	19	25	160	1200	1324	14.5	44.1	44.4	23.9
9	HW1-9	17	25	160	1800	1500	16.7	43.5	44.8	26.8
10	HW1-10	17	15	165	600	1139	17.7	41.5	45.8	19.9
11	HW1-11	17	40	165	600	1405	15.8	41.9	46.5	24.2
12	HW1-12	17	25	165	1200	1362	12.7	43.8	44.7	24.4
13	HW1-13	17	25	165	1200	1237	15.6	42.7	49.4	20.0
14	HW1-14	17	15	165	1800	1413	15.9	42.7	43.4	26.1
15	HW1-15	17	40	165	1800	2233	13.5	44.0	44.7	40.0
16	HW1-16	15	25	170	1200	1515	25.8	40.3	41.3	29.4
17	HW1-17	19	25	170	1200	1448	13.6	43.0	43.9	26.4
18	HW1-18	17	15	170	1200	1686	25.8	37.8	40.2	33.6
19	HW1-19	15	25	165	1800	2851	15.2	44.9	45.6	50.1
20	HW1-20	19	25	165	1800	1874	11.6	44.2	44.5	33.7
21	HW1-21	17	25	165	1200	1628	14.1	44.2	45.3	28.8
22	HW1-22	15	25	165	600		15.1	42.8	44.9	
23	HW1-23	19	25	165	600	1614	17.9	40.4	47.3	27.3
24	HW1-24	15	25	160	1200	1525	14.8	43.9	45.6	26.8
25	HW1-25	17	15	160	1200	1734	13.3	43.7	44.2	31.4
26	HW1-26	17	40	160	1200	2183	14	43.8	44.8	39.0
27	HW1-27	17	40	170	1200	1577	16.1	43.3	51.5	24.5

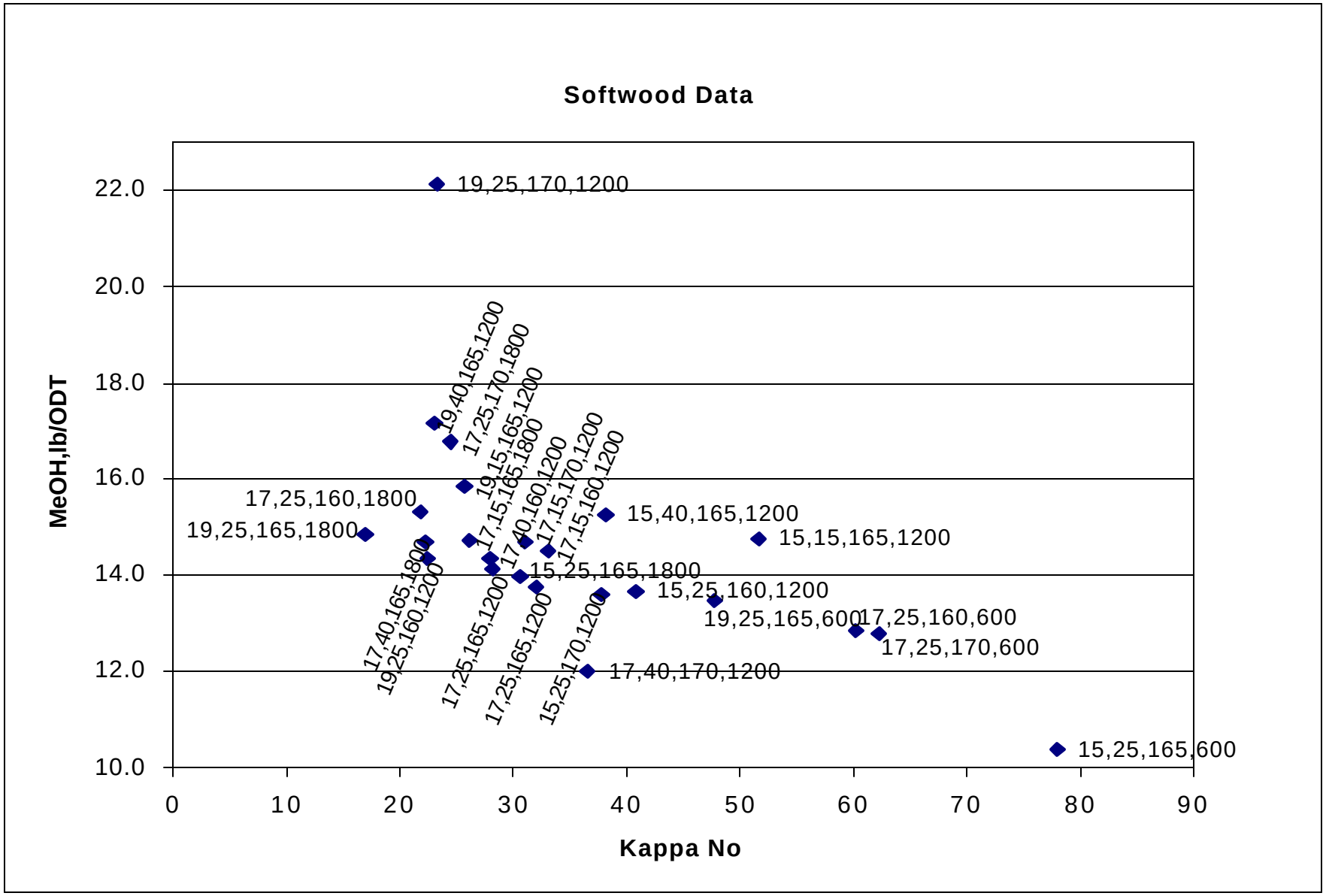

Fig. 4.A1. Softwood data including pulping condition labels

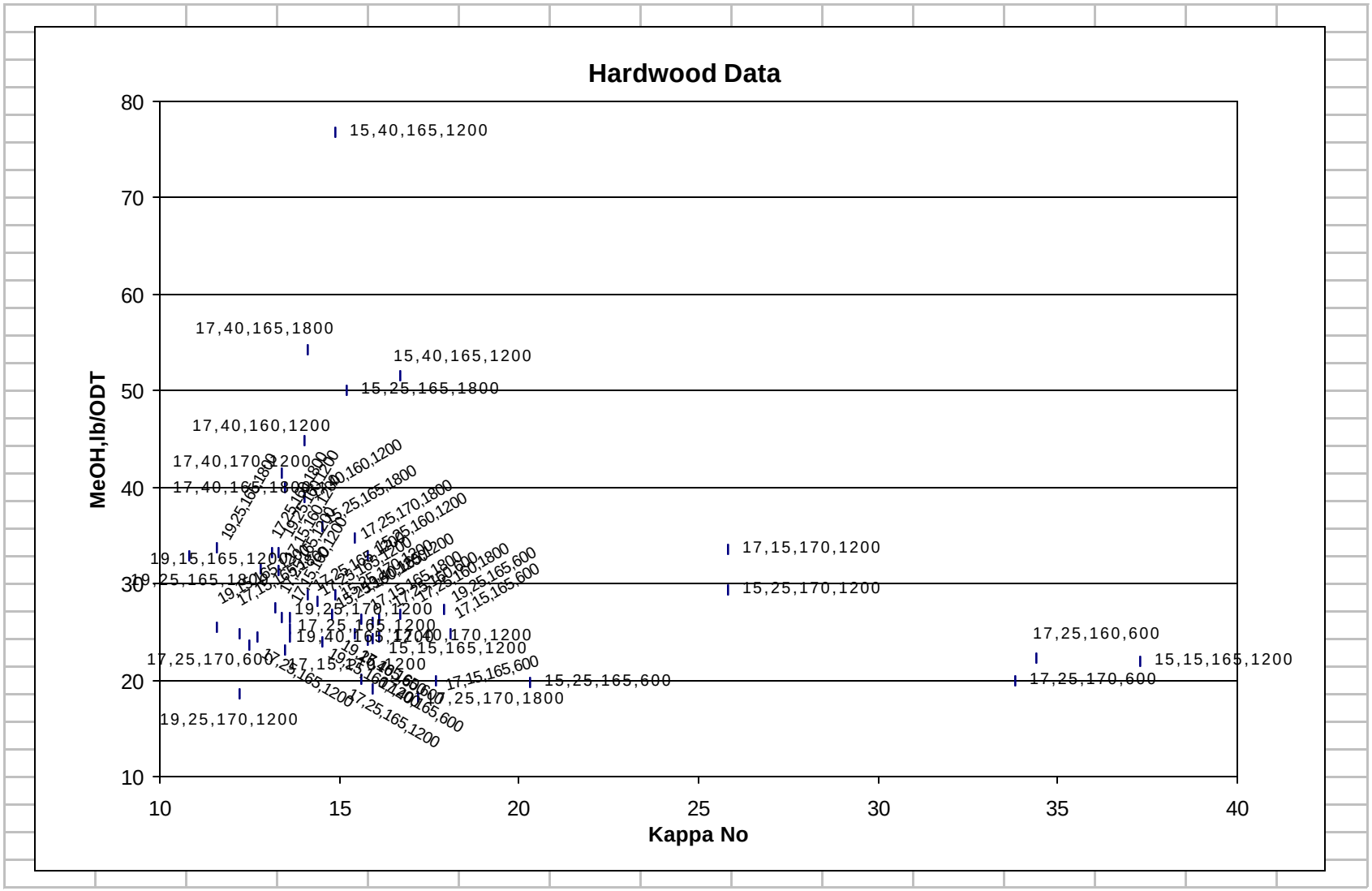

Fig. 4.AII. Hardwood data including pulping condition labels

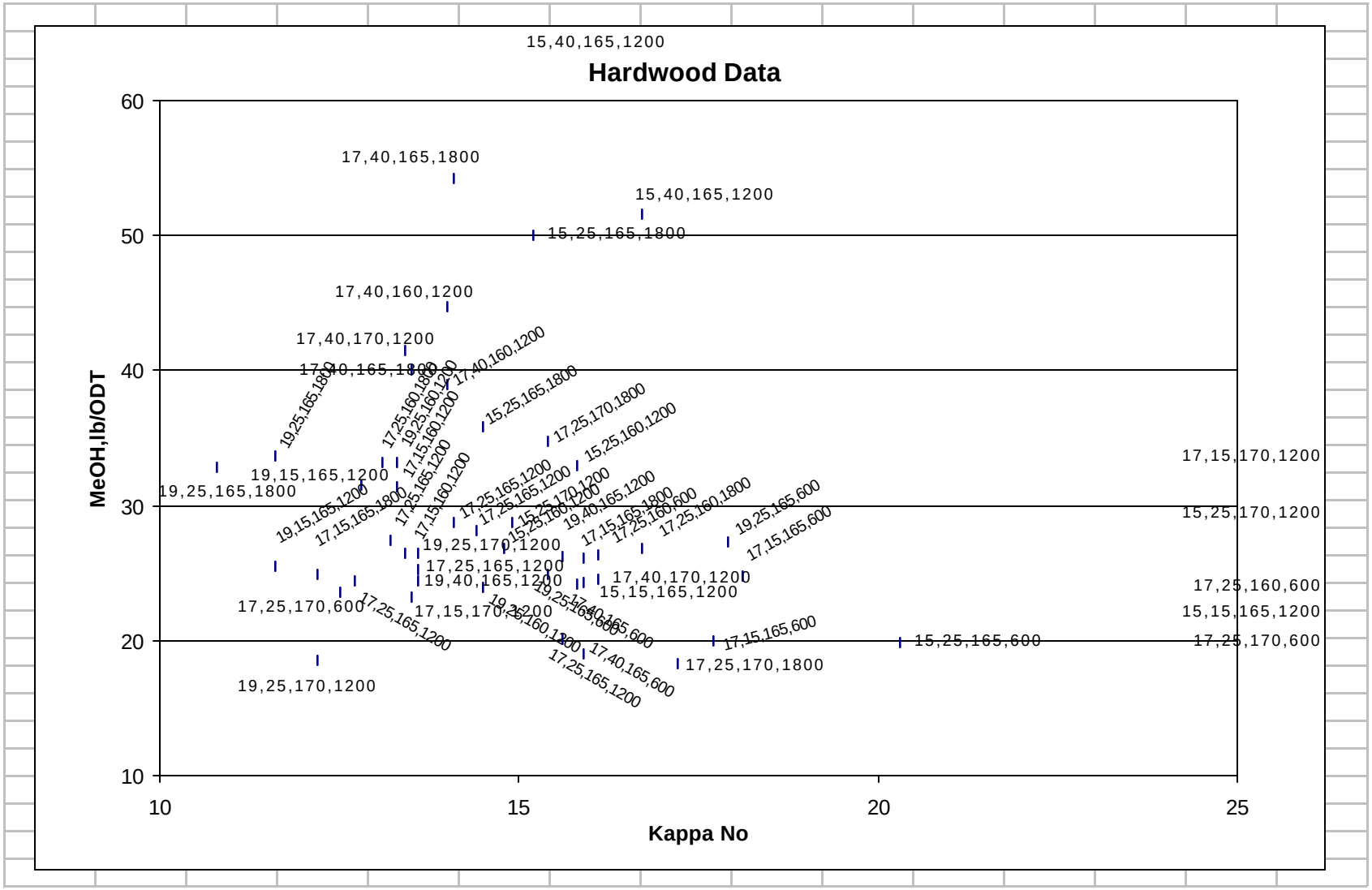

Fig. 4.AIII. Hardwood data including pulping conditions labels – expanded section

CHAPTER 5: VOC AIR EMISSION PREDICTIVE MODEL

Computer based process simulation models is a tool capable of predicting process parameters in kraft mills. Developing a simulation tool for the predicting of VOC air emission in kraft mill is the objective of Task A of this research. In this chapter, basic chemical engineering concepts are used to develop sub-models of VOC vapor-liquid equilibrium, formation, and air emission.

Different from the pure methanol and water system as discussed previously, methanol vapor-liquid equilibrium calculation for kraft pulp mills needs the following special considerations: Methanol content in most liquors is very low and there are significant amounts of other dissolved organics and inorganics in kraft liquors. The new equilibrium model developed is based on the traditional equilibrium calculation approach and addresses the special requirements for kraft pulp mills. The model was validated by laboratory measurements at different temperatures and various concentrations of dissolved compounds. Also, direct mill measurements were compared with laboratory measurements and model predictions. The new equilibrium model is an essential part of a complete tool kit that can predict methanol concentrations in all kraft mill vapor streams (fiberline, evaporators, strippers and recaustizing). Application of these tools will help minimize the cost of cluster rule VOC compliance.

Methanol is mainly generated during cooking from methoxyl groups in hemicellulose and lignin as discussed in Chapter 4. Wood species and final cooking kappa number significantly affect methanol generation. Residual lignin on pulp carries methoxyl groups down the fiberline and methanol can be generated in oxygen delignification and bleaching stages. Demethylation in dissolved lignin causes methanol generation in black liquor evaporation. Mathematical models of methanol generation in kraft mills have been developed for cooking, bleaching and black liquor storage. The models relate methanol generation to methoxyl contents in hemicellulose and lignin, cooking conditions, final cooking Kappa, degree of delignification in bleaching stages and black liquor temperature and storage time. Experimental data presented in Chapter 4 are used to validate the models.

VOC air emission models are developed based on equilibrium calculations and mass transfer rates for commonly used equipment in kraft mills. These models quantify the interaction between methanol air emissions and liquor conditions (concentrations and temperature). Methanol air emission data collected in three kraft mills are used to validate these models. When the air emission models are integrated into existing process simulators, it is possible to evaluate the impact of process modification and operating changes on methanol air emissions. Besides methanol, the same models can be applied to other VOC components if their equilibrium constants are available.

5.1 VOC Vapor-Liquid Equilibrium Models

Methanol content in most filtrates and condensates is less than 2000 mg/kg [1]. For practical purposes, it is important to predict methanol equilibrium concentration near infinite dilution. However, methanol can be enriched to more than 50% in steam strippers. Also, methanol content in condensates generated from cooking can reach more than 10,000 mg/kg [1]. Because other VOC's in kraft mills have lower concentrations than methanol, the existence of these VOC's has little effect on methanol equilibrium. However, dissolved organic and inorganic solids are significant in kraft liquors, especially in evaporator areas. Previous studies have shown that these dissolved solids have a significant impact on methanol equilibrium [2, 3].

Blackwell et al. [4] summarized vapor and liquid equilibrium relationships for kraft foul condensates. It was shown that the methanol activity coefficient at infinite dilution is a function of temperature. However, the infinite dilution activity coefficients from literature data were increased by 10% by Blackwell et al. in order to match experimental measurements of stripper liquid concentration profiles. Because the relationships were developed for condensates, no dissolved solids effect on the equilibrium was included. Gupta [5] has summarized recent studies of the methanol activity coefficients at infinite dilution.

Chai and Zhu [6] have developed a headspace GC method for measuring methanol content and Henry's law constants. It was found that Henry's law constant for methanol is dependent on temperature and dissolved solids content [4]. Several empirical equations have

been developed to correlate Henry's law constant with these variables [2, 3]. This part of the report generalizes methanol equilibrium calculations for all kraft mill liquors and filtrates.

5.1.1. Equilibrium Theory

General vapor and liquid equilibrium theory is defined according to following equation (please see last page for nomenclature):

$$P_T y_i \phi_i = P_i^o(T) \gamma_i x_i \qquad (5.1)$$

In pulp mills, no equipment is under high pressure. Therefore, it can be assumed that the vapor phase is ideal. A general equilibrium constant can be expressed as:

$$K_i = \frac{y_i}{x_i} = \frac{\gamma_i P_i^o(T)}{P_T} \qquad (5.2)$$

For most VOC's, vapor pressure information, $P_i^o(T)$, can be found in the literature. Less information is available for activity coefficients, especially at infinite dilution.

There are various activity coefficient models in the literature. In this work, the NRTL (Non-Random Two-Liquid) model [7] has been chosen. For a binary mixture, it can be expressed as:

$$\ln(\gamma_1) = x_2^2 \left(\frac{\tau_{21} A_{21}^2}{(x_1 + x_2 A_{21})^2} + \frac{\tau_{12} A_{12}^2}{(x_2 + x_1 A_{12})^2} \right) \qquad (5.3)$$

in which,

$$A_{21} = \exp(-\alpha \tau_{21})$$
$$A_{12} = \exp(-\alpha \tau_{12})$$

The NRTL model has three parameters, τ_{21}, τ_{12} and α, which have to be determined from experimental measurements.

At fixed total pressure and composition, the effect of temperature on activity coefficients can be expressed as:

$$\left.\frac{\partial(\ln \gamma_i)}{\partial(1/T)}\right|_{P_T,x} = \frac{\Delta H_i}{R} \qquad (5.4)$$

The partial excess molar enthalpy, ΔH_i, has to be determined from measurements. If ΔH_i is constant, the natural logarithm of the activity coefficient is inversely proportional to absolute temperature.

5.1.2 Binary Methanol and Water System Equilibrium

5.1.2.1 Methanol Activity Coefficients

Figure 5.1 shows various direct measurements of methanol activity coefficients at infinite dilution for the mixture of methanol and water [5, 8-10]. Although the measurements vary, methanol activity coefficients generally increase with temperature. The methanol activity coefficient at 100°C is approximately 25% higher than at 60°C. If Equation (5.4) is applied, methanol partial molar excess free enthalpy at infinite dilution is -5200 J/mol. When the NRTL model parameters, τ_{21} and τ_{12}, are expressed as Equations (5.5) and (5.6), the temperature effect on the methanol infinite dilution activity coefficient is well represented by the NRTL model as shown by the solid line in Fig. 5.1.

$$\tau_{21} = 2.7967 - \frac{700}{T} \qquad (5.5)$$

$$\tau_{12} = 2.4362 - \frac{200}{T} \qquad (5.6)$$

A comparison of the NRTL model prediction and measurements for methanol infinite dilution activity coefficient is shown in Fig. 5.1. Also, shown in Fig. 5.1 are methanol, infinite dilution, activity coefficients calculated from vapor-liquid equilibrium measurements. The activity coefficients (from VLE) in Fig. 5.1 are calculated from Wilson parameters provided in the literature [11]. Figure 5.1 shows that the direct measured methanol, infinite dilution, activity

coefficients are generally higher and more temperature sensitive than those calculated from vapor-liquid equilibrium measurements.

The impact of methanol concentration on the methanol activity coefficient is shown in Fig. 5.2 for the methanol and water system. The measurements were obtained by using a method emphasizing accuracy at low methanol concentration [8]. When Eqs. (5.5) and (5.6) are used to calculate the temperature effect on NRTL parameters, the NRTL model accurately represents the methanol activity coefficient for the whole methanol concentration range. In Fig. 5.2, the methanol activity coefficient approaches the infinite dilution activity coefficient at methanol concentration lower than 0.001 mole fraction in the liquid phase. In other words, the methanol equilibrium concentration can be calculated from Henry's law when the methanol concentration in the liquid phase is lower than 0.001 mole fraction.

5.1.2.2 Methanol Equilibrium Constant

It is shown in Eq. (5.2) that temperature affects the equilibrium constant through both the saturated vapor pressure, $P_i^o(T)$, and activity coefficient, Eq. (5.4). The effect of temperature on saturated vapor pressure is much stronger than on the activity coefficient. At atmospheric pressure, the model predicted temperature effect on the methanol equilibrium constant at very low methanol concentration is compared with laboratory measurements in Fig. 5.3. The measurements in Fig. 5.3 were converted from Henry's law constants obtained from a headspace GC method [6]. The methanol content in the liquid phase was 800 mg/L. Both the NRTL model and measurements show that the methanol equilibrium constant is very strongly dependent on temperature (e.g. at 80^{o}C it is 2.6 times higher than at 60^{o}C).

5.1.2.3 Methanol Equilibrium Concentrations

Using Eqs. (5.2), (5.3), (5.5) and (5.6), methanol vapor equilibrium concentrations can be predicted for binary mixtures of methanol and water. The comparison of predicted equilibrium concentration with measurements is shown in Fig. 5.4. The model gives good predictions over the whole range of methanol concentrations. When methanol concentration in the liquid is lower than 0.001 mole fraction (1800 mg/kg), the embedded figure in Fig. 5.4 shows that Henry's law is acceptable (1% error) for methanol equilibrium calculations. At 0.006 mole fraction methanol

in the liquid phase, the error from Henry's law is 5%. For streams with high methanol concentrations, such as foul condensates, stripper feed and stripper overheads, it is necessary to use the NRTL model presented in this paper for equilibrium calculation.

Methanol is the most abundant VOC in kraft mills. Except in steam strippers and foul condensates, methanol concentration in most mill streams is lower than 0.001 mole fraction (1800 mg/kg). At such low concentrations, the methanol equilibrium constant only depends on the interaction between methanol and water. The existence of other VOC's in kraft mills will not affect the interaction between methanol and water. Therefore, methanol equilibrium constants from the binary mixture of methanol and water can be applied to most condensate streams in kraft mills.

5.1.3 Impact of Dissolved Solids on Methanol Equilibrium Constants

Although the existence of other VOC's in pulp mill streams does not affect methanol equilibrium in these streams, the existence of other dissolved solids in kraft mill filtrates and liquors does affect methanol equilibrium [2, 3]. Dissolved solids in kraft liquors can be generally divided into dissolved organics and dissolved inorganics. Their impacts on methanol equilibrium have been examined separately and are discussed below.

5.1.3.1 Dissolved Organics

The composition of dissolved organics in kraft spent liquors is not well defined. The impacts of sulfonated lignin and wood lignin have been studied experimentally [3]. The wood lignin is from kraft pulping of softwood to liner board grade pulp. pH 9.8 was used to dissolve wood lignin for equilibrium measurements. The effect is expressed as a relative equilibrium constant according to Eq. (5.7):

$$R_K = \frac{K \ \ for \ \ Kraft \ \ Liquors}{K \ \ for \ \ Methanol \ \ and \ \ Water \ \ Only} \qquad (5.7)$$

While sulfonated lignin has little impact on methanol equilibrium, kraft lignin slightly increases the methanol equilibrium constant. The impact of kraft lignin on methanol equilibrium is shown

in Fig. 5.5. Because the molecular weights of the dissolved organics are generally unknown, methanol mole fraction in the liquor is calculated according to Eq. (5.8):

$$x\ (methanol) = \frac{Moles\ \ of\ \ Methanol}{Moles\ \ of\ \ Water\ \ and\ \ Methanol\ \ in\ \ the\ \ Liquor} \quad (5.8)$$

Dissolved organics are excluded in the calculation of methanol mole fractions. The impact of kraft wood lignin on relative methanol equilibrium constant can then be expressed as:

$$R_K = 1 + 1.3 W_{DOS} \quad (5.9)$$

The comparison of Eq. (5.9) with measurements is shown in Fig. 5.5. The measurements were conducted using a commercial kraft lignin and a standard aqueous methanol solution with methanol concentration of 800 mg/L. A headspace gas chromatographic (GC) technique [6] were used to determine the methanol partitioning coefficients.

5.1.3.2 Dissolved Inorganics

Dissolved inorganics in kraft mill liquors can significantly increase the methanol equilibrium constant. The measured effects at low methanol concentration are shown in Fig. 5.6 [3]. The existence of 10 wt.% inorganics can cause a 60% increase in the methanol equilibrium constant. It seems that different inorganics have the same effect on the equilibrium constant. An empirical equation, Eq. (5.10), is used to describe the impact of dissolved inorganics.

$$\ln(R_K) = 4.5 W_{DIS} \quad (5.10)$$

The comparison of Eq. (5.10) with measurements is also shown in Fig. 5.6. The same approach used in studying the effect of kraft lignin (Fig. 5.5) was used to obtain the measurements in Fig. 5.6.

5.1.3.3 Kraft Black Liquors

Black liquors from several kraft mills were collected to investigate the effect of kraft pulping dissolved solids on methanol equilibrium. The liquors were for various pulping conditions of southern pine and birch for bleachable and liner board grade pulps. Methanol

equilibrium constants were measured at 50°C and 60°C. The dissolved inorganics contents were calculated by subtracting measured dissolved organics from the measured total solids content. When dissolved organics were not measured, the average content of dissolved organics measurements, 63% of total dissolved solids, is used in the calculation. The results are shown in Fig. 5.7. Also, the combined model correction for dissolved solids from Eqs. (5.8), (5.9) and (5.10) is shown in Fig. 5.7. Although Eq. (5.9) is only from lignin, it was applied to all dissolved organics in the black liquors in the calculation shown in Fig. 5.7. The current model can reflect the general trend of dissolved solids impact. However, the measurements in Fig. 5.7 suggest that there are more influencing factors than those considered in the current models.

5.1.4 Mill Measurements of Equilibrium Constants

Air and filtrate have intensive contact in vacuum drum washer drop legs before they are separated in the seal tanks. Temperature measurements indicate that the vented air from seal tanks is close to equilibrium with the filtrates. Several seal tank methanol measurements in vented air and filtrates are shown in Table 5.I. Air samples were collected and analyzed by NCASI. The listed measurements are the average of triplicate samples. The methanol concentration ratios of air to liquor (i.e. K-values) from these measurements are 37% lower than methanol equilibrium constants predicted by the equilibrium model described earlier in this paper at the measured temperatures.

Methanol equilibrium constants for these mill liquor samples were also measured at 70°C by the headspace GC method [6]. The laboratory measurements are 20% lower than the model prediction. Based on laboratory measurements, the prediction of methanol infinite dilution activity coefficient is adjusted to eliminate the 20% difference. The adjusted NRTL parameter, τ_{21}, is shown in Eq. (5.11).

$$\tau_{21} = 1.7774 - \frac{400}{T} \qquad (5.11)$$

The comparison of these measurements with adjusted model predictions (i.e. Eq. (5.11) rather than Eq. (5.5)) is shown in Table 5.I. Also, measurements from an oxygen delignification blow tank are included. Because the temperature in the blow tank is much higher than that in seal

tanks, the methanol equilibrium constant is much higher than those for seal tanks. The model presented in this paper predicts well at high temperature, but more mill data are needed.

5.2 Methanol Formation Models

It is well known that methanol is generated in cooking processes [1, 15, 16]. Wood species affect the amount of methanol generation during cooking (from 28 lb/ADTP for red alder to 14 lb/ADTP for Douglas-fir [16]. Recent studies of methanol generation also found 8.5 kg/ADTP from Douglas fir and 10 kg/ADTP from birch [17, 18] as reported in Chapter 4. Cooking Kappa also affects methanol generation. Previous research has shown that methanol can also be generated from chlorine and chlorine dioxide bleaching as well as oxygen delignification [19-21]. Mathematical models for methanol generation can combine various measurements for practical applications.

It is believed that methanol generated in kraft mills is from methoxyl groups in wood compounds [17]. Earlier research [15] has shown that 53% of methoxyl in a hardwood 4-*O*-methyl-glucuronoxylan is recovered as methanol during alkaline degradation. Laboratory cooking [17] has shown that methanol is generated from lignin. Also, methanol is generated during black liquor storage [22]. Available data suggest that methanol is generated during and after lignin dissolution from pulp.

After cooking, a significant amount of lignin is still left on pulp. To make bleached pulp, the residual lignin will be removed during oxygen delignification and various bleaching stages. Methanol is also generated in these stages. Compared to cooking, only a relatively small amount of methanol is generated in bleaching stages. However, the generation affects methanol air emissions [13, 14].

Instead of describing the mechanisms of methanol generation in kraft mills, the major purpose of our models is to predict methanol content in mill streams. Existing literature data and results are re-organized in this study to predict methanol generation.

5.2.1 Methanol Generation During Kraft Cooking

Since the dissolution of hemicellulose is much faster than delignification during kraft cooking, it is necessary to separately model methanol generation from hemicellulose, G_H, and lignin, G_L:

$$G_C = G_H + G_L \tag{5.12}$$

5.2.1.1 Methanol Generation from Hemicellulose

Wood species significantly affects methanol generation [16-18]. Methanol generation from hemicellulose is mainly determined by 4-*O*-methyl-glucuronoxylan content in woods. The maximum methanol generation from hemicellulose, $G_{H\,max}$, can be expressed as:

$$G_{H\,\max} = 0.0295 f_x H_W \tag{5.13}$$

in which, H_W is hemicellulose content in wood and f_x is the fraction of 4-*O*-methyl-glucuronoxylan in hemicellulose. Wood species affects 4-*O*-methyl-glucuronoxylan content [23]. Hardwood 4-*O*-methyl-glucuronoxylan content (average 25.7%) is significantly higher than softwood (average 9.3%).

Although maximum methanol generation from hemicellulose is only dependent on wood species, cooking conditions affect the actual conversion of methoxyl groups into methanol. Eq. (5.14) is proposed to predict methanol generation from hemicellulose at various cooking conditions:

$$G_H = A_H G_{H\,\max} F_{HD} F_S F_{AQ} F_{HC} \tag{5.14}$$

in which, F_{HD} is the effect of hemicellulose dissolution degree on methanol generation, F_S is the effect of sulfidity, F_{AQ} is the effect of anthraquinone (AQ) addition and F_{HC} is the conversion factor of methoxyl groups into methanol.

Methanol generation from hemicellulose is proportional to the degree of hemicellulose dissolution [15]. F_{HD} in Eq. (5.14) can be expressed as:

$$F_{HD} = 1 - \frac{C_H}{C_{Hi}} \tag{5.15}$$

In some modern cooking technologies, such as Lo-Solids^{TM} cooking, a significant amount of spent liquor is extracted at the early stage of cooking. In order to predict methanol content in spent liquor from the early stage of cooking, cooking time has to be included in the model. There are various kinetic models for hemicellulose dissolution in the literature [24]. Equation (5.16) is derived based on theoretical propagation rate [25]:

$$\frac{C_H}{C_{Hi}} = \frac{C_{H\_Inf}}{C_{Hi}} + (1 - \frac{C_{H\_Inf}}{C_{Hi}}) Exp(-A_{DH} t / X_n \, e^{-E_{DH}/RT}) \tag{5.16}$$

A comparison of the model with laboratory measurements is shown in Fig. 5.8. Almost all dissolvable glucuronoxylan is dissolved within 30 minutes at 170^{o}C. Model parameters used for Fig. 5.8 are listed in Table 5.II.

5.2.1.2 Methanol Generation from Lignin

Table 5.III shows that the degree of delignification in cooking does not affect the content of methoxyl group in residual lignin on pulp [21]. However, methoxyl content in residual kraft lignin is lower than wood lignin. This suggests that some methoxyl groups may be removed from all wood lignin at a very early stage of cooking.

Methanol generation from wood lignin is divided into initial generation, $G_{Li,}$ and delignification generation, G_{Ld}:

$$G_L = G_{Li} + G_{Ld} \tag{5.17}$$

Initial generation is defined as methanol generated before the cooking temperature reaches 100^{o}C. It is expressed as:

$$G_{Li} = A_L R_{Li} G_{L\max} F_{LCi} \tag{5.18}$$

$$G_{LW\max} = 32 n_M L_W / 196 \tag{5.19}$$

in which, R_{Li} is the fraction of initial methoxyl removal from lignin on pulp; F_{LCi} is the fraction of methoxyl conversion into methanol; n_M is the number of methoxyl group in each lignin monomer (C_9 units) and L_W is wood lignin content. Although softwoods have a higher lignin content (average 29.7%) than hardwoods (average 21.0%), hardwoods have a higher methoxyl content (22% on lignin, n_M=1.4) than softwood lignin (16%, n_M=0.95) [23].

Methanol generation during delignification, G_{Ld}, is expressed as:

$$G_{Ld} = A_L (1 - R_{Li}) G_{LW\ \max} F_{LD} F_S F_{AQ} F_{LC} \tag{5.20}$$

in which, F_{LC} is the conversion from methoxyl into methanol and F_{LD} is the degree of delignification.

$$F_{LD} = 1 - \frac{C_L}{C_{Li}} = 1 - \frac{C_{L\_Inf}}{C_{Li}} - (1 - \frac{C_{L\_Inf}}{C_{Li}}) Exp(-k_L t) \tag{5.21}$$

Only a fraction of lignin methoxyl is converted into methanol during cooking. Laboratory study [19] has shown that dissolved lignin from the early stage of cooking (yield > 80%, degree of delignification <20%) has lower methoxyl content than lignin dissolved at the end of cooking (10.5% vs. 12.5% on lignin). This suggests that methanol conversion factor, F_{LC}, is lower for bulk delignification than initial delignification.

5.2.1.3 Determination of Model Parameters

Laboratory batch cooking (Southern Pine. Cooking conditions: AA = 18%, Sulfidity = 30%, Max T = 170^{o}C) has been conducted to determine the model parameters. A set of typical dissolved lignin and Kappa during laboratory batch cooking is shown in Fig. 5.9. Also, the model prediction is compared with measurements in Fig. 5.9. Model parameters used for Fig. 5.9 are listed in Table 5.II.

Figure 5.10 shows the methanol generation for the cooks shown in Fig. 5.9. Model predictions for methanol generation from hemicellulose, lignin and total methanol generation are also shown in Fig. 5.10. Although no detailed kinetic models are used, methanol generation

during cooking can be represented by the current models. Model parameters used for Fig. 5.10 are also listed in Table 5.II.

Figure 5.10 shows that 45% of the total methanol generation is from hemicellulose. Sixty percent of the methanol generation from hemicellulose has happened before reaching final cooking temperature and 95% of the methanol generation from hemicellulose is finished at 20 minutes after reaching final cooking temperature.

The effect of sulfidity and AQ on methanol generation has been studied by laboratory batch cooking [18]. Eqs. (5.22) and (5.23) are proposed to describe the impact of sulfidity and AQ on methanol generation. The comparison of these models with laboratory measurements is shown in Fig. 5.11.

$$F_S = 1 + 1.165(0.3 - S/100) \tag{5.22}$$

$$F_{AQ} = 1 - 0.75(AQ) \tag{5.23}$$

Laboratory batch cooking has been conducted to investigate wood species effect on methanol generation during cooking [18]. Methanol generation was measured for two levels of final Kappa (Kappa 70 & 30 for softwoods, Kappa 45 & 15 for hardwoods). Measured methanol generations are shown in Figs. 5.12 and 5.13.

In the current model, the effect of wood species has been included in $G_{H\,max}$ and G_{LWmax}, (Eqs. (5.13) and (5.19)). Hemicellulose content, lignin content and methoxyl content affect methanol generation from different wood species. Based on parameters listed in Table 5.II and hemicellulose and lignin data in the literature [23], the methanol generation from various wood species has been predicted successfully by the model. The comparison of model predictions with laboratory measurements for softwoods is shown in Fig. 5.12 and hardwoods in Fig. 5.13. Because no H_w, f_x and L_w are available for Bass, Oak and Sweet Gum, the average of hardwood values is used for these species.

5.2.1.4 Simplified Cooking Model

For most practical mill applications, the model described above for methanol generation during cooking can be simplified. The dissolution of hemicellulose is very fast (Fig. 5.8), about 95% of methanol generation from hemicellulose is completed within 20 minutes after reaching cooking temperature (Fig. 5.10). Except for predicting methanol content in extraction liquors from the early stage of cooking, F_{HD} in Eq. (5.14) can be set to one. Methanol generation from hemicellulose can be simplified as:

$$G_H = 0.0295 A_H f_x H_W F_S F_{AQ} F_{HC} \tag{5.24}$$

When Kappa number is used as an indicator of pulp lignin content in the model, methanol generation from lignin for cooking can be expressed as:

$$G_L = 0.163 A_L n_M L_W (R_{Li} F_{LCi} + (1 - R_{Li}) F_{LD} F_S F_{AQ} F_{LC}) \tag{5.25}$$

in which, y_P is pulp yield at given Kappa number.

$$F_{LD} = 1 - \frac{1.53(Kappa - 25) y_P}{L_W - 38.3 y_P} \tag{5.26}$$

Figure 5.14 shows methanol generation from a laboratory cooking of Southern Pine. A linear relationship exists for a wide range of Kappa numbers (Kappa<90). The prediction of the simplified model is also shown in Fig. 5.14. The hemicellulose and lignin contents of Jack pine [23] are used in the prediction. The simplified model predictions are about 7% higher than the laboratory measurements for Kappa numbers less than 90. The difference between simplified model and the measurements at high Kappa numbers of about 145 in Fig. 5.14 indicates that methanol generation from hemicellulose is not completed at these Kappa numbers. This suggests that the simplified model can be used for Kappa lower than 90, which covers most mill applications.

5.2.2 Methanol Generation in Oxygen Delignification and Bleaching Plants

For each O_2 delignification or bleaching stage, the total methanol generation is expressed as:

$$G_S = A_S G_{S\max} F_{SD} \tag{5.27}$$

in which, A_S is a coefficient related to bleaching chemicals; $G_{S\,max}$ is the maximum methanol generation and F_{SD} is the degree of delignification. $G_{S\,max}$ and F_{SD} are expressed as:

$$G_{S\max} = 0.163 n_M (1.53 Kappa_i) \tag{5.28}$$

$$F_{SD} = 1 - \frac{Kappa_o}{Kappa_i} \tag{5.29}$$

The impacts of operating conditions on methanol generation can be reflected from the change of Kappa numbers.

5.2.2.1 Oxygen Delignification

The data in Table 5.III indicate that the residual lignin in O_2 pulp has a lower methoxyl content (25% lower) than that in kraft pulp. It is suggested that methanol is not only generated from lignin dissolution but also from residual lignin on pulp during oxygen delignification. Lower methoxyl content is observed in dissolved lignin from oxygen delignification than from kraft cooking [20]. Therefore, oxygen delignification generates more methanol than kraft cooking for the same amount of lignin removal from pulp. The methoxyl content in O_2 dissolved lignin remains almost the same during O_2 delignification [20]. This suggests that the degree of delignification does not affect the conversion of lignin methoxyl into methanol. Therefore, A_S in Eq. (5.27) is a constant for O_2 delignification.

Mill methanol has been measured for southern pine cooked to Kappa 37 in a two-vessel Kamyr digester with Lo-Solids^{TM} cooking. The final Kappa after oxygen delignification is 17.5. Methanol generation from mill measurements is 1.22 kg/ODMTP. Based on these data, A_S in Eq. (5.27) is estimated as 0.265.

5.2.2.2 Chlorination and ClO_2 Bleaching

Methanol generation during chlorination is well understood based on studies of the chlorination mechanism [26]. Lignin has to go through demethylation before it can be dissolved from pulp. All methoxyl groups removed during kraft pulp chlorination are converted into methanol [27]. Also, the methoxyl content in the lignin of chlorinated pulp remains constant. Therefore, methanol generation during chlorination is determined by the amount of lignin dissolved during chlorination and the methoxyl content in lignin. When Kappa is used to measure lignin content, final Kappa after chlorination, i.e. CW Kappa (instead of CE Kappa, See reference [27] for CW Kappa measurement), should be used in Eq. (5.29).

In Fig. 5.15, the model is compared with laboratory measurements for softwood Cl_2 bleaching [26]. For this specific pulp, each lignin monomer has 0.79 methoxyl groups and 0.15 kg of methanol is generated from dissolving 1 kg of lignin (i.e. A_S = 1.15). For the same amount of lignin dissolution, more methanol is generated from chlorination than from oxygen delignification.

Different from chlorination, chlorine dioxide does not remove methoxyl groups before dissolving lignin from pulp. Only part of the lignin methoxyl groups are converted into methanol [28]. Sixty-two percent of methoxyl has been recovered as methanol from softwood ClO_2 laboratory bleaching [28]. Laboratory measurements of softwood ClO_2 bleaching [28] are shown in Fig. 5.15. For this specific pulp, 0.065 kg of methanol is generated from dissolving 1 kg of lignin (i.e. A_S = 0.50). Methanol generation from ClO_2 bleaching is much lower than Cl_2 bleaching. Because oxygen delignified pulp has a lower methoxyl content than kraft pulp, it is expected that less methanol will be generated from ClO_2 bleaching of oxygen delignified pulp.

Table 5.IV lists available model parameters for methanol generation in oxygen delignification and bleach plants. Although no methanol generation data are available for caustic extraction (E/Eop), it is expected that methanol is generated during caustic extraction due to methoxyl groups on residual lignin. However, the A_S of caustic extraction will be lower than oxygen delignification.

5.2.3 Methanol Generation in Black Liquor

From a laboratory study it was found that methanol can be formed during black liquor storage and evaporation [19]. Since methanol is also generated in a caustic solution of model lignin, it is suggested that methanol generated during storage and evaporation is from the continuation of dissolved lignin demethylation.

Although it is difficult to determine black liquor temperatures and residence times in a multiple effect evaporator system, the mechanism of methanol generation from black liquor during evaporation should be the same as liquor storage and the same generation model can be applied. Because methanol generation in black liquor is the continuation of demethylation from dissolved lignin, the generation is related to the generation during cooking.

Equation (5.30) is proposed to incorporate various impacts on methanol generation during storage and evaporation:

$$G_{BL} = A_{BL} G_{BL\max} F_{BLC} \tag{5.30}$$

in which, $G_{BL\,max}$ is the maximum methanol generation from black liquors and F_{BLC} is the degree of methoxyl conversion. $G_{BL\,max}$ is expressed as:

$$G_{BL\max} = G_{L\max} - G_C \tag{5.31}$$

Methanol generation during cooking, G_C, affects methanol generation from black liquors. F_{BLC} is expressed as:

$$F_{BLC} = 1 - \frac{C_L}{C_{Li}} \tag{5.32}$$

Because methanol generation during black liquor storage and evaporation is time dependent, a kinetic model is needed. The following equations are proposed to calculate F_{BLC}:

$$-\frac{dC_L}{dt} = A_C e^{-E_{BL}/RT}(C_L - C_{Inf}) \tag{5.33}$$

$$C_{Inf} = C_{Li}(a + bT) \tag{5.34}$$

Temperature affects not only the rate of methoxyl group conversion in Eq. (5.33), but also how many methoxyl groups can be converted into methanol in Eq. (5.34).

Figure 5.15 shows methanol generation during black liquor storage. The black liquor is from laboratory batch kraft cooking of Southern Pine [22]. Five hours storage time generates about 10% (70^{o}C) to 15% (80^{o}C) of the methanol generated during cooking. Based on these data, the parameters in Eqs. (30)~(34) have been determined. The results are listed in Table 5.V. The comparison of model predictions with laboratory measurements is also shown in Fig. 5.16.

5.3. VOC Air Emission Models

Kraft mill VOC air emissions originate from various liquors or filtrates. Although some studies have been done to correlate VOC air emissions with liquor concentrations [29, 30], little work has been done to explain how VOC air emissions are affected by processes, equipment and operating conditions. Now, the Cluster Rule directly links air and water emissions through programs such as the Clean Condensate Alternative in MACT II [31]. For minimum cost compliance, it is essential to understand the interaction between air and water emissions.

In this part of the research program, VOC air emission models were developed to predict VOC air emissions as a function of liquid phase VOC concentrations, liquid temperature, equipment type, etc. A VOC air emission model for vacuum drum washer hoods was developed previously [32]. The model is based on mass transfer and equilibrium calculations. Some improvements have been made to generalize this model in the research. Also, more equilibrium measurements [2, 3] have been made and a better equilibrium calculation model for kraft mills has been developed [33]. Based on the same modeling principles, new air emission models have been developed for other equipment in kraft mills (atmospheric diffusers, filtrate tanks, smelt dissolving tanks and paper machines).

5.3.1 Single Source Model

If the filtrate concentration and temperature in the equipment can be represented by single value, such as the seal tank for vacuum drum washers, a single source emission model can be applied. VOC emission from a single source can be described as (see last page for nomenclature):

$$y_o = \frac{Kx_i}{1 + G(1/K_G a + K/L)} \tag{5.30}$$

$$E_{VOC} = \frac{Kx_i}{1/G + 1/K_G a + K/L} \tag{5.31}$$

For good mass transfer conditions ($K_G a >> G$), Eq. (5.31) can be approximated by Equations (5.32). VOC emission concentration is equal to the final VOC equilibrium concentration in the filtrate. Air flowrate and gas-liquid contact have a strong effect on VOC emission. The emission from vacuum drum washer seal tanks is a good example of this case.

$$E_{VOC} = GKx_o = \frac{Kx_i}{1/G + K/L} \tag{5.32}$$

For poor mass transfer conditions ($K_G a << G$), Equation (2) can be approximated by Eq. (5.33). The major influence of air flowrate is on VOC concentration, not on total VOC emission, although air flowrate will have some effect on mass transfer. Filtrate storage tank vents are a good example of this case.

$$E_{VOC} = \frac{Kx_i}{1/K_G a + K/L} \tag{5.33}$$

The same model has also been applied to atmospheric diffusers, bleach towers and oxygen blow tanks. Different mass transfer coefficients and vent air flowrates are required when the model is applied to different equipment.

5.3.2 Multi-Source Model

An air emission model for vacuum drum washers has been described in our previous paper [32]. To make the model more general, the following modifications have been made since that publication:

1. Equilibrium constants have been substituted for Henry's law constants. This allows the same equilibrium model to be used throughout the mill (e.g. for evaporator methanol equilibrium calculations).

2. Wet basis methanol concentration for the air stream has been substituted for dry air based methanol concentration.

The improved model can be expressed as follows:

$$E_{VOC} = G\frac{(K_G a)_v K_v x_v + (K_G a)_s K_s x_s}{G + (K_G a)_v + (K_G a)_s} \tag{5.34}$$

in which, x_v is vat VOC concentration and x_s is shower VOC concentration.

When Eq. (5.35) is applied to a split shower washer, the mass transfer coefficient is divided in proportion to the shower flowrates.

$$E_{VOC} = G\frac{(K_G a)_V K_V x_V + (K_G a)_{ST} K_{ST} x_{ST} + (K_G a)_{SB} K_{SB} x_{SB}}{G + (K_G a)_V + (K_G a)_{ST} + (K_G a)_{SB}} \tag{5.35}$$

Because the equilibrium constant is very sensitive to temperature, equilibrium constants at corresponding filtrate and shower temperatures are required in the model. In mill situations, the amount of VOC air emission is relatively small when it is compared with the amount of VOC in the filtrates. The impact of VOC air emission on VOC concentration in filtrates has been neglected in Eqs. (5.34) and (5.35).

5.3.3 Paper Machine/Pulp Dryer Model

Depending on the VOC emission mechanism, paper machines or pulp dryers can be divided into two parts: sheet formation and sheet drying.

In the sheet drying section of paper machines, VOC is evaporated with the water. Because the residual VOC in the dried sheet is negligible and generally no condensate is collected from the drying section, all VOC carryover after pressing will be evaporated and released into the air.

$$E_{VOC} = Px(100/c - 1) \tag{5.36}$$

in which, P is dry pulp rate into the dryer section, x is the VOC concentration in the white water and c is the press discharge consistency. Because white water in paper machines is circulated at high flowrates, VOC carryover concentrations at the press are almost equal to those in the headbox.

In the sheet formation area, from the headbox to the press, VOC emission is caused by VOC vaporization from white water and the pulp on the wire. Vents in this area can be divided into general vents and vacuum system vents. The emission from general vents is less predictable because the fans used for these vents play a significant role. Considering the significant white water circulation, Eq. (5.37), simplified from Eq. (5.33), is proposed to predict VOC air emissions from general vents in the sheet formation area:

$$E_{VOC} = K_G aKx \tag{5.37}$$

The vented air from the vacuum system has much more intimate contact with white water and the air flowrate is more predictable. If the change of VOC content in white water is neglected, Eq. (5.38), which is simplified from Eq. (5.31), is proposed to predict VOC air emission from vacuum system vents:

$$E_{VOC} = GKx \tag{5.38}$$

Air flowrate, VOC concentration in the white water and white water temperature affect VOC air emission.

5.3.4 Smelt Dissolving Tank Model

In order to model VOC air emission from smelt dissolving tanks, it is necessary to separate the smelt dissolving tank itself from the scrubber. Molten smelt from the recovery boiler

evaporates water in the smelt dissolving tank. When there are VOC's in the weak wash, VOC's will be evaporated along with water. Because of total evaporation in the vicinity of the molten smelt entry points, the methanol content in vapor can be assumed the same as that in weak wash. VOC air emission from the smelt dissolving tanks without scrubbers can be expressed as:

$$E_{VOC} = 0.35 M_{SM} \frac{T_{SM} - T_i}{646 - T_{WW}} x_{WW} \qquad (5.39)$$

The vapor, V_T, is estimated according to the equation used in GEMS [35]. Although the air entering smelt dissolving tanks affects the VOC concentration, it does not affect the amount of VOC air emission.

The vapor generated in the smelt dissolving tank mixes with air before entering the smelt dissolving tank scrubber. If a mixed tank model is used to represent the scrubber, methanol content in the exit gas stream can be expressed as:

$$y_o = \frac{(G + K_G aKG / L_C) y_{si} + K_G aKx_i}{G + K_G a + K_G aKG / L_C} \qquad (5.40)$$

Normally, there is a liquor circulation in the scrubber. If the liquor flow is much bigger than the gas flow ($L_C >> G$), Eq. (5.40) can be simplified:

$$y_o = \frac{G + K_G a \dfrac{Kx_i}{y_{si}}}{G + K_G a} y_{si} \qquad (5.41)$$

If VOC content in the scrubbing liquor is low, ($Kx_i < y_{si}$), VOC content in the exit gas will be lower than that in the inlet gas. High VOC content in the scrubbing liquor, ($Kx_i > y_{si}$), can increase VOC content in the exit gas. If the same weak wash is used for smelt dissolving and makeup scrubber liquor, Eq. (5.41) can be expressed as:

$$y_o = \frac{K_G aK(1 + V_T / L_M) + V_T}{G + K_G a(1 + K G / L_M)} x_{WW} \qquad (5.42)$$

In which, K is the equilibrium constant at the temperature of scrubbing liquor. VOC content in weak wash, gas flowrate, makeup liquor flowrate, scrubbing liquor temperature and the mass transfer coefficient affect VOC emission from smelt dissolving tank scrubber vents.

5.3.5 Validation of Air Emission Models Using Mill Data

5.3.5.1 Single Source Emissions

If the VOC concentration related to air emissions in equipment can be represented by one concentration and one temperature, it is classified as "single source". A typical example is vacuum drum washer seal tanks. The single source air emission model can also be applied to oxygen delignification blow tanks, bleaching towers, filtrate tanks and atmospheric diffusers. A comparison of methanol concentrations in vent gases from model predictions, Eq (5.30), and mill measurements is shown in Fig. 5.17. All mill measurements are from the same fiberline in a southern softwood kraft mill. All air samples were collected and analyzed by NCASI. The reported data are the average of triplet samples. Liquor samples were collected at the same time and analyzed by the headspace GC method at IPST [36]. Detailed liquor methanol profile along the fiberline is presented in other publications [37, 12].

The methanol air emissions from those sources shown in Fig. 5.17 can be calculated from Eq. (5.31). The result is shown in Fig. 5.18. The only difference between Eqs (5.30) and (5.31) is vent air flowrate, G, in Eq. (5.31). The significance of air flowrate on air emissions can be demonstrated by comparing Fig. 5.17 and Fig. 5.18. Although methanol concentration in the O_2 blow tank vent is approximately 10 times higher than that in the O_2 atmospheric diffuser vent, methanol emission from the O_2 blow tank is only half of that from the O_2 atmospheric diffuser due to its low air flowrate. Although reducing air flow causes higher methanol concentration in vents, methanol emission can be reduced.

It is difficult and costly to measure methanol concentrations in vents. However, they can be reliably calculated from methanol liquor concentrations and liquor temperatures. Therefore, the prediction of methanol concentrations in vents is relatively certain. On the other hand, vent flowrate is very equipment specific. For example, air flowrate from a vacuum drum washer hood is mainly determined by the discharge fan. Different washers may use very different fan

sizes. It is difficult to develop reliable methods to predict air flowrates for various equipment. However, it is relatively easy to measure or estimate air flowrate from the specific equipment used. Therefore, a reliable approach to predict methanol air emission is combining the model, Eq. (5.30), with measured air flowrate. In this paper, all air flowrates are from mill measurements.

5.3.5.2 Multi-Source Emissions

A vacuum drum washer hood is a typical example of multiple source air emission. Methanol air emissions from washer hoods are affected by methanol concentrations in both the vat and showers. Some mills use two different shower liquids, (i.e. split showers) on the same washer. Therefore, three liquid concentrations and three temperatures affect air emissions from a single washer hood.

Measurements from three kraft mills have been collected to test the model. The result is shown in Fig. 5.19. Mill A and B produce bleached pulp. Mill B uses split showers for the two washers shown in Fig. 5.19. Mill C is a linerboard mill that has three parallel washing lines. The Mill C data shown in Fig. 5.19 are the average of the three lines.

Liquor samples and process operating conditions were also collected during the air sampling. Methanol air emissions from similar washers in the same fiberline vary significantly. In Mill A, the emission from No.1 brown stock washer (#1BSW) is approximately 10 times higher than that from No.2 post oxygen washer (#2POW). Also, the measurements show that the emission from the decker is higher than that from the No.2 brown stock washer (#2BSW). However, the methanol concentrations in filtrates decrease from (#1BSW) to (#2POW). Therefore, filtrate concentration is not the only factor affecting air emission. The difference from mill to mill is also significant. In Mill A and Mill C, the methanol concentrations of No.1 brown stock washers (#1BSW) are similar. However, methanol air emission of #1BSW in Mill C is only about 1/5 of that of #1BSW in Mill A.

The methanol air emissions from these hoods are calculated using Eqs. (5.34) and (5.35) and shown in Fig. 5.19. The same methanol equilibrium model (7) has been applied to all calculations. The equilibrium model automatically takes consideration of filtrate temperature on

methanol air emissions. The same values of $(K_Ga)_v$ and $(K_Ga)_s$ were used for all four hoods in Mill A. The model correctly predicts the low emission at No.2 brown stock washer. The low temperatures at No.2 brown stock washer is responsible for its low air emission. Filtrate temperature plays an important role in methanol air emissions. The effect of filtrate temperature on air emission is also demonstrated in Fig. 5.20. If decker shower temperature in Mill A is reduced 20^{o}C, emission is reduced over 50% according to the model. Of course, washing efficiency has to be considered in choosing the best shower temperature.

In Mill A, the vent flowrate from #1BSW and #2BSW is twice that of the decker and #2POW. The hood air flowrates in Mill B are approximately 1/7 of those in Mill A. One difference between Mill A and Mill B is that sampled vents in Mill B (D_0 and Eop) are collected and go through a caustic scrubber to remove chlorine species. Perhaps, due to that concern, the vent system was not over-designed and is operated carefully. To control odor on the washing floor, large hood vent flows are traditionally used to improve the operating environment. This study has shown that large vent flows can result in higher VOC air emissions. A tradeoff between VOC emissions and odor should be considered in the operation of vent systems. However, some simple practices, such as closing washer hood doors, are good for VOC emission reduction and improving the operating environment.

The impact of air flowrate on methanol emission from washer hoods is demonstrated in Fig. 5.20. If the air flowrate of #1BSW in Mill A is cut to Mill B level, methanol air emission from #1BSW in Mill A will be reduced to 1/5 of current emission. This is close to the situation of the D_0 washer hood in Mill B.

The same pulp production adjusted mass transfer coefficients, $(K_Ga)_v$ and $(K_Ga)_s$, are used in the calculations for all washer hoods of Mill A and Mill B in Fig. 5.19. This means that mass transfer conditions in these hoods are similar. When the same production adjusted mass transfer coefficients are applied to the hoods of Mill C, the predicted methanol emissions are much higher than measurements. Much lower mass transfer coefficients are needed for the model to match the measurements. Mass transfer conditions in the hoods of Mill C are very different from those of Mill A and Mill B. Physically, the open hood structure of Mill C is also very different from those in Mill A and Mill B.

The vent air temperature is a good indicator of mass transfer conditions. When the air temperature is close to the vat and shower temperatures, there are good mass transfer conditions in the washer. Theoretically, there is a relationship between mass transfer and heat transfer. Since it is easy to measure temperatures, it is possible to calculate mass transfer coefficients from various temperature measurements. More study is needed to develop a reliable approach to predict mass transfer coefficients.

5.3.5.3 Paper Machine / Pulp Dryer Emissions

Table 5.VI compares model predictions with NCASI mill measurements [34] for methanol air emissions from paper machines / pulp dryers. Each measurement represents a different paper machine / paper dryer. The mill data for the wet end general vents are calculated by subtracting the measured vacuum vent emissions from the measured total wet end emissions. Only methanol concentration in white water was measured during the study. In the model predictions for the dry section, Eq. (5.36), 40% press consistency is used because pulp consistency at the press discharge was not measured. Measured air flowrates and methanol concentrations in the white water are used in Eq. (5.38) to predict air emissions from vacuum vents. The same mass transfer coefficient adjusted by production is used for all five mills. Also, the same mass transfer coefficient adjusted by production is used in Eq. (5.37) to predict methanol air emission from the wet end general vents for all mills.

5.3.5.4 Smelt Dissolving Tank Emissions

Very limited data are available to test the air emission model for smelt dissolving tanks. The scrubber plays an important role in the air emission of smelt dissolving tanks. In the previous NCASI study [38], not enough data were collected to validate the currently proposed model. Based on our best estimation for all parameters in Equation (??), a model predicted methanol concentration in SDT vent air is calculated from the measured methanol concentration in the weak wash. The same set of parameters is used for all three cases in Fig. 5.21. A comparison of model prediction with mill measurements is shown in Fig. 5.21. The proposed model reflects the difference between No.1 SDT and No.2 SDT in Mill D in which the same weak wash was used.

5.3.6 Prediction of Other VOC Emissions

The same air emission models validated by methanol can be applied to other volatile compounds, such as TRS and chlorine species. Because the mass transfer coefficient is mainly determined by the mass transfer conditions in the equipment involved, the same value used for methanol can be applied to other VOC's. However, the equilibrium constant is totally determined by the species involved and the temperature.

In Fig. 5.22, it is demonstrated that acetone air emissions can be predicted by the same model, Eq. (5.34), with the same mass transfer coefficients for all washer hoods. Methanol air emission predictions are shown in Fig. 5.19. Because acetone concentration in filtrates is much lower than methanol, acetone air emissions are much lower.

5.4 Conclusions

A general methanol and water equilibrium model has been developed with special emphasis on low methanol concentrations. The methanol infinite dilution activity coefficient is temperature dependent. Temperature is the single most important factor influencing methanol equilibrium. Henry's law is acceptable when methanol concentration in the liquid phase is lower than 1800 mg/kg. Dissolved solids in kraft liquors increase methanol equilibrium constants. Dissolved inorgnics have stronger impact than dissolved organics. The impact of dissolved inorganics is not species dependent for the investigated inorganics.

Methanol is mainly generated during cooking in kraft mills. Methanol is produced from methoxyl groups in hemicellulose and lignin. Methanol can also be generated during oxygen delignification and bleaching. The methoxyl groups in dissolved lignin causes methanol generation during black liquor storage and evaporation. Wood species and the final cooking Kappa are two major factors that affect total methanol generation in kraft mills. Model parameters for predicting methanol generation are determined from limited available measurements. From these models, methanol generation can be predicted for different wood species and operating conditions. A simplified cooking model (Eqs. (5.24)~(5.26)) is applicable for most mill digesters. At Kappa numbers lower than 90, there is a linear relationship between methanol generation and final digester Kappa number. Methanol generation in oxygen

delignification and bleaching is determined by the type of bleaching chemical and the degree of Kappa reduction.

VOC air emissions can be calculated from VOC liquor concentrations and temperatures by the models presented in this paper. These models are based on mass transfer and equilibrium calculations. Equipment and its operating conditions affect the mass transfer coefficients and the air flowrate in these models. The same principles of mass transfer and equilibrium calculation can be applied to VOC air emission calculations for all situations. However, a specific model has to be developed for each kind of equipment. In this paper, models for vacuum drum washer hoods, washer seal tanks, atmospheric diffusers, oxygen delignification blow tanks, bleaching towers, paper machines/pulp dryers and smelt dissolving tanks are presented. The models are validated by methanol mill measurements in three kraft mills. The same models and mass transfer coefficients are able to predict the air emissions of other VOC species.

Reducing vent air flowrate can reduce the amount of VOC air emissions although it will increase VOC concentrations in the vent air. Reducing liquor temperatures can also reduce methanol air emissions due to lower equilibrium constants.

NOMENCLATURE

A = Coefficient for methanol generation
or pre-exponential coefficient of reaction rate
AQ = Anthraquinone charge, % on wood
C = Hemicellulose or lignin concentration, kg/L
c = Pulp consistency at press discharge, %
E = Activation energy, j/mol.K
E_{VOC} = VOC air emission, mt/h
F = Influence factors in methanol generation, fraction
f_x = Fraction of methoxyl in hemicellulose, mass fraction
G = Methanol generation, kg/ODTW
or Gas flowrate (vented wet air), mt/h
G_H = Methanol generation from hemicellulose, kg/ODTW
G_L = Methanol generation from lignin, kg/ODTW (cooking) or kg/ODTP
H_W = Hemicellulose content in wood, kg/ODTW
K = VOC equilibrium constant
k = Rate constant, 1/minute
K_Ga = Overall mass transfer coefficient, mt/hr
K_i = Equilibrium constant of component i
Kappa = Kappa number
L = Liquor flowrate, mt/h
L_C = Circulation liquor flowrate in smelt dissolving tank scrubber, mt/h
L_M = Liquor makeup to smelt dissolving tank scrubber, mt/h
L_W = Lignin content in wood, kg/ODTW
M_{SM} = Smelt mass flowrate, mt/h
n_M = Number of methoxyl in each lignin monomer
P = Pulp rate into the dryer section, ODmT/h
$P_i^o(T)$ = Saturated vapor pressure of pure component i at temperature T, mmHg
P_T = Total pressure on system, mmHg
R = General gas constant, J/mol.K
R_K = Ratio of liquor equilibrium constant to water equilibrium constant, see Eq.(5.7)
R_{Li} = Fraction of demethylation during initial cooking stage, fraction
S = Sulfidity, %
T = Temperature, K
t = Time, minutes
T_i = Intermediate smelt temperature, ^oC
T_{SM} = Smelt temperature, ^oC
T_{WW} = Temperature of weak wash entering smelt dissolving tank, ^oC
V_T = Evaporated water flowrate from smelt dissolving tank, mt/h
W_{DIS} = Dissolved inorganic solids content, mass fraction
W_{DOS} = Dissolved organic solids content, mass fraction
X_n = Number average degradable chain length
x_i = VOC content in inlet liquor stream, mass fraction
or Mole fraction of component i in liquid phase at equilibrium
x_o = VOC content in outlet liquor stream, mass fraction

x_{WW} = VOC content in weak wash, mass fraction
y_e = VOC equilibrium concentration, mass fraction
y_i = Mole fraction of component i in vapor phase at equilibrium
y_o = VOC content in outlet gas stream, mass fraction
y_P = Pulp yield of cooking, fraction
y_{si} = VOC content in inlet stream of SDT scrubber, mass fraction
ΔH_i = Partial molar excess enthalpy of component i, j/mol
γ_i = Activity coefficient of component i
ϕ_i = Fugacity coefficient of component i
τ_{12}, τ_{21}, α = NRTL activity coefficient model parameters

Subscripts:

- AQ = Anthroquinone
- BL = Black liquor
- C = Conversion of methoxyl into methanol
- D = Degree of dissolution for hemicellulose or lignin
- d = Delignification after initial dissolution
- H = Hemicellulose
- i = Initial value (time = 0)
- Inf = Value at infinite time
- L = Lignin
- max = Maximum
- S = Bleaching stage or sulfidity
- x = Xylan
- W = Wood

Subscripts:

- V = Vat
- S = Shower
- ST = Top shower
- SB = Bottom shower

REFERENCES

1. Blackwell, B.R., MacKay, W.B., Murray, F.E. and Oldham, W.K., *TAPPI J.,* **62**(10): 33, 1979.
2. Zhu, J.Y. and Chai, X.S., *TAPPI J.,* **82**(2): 123, 1999.
3. Zhu, J.Y., Liu, P.H., Chai, X.S., Bullock, K.R., and Teja, A.S. *Environ. Sci. & Techno.,* **34**(9):1742, 2000.
4. Blackwell, B.R., Murray, F.E. and Oldham, W.K., *TAPPI J.,* **63**(2): 151, 1980.
5. Gupta, A.K., MS thesis, Georgia Institute of Technology, 1998.
6. Chai, X.S. and Zhu, J.Y., *J. Chromatography A,* **799**:207, 1998.
7. Benedek, P. and Olti, F., Computer Aided Chemical Thermodynamics of Gases and Liquids, John Wiley & Sons.
8. Dalager, P., J. *of Chem. Eng. Data,* **14**(3): 298, 1964.
9. Richon, D., *Ind. Eng. Chem. Process Des. Dev.,* **24**:1160, 1985.
10. Pividal, K.A., Birtigh, A. and Sandler, S.I., *J. of Chem. Eng. Data,* **37**:484, 1992.
11. Hirata,M., Ohe, S. and Nagahama, K., *Computer Aided Data Book of Vapor-Liquid Equilibria,* Lodansha Ltd., Elsevier Scientific, Tokyo, 1975.
12. Gu, Y., Edwards, L.L., Zhu, J.Y. and Chai, X.S., Cluster rule compliance tools: Predicting kraft mill VOC's, Part 2 of 4. Methanol generation models, *TAPPI J,* **84**(4):65, 2001.
13. Gu, Y. and Edwards, L.L., Cluster rule compliance tools: Predicting kraft mill VOC's, Part 4 of 4. Mill validated air emission models, *TAPPI J,* **84**(4):65, 2001.
14. Clayton, D.W., *Svensk Papperstidning,* **66**(6):28, 1963.
15. Wilson, D.F., Johanson, L.N. and Hrufiord B.F., *TAPPI J.,* **55**(8):1244, 1972.
16. Zhu, J.Y., Chai, X.S. and Dhasmana, B., *J. Pulp & Paper Sci.,* **25**(7):256, 1999.
17. Zhu, J.Y., Yoon, S.H., Liu, P.H., and Chai, X.S., *TAPPI J.,* **83**(7):65, 2000.
18. Gellerstedt, G. and Lindfors, E.-L., *Holzforschung,* **38**:151, 1984.
19. Gellerstedt, G. and Lindfors, E.-L., *TAPPI J.,* **70**(6):119, 1987.
20. Jiang, Z.-H. and Argyropoulos, D.S., *J. Pulp & Paper Sci.,* **25**(1):25 1999.
21. Zhu, J.Y., Liu, P.H., Yoon, S.H., Chai, X.S. and Thomas, J.T., *1999 TAPPI Engineering Conference,* Anaheim, CA, Sept. 1999.
22. Rydholm, S. A., *Pulping Processes,* Interscience Publishers, p95, 1967.
23. Grace, T.M., Malcolm, E.W. and Kocurek, M.J., *Pulp and Paper Manufacture: Alkaline Pulping,* Joint Textbook Committee of the Paper Industry, 1989.
24. Kondo, R. and Sarkanen, K.V., *Holzforschung,* **38**:31, 1984.

25. Ni, Y., Kubes, G.J. and van Heiningen, A.R.P., *J. Pulp & Paper Sci.*, **16**(1):13, 1990.

26. Ni, Y., Kubes, G.J. and van Heiningen, A.R.P., J. Pulp & Paper Sci., **21**(1):30, 1995.

27. Ni, Y., A Fundamental Study of Chlorine Dioxide Bleaching of Kraft Pulp, Ph.D. Dissertation, McGill University, 1992.

28. Crawford, R.J., Rovell-Rixx, D.C., Jett, S.W., Jain, A.K. and Dillard, D.S., *TAPPI J.*, **78**(5):81, 1995.

29. Jain, A.K., Proceeding of TAPPI Minimum Effluent Mill Symposium, 1996.

30. Vice, K. and Carroll, R., *TAPPI J.*, **81**(2):91, 1998.

31. Gu, Y.X., Edwards, L.L., Haynes, J.B, and Euhus, L.E., *TAPPI J.*, **81**(2):173, 1998.

32. Gu, Y.X., Edwards, L.L., Zhu, J.Y., Liu, P.H. and Chai, X.S., Cluster rule compliance tools: Predicting kraft mill VOC's, Part 3 of 4. Methanol equilibrium calculations, *TAPPI J*, **84**(4):65, 2001.

33. NCASI Technical Bulletin No.681, NCASI, New York, NY, September, 1994.

34. Edwards, L.L., GEMS Documentation Manual. Moscow, Idaho: Idaho Research Foundation 1972, 1979, 1983, 1995.

35. Chai, X.S. and Zhu, J.Y., *Analytical Chemistry*, **70**(16):3481, 1998.

36. Gu, Y.X., Edwards, L.L., et al. *1998 International Environmental Conference*, Vancouver, Canada.

37. NCASI Technical Bulletin No.676, NCASI, New York, NY, September 1994.

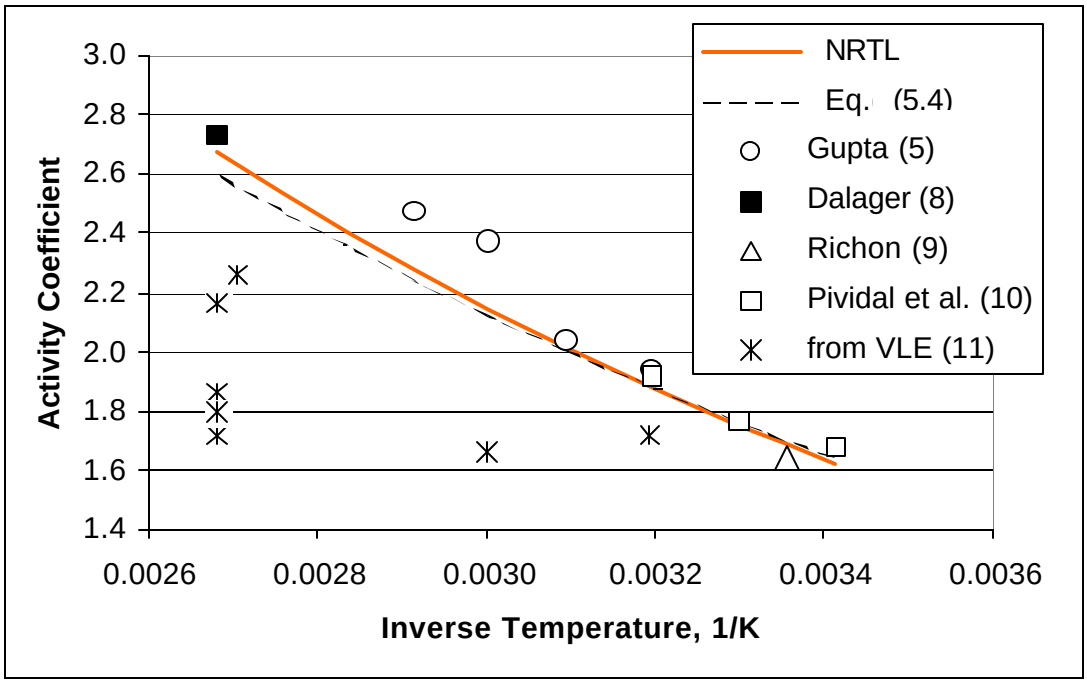

Fig. 5.1. Temperature Effect on Methanol, Infinite Dilution, Activity Coefficient

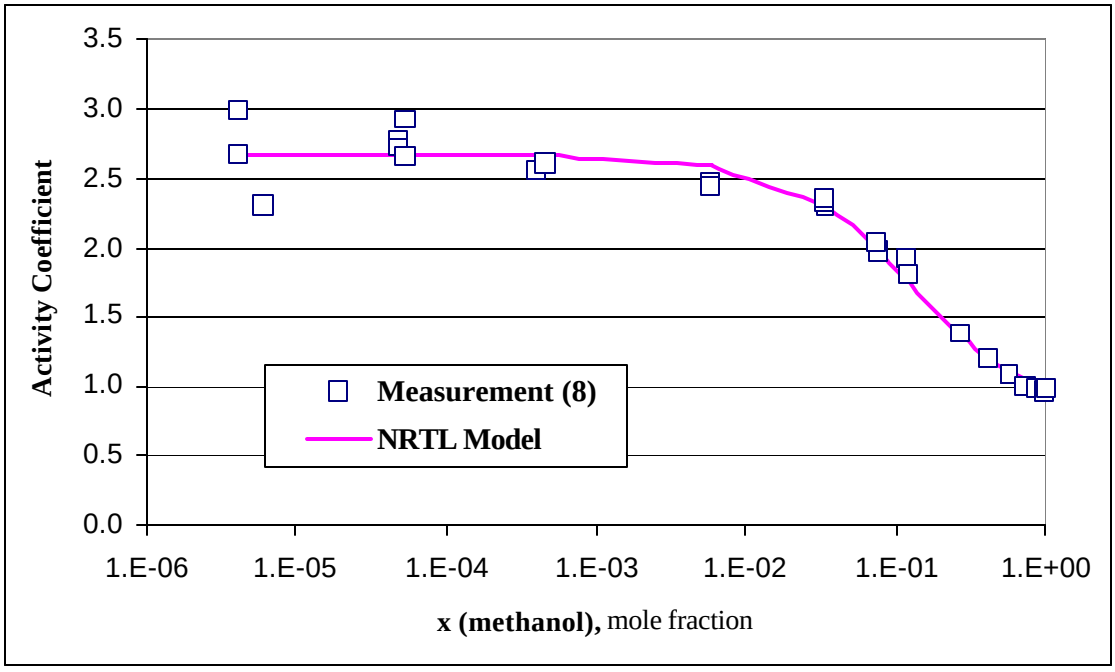

Fig. 5.2. Comparison of Model Prediction with Measurements for Methanol Activity Coefficients (760mmHg)

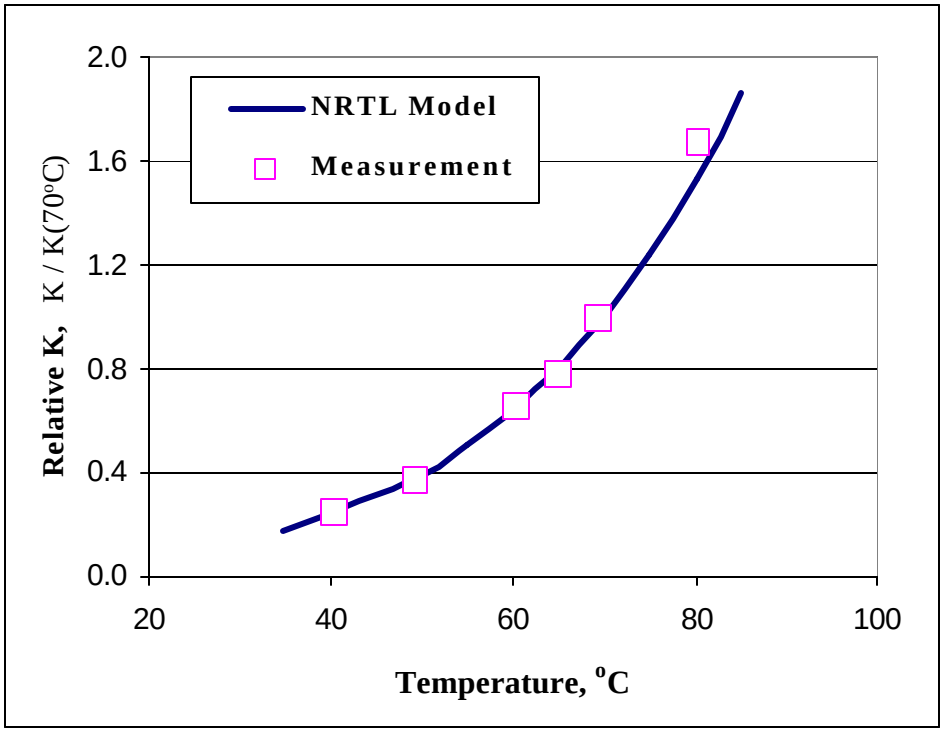

Fig. 5.3. Comparison of Model Prediction with Measurements: Temperature Effect on Methanol Equilibrium Constant (760 mmHg, and Infinite Dilution)

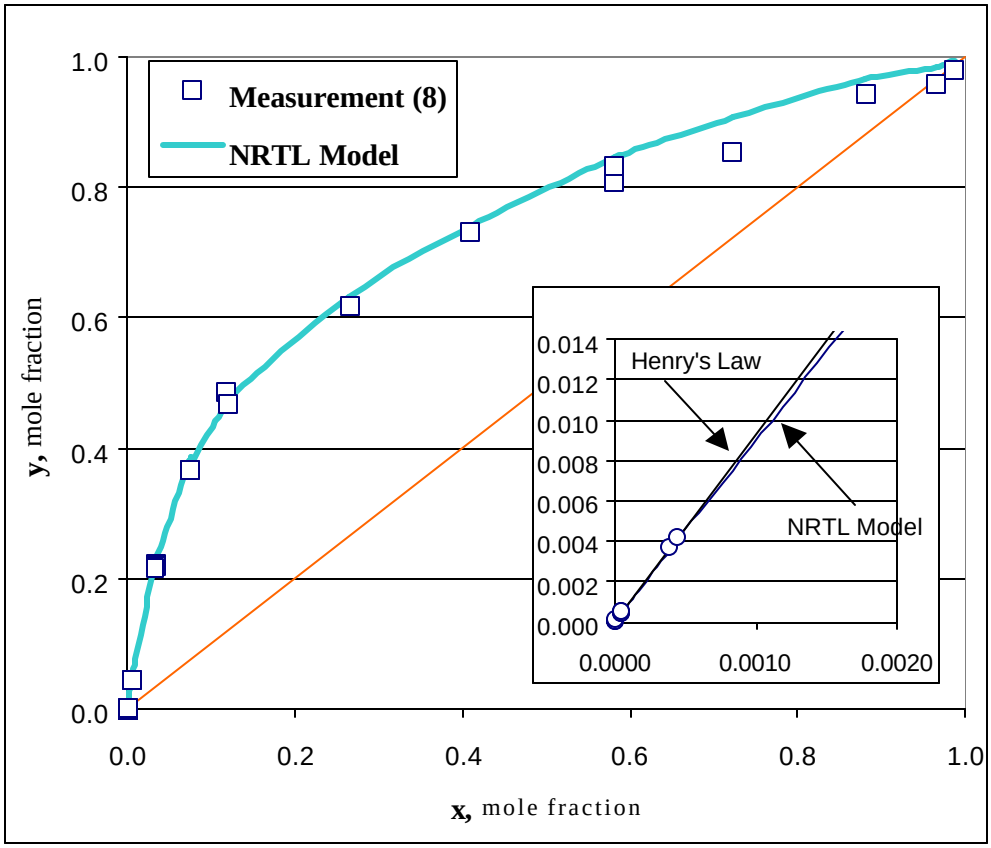

Fig. 5.4. Methanol Equilibrium Concentration in Methanol and Water System (760 mmHg)

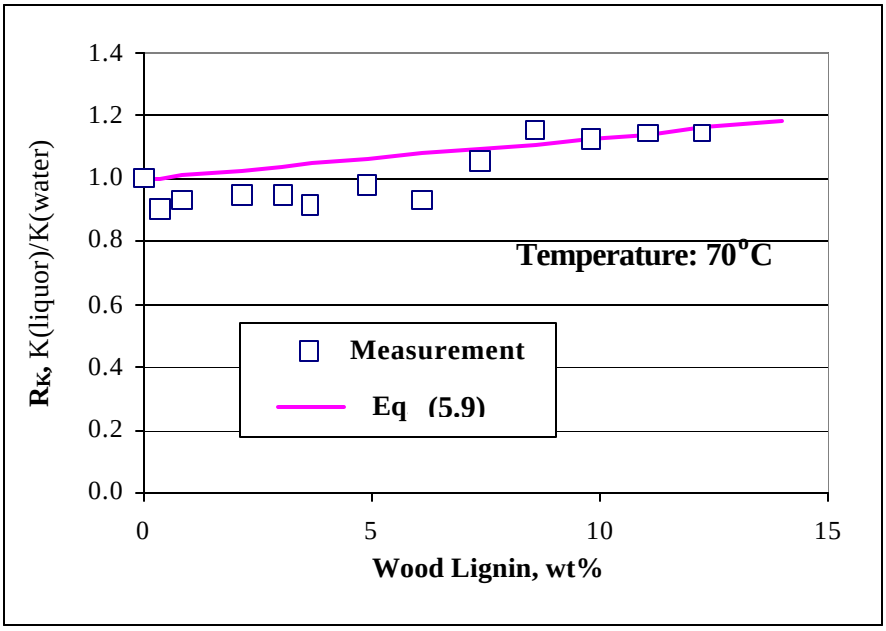

Fig. 5.5. Impact of Wood Lignin on Methanol Equilibrium Constants (pH 9.8)

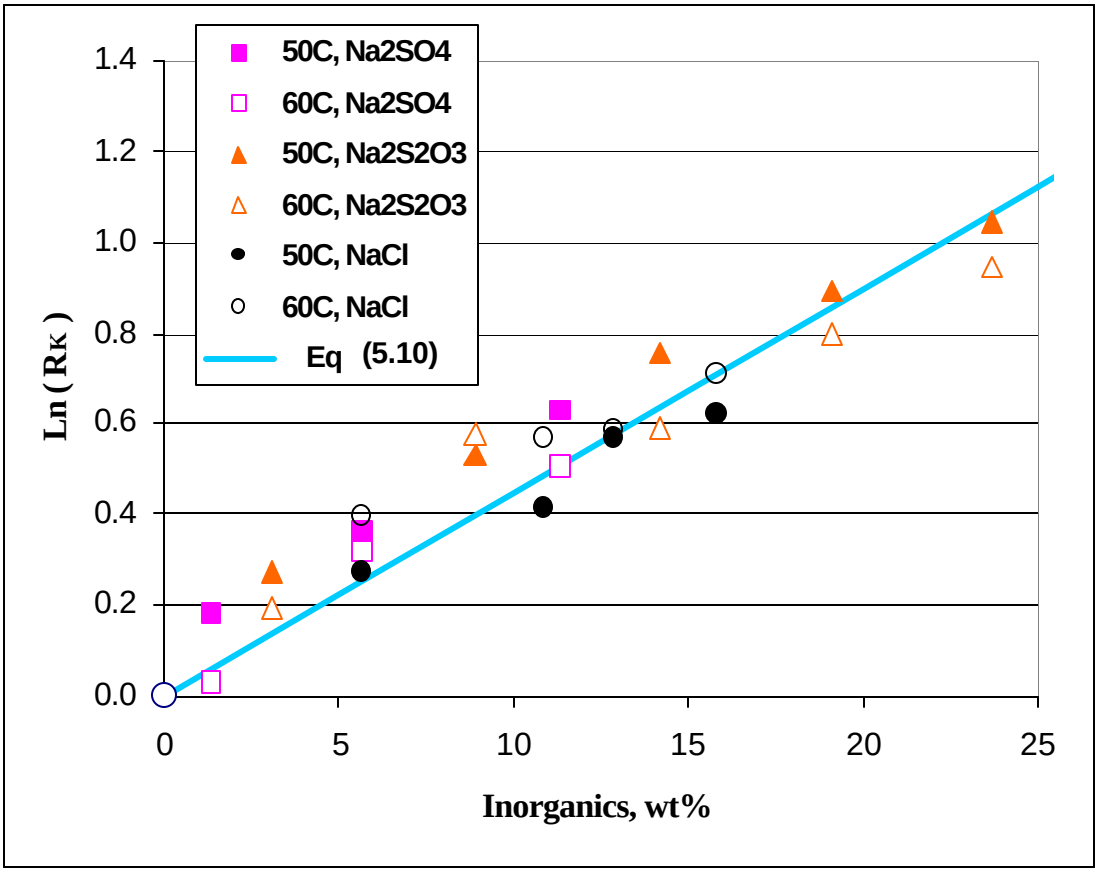

Fig. 5.6. Impact of Inorganics on Methanol Equilibrium Constants

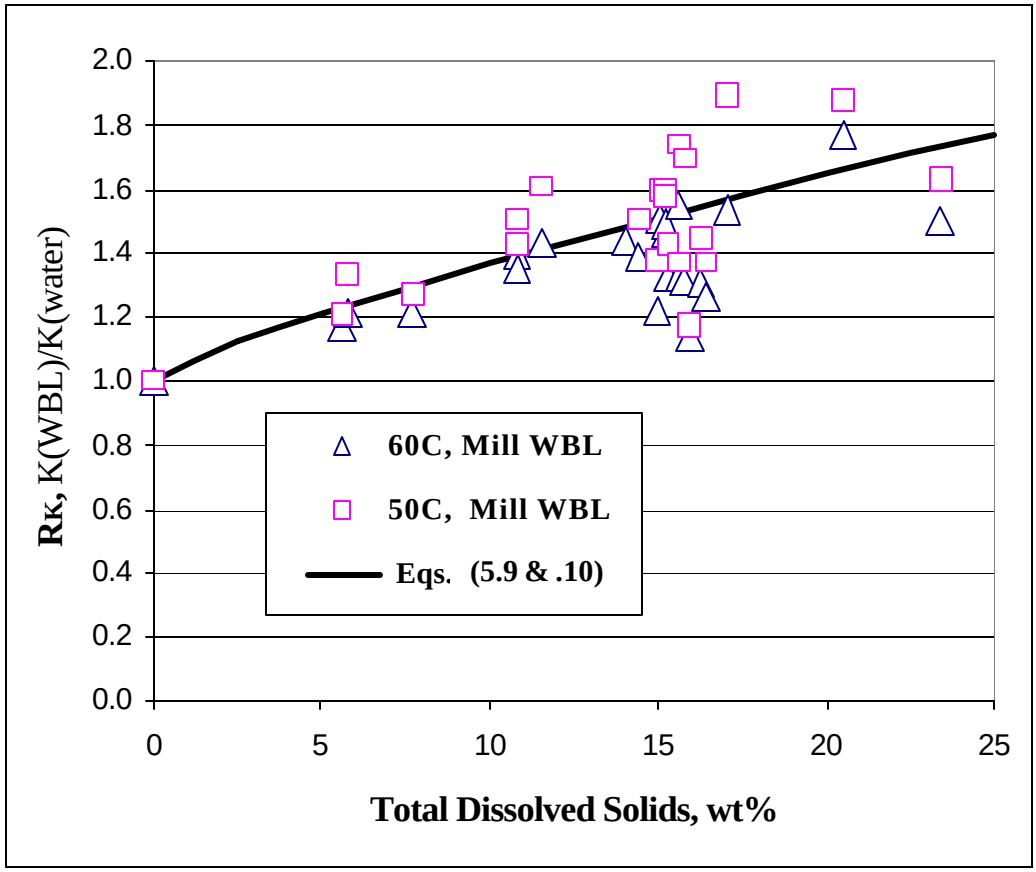

Fig. 5.7. Effect of Dissolved Solids in Kraft Liquors on Methanol Equilibrium Constants

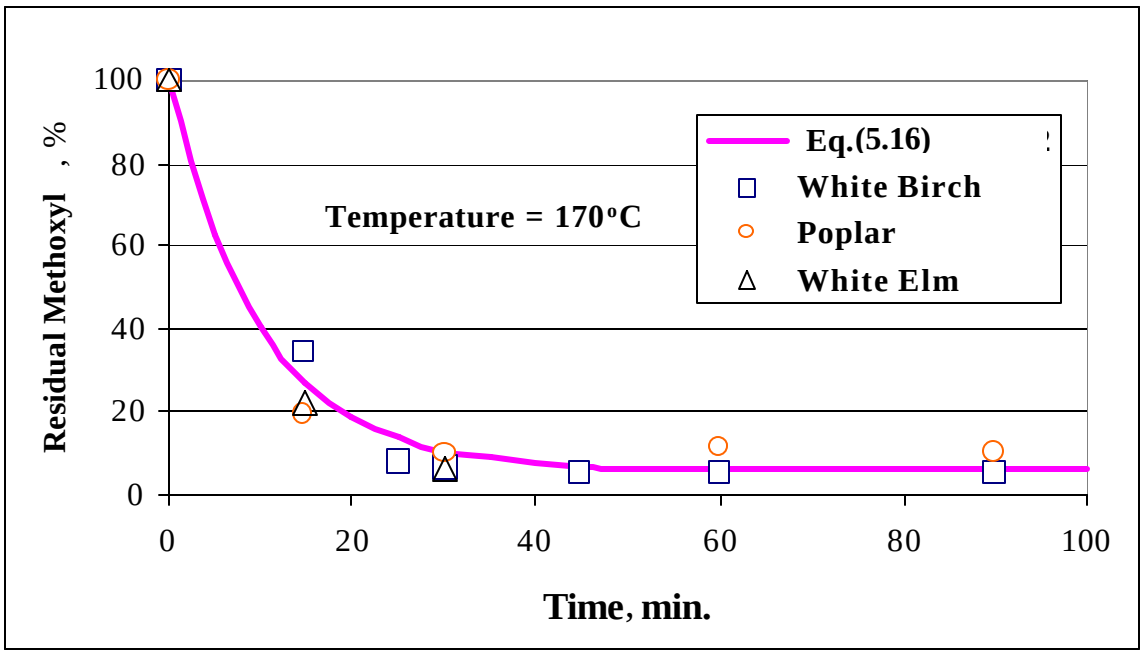

Fig. 5.8. Dissolution of Methoxyl from 4-*O*-Methyl-D-Glucuronoxylans [15]

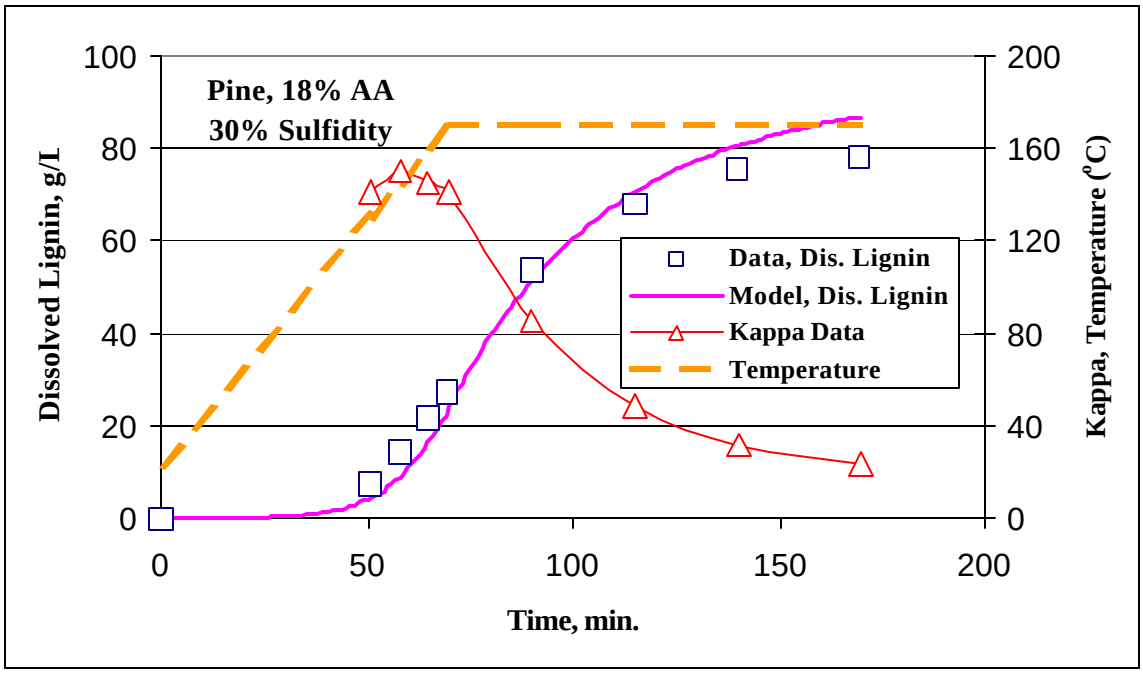

Fig. 5.9. Delignification during Laboratory Batch Cooking and Model Prediction

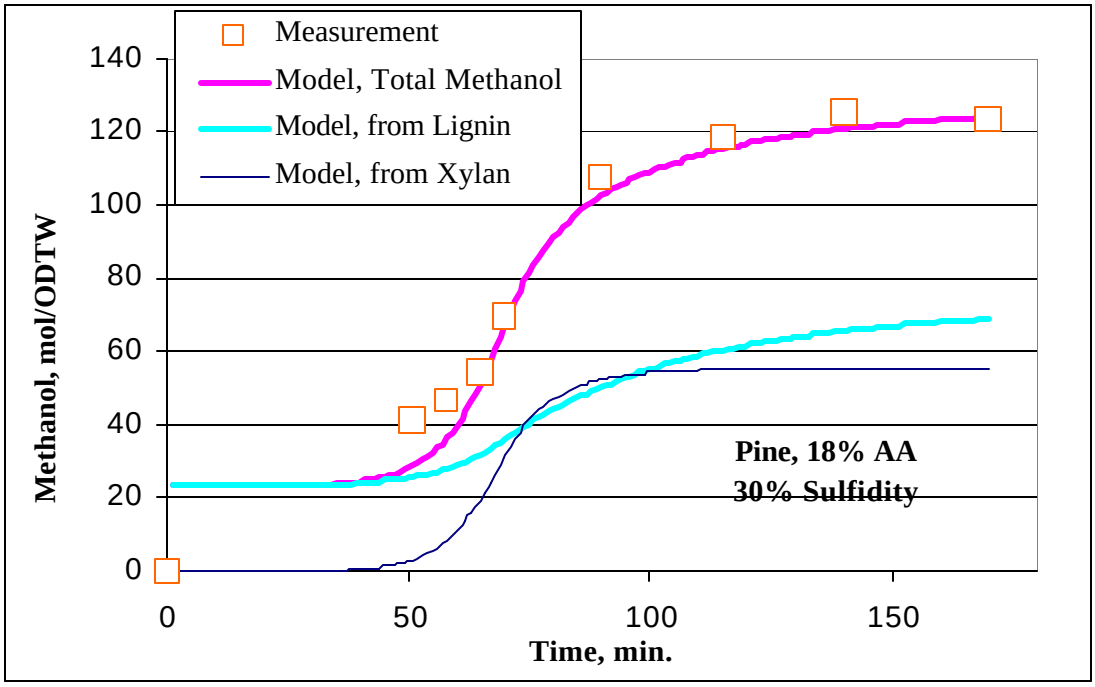

Figure 5.10. Model Prediction of Methanol Generation during Batch Cooking

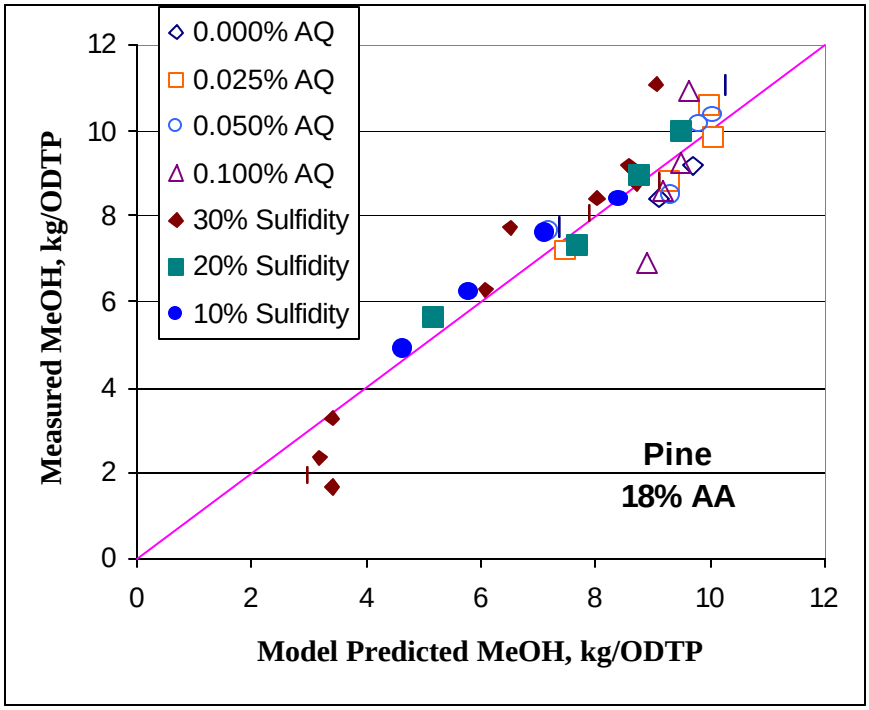

Figure 5.11. Comparison of Model with Measurements for Sulfidity and AQ Effect on Methanol Generation

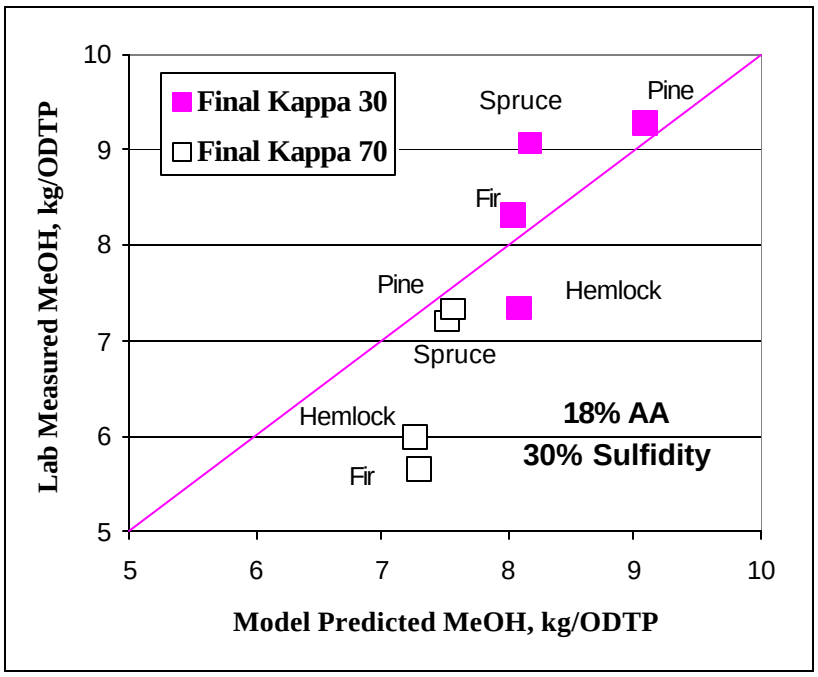

Figure 5.12. Comparison of Model Predicted Softwood Methanol Generation with Laboratory Measurements

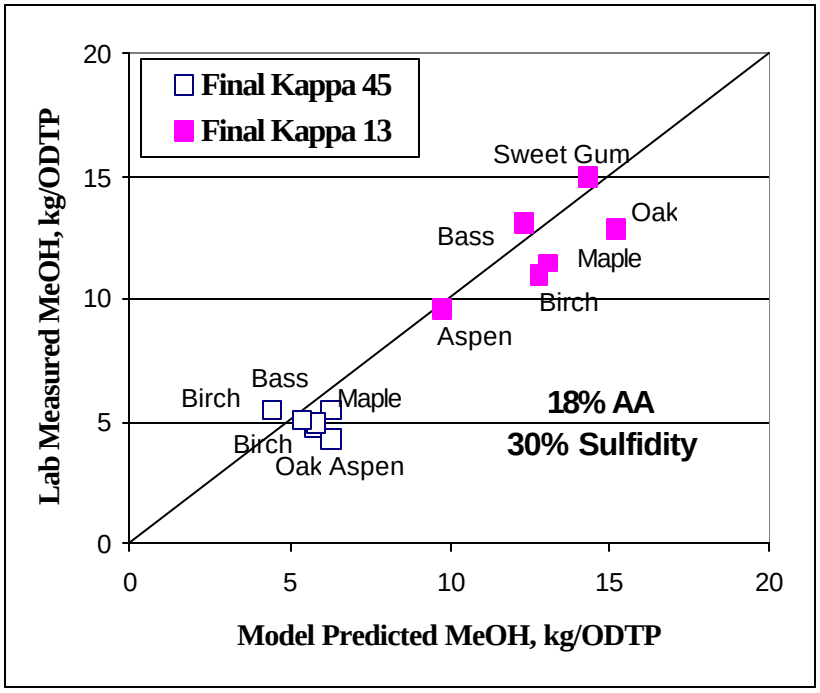

Figure 5.13. Comparison of Model Predicted Hardwood Methanol Generation with Laboratory Measurements

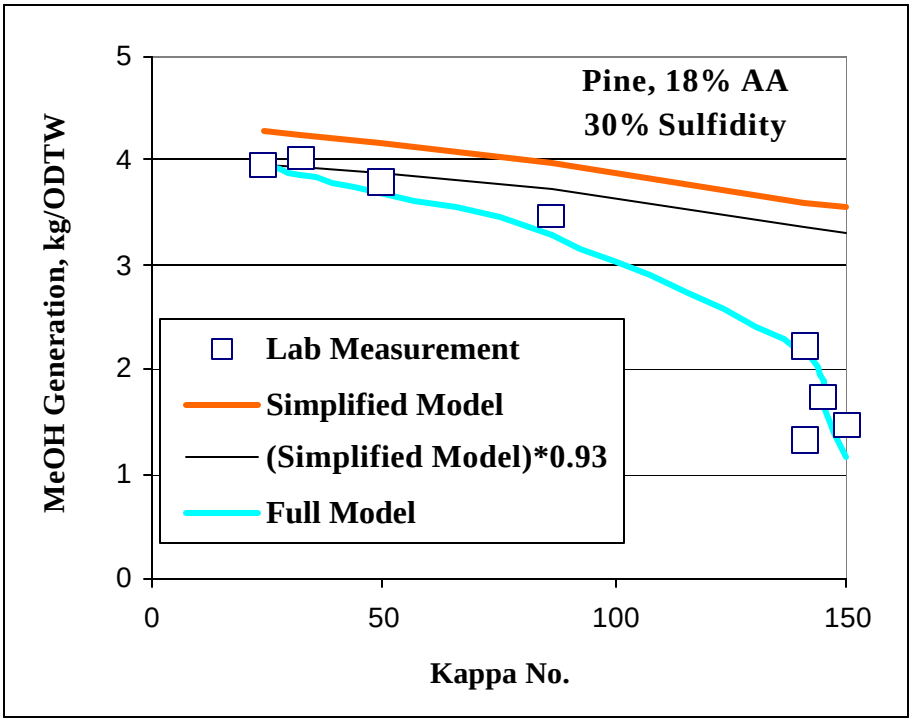

Figure 5.14. Impact of Kappa on Methanol Generation and Model Prediction

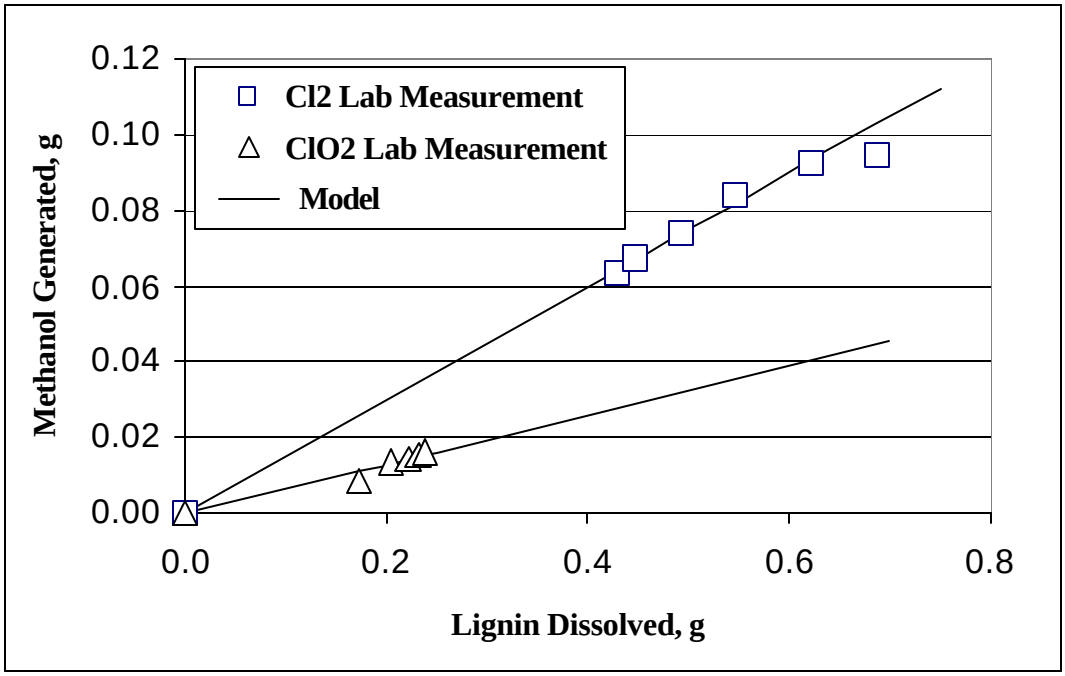

Figure 5.15. Methanol Generation from Chlorination [26] and ClO_2 Bleaching [28]

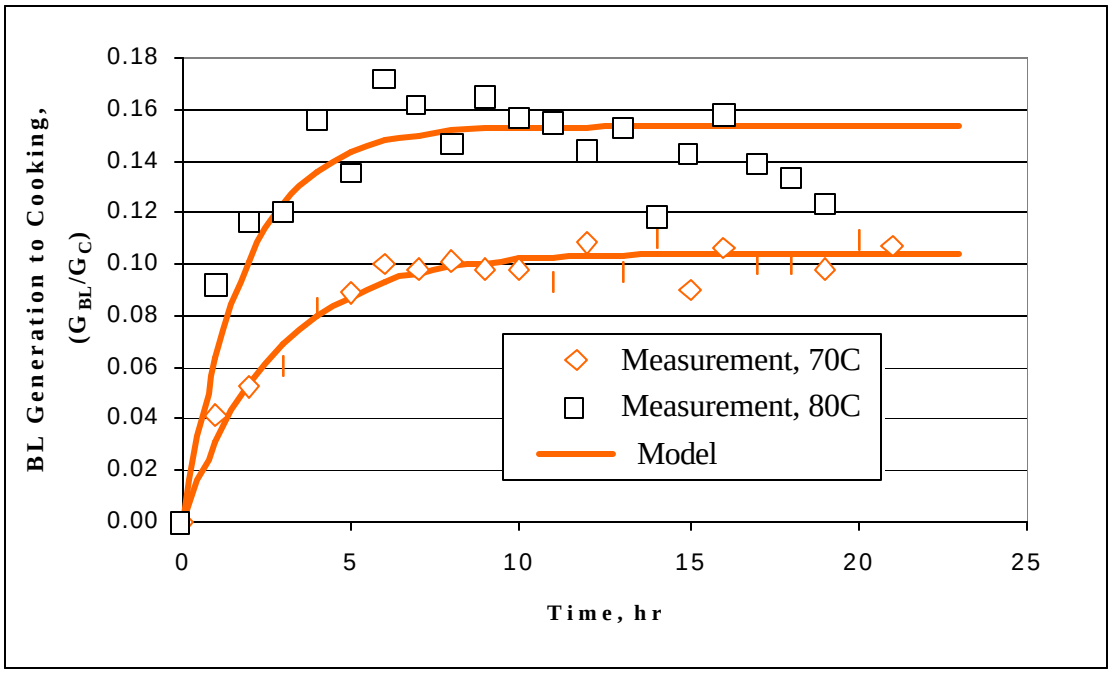

Figure 5.16. Methanol Generation during Black Liquor Storage

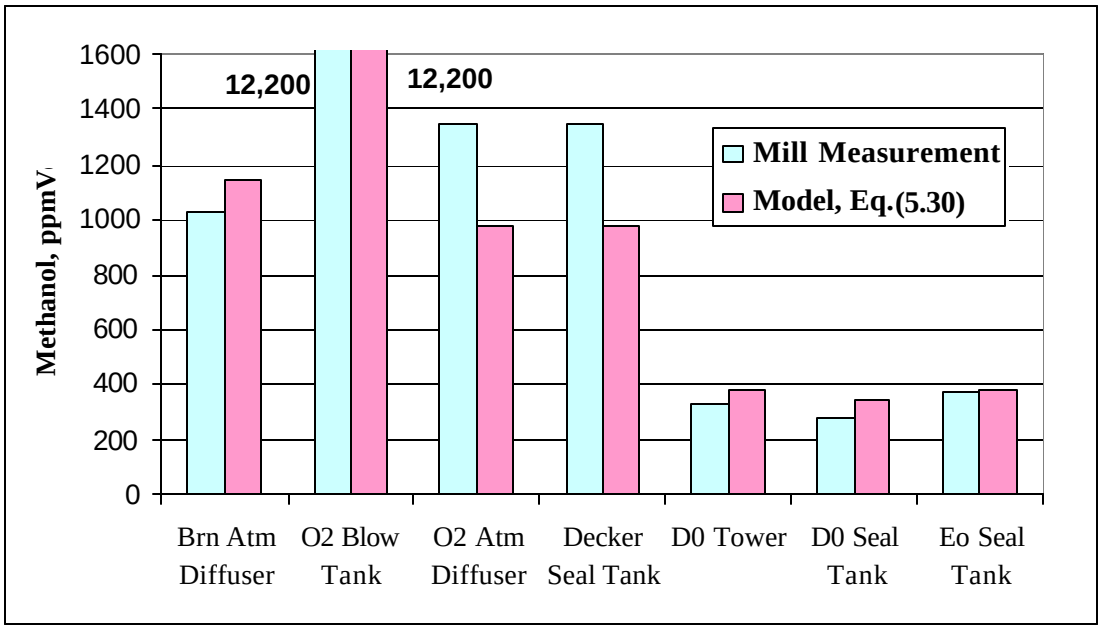

Figure 5.17. Comparison of Model Predictions with Mill Measurements: Methanol Vent Concentrations

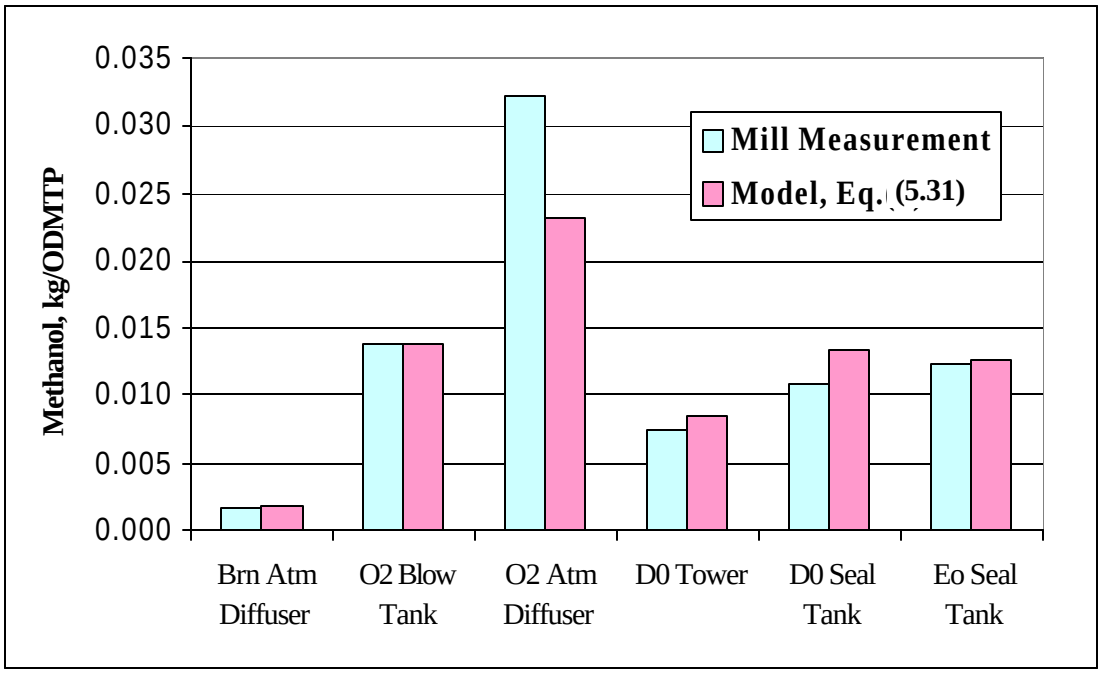

Figure 5.18. Comparison of Model Predictions with Mill Measurements: Methanol Vent Emissions

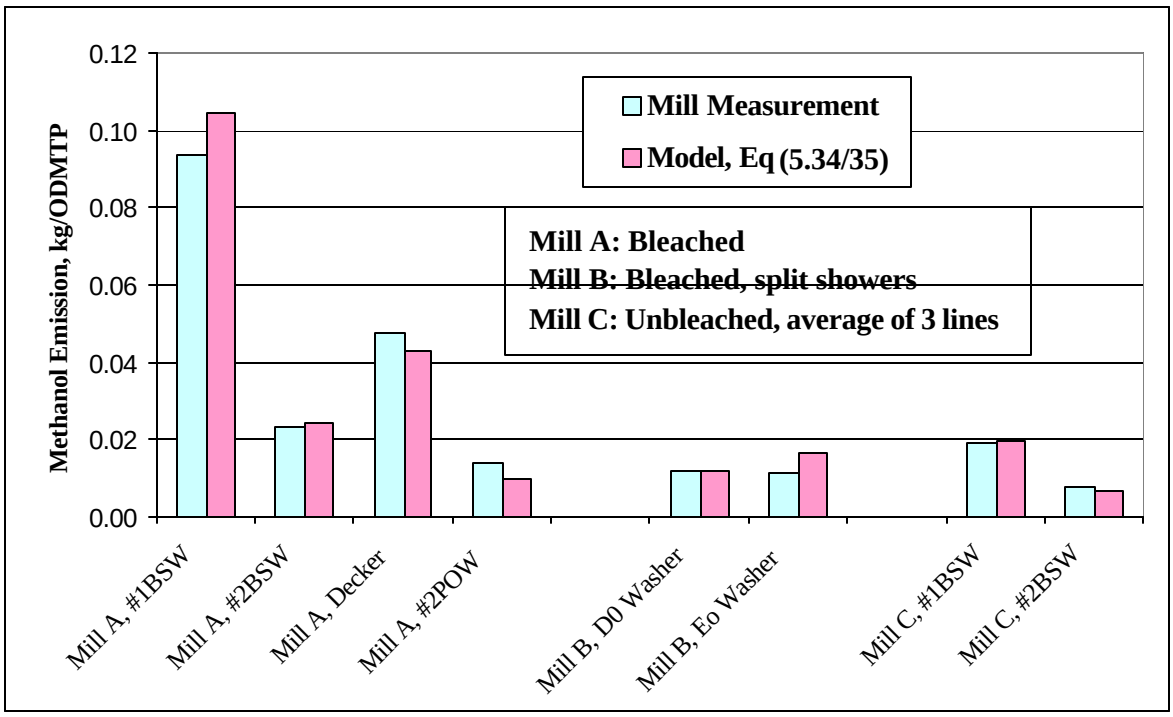

Figure 5.19. Comparison of Model Predictions with Mill Measurements: Methanol Air Emissions from Drum Washer Hoods in Three Kraft Mills

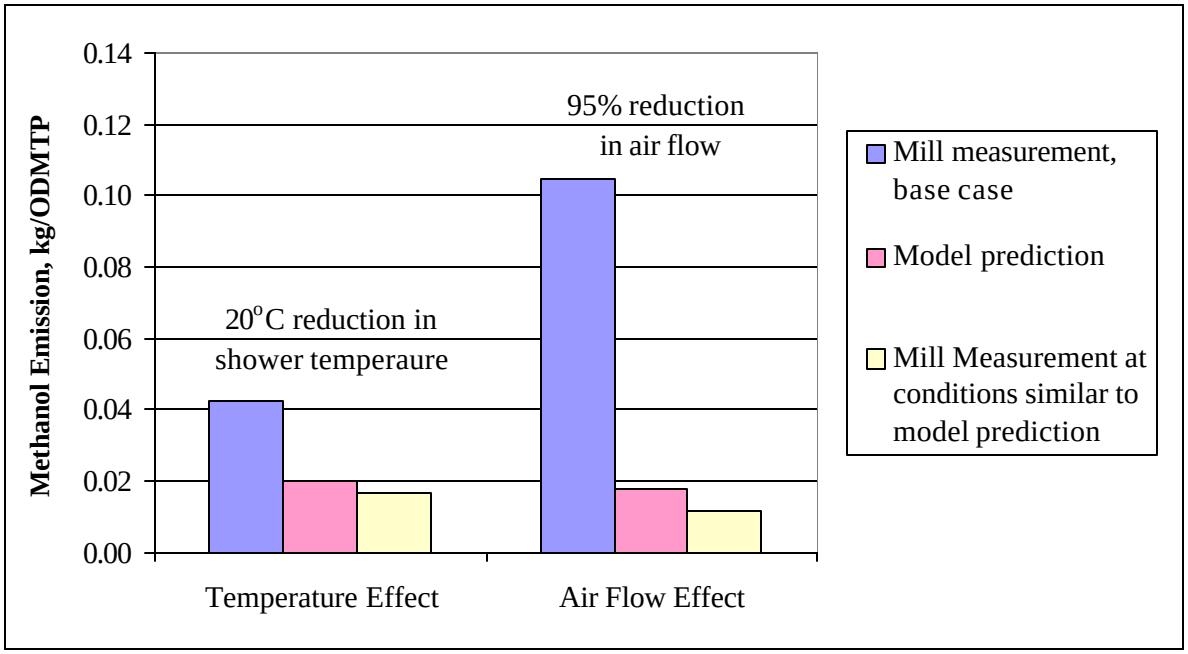

Figure 5.20. Impact of Operating Conditions on Air Emissions from Washer Hoods

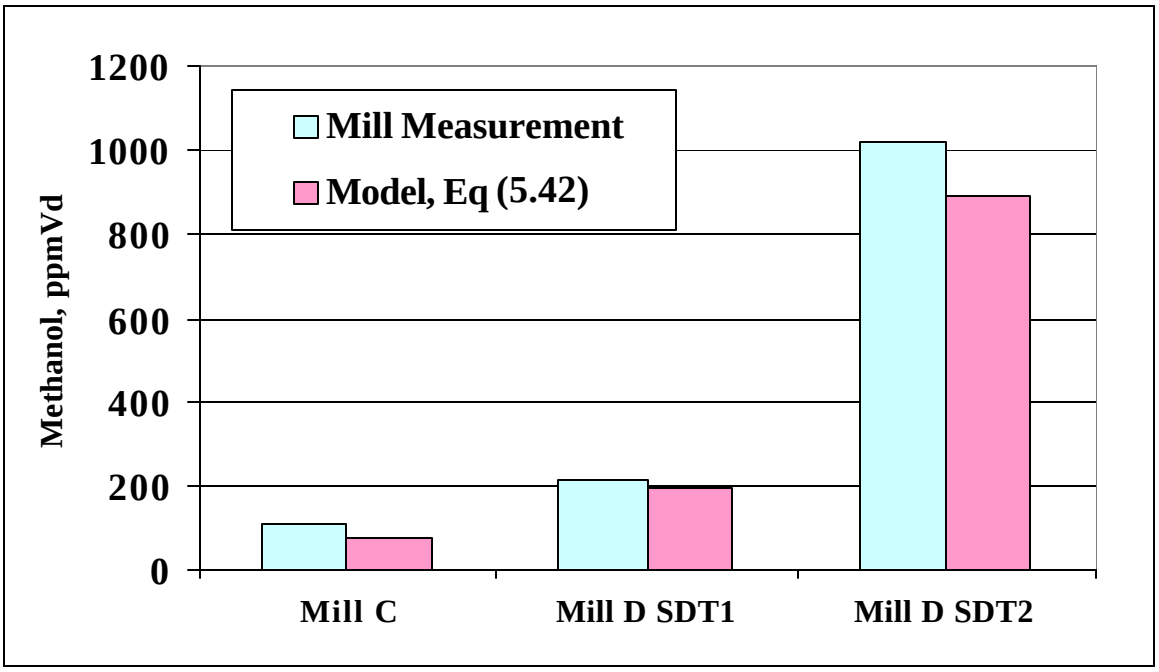

Figure 5.21. Comparison of Model Predictions with Mill Measurements: Methanol in Smelt Dissolving Tank Vent Air [38]

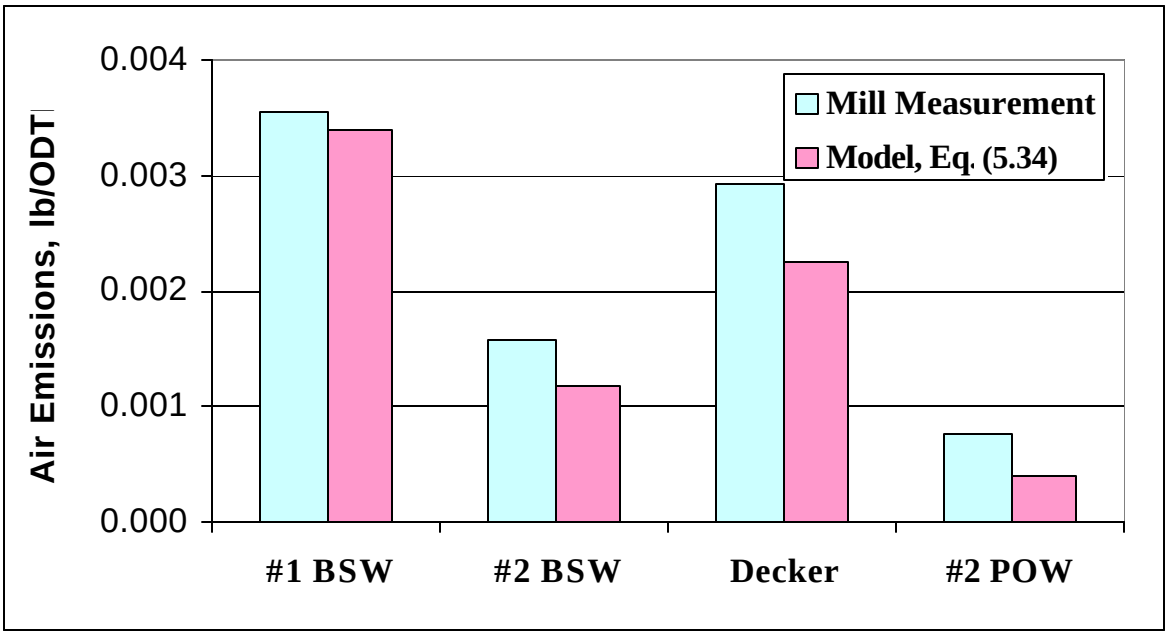

Figure 5.22. Comparison of Model Prediction with Mill Measurements: Acetone Emissions from Mill A Washer Hoods

Table 5.I. Methanol Measurements from a Southern Kraft Mill

Location	Liquor Temperature	Methanol		Equilibrium Constant		
		Air	Liquor	Measured [1]	Model [2]	Adj. Model [3]
	^{O}C	mol/kmol	mol/kmol	ratio of mole fractions		
Decker Seal Tank	71.9	0.8333	0.3021	2.76	3.06	2.64
D0 Washer Seal Tank	57.9	0.2253	0.1783	1.26	1.62	1.45
Eop Washer Seal Tank	77.3	0.2325	0.1082	2.15	3.85	3.27
O2 Blow Tank	92.2	2.9752	0.5490	5.42	6.99	5.73

Note: 1. Mill values from this table.
2. Model using Eq. (5.5)
3. Model using Eq. (5.11)

Table 5.II. Model Parameters of Methanol Generation during Kraft Cooking

		Softwood	Hardwood	Source
Hemicellulose/Lignin Dissolution				
C_{H_Inf}/C_{Hi}	fraction		0.06	Figure 5.8
A_{DH}/X_n	dimessionless		9.25E9	Figure 5. 8
E_{DH}	J/mol.K		9.3E4	[25]
C_{L_Inf}/C_{Li}	fraction	0.08		Figure 5.9
A_{DL}	dimessionless	3.0E5		Figure 5.9
E_{DL}	J/mol.K	6.0E4		Figure 5.9
Methanol Generation				
H_w	kg/ton	275	347	[23]
f_x	fraction	0.339	0.74	[23]
L_w	kg/ton	297	210	[23]
n_M	dimessionless	0.95	1.4	[23]
R_{LCi}	fraction	0.15	0	Figure 12/13
A_H	dimessionless		1.0	Figure 5.8
A_L	dimessionless	0.11		Figure 5.10
F_{HC}	fraction		0.53	[15]
F_{LCi}	fraction	1		Figure 5.10
F_{LC}	fraction	0.4		Figure 5.10

Table 5.III. Methoxyl Content from Residual Lignin of Spruce Kraft Pulp [21]

	Milled Wood	Unbleached Pulp			O2 Pulp
Pulp Kappa number		145.0	86.4	29.4	17.0
Degree of delignification on wood, %		39.8	71.3	92.5	95.7
Methoxyl groups on lignin, %	15.3	11.5	11.9	12.2	9.0

Table 5.IV. Model Parameters for Methanol Generation in Oxygen Delignification and Bleach Plants

Parameter	Softwood	Hardwood	Source
n_M	0.95	1.4	[24]
A_S, O_2	0.27		Mill Data
A_S, Cl_2	1.15		Figure 5.15
A_S, ClO_2	0.50		Figure 5.15

Table 5.V. Model Parameters for Methanol Generation from Black Liquors

Parameter	Softwood	Source
A_{BL}	0.017	Figure 5.16
A_C	4.07E+05	Figure 5.16
E_{BL}	5.14E+04	Figure 5.16
a	10.00	Figure 5.16
b	-0.028	Figure 5.16

Table 5.VI. Comparison of Model Predictions with Mill Measurements: Air Emissions from Paper Machines [34]

Mill ID	**Methanol Air Emission**, kg/ODMTP					
	PM Dryer Section		PM Vacuum Vents		PM Wet End Vents	
	Measured	Predicted	Measured	Predicted	Measured	Predicted
Mill G	0.352	0.467	0.286	0.236	0.234	0.283
Mill H	0.224	0.198	0.081	0.083	0.213	0.130
Mill K	0.010	0.002	0.002	0.001	0.012	0.001
Mill N	0.030	0.014	0.027	0.007	0.020	0.008
Mill Q	0.162	0.066	0.002	0.001	0.002	0.049

CHAPTER 6: PREDICTING EMISSIONS OF VOC's IN KRAFT MILLS

Process simulation is an effective and efficient approach to understand complicated processes and predict the impacts of process modification. However, reliable models for given issues are required when reliable simulation results are needed. Due to the complexity of real mill systems, it is difficult to get reliable regression models for mill process variables such as VOC air emissions. First principle models are more desirable. This chapter demonstrates the application of the VOC predictive models developed in this research based on first principle in krfat mills. Four kraft mill case studies (a continuous digester, two brownstock washing lines and a pre-evaporator system) are presented and compared with mill measurements. These case studies provide valuable, technical information for issues related to MACT I and MACT II compliance, such as condensate collection and Clean-Condensate-Alternatives (CCA).

Venkatesh [1, 2] demonstrated that simulation is able to predict mill wide methanol (and TRS) levels. Methanol modeling was applied to assessing the emission impact of installing a new washer and to developing an alternative condensate segregation strategy to size a stripper. Simulation is a useful tool for evaluating MACT compliance alternatives in kraft mills. When fundamental models [3-5] are available, detailed mill simulation and limited mill sampling can replace comprehensive mill VOC sampling, such as those in the Venkatesh paper [1]. The mill cases presented in this chapter show that process details play a significant role in methanol distribution and air emissions. With the new simulation tools, the impacts of process modifications on methanol distribution and air emission can be predicted.

Methanol is generated mainly during cooking and is separated into digester condensates, weak black liquor and the blow line filtrate. Because significant amounts of methanol can be recovered in digester condensates, digester operation is not only important for methanol generation, but also for methanol collection. Case I in this chapter demonstrates the potential for improved methanol collection from a continuous digester.

It is difficult and costly to conduct VOC air sampling. Simple correlations between liquid methanol concentrations and methanol emissions for certain types of unit operations have

been developed [6], but these do not consider effects of equipment configuration and operating conditions. The new air emission models [5] can handle these effects very well as shown in Case II. In Case III, these new models are applied to evaluate Clean-Condensate-Alternatives.

Although most all methanol in the weak black liquor will end up in evaporator condensates, the evaporator system details determine how methanol is separated among different evaporator condensates. Good condensate segregation in evaporators results in less condensate for treatment. Evaporator operation is important not only for collecting methanol rich condensates for treatment, but also for collecting "clean" condensates for re-use. Case IV in this paper shows how the new VOC models are used to optimize condensate segregation.

For the U.S. Industry, MACT I is understood to be the requirements for NCGs (both LVHC and HVLC systems); bleach plants; and kraft mill condensate collection and treatment. MACT II refers to the upcoming requirements for emissions from so-called combustion sources (recovery furnace, lime kiln, smelt dissolving tank). Collection of brownstock washer went gases is part of MACT I, even though the compliance date is not until April 2006.

6.1 New VOC Simulation Tools

6.1.1 Overview

For the reader's convenience the next paragraphs are a very brief summary of the simulation submodels developed in this research and discussed in Chapter 5.

1. Methanol generation models. Currently, new models are available for kraft pulping, bleaching and liquor storage.

2. Methanol equilibrium models, which are needed for the calculation of evaporators, flash tanks and air emission predictions.

3. VOC air emission models, which predict VOC air emissions from mill equipment at given operating conditions (also requires equilibrium models).

Figure 6.1 shows the general relationship among these models in a simulation project. When methanol generation is available, existing process simulators can predict filtrate methanol distribution in the process when evaporation (e.g., in flash tanks and evaporators) is not involved. During evaporation, methanol in the vapor is in equilibrium with methanol in the liquor. Therefore, methanol equilibrium calculation is needed to predict methanol in condensates. Emission models calculate air emissions from methanol concentrations in filtrates and filtrate temperatures. Equilibrium calculation is also needed for air emission prediction [5] as shown in Fig. 6.1.

When a mill process is simulated using a VOC enhanced process simulator, condensate flows, methanol concentrations in condensates and methanol air emissions are predicted. The impacts of process configuration changes and operating changes are predicted from these first principle models. This information is very valuable for process improvement, equipment design and on-going monitoring purposes for MACT I and MACT II compliance.

6.1.2 Methanol Generation [3]

In Kraft mills, methanol is generated mainly in cooking. Methanol originates from methoxyl groups in wood, so wood species affect methanol generation. Methanol generation from cooking can be estimated from wood species and final cooking Kappa. The details of methanol generation models can be found in Chapter 5 or in our publication [3].

Methanol is also generated during O_2 delignification and bleaching. Kappa change affects methanol generation in these stages. For a given Kappa change, chlorination generates more methanol than ClO_2 bleaching and ClO_2 bleaching generates more methanol than O_2 delignification. Methanol can also be generated from black liquor.

6.1.3 Methanol Equilibrium [4]

Temperature has the most influence on methanol equilibrium constants [4]. The methanol equilibrium constant at 100°C is 5.7 times higher than at 60°C. The impact of washer shower temperature on washer hood methanol air emission has been documented by mill measurements [4].

Laboratory measurements have shown that inorganic salts in liquors and filtrates also increase the methanol equilibrium constant while dissolved organics have limited impact [4].

6.1.4 VOC Air Emission [5]

Newly developed methanol air emission models [5, 7] are based on equilibrium and mass transfer calculation. Methanol concentrations in filtrates, filtrate temperatures, vent air flow and mass transfer coefficients affect air emissions. When these models are used in simulation, the effects of process modifications and operating conditions (e.g. condensate recycling and temperature adjustment) on methanol air emissions are reflected in the model prediction. When the methanol equilibrium constant is replaced with the equilibrium constants of other VOC's the same models can be used to predict air emissions.

Compared with NCASI's methanol air emission correlations [6], these new models can predict the impacts of process changes on air emissions from first principles. However, they are more complicated and are more suitable for applications in process simulators while NCASI's correlations [6] are good for quick estimations.

6.2 Kraft Mill Methanol Simulation: Case Studies

Four case studies using the new VOC models are included in this section. Mill measurements validate the simulation results.

Case I: Continuous digester, condensate methanol collection

Case II: Fiberline methanol air emissions

Case III: Clean condensate alternative

Case IV: Pre-evaporator condensate segregation

All simulations shown in this paper are calculated using VOC enhanced WinGEMS [8] although the new VOC models can be implemented in any modular process simulator.

6.2.1 Case I: Continuous Digester, Condensate Methanol Collection

Cooking is the major source of methanol generation in kraft mills. Also, digester operation determines how methanol is split among digester condensates, black liquor and the fiberline. The more methanol in black liquor, the more methanol in the evaporator condensates, the lower the condensate treatment cost and methanol air emissions from the fiberline are minimized.

Figure 6.2 shows a single vessel Kamyr digester simulation. In the simulation, 23 blocks are used for the calculation of the digester body. One methanol generation block predicts methanol generation before the UCC (Upper Cooking Circulation) and another for the rest of the cook. Methanol equilibrium calculation is included in the two flash tanks. Also, an air emission model is used to predict methanol content in NCGs (Non-Condensable Gases) from the blow tank.

An overall methanol mass balance is shown in Table 6.I for the process shown in Figure 6.2. Approximately 50% of methanol goes to brownstock washing and 11% goes to the second flash tank steam.

Black liquors extracted from digester have the highest methanol concentrations and high temperatures. Because steam generated from these liquors has even higher methanol concentrations, digester flash tank systems can be improved from the point view of methanol collection. Table 6.II demonstrates the significance of flash tank steam configuration on methanol distribution. If No.1 flash tank steam is removed from the steaming vessel, 2.7 kg/ODTP (vs. 1.1 kg/ODTP in Table 6.I) methanol can be collected from the No.1 and No.2 flash tank steam condensate. The flow of this condensate is only about 5% of the total condensate. Also, fiberline methanol concentrations (and air emissions) will be reduced 25%.

Batch digester heat recovery systems can also be improved to collect condensates with higher methanol concentrations.

6.2.2 Case II: Fiberline Methanol Air Emissions

6.2.2.1 Filtrate Methanol Profiles

When methanol generation is specified, methanol concentrations in filtrates can be calculated from mass balances for the process if evaporation is not involved. Compared with methanol in filtrates, methanol air emissions account for a small fraction of the total methanol and its effect on the filtrate methanol mass balance is very small. In Fig. 6.3, calculated filtrate methanol concentrations from mass balance calculations are compared with mill measurements for brownstock washing, O_2 delignification and the D_0 stage in a southern softwood kraft mill. Methanol is used for ClO_2 generation.

6.2.2.2 Prediction of Air Emissions

Figure 6.4 shows a two-stage O_2 delignification system with methanol air emissions from the blow tube vent, atmospheric diffuser vent, decker hood vent and decker seal tank vent. The new emission models [2] predict methanol air emissions from all these vents. In Fig. 6.5, model predicted methanol air emissions are compared with mill measurements.

The whole fiberline simulation of a southern softwood kraft mill has been built. The simulation includes digester, brownstock washing, O_2 delignification (Fig. 6.4), an ECF bleach plant and a pulp dryer. Simulated air emissions are also compared with mill measurements in Fig. 6.5.

Process changes can significantly affect methanol air emissions. Condensate with 470 ppm methanol is applied to the decker shower in the current mill situation, Fig. 6.4. When condensate with 100 ppm methanol is used on the decker shower, the simulation predicts that the total fiberline methanol air emissions will be 1/3 lower than current emissions. Fig. 6.5 clearly shows the significant impacts on the O_2 diffuser and the decker vent. Due to lower methanol carryover to the bleach plant, methanol air emission in the bleach plant is also lower, especially for D_0 stage vents. The impact of cleaner decker showers on filtrate methanol concentrations is also shown in Fig. 6.3.

6.2.3 Case III: Clean Condensate Alternative

In MACT II, the HVLC collection system from brownstock washing and screening can be replaced by the reduction of air emissions through using clean condensate (Clean-Condensate-Alternative). In order to evaluate CCA options for MACT II compliance, it is necessary to know methanol air emissions under current mill conditions and CCA conditions.

A mill study (3 brownstock drum washer and a decker) has been conducted to demonstrate that the new air emission models [2] can predict methanol air emissions at CCA operating conditions using fundamental model parameters determined from current mill conditions. Figure 6.6 shows methanol air emissions from brownstock washing at two levels of methanol in the decker shower. The air emission model parameters (i.e. mass transfer coefficients) are determined from Case A in Fig. 6.6, the air emissions for Case B are totally predicted from the models without any adjustment in model parameters. The same mass transfer coefficients are used for all three washers.

The breakdown of Hood Totals in Fig. 6.6 is shown in Fig. 6.7. Except for No.3 washer hood, the new air emission models are able to describe air emissions under current mill situation (Case A) and to predict air emissions under CCA (Case B). The No.3 (Case A) washer hood has higher air emission than the No.2 (Case A) washer hood but the No.3 washer has lower methanol concentration and temperature in the vat and shower than the No.2 washer. This is most likely a measurement error.

Figures 6.6 and 6.7 demonstrate that the new air emission models can predict the impact of a specific process modifications. Because the new air emission models are based on equilibrium and mass transfer calculations, it is expected that the impacts of other process and operating conditions (i.e. temperature, production) on air emissions can be predicted by these models.

Table 6.III demonstrates the possibility of using the Clean-Condensate-Alternative for this sampled line if the decker pulp is sent to a paper machine (i.e. a "brown" mill). Clean condensate significantly reduces methanol carryover to the paper machine and air emissions

from the paper machine and the simulation predicts this system can meet MACT II requirements under the Clean-Condensate-Alternative (Table 6.III).

6.2.4 Case IV: Pre-Evaporator Condensate Segregation

Evaporator operation is important for MACT compliance especially when a steam stripper or CCA is involved. Skillful condensate segregation minimizes the condensate flow that has to be collected to meet MACT requirements. The steam usage and size of condensate strippers are directly proportional to the feed rate.

Internal condensate segregation in evaporator bodies is a good approach to maximize condensate methanol concentration. Separating condensate from each effect in a multiple effect evaporator system is another approach. Increasing evaporator vent steam can also be considered if a separate surface condenser is used for the vent steam. In evaporators, methanol splits between condensate and black liquor according to equilibrium. Mass balances alone cannot predict the methanol distribution between liquors and condensates. Detailed mass balances, energy balances, heat transfer and methanol equilibrium calculation are required to study the effect of process, equipment and operating conditions on condensate methanol content.

Figure 6.8 shows a mill two-effect pre-evaporator simulation including methanol prediction. Weak black liquor (16% TDS) is concentrated to TDS 18.8% by using steam generated from accumulator condensate in a two-stage flash tank. There is internal condensate segregation in each evaporator body.

Methanol concentrations from the simulation are compared with mill measurements in Fig. 6.9. Except for two foul condensate samples, methanol concentrations in all other samples are matched very well by the simulation. Liquor flows, TDS, temperatures and pressures also match mill measurements.

For a simulation, such as Fig. 6.8, flows and methanol concentrations are calculated for all streams. Thus, it is easy to determine which condensate streams should be collected. If internal streams are collected, the simulation predicts the new evaporation capacity and methanol distribution.

Table 6.IV shows the overall methanol mass balance for Fig. 6.8 under the current mill operating conditions. Of the incoming methanol, 22% remains in black liquor after the pre-evaporator set. The foul condensate accounts for 23% of the total condensate flow and 42% of the total methanol input. Table 6.V shows the overall methanol mass balance when a third effect is added to evaporate black liquor to TDS 22.7% (18.8% for 2 effects). Methanol in the strong black liquor of this proposed 3-effect pre-evaporator set is very low (5% of the total input). Approximately 50% of the methanol input is collected in the foul condensate. The foul condensate flow accounts for about 25% of the total pre-evaporator condensate and 6% of the total condensate generated from TDS 16% to 70%. If 15.4 lb/ODTP methanol is generated from softwood linerboard cooking, this 6% foul condensate contains 7.4 lb/ODTP methanol, enough to meet MACT I requirement. This case shows that there is great potential to reduce the cost of MACT compliance through evaporator optimization.

A detailed simulation, such as Figure 6.8, predicts the effect of operating conditions on methanol distribution. This information can help mill operations in on-going MACT compliance. If input streams and sensitive operating conditions are collected online, the simulation can be used as a soft sensor for MACT compliance and thus reduce the monitoring cost.

6.3 Conclusions

Case studies presented in this paper show that simulation can "map out" methanol distribution and air emissions in kraft mills when newly developed VOC models are implemented in existing process simulators. These calculations provide information about how to collect methanol from condensates and can act as soft sensors for MACT I and MACT II compliance.

Mill data have demonstrated that the newly developed air emission models can predict changes in brownstock washing air emissions caused by changes in the methanol content of the decker shower. Because these emission models are based on fundamental equilibrium and mass transfer calculations, they can predict the impacts of process modification and operating changes.

When condensate is carefully segregated in evaporator systems, collecting a very small fraction of total condensate can meet the MACT I requirement. A simulated case shows that only

6% of the total condensate is needed. Also, the condensate from continuous digester black liquor flash steam is a good source for methanol collection when its heat can be recovered indirectly.

REFERENCES

1. Venkatesh, V., Owens, T., and Kirkman, A. *TAPPI Intl. Environmental Conf.*, Denver May, 2000.
2. Venkatesh, V., Lapp, W.L. and Parr, J.L., *TAPPI J.*, **80**(2):171, 1997.
3. Gu, Y.X., Edwards, L.L., Zhu, J.Y. and Chai, X.S., Cluster rule compliance tools: Predicting kraft mill VOC's, Part 2 of 4. Methanol generation models, *TAPPI J.*, **84**(4):65, 2000.
4. Gu, Y.X., Edwards, L.L., Zhu, J.Y., Liu, P.H. and Chai, X.S., Cluster rule compliance tools: Predicting kraft mill VOC's, Part 3 of 4. Methanol equilibrium calculations, *TAPPI J.*, **84**(4): 65, 2001.
5. Gu, Y.X. and Edwards, L.L., TAPPI J. Cluster rule compliance tools: Predicting kraft mill VOC's, Part 4 of 4. Mill validated air emission models, *TAPPI J.*, **84**(4):65, 2001.
6. Jain, A.K., *Proceeding of TAPPI Minimum Effluent Mill Symposium*, 1996.
7. Gu, Y.X., Edwards, L.L., Haynes, J.B. and Euhu, L.E., *TAPPI J.*, **81**(2):173, 1998.
8. Pacific Simulation, Inc., WinGEMS Manual, Pacific Simulation, Inc., Moscow, Idaho, 1995.

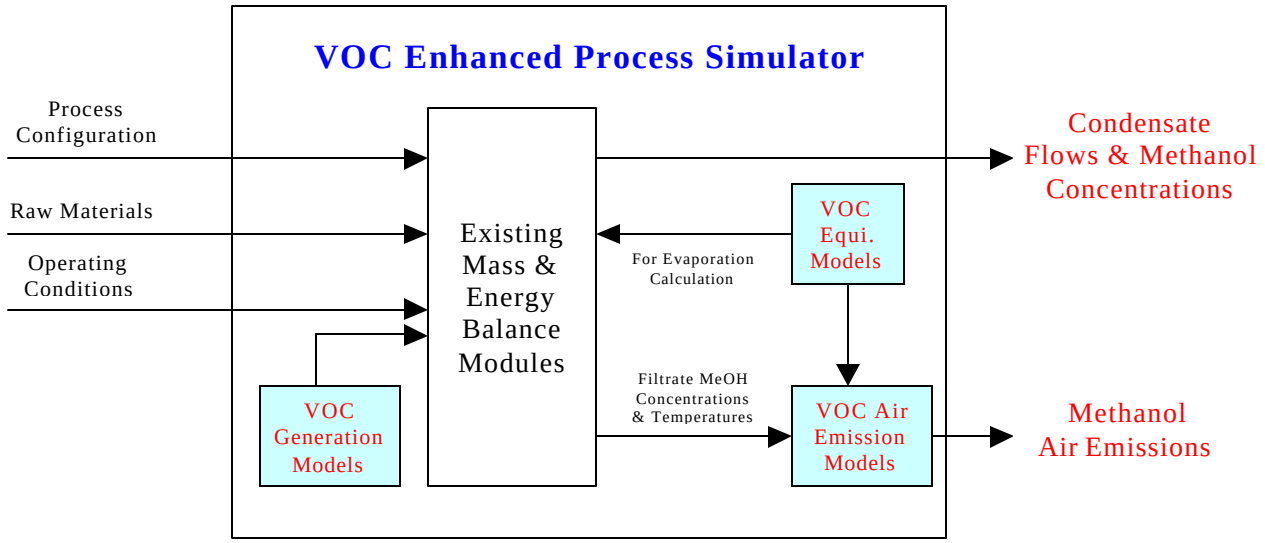

Figure 6.1. Overview of VOC Simulation for Kraft Mills

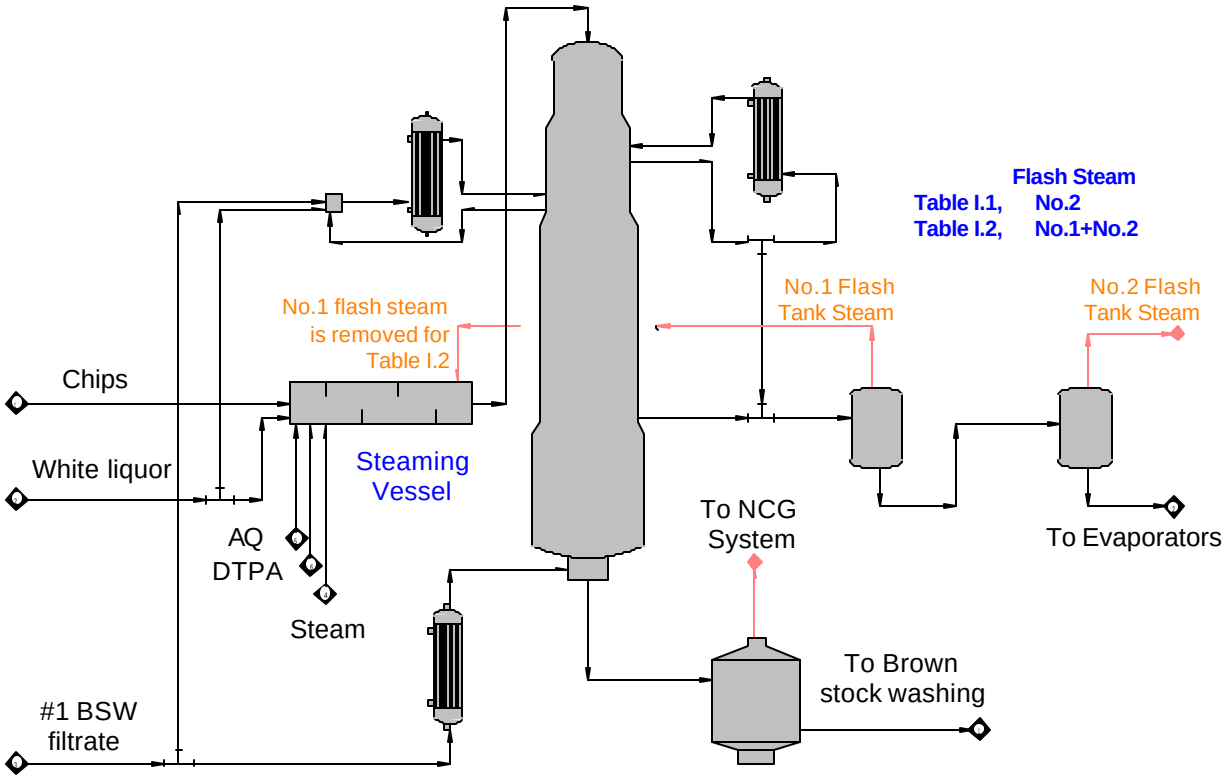

Figure 6.2. Kamyr Digester Methanol Simulation

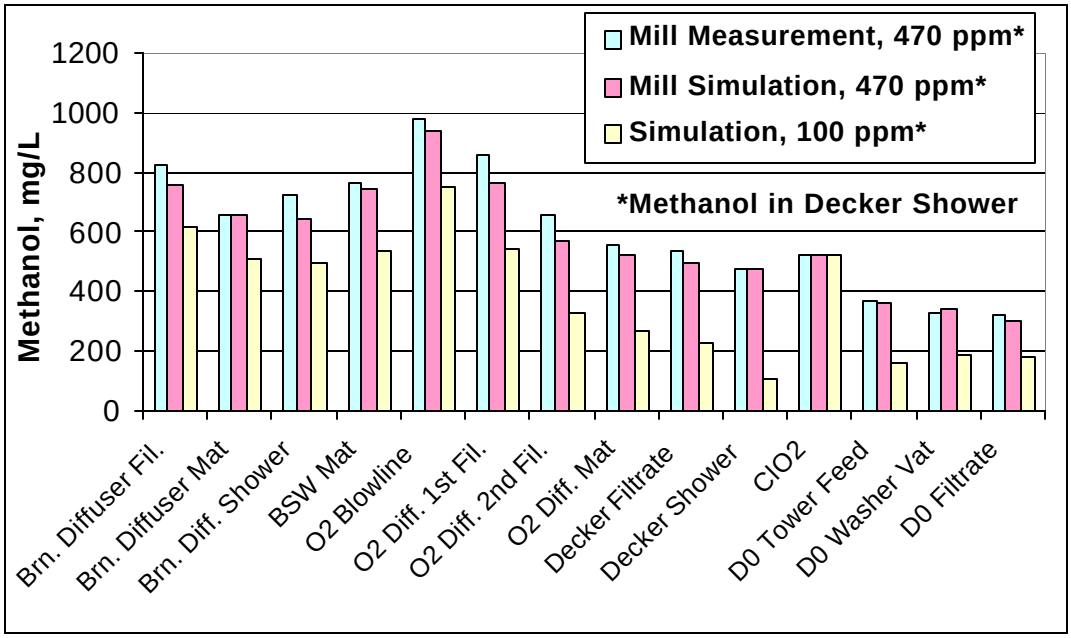

Figure 6.3. Comparison of Simulation with Mill Measurement: Filtrate Methanol Concentrations

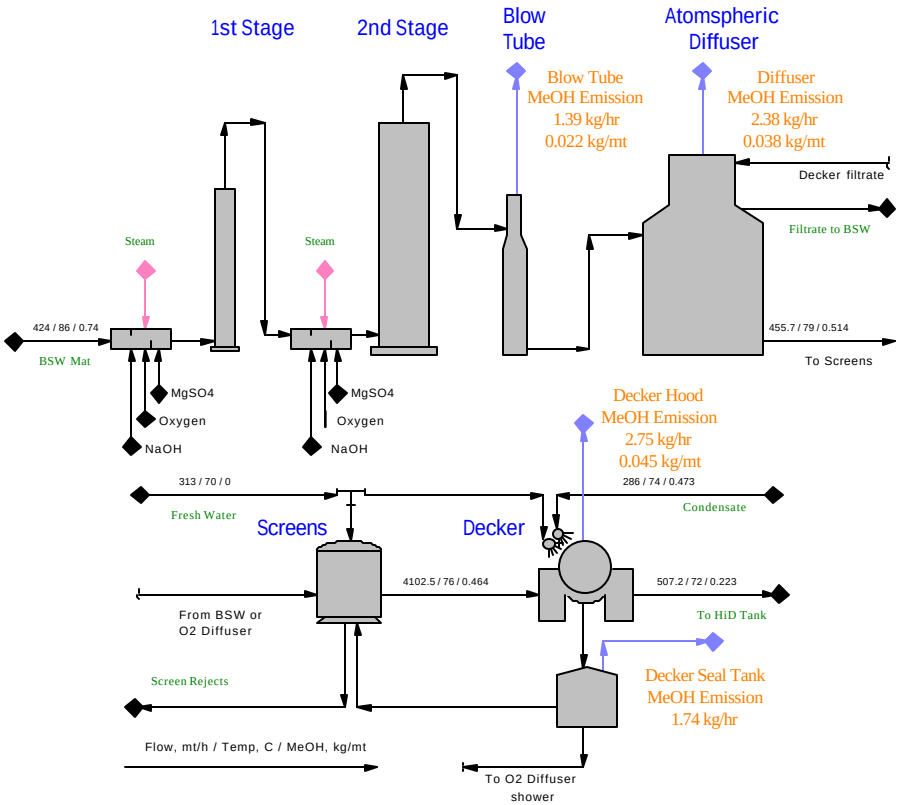

Figure 6.4. Simulation of O_2 Delignification with Methanol Air Emissions

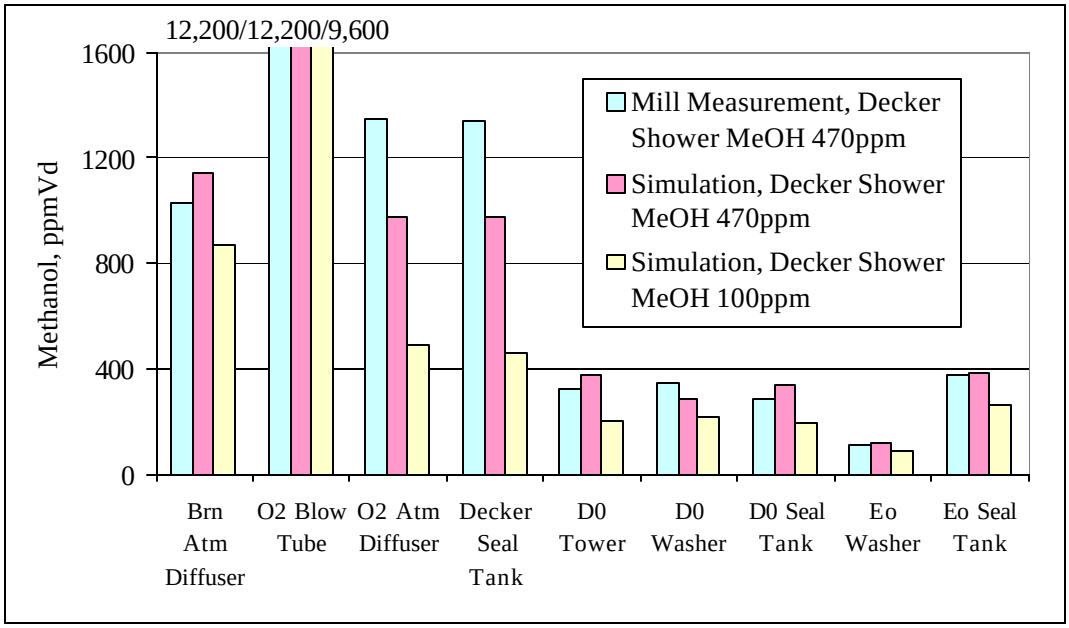

Figure 6.5. Comparison of Mill Measurements with Simulation for Fiberline Air Emissions and Impact of Using Cleaner Condensate

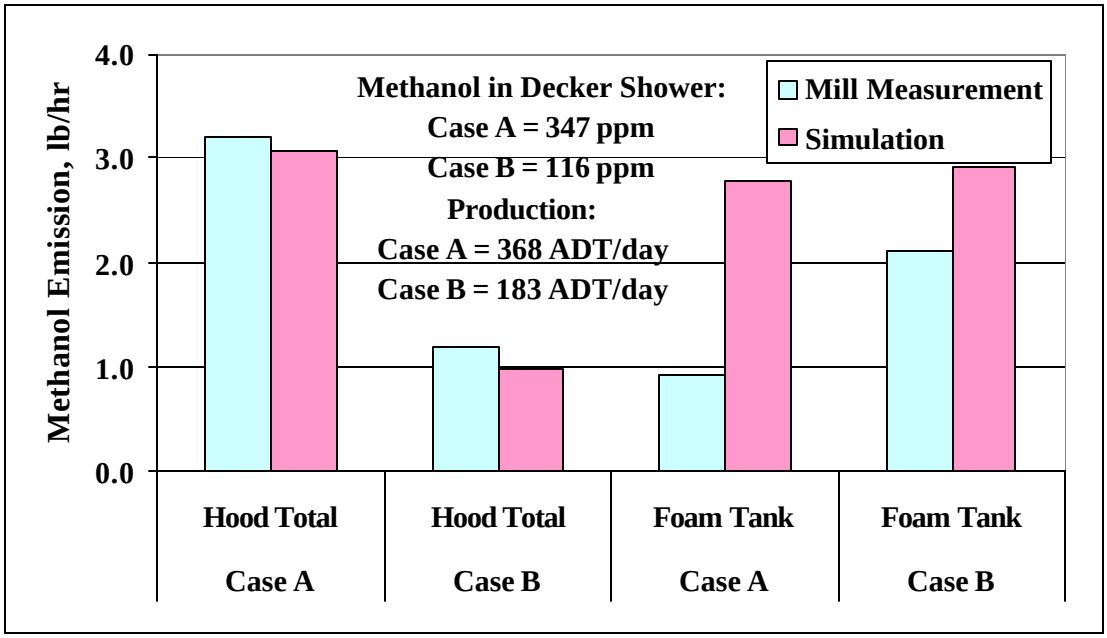

Figure 6.6. Comparison of Methanol Air Emission Simulation with Mill Measurements at Current Mill (Case A) and Clean-Condensate-Alternative Conditions (Case B): Washer Hood Totals and Foam Tanks

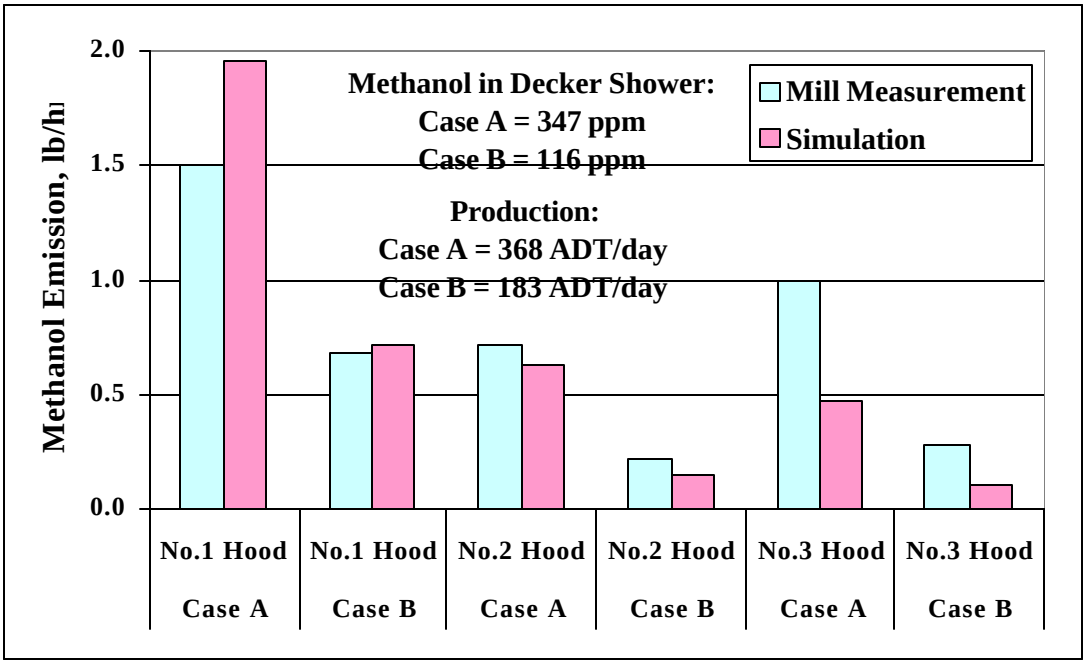

Figure 6.7. Comparison of Methanol Air Emission Simulation with Mill Measurements at Current Mill (Case A) and Clean-Condensate-Alternative Conditions (Case B): Individual Washer Hoods

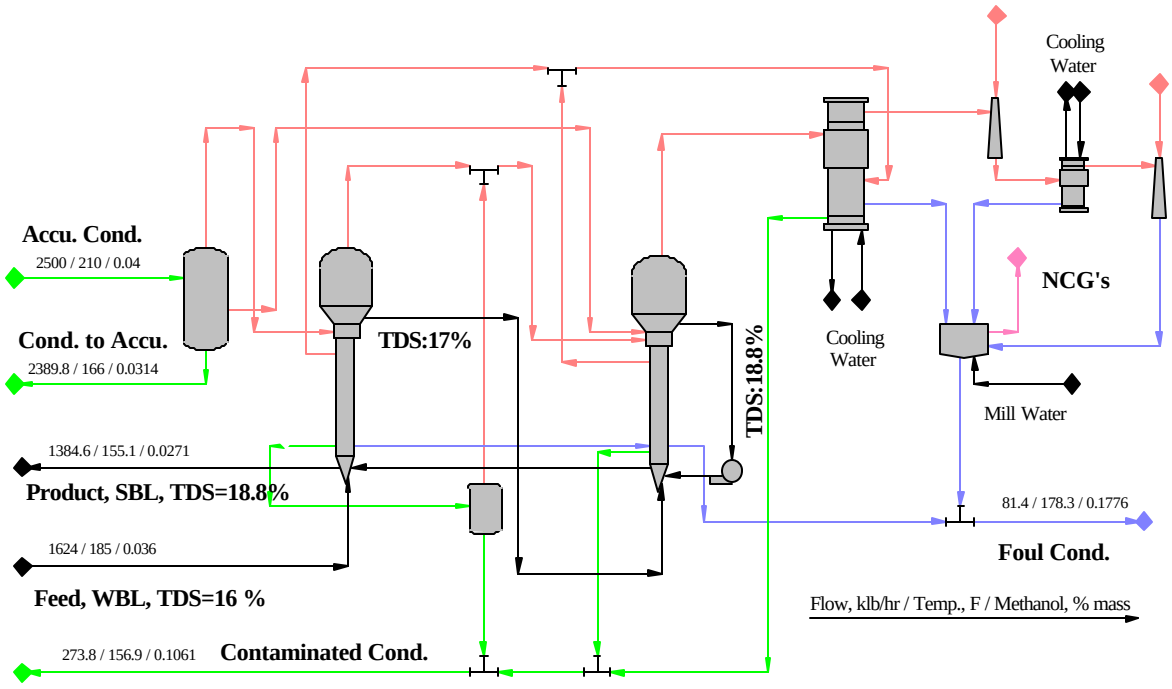

Figure 6.8. Mill Pre-Evaporators Methanol Simulation

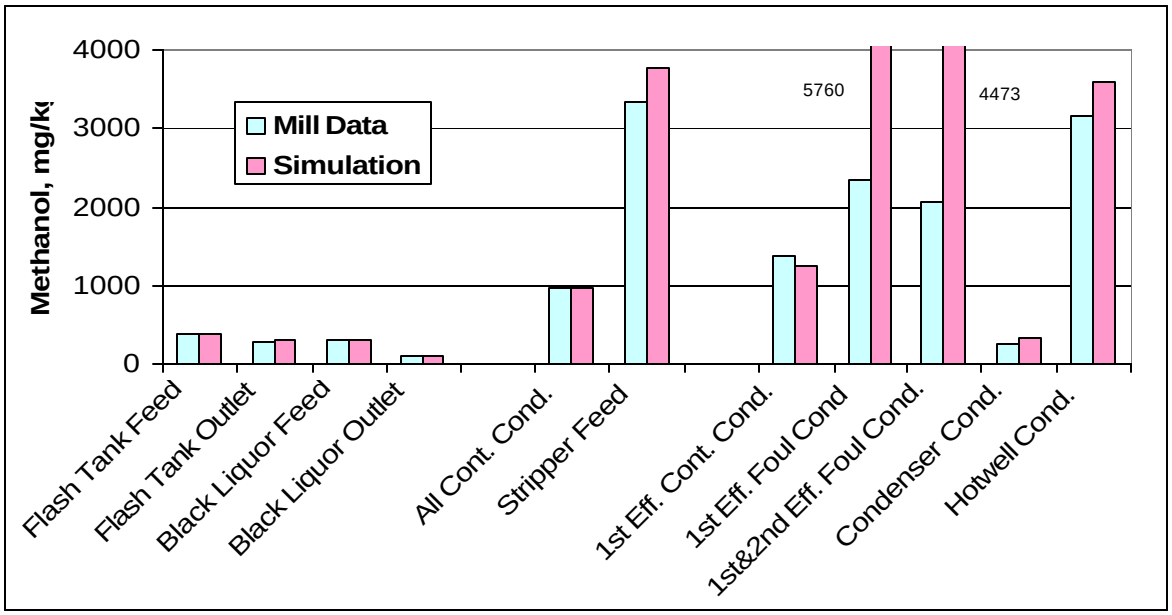

Figure 6.9. Comparison of Simulation with Condensate Methanol Mill Measurements in Pre-Evaporator Set.

Table 6.I. Overall Methanol Mass Balance in Digester Area

Input	Methanol			Output	Methanol		
	ppm	kg/ODTP	%		ppm	kg/ODTP	%
UCC Generation		3.10	32.4	Pulp	523	5.09	53.1
Bulk Generation		3.68	38.5	Black Liquor	511	3.36	35.0
#1 BSW Filtrate	380	2.79	29.2	Flash Steam	4917	1.11	11.5
				Blowtank NCG	1647	0.04	0.4
Total		9.56		Total		9.59	

Table 6.II. Effect of Removing No.1 Flash Tank Steam on Methanol Distribution

Input	Methanol			Output	Methanol		
	ppm	kg/ODTP	%		ppm	kg/ODTP	%
UCC Generation		3.10	35.0	Pulp	385	3.75	42.3
Bulk Generation		3.68	41.5	Black Liquor	371	2.43	27.4
#1 BSW Filtrate	284	2.08	23.5	Flash Steam	4114	2.66	30.0
				Blowtank NCG	1215	0.03	0.3
Total		8.86		Total		8.88	

Table 6.III. Model Predicted Methanol Air Emissions under Current Mill and Clean-Condensate-Alternative (CCA) Conditions

Methanol in Decker Shower:	**350 ppm / Current**	**100 ppm / CCA**
	lb/ADsTP	lb/ADsTP
Brownstock Washing Total	0.38	0.27
Paper Machine Total	1.32	0.38
Breakdown of Brownstock Washing Air Emissions		
No.1 Washer Hood	0.13	0.10
No.2 Washer Hood	0.04	0.02
No.3 Washer Hood	0.03	0.01
No.1 Seal Tank	0.13	0.12
No.2 Seal Tank	0.03	0.01
No.3 Seal Tank	0.02	0.01
Breakdown of Paper Machine Air Emissions		
General Vents	0.38	0.11
Vacuum Vents	0.41	0.12
Dryer	0.53	0.15

Table 6.IV. Methanol Distribution for Existing 2-Body Pre-Evaporators

Input Streams	Flowrate	Methanol			Output Streams	Flowrate	Methanol	
	klb/hr	lb/hr	%			klb/hr	lb/hr	%
Flash Tank Inlet	2500				Product, SBL	1385	184	22
Net Change of Accu. Cond.		257	31		Contanimated Condensate	274	295	35
Weak Black Liquor	1624	585	69		Foul&Hotwell Condensate	81	357	42
					NCG's	1	5	1
Total Input		841			Total Output		841	

Table 6.V. Methanol Distribution for Proposed 3-Body Pre-Evaporators

Input Streams	Flowrate	Methanol			Output Streams	Flowrate	Methanol	
	klb/hr	lb/hr	%			klb/hr	lb/hr	%
Flash Tank Inlet	3380				Product, SBL	1116	54	5
Net Change of Accu. Cond.		543	48		Contanimated Condensate	611	524	47
Weak Black Liquor	1624	585	52		Foul&Hotwell Condensate	161	547	48
					NCG's	1	2	0
Total Input		1128			Total Output		1128	

DE-FC07-96ID13438

VOC Control in Kraft Mills
Task B:
Development of a Membrane Separation Technology

By

Peter H. Pfromm, Institute of Paper Science and Technology
Mary E. Rezac, Georgia Institute of Technology

June, 2001

Work Performed Under Contract No: DE-FC07-96ID13438

For

U.S. Department of Energy
Office of Industrial Technologies
Washington, D.C. 20585

By

Institute of Paper Science and Technology, Atlanta, GA
Georgia Institute of Technology, Atlanta, GA

TABLE OF CONTENTS

PREFACE AND ACKNOWLEDGEMENTS

A joint research effort was carried out in this program towards detection and control of volatile organic compound (VOC) emissions form kraft pulp mills. The program was selected by the Office of Industry Technologies of the US Department of Energy and American Forest and Paper Association (AF&PA) as a successful story project in 1998. The program consists of Tasks A (see separate report) and Task B (reported here).

This report deals with Task B. This Task was to develop a membrane technology for the control of the emission of VOC's from bleached kraft pulp mills. The main contribution of Task B is material science and laboratory experimentation towards development of a membrane technology to selectively remove methanol (as a VOC surrogate) from humid air streams that occur in a bleached kraft pulp mill.

This effort consists of two main areas:

1. Fundamental materials research to investigate the possibility to use the transport properties of polymers for selective methanol removal via polymeric membranes (performed mainly at Georgia Tech)

2. Laboratory experimentation on realistic mixed feed streams for selective separation of methanol via membrane permeation (performed at the Institute of Paper Science and Technology).

This work would not have been possible without the dedicated work of students, post doctoral researchers, and technical staff at Georgia Tech and the Institute of Paper Science and Technology. The publication and thesis listings reflect the names of these individuals. Special recognition goes to Professor Czermak of the University of Applied Sciences in Giessen, Germany, Professor Staude of the University of Essen, Germany, and Professor Schlünder of the University of Karlsruhe, Germany, who made it possible for several students from their institutions to join this effort.

LIST OF RELEVANT PUBLICATIONS

Refereed Publications

1. Klug, A., Pfromm, P. H., Rezac, M. E., Czermak, P., "Selective Removal of Methanol from Humid Air Streams using a Water Vapor-Purged Membrane Separator", *Industrial and Engineering Chemistry Research*, **40**, 12, 2685-2692, 2001.

2. Dorkenoo, K., Pfromm, P. H., Rezac, M. E., "Gas Transport Properties of a Series of High T_g Polynorbornenes with Aliphatic Pendant Groups", *Journal of Polymer Science, Part B: Polymer Physics*, **36**, 797-803, 1998

3. Rezac, M. E., John, T., "Correlation of Penetrant Transport with Polymer Free Volume: Additional Evidence from Block Copolymers", *Polymer*, **39**, 599-603, 1998.

4. Rezac, M. E., John, T., Pfromm, P. H., "Effect of Copolymer Composition on the Solubility and Diffusivity of Water and Methanol in a Series of Polyether Amides", *Journal of Applied Polymer Science*, **65**, 1983-1993, 1997.

Theses

5. John, T., "Transport Properties of a Series of Block Copolymers", M.S. Thesis, University of Karlsruhe, Germany, (Advisor Professor Schlünder), graduation Fall 1996

6. Thrasher, S., "Polymeric Membranes for Organic Vapor Recovery", M.S. Thesis, Georgia Institute of Technology, Atlanta, (Advisor Professor Rezac), graduation Fall 1998.

7. Christ, I., "Methanol removal from wet air streams via membrane vapor permeation", M.S. Thesis, University of Essen, Germany, (Advisor Professor Staude), graduation Fall 1998.

8. Klug, A., "Methanol removal from wet air streams: purge driven vapor permeation", M.S. Thesis, University of Applied Sciences Giessen, Germany, (Advisor Professor Czermak), graduation Spring 1999.

EXECUTIVE SUMMARY

Four peer-reviewed publications are appended below.

The first three publications (Appendices A through C) deal with the measurement of transport properties (sorption and diffusion) of small molecules in polymers. This was done early in the project to identify whether there are polymers that would show a sufficiently high selectivity for methanol over water and air to allow design of a simple separation process where methanol is directly removed from a humid air stream by contacting the stream with a polymer membrane and providing a partial pressure driving force for methanol permeation (for example using a partial vacuum on the permeate side). Although we found polymers with a selectivity for methanol over water, the selectivities are not very high and permeation of air is an additional issue. Therefore, a simple process based on the selectivity of the membrane material seems not viable.

The fourth publication (Appendix D) deals with the final approach that we took to remove methanol from humid air streams via membrane permeation through a tight polymer layer (solution/diffusion transport). We produced defect-free polymer/ceramic thin film composite membranes at the laboratory scale. We applied a water vapor purge stream on one side of the membrane to supply a partial pressure driving force to remove methanol from the feed, while not removing water vapor from the feed. The feed was a realistic mixture of methanol, air, and water vapor. Parasitic air permeation turned out to be a significant problem, and we point out routes to improved membranes. Our results show that minimized air permeation (diluting the permeate and making it hard to condense) might be more important than to concentrate on methanol/water selectivity. Process design calculations are shown to prove how this system could work in reality.

Appendix A: Effect of Copolymer Composition on the Solubility and Diffusivity of Water and Methanol in a Series of Polyether Amides

Effect of Copolymer Composition on the Solubility and Diffusivity of Water and Methanol in a Series of Polyether Amides

MARY E. REZAC,[1] TILO JOHN,[2]* PETER H. PFROMM[3]

[1] Georgia Institute of Technology, School of Chemical Engineering, Atlanta, Georgia 30332-0100

[2] Institute für Thermische Verfahrenstechnik, Universität Karlsruhe, Germany

[3] Institute of Paper Science and Technology, Atlanta, Georgia 30318

Received 4 September 1996; accepted 24 December 1996

ABSTRACT: Sorption and diffusion of water and methanol in polydimethylsiloxane and a series of PEBAX™ copolymers (polyether block amide copolymers) were measured over a wide range of activities near room temperature. The goal was to identify a membrane material for separation of the hazardous air pollutant methanol from wet air streams in the pulp and paper industry. The PEBAX™ copolymer series used here allows a unique insight into transport of small molecules, because solubilities are virtually constant, while diffusion coefficients vary. This is due to the similar chemical structure, but different chain mobility of the homopolymers. The grade PEBAX™ 2533 is most promising for the separation process due to high solubility and diffusivity. The unwanted simultaneous highly selective separation of methanol and water from the targeted air/vapor streams will be addressed in future work. © 1997 John Wiley & Sons, Inc. J Appl Polym Sci **65:** 1983–1993, 1997

Key words: PEBAX™; methanol and water sorption and diffusion; membrane vapor separation; pulp and paper industry

INTRODUCTION

Methanol vapor present in water wet air streams has clearly been identified as one of the major hazardous air pollutants emitted from pulping and papermaking operations.[1] In a typical pulp and paper mill using the Kraft process,[2] methanol is emitted at many points in the process. As wood is chemically treated to liberate individual cellulose fibers that will be made into paper, the lignin, an organic network polymer present in the wood, is decomposed into lower molecular weight organic compounds. These processes are carried out in an aqueous phase medium at high pH. Very large amounts of water are employed. Conventional equipment (washers, holding tanks) is not pressure tight, and operates above ambient temperature. Many of the separation stages operate in "open" systems where loss of some of the aqueous phase in the form of vapors occurs. The dissolved organics present as byproducts from chemical pulping may have a much higher vapor pressure than water, and therefore, partition preferentially into the vapor phase. Methanol is the most significant example.

Major equipment and processing changes would be required to eliminate all air–liquid contacts currently present in pulp and paper mills.

Correspondence to: M. E. Rezac.
* *Current address:* BASF, Mannheim, Germany.
Contract grant sponsors: Technical Competitiveness in the Pulp and Paper Industry Initiative (State of Georgia); Ernest Solvay Foundation.

Failing this, the partial migration of organics from the liquid to the air phase will continue. It is unrealistic to expect that complete renovation of a majority of mills will occur, due to the prohibitive investment costs that are involved. Entirely novel methanol control technologies are not currently realistic. However, methanol must be captured, because it will have to be removed from the process in a controlled fashion. Therefore, we have chosen to focus our efforts on the recovery of organics from mixtures with air, with methanol as the representative example.

The ultimate goal of our work is a technology that can be used as a retrofit to existing mills to control hazardous air pollutant emissions. Methanol is the most prominent contributor to these emissions and will serve as our model compound.[1] We chose to investigate membrane vapor separation for this purpose.

Polymeric membranes have inherently high selectivities for organics over air. Membrane vapor separation units are rugged and can be built to treat point sources.[3] The organics are recovered as liquids without cumbersome regeneration or disposal problems that occur with adsorption or bioremediation.

Membrane vapor separation is being evaluated here as a potential technology for the recovery of methanol. In this process, organic vapors are separated from the feed stream by permeation through an ultrathin polymeric membrane with outstanding affinity for the organic component. Current industrial-scale applications of this process include recovery of fuel vapors from tank farms and recycling of solvents and chemicals.[4]

The vapor separation membrane module itself contains no moving parts. Modularity of the system allows expansions and adaptation to the volume to be treated. Ideally, the result of the membrane separation process is recovery of nearly all organics in liquid form for easy reuse, transport, or disposal. Through internal recycling schemes, the process can be adapted to feeds with low or high concentrations.

TECHNICAL APPROACH

A membrane material capable of recovering methanol while allowing the majority of the water and air to pass through the unit is required for this application. The affinity of the membrane material for a minor component of the feed stream (methanol) allows removal of a highly concentrated solvent vapor by permeation through the membrane.

As only limited data regarding diffusivity of water and methanol from the vapor phase through polymers is available, experimental evaluation of candidate polymers was made. This entails determination of basic transport properties (sorption, diffusion) of candidate polymers when contacted with methanol, water, and air. The initial material evaluation is reported here.

PREVIOUS STUDIES

The system polydimethylsiloxane (PDMS)/water was included in the work presented here to validate the experimental technique by comparison with existing data (see discussion). After many years of experimental work (e.g., refs. 5–7), the diffusivity of water in PDMS remains under discussion. A review and additional data has recently been published.[8] Watson and Baron challenge the view that clustering of water molecules decreases the diffusion coefficient with increasing water sorption. Our data appears to support this view.

The literature yielded no comparable results for the diffusivity of methanol in PDMS beyond Favre et al.[5]

The transport properties of polyether block amides (PEBAX™), especially for water and methanol, have rarely been reported in the literature. Some PEBAX™ grades show a very high affinity for water. Therefore, this polymer was chosen to investigate the separation of methanol from air streams. The availability of a wide range of copolymers allows unique insights in structure/property relationships. Optimization of the polymer for the separation process may then be possible. Depending on chemical composition, PEBAX™ grades can exhibit two glass transition temperatures far below and above room temperature. PEBAX™ has been evaluated for the separation of liquid acetone/water mixtures by pervaporation.[9] Although the grade of PEBAX™ was not given, the low acetone selectivity may indicate a grade with low polyamide content. Permeability coefficients cannot be derived, because the effective membrane thickness was not given.

It is of some interest to investigate the literature for the transport properties of homopolymers made from the monomer units of PEBAX™. Copolymer properties could then potentially be predicted.[10] The transport properties of the system polyamide/water have been reviewed.[11] This re-

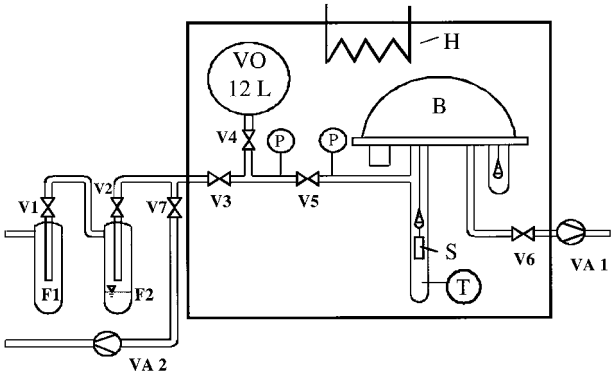

Figure 1 Schematic of apparatus for dynamic sorption–desorption measurements. (B) Cahn microbalance, (H) heater, (V) valve, (VO) ballast volume, (F) flask, (VA) vacuum pump, (S) sample, (T) temperature indicator, (P) pressure gauge.

view lists experimental data for water uptake in Nylon 12 of 12.6 to 13.8 cc(STP)/cc Polymer at 25 ± 5°C and an activity of 0.6. This data clearly confirms the magnitude and trend of water sorption in PEBAX™ grades with increasing polyamide content (Fig. 5). Using a model,[11] a diffusion coefficient of 5.4×10^{-9} cm^2/s of water in Nylon 12 at unit activity and 30°C can be predicted. Considering the many assumptions for the model, this value corresponds reasonably well with another source.[12] The decrease in the diffusion coefficient of water with increasing polyamide content of PEBAX™ grades as found in this work is generally confirmed.

Unfortunately, no studies of the diffusivity of water or methanol in polytetramethylene oxide (PTMO) were found in the literature. Therefore, no attempt could be made at predicting copolymer properties from the homopolymers.

EXPERIMENTAL

The absorption–desorption kinetics and the solubility of methanol vapor, water vapor, and dry air in a series of PEBAX™ polymers and PDMS were studied by a gravimetric method. This method consists of measuring the rate of weight gain or loss of a sample due to sorption or desorption. The weight change is determined with an automatic electromicrobalance incorporated in a vacuum system as shown in Figure 1.

An electronically controlled beam balance was used (Cahn Instruments, Inc.; Cerritos, CA; Model D-200). On both sides of the beam, hang-down wires with sample baskets were suspended in glass tubes. One basket holds sheets of the sample material; the other holds tare weights. For the configuration employed, the balance had a maximum load-carrying capacity of 3.5 g and was capable of registering weight changes of up to 750 mg with a sensitivity of 1 mg.

The vacuum system consisted of two flasks, F1 and F2, to generate the solvent vapor, a ballast volume (approximately 12 L) to reduce pressure fluctuations during the runs due to absorption, and two vacuum pumps with cold traps (VA1: Precision Scientific, Model D25. VA2: Edwards, Model E2M2). Pump VA1 was used to evacuate the system up to valve V5 during the desorption runs, and pump VA2 was used to evacuate the remainder of the system and to adjust the vapor pressure prior to sorption experiments. The pressure was measured with two absolute pressure transducers (MKS, range 0–1000 cmHg and 0–100 cmHg). The temperature inside the isolated chamber (black box in Fig. 1) was held at 30 ± 0.1°C.

For gas absorption, a sample of known thickness is placed on the hangdown wire. Valve V5 is closed and the system evacuated with pump VA1. In this stage, any remaining penetrants are removed. Solvent is filled in Flask F2 at room temperature. Valve V1 was closed and the left part of the system was evacuated with pump VA2 to remove any air. To start the run, valve V6 is closed and data recorded every 5 s. After 60 s valve V5 is carefully opened and the sample exposed to the solvent vapor. Typically, about 30 s is required for the pressure in the balance system to reach steady state. No data for this initial transient pressure period was used in the analysis. Sorption was allowed to continue for a period of at least 20 times the half-time (time for 50% final penetrant uptake).

Desorption measurements followed each absorption measurement. Valve V5 was closed and the data recording started. After 60 s, valve V6 was opened to evacuate the system. This pump was capable of evacuating the system within several seconds. The run was terminated after the same time had elapsed as during absorption.

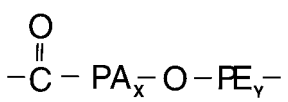

Figure 2 Chemical structure of PEBAX™.

Table I Physical Properties of the Different PEBAX™ Grades

	PEBAX™			
	2533	3533	5533	6333
"x" (number of PTMO groups per repeat unit)	2.68	3.42	14.85	19.30
"y" (number of PA groups per repeat unit)	27.80	26.00	24.70	16.60
Weight percent PA	21.6	27.1	62.2	75.8
T_g PTMO (°C)	−76	−72	−65	−60
T_m crystalline PTMO (°C)	12	7	None detected	None detected
T_g PA (°C)	All between 65 and 75			
T_m crystalline PA (°C)	137	142	160	170

MATERIALS

Polymers

The polymers used in this study were Polydimethylsiloxane (PDMS) and polyether block amide (PEBAX™).

The PDMS films were cast from commercially available components (General Electric) with no fillers or additives. As solvent, toluene was used. The sample was dried at room temperature for 2 weeks and at 100°C for 48 h under vacuum (vacuum pump equipped with an aluminum oxide backdiffusion trap). The density of PDMS is reported to be 1.02 g/cm^3.[13] The thickness, δ, was evaluated with a thickness gauge at 21 positions on the sample. The arithmetic average was 0.502 ± 0.074 mm. The glass transition temperature, T_g, was measured using differential mechanical thermal analysis to be −123°C. This is in good agreement with the published value.[13]

A series of PEBAX™ samples in the form of pellets was generously supplied by Elf Atochem (Philadelphia, PA). PEBAX™ 2533, 3533, 5533, and 6333 were evaluated. The general chemical structure of PEBAX™ is given in Figure 2.

PA represents polyamide, and PE is a polyether segment. In the PEBAX™ series studied here, Nylon 12 and polytetramethylene oxide (PTMO) were present in varying ratios. An elemental analysis for carbon, hydrogen, nitrogen, and oxygen was performed by Huffman Laboratories (Golden, CO). The number of repeat units of polyamide and polyether in each monomer segment (subscripts "x" and "y" in Fig. 2) were calculated. Initial guesses for "x" and "y" were based on the literature.[14,15] Using these guesses and the known structure of Nylon 12 and PTMO, the resultant mass fraction of each element was calculated. These calculated values were compared to the experimentally measured mass fractions and an overall error (defined as the sum of the error for each element) was minimized via iteration. The results are reported in Table I.

The T_gs were measured using differential scanning calorimetry (DSC) under nitrogen. Scans were run from −100 to 200°C at a heating rate of 10°C/min. The measured values are reported in Table I. Thermal analysis of the PEBAX™ grades indicated two distinct glass transition temperatures as well as crystalline melting peaks near 10 and 140°C.

PEBAX™ films were melt extruded using a Haake Buckler extruder fitted with a flat film die. The extrusion temperature ranged from 140 to 180°C, depending on the material. The motor speed was varied between 5 and 30 rpm. Sample thickness was controlled by the motor speed and the speed of the take up roller. Sample thicknesses are reported in Table II.

All films were optically clear and remained so throughout the preparation and testing process. Samples were dried under vacuum for 14 days at 40°C. The vacuum pump was equipped with an aluminum oxide backdiffusion trap. Following

Table II Thickness and Standard Deviation for PEBAX™ Samples

	PEBAX™ 2533	PEBAX™ 3533	PEBAX™ 5533	PEBAX™ 6333
Thickness, δ (mm)	0.470 ± 0.011	0.470 ± 0.023	0.432 ± 0.023	0.125 ± 0.005

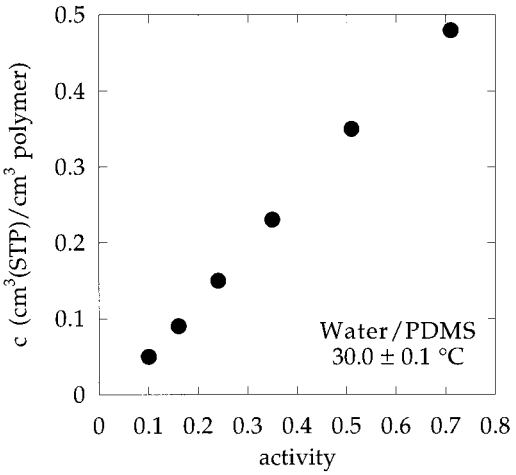

Figure 3 Solubility of water in PDMS as a function of activity at 30°C.

drying, all samples were stored in a desiccator until further use. The density of the PEBAX™ grades tested was reported to be 1.01 g/cm^3.[16]

Solvents

Methanol (Fisher Chemical, technical grade, 99.9% purity) and water were used. Both penetrants were subjected to a series of freeze–thaw cycles before use. The measured vapor pressures were in good agreement with those reported by Reid, Prausnitz, and Poling.[17]

TREATMENT OF EXPERIMENTAL DATA

Solubility

The equilibrium sorption for each penetrant was calculated using

$$c = \frac{22414\,|M_f - M_i|}{MW \cdot V_p} \qquad (1)$$

where c is the equilibrium concentration of the penetrant [cm^3(STP)/cm^3 polymer]; 22414 is the volume (cm^3) of 1 mol of penetrant at standard temperature and pressure; M_i and M_f are the initial and final masses (g), respectively; MW is the molecular weight of the penetrant (g/mol); and V_p is the polymer volume (cm^3). Standard conditions were taken as 0°C and 1 atm.

The solubility coefficient, S, is defined as:

$$S = c/p \qquad (2)$$

where p is the vapor pressure. Solubility coefficients were needed to calculate permeability coefficients. The permeability coefficients at low activities were of interest for the methanol separation process. Therefore, eq. (2) could be used directly, because the concentration c is linearly related to the vapor pressure in this range.

Diffusion Coefficients

The diffusion coefficient can be determined from the transient portion of the sorption process. The necessary relationships were obtained from the solution of Fick's second law by Crank[18] obeying boundary conditions equivalent to the ones in this study. At short times, the diffusion coefficient can be estimated from a plot of M_t/M_∞ versus the square root of time:

$$\frac{M_t}{M_\infty} = \frac{4}{\sqrt{\pi}}\left(\frac{Dt}{\delta^2}\right)^{1/2} \qquad (3)$$

where M_t and M_∞ are the weight gain by the sample at time t and at equilibrium, respectively, δ is the thickness of the sample, and D is the mutual diffusion coefficient. This equation is only valid for applications with a constant diffusion coefficient. However, Crank and Park[19] showed that for cases of nonconstant D, the average diffusion coefficient over the entire experimental range is calculated. This method can be applied up to a normalized mass uptake M_t/M_∞ of 0.6 with negligible devia-

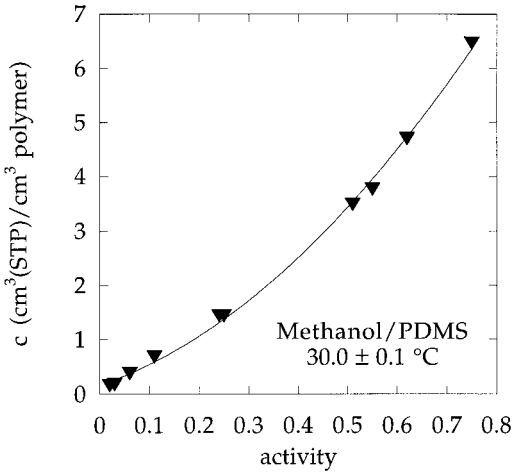

Figure 4 Solubility of methanol in PDMS as a function of penetrant activity. The dark line represents the data published by Favre.[5]

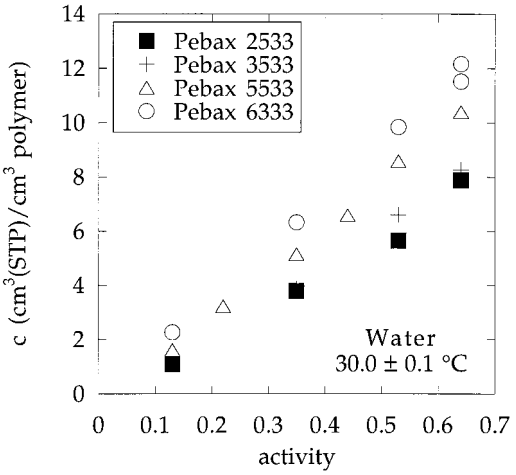

Figure 5 Solubility of water in a series of PEBAX™ polymers as a function of activity.

tions from the exact solution of Fick's second law. The short-term method was used in this study to analyze the data. The time required to bring the sample environment from vacuum to the vapor pressure of the run is small compared to the experimental timescale, but not zero. The raw experimental data (weight vs. time) was therefore shifted so that a zero time/zero uptake intercept of the linear regression (up to $M_t/M_\infty = 0.6$) was obtained.

Crank and Park[19] also introduced the long-term method to calculate the diffusion coefficient from experimental data. The long-term method proposes a linear relationship in a plot of $\ln(1 - M_t/M_\infty)$ versus time t:

$$\ln\left(1 - \frac{M_t}{M_\infty}\right) = \ln\left(\frac{8}{\pi^2}\right) - \left(\frac{\pi^2 D}{\delta^2}\right)t \qquad (4)$$

This method was used for a normalized mass uptake between 0.5 and 0.85. The uncertainty of the starting time has negligible influence on the results of the long-term method. The starting time determined through the shift of the raw experimental data to satisfy the zero time/zero uptake intercept was used (see above). Agreement between the diffusion coefficients from the short- and long-term methods was very good. This shows the high reliability of the results obtained here.

The reported diffusion coefficients were calculated by first averaging the results of the short-term and the long-term method for each sorption and desorption experiment. Then, the final value is obtained by averaging the results of the corresponding sorption–desorption runs.

Permeation Coefficients

The permeation coefficient of each penetrant has been calculated as the product of the diffusion and sorption coefficients according to

$$P = DS \qquad (5)$$

RESULTS

Solubility Measurements

To ensure that the data obtained were accurate, the sorption of water and methanol in PDMS was measured and compared to values reported in the literature.

PDMS/Water

The solubility of water in PDMS was determined at 30.0 ± 0.1°C over the pressure range of 4 to 21 cmHg, or an activity range of 0.13 to 0.64. Experimental results are presented in Figure 3 in the form of a solubility isotherm. The isotherm is linear, indicating that the sorption can be described by Henry's law for this activity range. The solubility of water in PDMS is quite low (<0.5 $cm^3(STP)/cm^3$ polymer at an activity of 0.7).

The behavior of water in PDMS has been the subject of recent analysis by a number of researchers. Unfortunately, there is some discrepancy as to the exact numerical results. The compliance with Henry's law over this activity range, and the order of magnitude of the sorption found in our work are consistent with the published data.[5]

PDMS/Methanol

The solubility of methanol in PDMS was measured at 30.0 ± 0.1°C over the pressure range 4 to 122 cmHg, or an activity range from 0 to 0.75. Experimental results are presented in Figure 4. As with the sorption of water, the sorption of methanol is linearly related to the applied penetrant pressure at low penetrant activities. However, at activities above about 0.3, there is clear curvature in the sorption isotherm, indicating that Henry's law no longer applies. Furthermore, the absolute value of sorption of methanol is an

order of magnitude greater than the sorption of water.

The results for the measurements with PDMS were compared to those reported by Favre[5] after correcting for temperature (solid line in Fig. 4). Temperature correction was performed using the interaction parameter calculated with the equations from Koningsveld and Kleinjtens.[20] The Favre data was obtained with a vapor permeation module. The agreement between our data and that of Favre is quite good. This is a very good validation of our experimental method.

PEBAX™/Water

The solubility of water in a series of PEBAX™ polymers was determined at 30.0 ± 0.1°C over the pressure range of 4 to 21 cmHg, or an activity range of 0.13 to 0.64. Experimental results are presented in Figure 5. Each of the isotherms is essentially linear with activity and shows no pronounced swelling or plasticization behavior. Interestingly, the total sorption, at a given activity, is not markedly affected by the polymer composition. Slight increases in the sorption of water are observed in the order of increasing PA content of PEBAX™ 2533 < 3533 < 5533 < 6333.

PEBAX™/Methanol

The solubility of methanol in the PEBAX™ series was determined at 30.0 ± 0.1°C over the pressure range of 4 to 90 cmHg, or an activity range of 0.02 to 0.55. Experimental results are presented in Figure 6. Each of the isotherms is essentially linear and shows no pronounced swelling or plasticization behavior. The total sorption, at a given penetrant activity, is essentially unaffected by the polymer composition. Within experimental error, all four polymers exhibit the same total sorption.

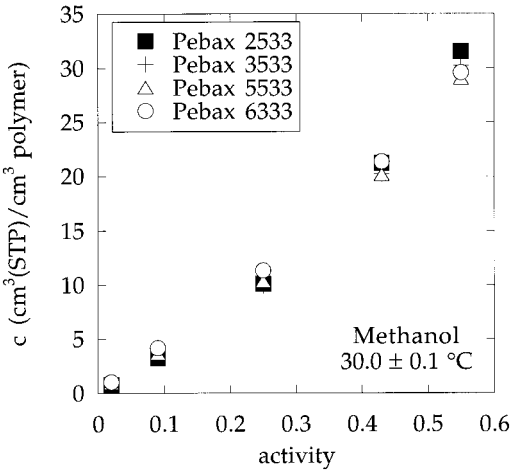

Figure 6 Solubility of methanol in a series of PEBAX™ polymers as a function of activity at 30°C.

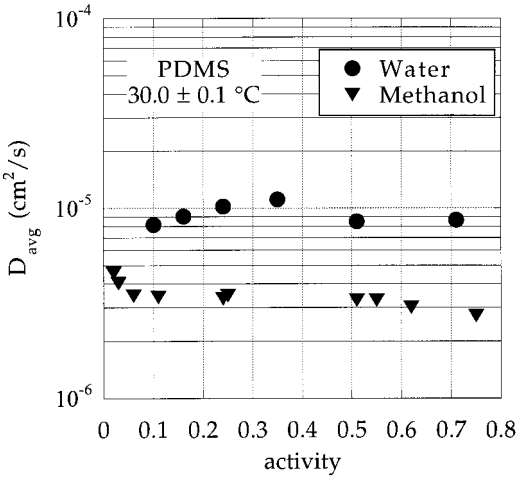

Figure 7 Average diffusion coefficient for water and methanol in PDMS as a function of penetrant activity.

DIFFUSION COEFFICIENTS

PDMS/Water/Methanol

The mutual diffusion coefficients, D, for water and methanol in PDMS were determined from the absorption and desorption rates using both the short-time and long-time methods as discussed above. The results are presented in Figure 7. The diffusion coefficients for both water and methanol are nearly independent of activity over the conditions investigated.

A recent publication by Watson and Baron reviews published diffusion coefficients for water in PDMS.[8] In contrast to previously published data,[5,6] which demonstrate decreases in the diffusion coefficient with increasing penetrant concentration, Watson and Baron report an essentially constant diffusion coefficient over a wide concentration range. The published values of diffusion coefficients as summarized by Watson and Baron vary by nearly an order of magnitude.

The data reported here is in acceptable agreement with that of Watson and Baron. In both data sets, the diffusion coefficient is observed to be independent of penetrant concentration. The average diffusion coefficient measured by Watson and Baron was 1.2 to 1.9 $\times$ 10^{-5} cm^2/s.[8] The values

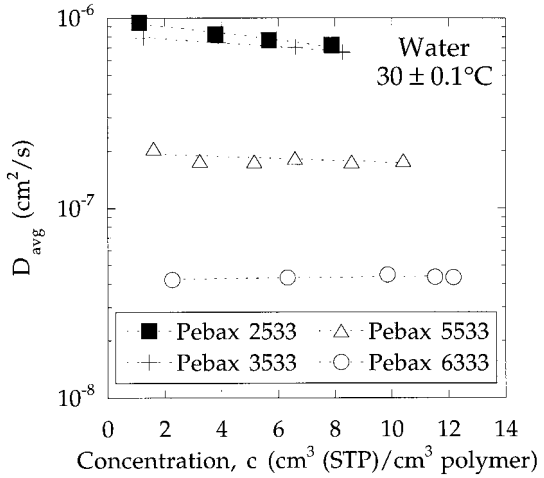

Figure 8 Average diffusion coefficient for water in a series of PEBAX™ polymers as a function of penetrant concentration. Lines drawn as visual aid.

measured here range from 0.8 to 1.1 $\times$ 10^{-5} cm^2/s. Considering the variability in the previously reported data, this agreement was deemed acceptable.

PEBAX™/Water

The diffusion coefficient of water in the PEBAX™ series was measured under the same conditions as the sorption isotherms. The results are presented in Figure 8, which shows that the diffusion coefficients are essentially independent of concentration over the interval investigated. However, there are marked differences in the diffusion coefficient of water in each of the four PEBAX™ grades. The trend is (increasing diffusion coefficient with decreasing polyamide content): 2533 $\approx$ 3533 $>$ 5533 $>$ 6333.

The absolute value of the diffusion coefficients ranges from approximately 3 $\times$ 10^{-8} to 1 $\times$ 10^{-6} cm^2/s.

PEBAX™/Methanol

The mutual diffusion coefficient of methanol in the PEBAX™ series was measured under the same conditions as the sorption isotherms. The results are presented in Figure 9, which shows that for grades 2533 and 3533, the diffusion coefficients are essentially independent of concentration over the interval investigated. Concentration dependence, which was not apparent in Figure 6, is clearly apparent here for PEBAX™ grades 5533 and 6333. This is most likely due to the plasticization of PEBAX™ grades 5533 and 6333 by methanol.

There are marked differences in the diffusion coefficient of methanol in each of the four polymers investigated. The trend in diffusion coefficients is the same as for water (increasing diffusion coefficient with decreasing polyamide content). The absolute values of the diffusion coefficients range from approximately 1.5 $\times$ 10^{-8} to 4 $\times$ 10^{-7} cm^2/s.

Permeation Coefficients

In the analysis of the membrane separation process, the relative rates of permeation through the polymer matrix is the key material property. Therefore, for each of the penetrants, the permeability has been calculated from eq. (5). In Table III, the calculated permeability for each material is reported at an activity similar to the level that would be encountered in the methanol recovery application of interest.

Due to the very low sorption of air in the polymer samples, the inaccuracy of the reported permeabilities for this penetrant is relatively high, estimated as ±50%. The relative inaccuracies are only approximately ±2% for the reported permeability coefficients of methanol and water.

DISCUSSION OF RESULTS

Membrane Separation Process

Ideally, if a membrane process were to be employed in recovery of vaporous methanol from hu-

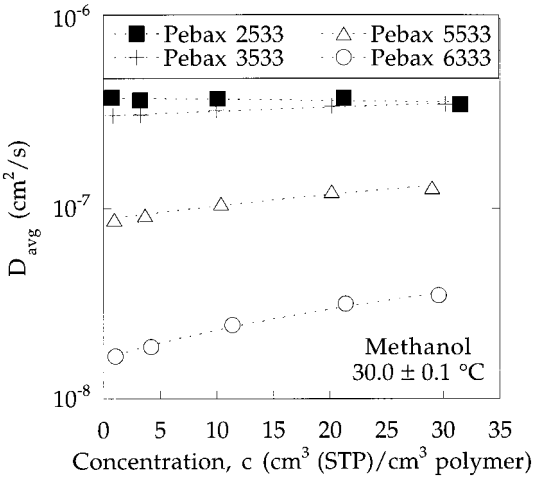

Figure 9 Average diffusion coefficient for methanol in a series of PEBAX™ polymers as a function of penetrant concentration. Lines drawn as visual aid.

Table III Calculated Permeability Coefficients and Selectivities for Methanol, Water, and Air Transport through PEBAX™ Polymers

	Permeability (Barrer)			Ideal Selectivity	
PEBAX™ Grade	Methanol[a]	Water[b]	Air[c]	Methanol/Air	Methanol/Water
2533	8090	25600	4.4	1840	0.32
3533	6840	27450	5.1	1340	0.25
5533	2250	8910	2.1	1070	0.25
6333	520	2590	0.3	1730	0.20

1 barrer = 10^{-10} cm^3 (stp) cm/cm^2 s cmHg.
[a] Methanol activity, 0.09.
[b] Water activity, 0.53.
[c] Air pressure, 73 cmHg.

mid air streams, it would preferentially permeate the methanol while excluding nearly all water and air from the permeate. Further, the rate of methanol transport should be as fast as possible, thereby minimizing the size of the membrane unit required. An appreciation for the ability of a particular material to complete this separation can be gained by evaluation of the ideal separation factors in Table III.

The ideal separation factor, defined as the ratio of the independently measured single-component permeation coefficients, provides a useful measure of the actual separation for polymers that exhibit Henry's law type sorption if there is no strong interaction of the various penetrants, and if the polymer does not undergo plasticization or swelling.[21] For the activity ranges of interest, swelling was not evident from the sorption measurements.

Each of the polymers in the PEBAX™ series evaluated here exhibits an outstanding ability to separate methanol from air, with selectivities of greater than 1000. PEBAX™ grade 2533 would appear to be the most attractive for this separation based on its high methanol permeability.

However, none of these polymers demonstrates the ability to selectively remove methanol from a water-wet air stream. Because these materials actually transport water faster than methanol, the permeate would consist of a methanol/water mixture, and the retentate would be a well-dried air stream. Thus, the goal of methanol recovery could be realized, but only at the added expense of a very large membrane area, which would be required to transport both the minor constituent (methanol) and the contaminant water.

Efforts are underway to overcome these limitations. We will report in the future on modifications of the mode of operation that will make full use of the high methanol selectivities, while avoiding problems with water permeation.

Transport Properties of Copolymers

The series of PEBAX™ polymers investigated is interesting in that although the films evaluated are optically clear, thermal analysis clearly demonstrates two distinct T_gs. Evaluation of Table I indicates that the thermal properties of the polymer are not influenced by the relative composition of polyether and polyamide segments. This is indicative of a microphase separated polymer.[22,23] The possible presence of two distinct phases in the polymers evaluated introduces some complications in the analysis.

The polyether phase has a T_g well below room temperature. Therefore, sorption into this phase would be expected to obey Henry's law with linear sorption isotherms up to the activity at which swelling becomes apparent. However, the polyamide segment has a T_g of approximately 40°C above the measurement temperature. Therefore, dual-mode type sorption isotherms, as are typical of glassy materials, may be expected from this fraction of the polymer.

Evaluation of the sorption isotherms for water and methanol in PEBAX™ (Figs. 5 and 6) indicates that, within the experimental error, all isotherms are linear with penetrant activity. Even for grade 6333, which is approximately 75 wt % glassy polyamide, no dual-mode behavior is observed.

A number of factors may be contributing to this behavior. First, the overall sorption measured is the sum of sorption into the rubbery PTMO phase and into the glassy PA phase. Any dual-mode be-

havior that may be present in the PA phase could be masked when superimposed on that of the PTMO phase.

It is further possible that the PA phase itself exhibits little or no dual mode sorption behavior. Stern has reported on the sorption of ethane and butane into polybutylmethacrylate over a range of temperatures traversing the T_g.[24] Even at temperatures 30°C above T_g, the sorption isotherm exhibited no dual-mode behavior. Rather, for the entire temperature range that was covered, the sorption isotherms were well described by Henry's law. Stern attributed this to the fact that the T_g is a temperature range, rather than a singular temperature.

Influence of Polymer Structure on Transport Properties

The copolymers evaluated here provide a unique look at a series of materials with essentially constant solubility, but varying diffusion coefficients.

Equilibrium sorption is determined by thermodynamic interactions between the polymer and the penetrant.[25] Thus, changes in the chemical nature of the polymer (such as changes in polarity) may manifest themselves as changes in the level of equilibrium sorption. In the series of polymers evaluated here, the relative content of polyether and polyamide groups is varied. The two constituents, PTMO and PA, have the chemical structures of $—(CH_2)_4—O—$, and $—NH—(CH_2)_{11}—CO—$, respectively. Because both materials have rather long aliphatic components, the chemical affinity of each for water and methanol is expected to be similar. This is consistent with the virtually constant equilibrium sorption for each of the block copolymers.

While the chemical nature of each of the blocks of the copolymer are nearly equivalent, their thermal behavior is not. At the evaluation temperature, the PTMO is in the rubbery range, and the PA has glassy characteristics. Thus, the kinetic behavior (chain mobility) of the two, which controls the rate of diffusion, is markedly different. These differences manifest themselves as differences in the diffusion coefficients. As the content of PA in the copolymer increases, the measured, average diffusion coefficient decreases. The diffusion coefficient in these materials is well correlated with the weight fraction of PA in the copolymer.

CONCLUSIONS

The PEBAX™ materials evaluated here can be used to selectively separate methanol from air, but not methanol from water. The 2533 grade appears to be the most promising based on its high permeation rates. If one of these materials were to be used in a membrane system for the recovery of methanol from water-wet air streams, the permeate product would be a mixture of methanol and water. Research is under way that will address this limitation, while simultaneously making full use of the very high methanol/air selectivities.

The PEBAX™ materials are unique in several respects. Because of the similar chemical nature of the two components of the copolymer, the equilibrium sorption of water and methanol in each of the polymers is essentially equivalent. However, the diffusion coefficient decreases markedly as the glassy polyamide content is increased.

Although the PEBAX™ polymers exhibit two T_gs, they are optically clear. Therefore, microphase separation is probable, but, if present, it must be present on a local scale only. The sorption isotherms of these materials (even those with up to 75 wt % glassy polyamide) obey Henry's law and show no evidence of dual-mode behavior. This may be attributable to masking of the sorption in the glassy phase by sorption into the rubbery phase. In addition, the presence of only minimal dual-mode behavior in the glassy phase could be explained by the close proximity of the measurement temperature to T_g.

Acknowledgment is made to the State of Georgia through its Technical Competitiveness in the Pulp and Paper Industry Initiative for partial support of this research. T. John also acknowledges financial support from the Ernest Solvay Foundation.

REFERENCES

1. NCASI, National Council of the Paper Industry for Air and Stream Improvement, Technical Bulletin 675 (1994).
2. P. M. Grace, B. Leopold, and E. W. Malcolm, Technical Eds., in *Pulp and Paper Manufacture,* Vol. 5, M. J. Kocurek and F. Stevens, Eds., Joint Textbook Committee of the Paper Industry of the United States and Canada, TAPPI Press, Atlanta, 1991.
3. R. W. Baker and J. G. Wijmans, in *Polymeric Gas Separation Membranes,* D. R. Paul and Y. P. Yampol'skii, Eds., CRC Press, Boca Raton, FL, 1994.

4. K. Ohlrogge, K.-V. Peinemann, J. Wind, and R.-D. Behling, *Sep. Sci. Technol.,* **25,** 1375 (1990).
5. E. Favre, P. Schaetzel, Q. T. Nguygen, and J. C. Neel, *J. Membr. Sci.,* **92,** 169 (1994).
6. J. A. Barrie and D. Machin, *J. Macro. Sci. Phys.,* 645 (1969).
7. I. Blume, P. J. F. Schwering, M. H. V. Mulder, and C. A. Smolders, *J. Membr. Sci.,* **61,** 85 (1991).
8. J. M. Watson and M. G. Baron, *J. Membr. Sci.,* **110,** 47 (1996).
9. M. E. Hollein, M. Hammond, and C. S. Slater, *Sep. Sci. Technol.,* **28,** 1043 (1993).
10. H. B. Hopfenberg and D. R. Paul, in *Polymer Blends,* D. R. Paul and S. Newman, Eds., Academic Press, New York, 1978.
11. L. P. Razumovskii, V. S. Markin, and G. Ye. Zaikoz, *Polym. Sci. USSR,* **27,** 751 (1985).
12. J. Agranoff, *Modern Plastics Encyclopedia,* McGraw Hill, New York, 1984.
13. J. Brandrup, E. H. Immergut, *Polymer Handbook,* John Wiley and Sons, New York, 1989.
14. H. S. Faruque and C. Lacabanne, *J. Phys., Appl. Phys.,* **20,** 939 (1987).
15. J. R. Flesher, Jr., in *High Performance Polymers: Their Origin and Development,* R. B. Seymour and G. E. Kirshenbaur, Eds., Elsevier Science Publishing, New York, 1986.
16. ELF Atochem North America, Inc., PEBAX™ Technical Brochure.
17. R. C. Reid, J. M. Prausnitz, and B. E. Poling, *The Properties of Gases and Liquids,* McGraw–Hill, New York, 1987.
18. J. Crank, *Mathematics of Diffusion,* Oxford University Press, London, 1956.
19. J. Crank and G. S. Park, *Diffusion in Polymers,* Academic Press, New York, 1968.
20. R. Koningsveld and L. A. Kleinjtens, *Macromolecules,* **4,** 637 (1971).
21. W. J. Koros, R. T. Chern, V. Stannett, and H. B. Hopfenberg, *J. Polym. Sci., Polym. Phys.,* **19,** 1513 (1981).
22. D. R. Paul and J. W. Barlow, *J. Macromol. Sci.-Rev. Macromol. Chem.,* **C18,** 109 (1980).
23. F. S. Bates, *Science,* **25,** 898 (1991).
24. S. A. Stern, U. M. Vakil, and G. R. Mauze, *J. Polym. Sci., Polym. Phys.,* **27,** 405 (1989).
25. W. J. Koros, G. K. Fleming, S. M. Jordan, T. H. Kim, and H. H. Hoehn, *Prog. Polym. Sci.,* **13,** 339 (1988).

Appendix B: Correlation of Penetrant Transport with Polymer Free Volume: Additional Evidence from Block Copolymers

ELSEVIER

PII: S0032-3861(97)00302-9

Polymer Vol. 39 No. 3, pp. 599–603, 1998

0032-3861/97/$17.00+0.00

Correlation of penetrant transport with polymer free volume: additional evidence from block copolymers

Mary E. Rezac[a,*] and Tilo John[†b]

[a]*Georgia Institute of Technology, School of Chemical Engineering, Atlanta, GA 30332-0100, USA*

[b]*Institute für Thermische Verfahrenstechnik, Universität Karlsruhe, Karlsruhe, Germany*

(Received 3 January 1997; revised 24 February 1997)

The transport rates of methanol and water through a series of PEBAX® block copolymers were measured and correlated with the fractional free volume. Excellent agreement between the logarithm of the diffusion coefficient and the inverse of the fractional free volume of the polymer was observed. This provides new evidence of the utility of the free volume theory to describe the transport of highly condensable vapours. Correlation was also quite good when the logarithmic additivity relationship was employed. This relationship has been previously shown to correlate the properties of homogenous blends with copolymer composition. The successful use of this theory for a series of blends that exhibit two glass transition temperatures is discussed. © 1997 Elsevier Science Ltd.

(Keywords: diffusion in polymers; free volume theory; copolymers)

INTRODUCTION

The rate of gas transport across a solid polymeric film is determined by the process conditions (feed composition, temperature and partial pressure) as well as by the chemical structure of the polymer. Many studies have attempted to quantify and generalize the relationship between chemical structure and gas transport. Notable are those of Stern and coworkers[1–4] and Koros, Paul and others[5–8]. These studies have focused on the use of permanent gases as test penetrants and on systematic variation of the polymeric backbone or side groups. Our analysis of a series of block copolymers minimizes ambiguities in the interpretation of the results due to variations in the chemical makeup of the polymer backbone or pendant groups. The research reported here examines the gas transport of highly condensable penetrants in a series of block copolymers. Block copolymers are rarely examined. Yet, they offer the unique opportunity to systematically examine gas transport without the influence of side-group interactions. The physical properties of these materials vary as the copolymer content changes; however, the chemical constituents of the polymer remain constant.

Through a detailed analysis of the transport of condensable penetrants in a series of block copolymers, we have provided further information in the continuing attempt to correlate the polymer structure with transport properties.

BACKGROUND

Cohen and Turnbull have suggested that diffusion in a rubbery polymer is the result of redistribution of free volumes within a matrix and migration of the penetrant among these free volumes[9]. Diffusion can therefore occur if a hole exists that is large enough for a molecule to enter this newly formed hole. From the evaluation of transport in liquids, Cohen and Turnbull found that the probability that a volume large enough exists for such a jump could be described by the following equation:

$$P(v^*) = \exp(-\gamma v^*/v_F) \tag{1}$$

where P is the probability for a hole of sufficient size v^*, γ is a constant and v_F is the average free volume in the material. Barrer and Fergusson[10] found linear relations between the probability of the existence of a hole and the diffusivity. Therefore, the free volume model suggests a linear relationship if the logarithm of the diffusion coefficient is plotted *versus* the polymer's free volume. Lee has shown that such a correlation can be applied both above and below the polymer's glass transition temperature[11].

A major limitation of the quantitative use of this theory is the lack of a clear working definition of 'free volume'[12–14]. Specific free volume and fractional free volume have been suggested. Each method has proven useful. The following simple definitions for specific and fractional free volume have been proposed and employed. Specific free volume can be found by

$$V_F = V - V_0 \tag{2}$$

Where V is the experimentally observed specific volume and V_0 is an estimate of the specific volume occupied by the polymer at zero Kelvin. The specific volume is taken as the inverse of the polymer bulk density. A group contribution approach was used in the calculation of V_0. The van der Waals specific volume, V_W, of the polymer was calculated by group contribution and equated to the occupied volume

* To whom correspondence should be addressed
† Present address: BASF, Mannheim, Germany

by

$$V_0 = 1.3V_W \quad (3)$$

as suggested by Bondi[12].

The fraction free volume has been defined as the ratio of the specific free volume to the observed specific volume:

$$FFV = \frac{V_F}{V} \quad (4)$$

Cohen and Turnbull's theory has been used to correlate the rate of penetrant diffusion in a polymer with its 'free volume'. Examination of penetrant transport in polymers is often concerned with the rate of penetrant migration across a film or the permeation rate. This rate can be used in the design of polymeric membranes for separation or barrier packaging. For the case of negligible downstream pressure, the permeability coefficient can be written as the product of a diffusion coefficient and a sorption coefficient:

$$P = DS \quad (5)$$

In principle, each of these coefficients can be measured independently. However, for low sorbing penetrants such as oxygen, nitrogen and helium, accurate measurement of the sorption and diffusion coefficients is difficult. Yet, direct measurement of the permeability coefficient of such gases is straightforward[15]. Therefore, the literature frequently reports permeability coefficients exclusively. As a result, several authors have attempted to apply Cohen and Turnbull's theory to correlate permeability coefficients with the free volume[16–22]. While such an extension has little theoretical basis, the correlations are often quite good. Successful correlations supports the proposition by these authors that the expected level of sorption is nearly constant for a given penetrant over a wide range of free volumes if the chemical nature of the polymer is varied only minimally. For systems in which D and S were independently measured, this proposition is generally confirmed[21].

Several modern theories of gas transport in polymers have been developed based on work of Cohen and Turnbull. Notable among these are those of Vrentas, Duda and coworkers[23–25]. These authors have attempted to develop a predictive theory and to account for differences in the chemical nature of the polymer and the penetrant. However, the complexity of the Vrentas and Duda model has limited its use.

While the Cohen and Turnbull model can accurately correlate transport rates to a single parameter, the polymer free volume, the Vrentas and Duda model requires information relating to variations in polymer viscosity above and below T_g, thermal expansion coefficients of the glassy and rubbery state, molar volume of solvent, rheological data and diffusivity data for the solvent in the glassy polymer as a function of temperature. The correlative power of the model appears to be quite high, better than that of Cohen and Turnbull in certain circumstances. However, the use of the model has been limited by the amount of experimental data required.

Weinkauf and Paul used free volume theory to describe the behaviour of a series of copolymers[26]. The copolymers exhibited only a single melting exotherm and a single glass transition temperature. The theory showed a good correlation with the experimental data.

Weinkauf and Paul also demonstrated that the copolymer permeability could be correlated using logarithmic additivity as shown in equation (6):

$$\ln P = x_1 \ln P_1 + x_2 \ln P_2 \quad (6)$$

where x_i is the volume fraction of component i, and P_i is the permeability of the homopolymer. equation (6) provides a simple model by which to predict the behaviour of miscible mixtures or copolymers prior to actual synthesis and evaluation.

EXPERIMENTAL

The absorption–desorption kinetics and the solubility of methanol and water in a series of polyamide–polyether block copolymers were studied by a gravimetric method. This method consists of measuring the rate of weight gain or loss of a sample material due to absorption or desorption, respectively, of the penetrant. The weight change was determined with an electromicrobalance incorporated in a vacuum system that allowed the exposure of the candidate material to a vapour of the solvent of interest. The system has been previously described in detail[27].

Materials

Polymers. A series of PEBAX® block copolymer samples in the form of pellets was kindly supplied by Elf Atochem (Philadelphia, PA). PEBAX® grades 2533, 3533, 5533 and 6333 were evaluated. The general chemical formula for PEBAX® is given in *Figure 1*.

PA represents polyamide and PE is a polyether segment. In the PEBAX® series studied here, Nylon 12 and polytetramethylene oxide (PTMO) were used in varying ratios. An elemental analysis for carbon, hydrogen, nitrogen and oxygen (C, H, N and O) was performed by Huffman Laboratories (Golden, CO). The number of repeat units of polyamide and polyether in each monomer segment (subscripts 'x' and 'y' in *Figure 1*) was calculated. In this calculation, initial guesses for 'x' and 'y' were based on those reported by Faruque and Lacabanne for this PEBAX® polymer[28]. Using these values and the known structure of Nylon 12 and PTMO, the resultant mass fraction of each element was calculated. These calculated values were compared to the experimentally measured mass fractions and an overall error (defined as the sum of the error for each element) was minimized via iteration. The results are reported in *Table 1*. The fractional free volume for each material is also reported. Fractional free volumes were calculated using the method of Bondi[12] with values for the structural groups from van Krevelen[29].

The glass transition temperatures of the various polymers were measured using differential scanning calorimetry (DSC) under nitrogen. Scans were run from −100 to 200°C at a heating rate of 10°C min^{-1}. The measured values are reported in *Table 1*. Thermal analysis of these materials indicated two distinct glass transition temperatures as well as crystalline melting peaks near 10 and 140°C.

PEBAX® films were melt extruded using a Haake Buckler extruder fitted with a flat film die. The extrusion temperature ranged from 140 to 180°C depending on the material. The motor speed was varied between 5 and

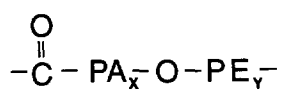

Figure 1 General monomeric repeat structure of PEBAX®

Table 1 Physical properties of the PEBAX® samples

	PEBAX® 2533	3533	5533	6333	Nylon 12
'x'	2.68	3.42	14.85	19.30	–
'y'	27.80	26.00	24.70	16.60	–
Weight percentage of PA	21.6	27.1	62.2	75.8	100
FFV	0.172	0.168	0.141	0.131	0.120[a]
$T_{g\ PTMO}$ (°C)	−76	−72	−65	−60	–
$T_{m\ Crystalline\ PTMO}$ (°C)	12	7	None detected	None detected	–
T_g Nylon (°C)	70	68	66	72	–
$T_{m\ Crystalline\ PA}$ (°C)	137	142	160	170	178[a]

[a]Reference [33]

30 rpm. Sample thickness was controlled by the motor speed and the speed of the take-up roller. Sample thicknesses were between 0.0125 and 0.0470 cm.

All films were optically clear and remained so throughout the preparation and testing process. Samples were dried under vacuum for 14 days at 40°C. The vacuum pump was equipped with an aluminium oxide backdiffusion trap. Following drying, all samples were stored in a desiccator until further use. The density of the PEBAX® grades tested was reported to be 1.01 g cm^{-3} [30].

Solvents

Methanol (Fisher Chemical, technical grade, 99.9% purity) and water were used. Both penetrants were subjected to a series of freeze–thaw cycles before use. The measured vapour pressures were in good agreement with those reported by Reid *et al.*[31]

TREATMENT OF EXPERIMENTAL DATA

Sorption

The equilibrium sorption for each penetrant was calculated using

$$c = \frac{22414|M_f - M_i|}{MW \cdot V_p} \tag{7}$$

where c is the equilibrium concentration of the penetrate absorbed in cm^3 (STP) cm^{-3} polymer, at a pressure, p, and at the given temperature. The constant 22414 represents the volume, in cm^3, of one mole of penetrant at STP (0°C and 1 atm), M_f is the mass shown by the balance at equilibrium (final) and M_i is the mass shown at the beginning of an experiment (initial), both in grams. MW is the molecular weight of the penetrant (in g mol^{-1}) and V_p is the polymer volume, in cm^3.

Diffusion coefficients

Diffusion coefficients were evaluated using the non-steady state of the sorption and desorption curve according to Crank[32]. At short times,

$$\frac{M_t}{M_\infty} = \frac{4}{\sqrt{\pi}}\left(\frac{Dt}{\delta^2}\right)^{1/2} \tag{8}$$

where M_t and M_∞ are the weight gain by the sample at time t and at equilibrium, respectively, δ is the thickness of the sample and D is the mutual diffusion coefficient. This equation is only valid for applications with a constant diffusion coefficient. However, Crank and Park[15] showed that for cases of non-constant D, the average diffusion coefficient over the entire experimental range is calculated. This method can be applied up to a normalized mass uptake M_t/M_∞ of 0.6 with negligible deviations from the exact solution of Fick's second law. This 'short-time method' was used in this study to analyse the data.

Crank and Park[15] also introduced the long-time method to calculate the diffusion coefficient from experimental data. The long-time method proposes a linear relationship in a plot of $\ln(1 - M_t/M_\infty)$ *versus* time t:

$$\ln\left(1 - \frac{M_t}{M_\infty}\right) = \ln\left(\frac{8}{\pi^2}\right) - \left(\frac{\pi^2 D}{\delta^2}\right)t \tag{9}$$

Agreement between the values of the diffusion coefficient calculated using those two methods was very good, supporting the accuracy of the calculated values.

The diffusion coefficients reported in this paper are the average of the results of the short- and long-time values. Furthermore, the average of the results of the sorption and the desorption runs is used.

Permeation coefficients

The permeation coefficients reported were calculated using equation (5), where S is the sorption coefficient and is defined as $S = C/p$. Here, the average slope of a plot of equilibrium sorption *versus* pressure up to the activity reported is used as S.

RESULTS

Sorption isotherms for both methanol and water in each of the PEBAX® polymers were measured over the activity range of 0 to approximately 0.75 at 30°C. Complete analysis of the influence of activity on molecular transport is provided in a separate publication[27]. Here, we have chosen to evaluate only a single intermediate activity for each penetrant. Up to the activities discussed, the sorption isotherms were linear with respect to penetrant activity. Therefore, one may conclude that no significant swelling of the polymer matrix has occurred.

Measured solubility coefficients, diffusion coefficients and calculated permeability coefficients for each of the polymers are reported in *Table 2* for methanol and in *Table 3* for water. Each of the values reported is the average of the measured values obtained from a paired absorption–desorption run.

For the polymers and penetrants examined, the solubility is essentially constant. Therefore, variations observed in the permeability coefficient can be attributed almost

Table 2 Solubility, diffusion, and permeability coefficients for methanol in a series of PEBAX® polymers at 30°C and methanol partial pressure of 40 cmHg (methanol activity = 0.25)

Polymer	S [cm^3 (STP) cm^{-3} polymer cmHg^{-1}]	$D_{AVG} \times 10^8$ (cm^2 s^{-1})	$P \times 10^{10}$ [cm^3 (STP) cm cm^{-2} cmHg^{-1} s^{-1}]
Pebax 2533	2.53	38.0	9600
Pebax 3533	2.48	33.0	8200
Pebax 5533	2.58	10.6	2740
Pebax 6333	2.86	2.45	700

Table 3 Solubility, diffusion, and permeability coefficients for water in a series of PEBAX® polymers at 30°C and water partial pressure of 20 cmHg (water activity = 0.64)

Polymer	S [cm^3 (STP) cm^{-3} polymer cmHg^{-1}]	$D_{AVG} \times 10^8$ (cm^2 s^{-1})	$P \times 10^{10}$ [cm^3 (STP) cm cm^{-2} cmHg^{-1} s^{-1}]
Pebax 2533	4.37	73.0	31870
Pebax 3533	4.06	66.4	26930
Pebax 5533	5.11	17.9	9150
Pebax 6333	5.70	4.35	2480

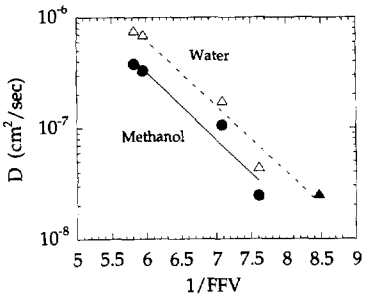

Figure 2 Correlation between inverse fractional free volume of PEBAX® polymers and the measured diffusion coefficients for methanol and water at 30°C. Correlation coefficients for water and methanol are 0.996 and 0.993, respectively. Water data denoted with solid triangle (at $1/FFV = 8.5$) is for the transport of water through pure Nylon 12[33]

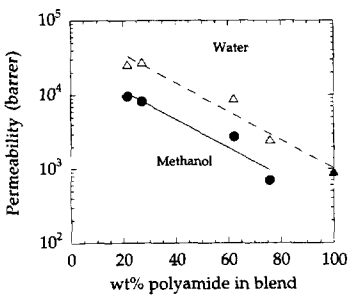

Figure 3 Influence of PEBAX® blend composition on the permeability of water and methanol at 30°C. Correlation coefficients for water and methanol are 0.966 and 0.990, respectively. Water data denoted with solid triangle (at polyamide content = 100%) is for the transport of water through pure Nylon 12[33]

entirely to changes in the measured diffusion coefficient. This supports the use of the free volume theory for correlations of the permeability coefficient with minimal inaccuracy.

DISCUSSION OF RESULTS

A plot of the diffusion coefficients of both water and methanol in the PEBAX® series as a function of inverse fractional free volume is presented in *Figure 2*. An excellent correlation between the fractional free volume of the copolymer and the diffusion coefficient of either water or methanol is demonstrated. Furthermore, data from the literature is included for water transport through pure Nylon 12. This data fits well with the experimentally measured trend. No data for the transport of methanol through the homopolymers was found in the literature.

Several, potentially significant variations exist between the results reported here and those reported in the literature for the correlation of transport properties with a polymer's free volume. The polymers studied here exhibit two glass transition temperatures indicative of phase separation. Yet the materials are optically clear and the molecular weight of each segment in the repeat unit is relatively short. Thus, any phase separation present is on a local molecular scale. Nevertheless, the free volume theory provides very good correlation for the transport properties of these materials.

The highly condensable components water and methanol were used as test penetrants. While the free volume theory is hypothetically applicable to any penetrant in any pseudo-liquid system, essentially all of the published correlations are for test penetrants that are much less condensable than water and methanol, typically carbon dioxide, nitrogen or methane. We must note, however, that the analysis presented here is at relative vapour activities under which no swelling of the polymer matrix was observed. Under bulk swelling conditions, this correlation may not provide sufficient detail to fully describe the diffusion process.

The extension of the free volume theory of Cohen and Turnbull to highly condensable components in block copolymers provides unique evidence for the usefulness of the theory to correlate transport properties and the fractional free volume of a polymer.

The permeability data for these polymers has been analysed using the logarithmic additivity model described in equation (6). While the permeability values for the homopolymers are not known, it appears that the block copolymers follow this simple relation (as can be seen in *Figure 3*). Our data confirms that equation (6) provides a simple method for the prediction of the properties of block copolymers. The excellent fit of equation (6) provides further support that the transport properties of the polymers examined here behave in a manner consistent with homogenous polymer blends[26].

CONCLUSIONS

Correlations between polymer free volume and penetrant diffusion coefficients, first proposed by Cohen and Turnbull have been successfully applied to a series of block copolymers with methanol and water as the test penetrants. The excellent agreement between the overall polymer free volume and the diffusion coefficients provides an opportunity to tune the copolymer content to achieve a wide range of desired transport properties. The successful extension of the free volume theory to a series of block copolymers and highly condensable penetrants provides further evidence of its general utility.

ACKNOWLEDGEMENTS

Acknowledgment is made to the State of Georgia through its Technical Competitiveness in the Pulp and Paper Industry Initiative for partial support of this research. T. John also acknowledges financial support from the Ernst Solvay Foundation.

REFERENCES

1. Stern, S.A., Liu, Y. and Feld, W.A., *Journal of Polymer Science, Polymer Physics*, 1993, **31**, 939.
2. Yamamoto, H., Mi, Y., Stern, S.A. and St. Clair, A.K., *Journal of Polymer Science, Polymer Physics*, 1990, **28**, 2291.
3. Stern, S.A., Mi, Y., Yamamoto, H. and St. Clair, A. K., *Journal of Polymer Science, Polymer Physics*, 1989, **27**, 1887.
4. Stern, S.A., Shah, V. and Hardy, B., *Journal of Polymer Science, Polymer Physics*, 1987, **25**, 1263.
5. Kim, T.H., Koros, W.J., Husk, G.R. and O'Brien, K.C., *Journal of Membrane Science*, 1988, **37**, 45.
6. Koros, W.J., Fleming, G.K., Jordan, S.M., Kim, T.H. and Hoehn, H.H., *Progress in Polymer Science*, 1988, **13**, 339.
7. Paul, D.R. and Maeda, Y., *Journal of Membrane Science*, 1989, **40**, 109.
8. Puleo, A.C., Muruganandam, N. and Paul, D.R., *Journal of Polymer Science, Polymer Physics*, 1989, **27**, 2385.
9. Cohen, M.H. and Turnbull, D., *Journal of Chemistry and Physics*, 1959, **31**, 1164.
10. Barrer, R.M. and Fergusson, R.R., *Transactions of the Faraday Society*, 1958, **54**, 989.
11. Lee, W.M., *Polymer Engineering and Science*, 1980, **20**, 65.
12. Bondi, A., *Physical Properties of Molecular Crystals, Liquids, and Glasses*. Wiley, New York, 1968.
13. Bondi, A., *Journal of Physics and Chemistry*, 1954, **58**, 929.
14. Haward, R.N., *Journal of Macromolecular Science—Review of Macromolecular Chemistry*, 1970, **C4**, 191.
15. Crank, J. and Park, G. S., *Diffusion in Polymers*. Academic, New York, 1968.
16. Aitken, C.L., Koros, W.J. and Paul, D.R., *Macromolecules*, 1992, **25**, 3651.
17. Pixton, M. R. and Paul, D. R., in *Polymeric Gas Separation Membranes*, ed. D. R. Paul and Y. P. Yampol'skii. CRC Press, Boca Raton, FL, 1994.
18. Walker, D.R.B. and Koros, W.J., *Journal of Membrane Science*, 1991, **55**, 99.
19. Coleman, M.R. and Koros, W.J., *Journal of Polymer Science, Polymer Physics*, 1994, **32**, 1915.
20. Costello, L.M. and Koros, W.J., *Journal of Polymer Science, Polymer Physics*, 1995, **33**, 135.
21. McHattie, J.S., Koros, W.J. and Paul, D.R., *Polymer*, 1992, **33**, 1701.
22. Hellums, M.W., Koros, W.J., Husk, G.R. and Paul, D.R., *Journal of Membrane Science*, 1989, **46**, 93.
23. Vrentas, J.S., Duda, J.L. and Ling, H.-C., *Journal of Polymer Science and Polymer Physics*, 1985, **23**, 275.
24. Vrentas, J.S., Duda, J.L., Ling, H.-C. and Hou, A.-C., *Journal of Polymer Science and Polymer Physics*, 1985, **23**, 289.
25. Vrentas, J.S., Duda, J.L. and Hou, A.-C., *Journal of Applied Polymer Science*, 1987, **33**, 2581.
26. Weinkauf, D.H. and Paul, D.R., *Journal of Polymer Science and Polymer Physics*, 1992, **30**, 837.
27. Rezac, M.E., John, T. and Pfromm, P.H., *Journal of Applied Polymer Science*, 1997, **0**, 0. (in press).
28. Faruque, H.S. and Lacabanne, C., *Journal of Physics, Applied Physics*, 1987, **20**, 939.
29. von Krevelen, D. W., *Properties of Polymers*, 3rd edn. Elsevier, New York, 1990.
30. ELF Atochem North America, Inc., Pebax® Technical Brochure.
31. Reid, R. C., Prausnitz, J. M. and Poling, B. E., *The Properties of Gases and Liquids*. McGraw-Hill, New York, 1987.
32. Crank, J., *Mathematics of Diffusion*. Oxford University Press, London, 1956.
33. Agranoff, J., *Modern Plastics Encyclopedia*, 1984, **61**, 463.

Appendix C: Gas Transport Properties of a Series of High Tg Polynorbornenes with Aliphatic Pendant Groups

Gas Transport Properties of a Series of High T_g Polynorbornenes with Aliphatic Pendant Groups

Kokou D. Dorkenoo, Peter H. Pfromm, and Mary E. Rezac

Institute of Paper Science and Technology
500 10th Street N.W., Atlanta, GA 30318-5794
School of Chemical Engineering, Georgia Institute of Technology
Atlanta, GA 30332-0100

ABSTRACT

A study of gas transport properties of novel polynorbornenes with increasing length of an aliphatic pendant group R (CH_3-, $CH_3(CH_2)_3$-, $CH_3(CH_2)_5$-, $CH_3(CH_2)_9$-) has been performed. These polymers were synthesized using novel organometallic complex catalysts via an addition polymerization route. This reaction route maintained the bridged norbornene ring structure in the final polymer backbone. Gas permeability and glass transition temperature were found to be higher than those for polynorbornenes prepared by ring-opening metathesis and reported in the literature. It was shown that for non-condensable gases such as H_2 and He the selectivity over N_2 decreased when the length of the pendant group increased, but remained relatively stable for the more condensable gases (O_2 and CO_2). The permeability coefficient is correlated well to the inverse of the fractional free volume of the polymers. The more condensable gases showed a deviation from this correlation for the longest pendant group, probably due to an increase of the solubility effect. This polymer series demonstrated a simultaneous increase in permeability and selectivity, uncommon for polymers.

(Keywords: Polynorbornene; gas separation; Membrane; free volume)

INTRODUCTION

Polynorbornenes have been synthesized for their excellent properties for dielectric applications, and also for their significant cost advantage in comparison with materials currently used as interlevel dielectrics in microelectronics.[1] Their transport properties are important not only for this application, but also for other potential uses in packaging[2] and gas separation.[3] The most familiar polynorbornene[4-9] (Figure 1) is prepared by ring-opening metathesis polymerization (ROMP) and has a varying content of cis and trans units depending on the polymerization catalyst used. The ROMP polynorbornenes have been the subject of a number of investigations; some of which are summarized below. In contrast, the polynorbornenes evaluated here have been synthesized via a novel addition polymerization, which maintains the norbornene ring structure. For simplicity, we will refer to these as addition polynorbornenes (APNB's). The molecular architecture of the APNB's, shown in Figure 2, is fundamentally different than the ROMP polymers shown in Figure 1. The impact of this difference on the physical and transport properties is the subject of this study.

Yampol'skii et al.[6] studied the transport properties of ROMP polynorbornenes with different stereoregular structures controlled by the synthesis. They showed that the polynorbornene with predominantly cis units in the backbone chain shows higher gas permeabilities than those with predominantly trans units. They also determined the free volume of their polymers by the positron annihilation method. Steinhäusler and Koros[7] have also investigated the influence of stereochemistry and tacticity of ROMP polynorbornenes on gas separation properties and reported findings similar to Yampol'skii.

Bondar et al.[8] studied permeation and sorption in polynorbornenes with varying substituents. They reported that the introduction of a $Si(CH_3)_3$ group to the backbone increased the glass transition temperature and the permeability of gases through the polymer. They concluded that if the size of the silicon-containing side group is too large the permeability and the glass transition decrease (see Table 4). Yampol'skii et al.[9] observed increased gas permeability, gas sorption, and elevated glass transition temperatures in polynorbornenes with fluorine-containing side groups.

In the research reported here, we have investigated a class of polynorbornenes, which retain the norbornene ring in the repeat unit as shown in Figure 2. This structure is substantially more rigid than the polynorbornenes prepared by ring-opening metathesis polymerization as previously discussed.[4-9] Thus, we anticipate that our materials will have enhanced glass transition temperatures and potentially improved separation selectivities. We have investigated the effect of the size of aliphatic pendant groups on transport properties.

EXPERIMENTAL

Materials

The repeat unit for the polynorbornene materials evaluated here is shown in Figure 2 where R represents different pendant groups. The polynorbornenes were supplied by the BFGoodrich corporation. They were produced via addition polymerization using an organometallic complex as catalyst.[10,11,12] APNBs with four different pendant groups have been evaluated here. The pendant groups are methyl,

butyl, hexyl, and decyl. The elongation-to-break of the unsubstituted APNB was insufficient to allow for formation of the film samples needed for permeation evaluation.

Polymer samples were cast from chloroform (Aldrich, 99.9% purity, used as received). Permeation samples were prepared by adhering aluminum foil masks to the polymer with an epoxy adhesive (Duro Master Mend).[13] All gases (minimum purity 99.9%) were obtained from Air Products and used as received.

Preparation

The films were cast from the chloroform solution containing approximately 3.6 wt% of polymer. The solution was filtered through a 0.45 μm Teflon filter and cast directly into a stainless-steel ring on a leveled mirror. A second glass plate was placed across the top of the casting ring to slow the evaporation of the solvent. The evaporation was performed in a glove bag in a solvent-enriched environment. Following 24 hours, the films were removed from the plates by immersion in water. The films were further dried under vacuum at 100°C to a constant weight. In the initial 7 hours of vacuum drying, a weight loss of 2% was measured. Continued drying to a total of 24 hours resulted in no further change in weight. The vacuum system was equipped with a trap to prevent oil vapor back diffusion.

Thickness and area measurement

After drying, the film thicknesses were measured. A known area of the film was weighed, and using the measured density (see below), the film thickness was calculated. The accuracy of this thickness measurement was determined by repeated measurements and was estimated to be within 2% of the reported value. The thickness of our films

ranged from 6-12 μm. Thickness measurements with a mechanical gauge (resolution 1μm) were in good agreement with the method described above.

The permeation area was determined by successive magnified photocopies of the masked permeation area taken after the end of the experiments. The image of the permeation area was then determined gravimetrically. The average area determined by the above procedure ranged from 1 to 13 cm^2 with an error of about 1%.

Permeation measurement

The permeability was studied by single-gas permeation using a constant-volume/variable-pressure apparatus. The permeation cell was maintained at $35^oC \pm 0.1^oC$. The feed pressure was 10 ± 0.05 atm; on the permeate side of the film, the gas pressure was less than 10 Torr and considered negligible. The leak rate into the vacuum system introduced an error for the permeability measurement of less than 0.01% for the slowest gas. These techniques have been described in greater detail, for example, by Koros.[14]

Density measurement

The density measurements were performed at 23 ± 0.1^oC with a density gradient column, using *iso*-propanol/water-calcium nitrate solutions. Samples were cut from the same samples used in the permeability measurement. Solvent uptake during the density measurement was less than 0.2 wt%.

RESULTS AND DISCUSSION

Physical properties

A polymer's glass transition temperature, T_g, is related, among other parameters, to the rigidity of the macromolecule. The thermal properties of these polynorbornenes were measured using dynamic mechanical thermal analysis at the BFGoodrich Corporation.[15] The results are summarized in the second column of Table 1. The increasing length of the flexible pendant group results in a decrease in the glass transition temperature and modulus of these polymers. The polynorbornene with the methyl side group has the highest glass transition temperature of this group (above 380^{o}C). The polynorbornene with the decyl side group has the lowest glass transition temperature (about 150^{o}C). For comparison, the glass transition temperatures of the ROMP polynorbornenes are presented in Table 2. The ROMP polymers have consistently lower T_g's. Thus, we can conclude that the APNB polynorbornene backbone is less flexible than the ROMP polymers.

Fractional free volume determination

The relation between the free volume and the coefficient of viscosity, η, was introduced by Doolittle in 1951[16] as:

$$\eta = A\exp[B/(v_o/v_f)] \qquad (1)$$

where A and B are constants. The fractional free volume (FFV) is defined as v_f/v_o:

$$FFV=(v-v_o)/v_o = v_f/v_o \qquad (2)$$

where v is the total specific volume of the polymer; v_o is the so-called "occupied volume," which cannot assist in penetrant transport; and v_f is the specific free volume of

the polymer. Using the Stokes-Einstein relation with a_o as the diameter of a sphere having the volume of the molecule, the diffusion coefficient, D, can be written as:

$$D = (kT / \pi a_o)/\eta \qquad (3)$$

where T is the temperature, and k is Boltzmann's constant.

Cohen and Turnbull[17] derived the relation between the diffusion coefficient and the fractional free volume as:

$$D=D_o\exp[-\gamma v^*/v_f] \qquad (4)$$

where v* is the critical volume just large enough to permit displacement of molecules. The permeability coefficient can be written as the product of the diffusion coefficient and the sorption coefficient, in the absence of significant swelling:

$$P = D\,S \qquad (5)$$

The pendant groups of our polynorbornenes can be written as $CH_3\ (CH_2)_x$-. As one evaluates the polymer series reported here, only the length of the aliphatic side chain changes (represented by x). If it is assumed that the solubility coefficient does not change significantly, the permeation coefficient, P, and the ideal selectivity, $\alpha_{A/B}$, can be described as follows:

$$P=P_o\exp[-\gamma v^*/v_f] \qquad (6)$$

$$\alpha_{A/B} = P_A/P_B \qquad (7)$$

where P_A and P_B are the permeation coefficients for two different gases A and B. P_o and γ are constants.

Table 1 presents the volumetric data of polynorbornenes. The free volume was calculated using the Bondi[18] method. The specific volume, v_{sp}, is defined as $1/\rho$, where

ρ, the density, was experimentally measured. The van der Waal's volume, v_w, was estimated by using van Krevelen's[19] data. Thus, the free volume is given by

$$v_f = v_{sp} - 1.3v_w \quad (8)$$

and the fractional free volume can be calculated as

$$FFV = v_f/v_{sp} \quad (9)$$

The greatest challenge for this calculation is the van der Waal's volume of the norbornene ring structure. We approximated this volume by building up the ring in a step-wise fashion from known components. While this may introduce error in the exact fractional free volume values calculated, errors in this calculation should not seriously influence the comparison between the different pendant groups, because the same ring is present in all polymers investigated here. The calculated fractional free volumes are presented in Table 1.

Permeation

Table 2 presents the permeability coefficients for different gases at 35^{o}C and 10 atm. The permeability coefficient decreased with increasing size of the pendant group except for the last value, which showed an increase in the permeability coefficient. Figure 3 presents the H_2 permeability coefficient versus the inverse fractional free volume for these polymers (numbered 1-4 in the figure) and selected data from the literature. The polynorbornenes evaluated here exhibit good correlation between the experimental permeabilities and the inverse of fractional free volume. Similar relationships also existed for the other gases examined. The good correlation observed for these polymers could be explained by the fact that our pendant groups present the

same structure, and therefore, the solubility of gases in these materials is approximately constant across the entire family.

The overall correlation between hydrogen permeability and the inverse of fractional free volume for our APNBs evaluated and the ROMP polymers from the literature shows some scatter. The inability of this correlation to account for differences in the polymer backbone has been previously observed.[20,21] Indeed, this behavior provides further evidence that differences in polymerization routes, which result in dissimilar polymer backbones, are important in determining the properties of the polymers.

Selectivity

Table 3 presents the ideal selectivity for different gases over nitrogen and methane. The selectivity decreased with increasing pendant group length for all gases. The percentage change was the largest for the non condensable gases such as He, H_2, and less pronounced for more condensable gases such as CO_2 and O_2. The CH_4/N_2 selectivity was the only gas pair that showed an increase in selectivity with increasing side group length.

Comparison to other polynorbornenes

Table 4 presents permeability coefficient data measured by other researchers. The first three lines of the table give Yampol'skii's[9] data for fluorinated polynorbornenes. Both the permeability of our polynorbornene with the CH_3 pendant group and its T_g are higher than for the polymers present in this table. For the rest of our polymers, some permeability coefficients are lower, but the high T_g is maintained. The second part of this

table presents Bondar's data.[8] Although glass transition temperatures of polynorbornenes with organosilicon substituents are consistently lower than those for our APNB's in Table 2, no clear trend in the permeability coefficients is apparent.

Direct comparison of ROMP and APNB polynorbornenes is complicated by the slight variations in the side groups of the materials studied. For the APNB series evaluated, both permeability and selectivity decrease as the length of the aliphatic side group is increased. Although extrapolation of this trend to predict the performance of other materials is should be viewed with caution, we hypothesize that the properties of the unsubstituted APNB would be similar to those of the APNB with the methyl side group. Indeed, the glass transition temperature of the unsubstituted material is above 400°C, as would be expected from extrapolation of data for the substituted materials.

Comparing the properties of the unsubstituted ROMP polynorbornene (polymer 5 in Table 4) with the methyl-substituted APNB (polymer 1 in Tables 1-3), one can gain insight into the importance of the rigidity of the polymer backbone in these polymers. The permeability of H_2 through these polymers is 500 Barrer for the APNB materials, but only 21 Barrer for the ROMP polymer. Hydrogen/nitrogen selectivities are 20.8 and 14, and the T_g's are 380°C and 31°C, respectively. Thus, the APNB has higher permeabilities, higher selectivities, and a higher glass transition temperature than the corresponding ROMP material. One might expect, therefore, that an APNB material with a fluorinated side group (such as the ROMP polymer 6) might have even more attractive properties.

Comparison to gas transport in other polymers

The polymers studied here show increasing permeabilities with increasing selectivities as can be seen in the H_2/N_2 trade-off curve in Figure 4. Robeson's upper bound[22] is also shown for reference. The behavior of this polymer family is somewhat unusual because for many polymers, permeability decreases with increasing selectivity. According to previous work by Hoehn[23] the behavior of our polymers can be rationalized by considering qualitatively the properties of the polymer chains and the free volume in the polymer. In the absence of significant sorption effects, the simultaneous selectivity increase with increased permeability can be explained as follows:

> The increasing selectivity with decreasing length of the flexible side chain is due to increasing influence of the rigidity of the polymer backbone. Rotational mobility decreases with increasing influence of the stiff backbone on the polymer properties. This, according to the ideas presented by Hoehn[17] and Koros,[24] will increase selectivity.
>
> The flexibility of our polymer molecules increases with the side chain length ($CH_3(CH_2)_x$-). This is evident from the decrease of T_g with increasing side chain length. At the same time, the side group is linear and packs well. Improved packing of the polymer chains is apparent from the decrease of fractional free volume with increasing side chain length. This is strongly related to a permeability loss.

The transport data for this family of polymers with a rather stiff backbone and a flexible side chain show how the properties of polymers can be tailored by molecular-level changes. It is even possible to reverse the trade-off between selectivity and permeability that is often found.

CONCLUSIONS

Maintaining the norbornene ring structure in the polymer backbone is important to obtain high glass transition temperatures and gas permeabilities. This study of the

transport properties of polynorbornenes with aliphatic pendant groups further shows that an increase in pendant group chain length is responsible for the simultaneous decrease in fractional free volume, glass transition temperature, permeation coefficients, and permselectivity. Interestingly, the APNB polymer family investigated shows simultaneous increases in selectivity and permeability as the pendant chain length is decreased. This behavior may prove important for future attempts to move beyond the performance of current polymers.

ACKNOWLEDGMENTS

This research was carried out with support of the State of Georgia, through its Technical Competitiveness in the Pulp and Paper Industry Initiative. The authors wish to thank Dr. Robert Schick of BFGoodrich for providing the various polymer samples and dynamic mechanical thermal analysis of these polymers.

REFERENCES

1. N. R. Grove, P. A. Kohl, S. A. Bidstrup-Allen, R. A. Shick, B. L. Goodall, and S. Jayaraman, Properties and Processing of AVATREL™ as a High Performance Dielectric, Proceedings of the International Conference on Multichip Modules, IMAPS and IEEE, 224-227 (April 7, 1997).

2. M. Salame, Use of Barrier Polymers in Food and Beverage Packaging, TAPPI Proceedings - Polymers, Laminations and Coatings Conference, TAPPI Press, 363 (1986).

3. V. T. Stannett, W. J. Koros, D. R. Paul, H. K. Lonsdale, and R. W. Baker, *Adv. in Polym. Sci*., **32**, 69 (1979).

4. D. R. Paul and Y. P. Yampol'Skii, *Polymeric Gas Separation Membranes*, CRC Press, Boca Raton (1994).

5. Y. Kawakami, H. Toda, M. Higashino, and Y. Yamashita, *Polym. J*., **4**, 285 (1988).

6. Y. P. Yampol'skii, E. S. Finkel'shtein, K. L. Makovetskii, I. Y. Ostrovskaya, E. B. Portnykh, M.L. Gringol'ts, Y. G. Ishunima, I. B. Kevdina, and V. P. Shantarovich, *Polym. Sci.*, **38**, 1480 (1996).

7. T. Steinhäusler, and W. J. Koros, *J. Polym. Sci, Poly. Phys.*, **35**, 91 (1997).

8. V. I. Bondar, Y. M. Kukharskii, Y. P. Yampol'skii, E. S. Finkel'shtein, and K. L. Makovetskii, *J. Polym. Sci, Poly. Phys.*, **31**, 1273 (1993).

9. Y. P. Yampol'skii, N. B. Bespalova, and E. S. Finkel'shtein, V. I. Bondar, and A. V. Popov, *Macromolecules*, **27**, 2872 (1994).

10. B. L. Goodall, G. M. Benedikt, L. H. McIntosh, III, D. A. Barnes, and D. A. Medina *U.S. Patent 5,468,819* (1995).

11. B. L. Goodall, G. M. Benedikt, L. H. McIntosh, III, D. A. Barnes, and L. F. Rhodes, *U.S. Patent* 5,569,730 (1996).

12. B. L. Goodall, G. M. Benedikt, L. H. McIntosh, III, D. A. Barnes, and L. F. Rhodes, *U.S. Patent 5,571,881* (1996).

13. P. H. Pfromm and W. J. Koros, *Polym.*, **36**, 2379 (1995).

14. W. J. Koros, Ph.D. Dissertation, University of Texas at Austin (1977).

15. R. A. Shick, Personal Communication, BFGoodrich Corporation (1997).

16. A. K. Doolittle, *J. Appl. Phys.*, **22**, 1031 (1951).

17. M. H. Cohen and D. J. Turnbull, *J. Chem. Phys*., **31**, 1164 (1959).

18. A. Bondi, *Physical Properties of Molecular Crystals, Liquids, and Glasses*, Wiley, New York (1968).

19. D. W. van Krevelen, *Properties of Polymers*, Elsevier, New York (1990).

20. Y. Maeda and D. R. Paul, *J. Polym. Sci., Polym. Phys*., **25**, 1005 (1987).

21. D. H. Weinkauf and D. R. Paul, *J. Polym. Sci., Polym. Phys*., **30**, 837 (1992).

22. L. M. Robeson, *J. Memb. Sci*., **62**, 165 (1991).

23. H. H. Hoehn, *U.S. Patent 3,822,202* (1974).

24. W. J. Koros, M. R. Coleman, and D. R. B. Walker, *Annu. Rev. Mater. Sci*., **22**, 47 (1992).

Table 1. Physical properties of APNB polynorbornenes.

Polynorbornene Pendant group (R)	**T_g**[15] **(^oC)**	**Young's modulus**[15] **(GPa)**	**r* (g/cm^3)**	**v_w (cm^3/g)**	**v_f (cm^3/g)**	**FFV**
1. CH_3 -	380>>	1.4	0.986	0.6302	0.1949	0.1922
2. $CH_3(CH_2)_3$ -	350>	0.9	0.970	0.6579	0.1756	0.1704
3. $CH_3(CH_2)_5$ -	280	0.6	0.965	0.6691	0.1664	0.1606
4. $CH_3(CH_2)_9$ -	150	0.2	0.946	0.6835	0.1685	0.1594

*at 23^oC

Table 2. Permeability coefficients at 35°C and 10 atm for APNB polynorbornenes.

Polynorbornene	**N_2**	**H_2**	**O_2**	**CO_2**	**CH_4**	**He**
Pendant group (R)			**Barrer***			
1. CH_3 -	24.1	502.1	89.2	396.3	30.3	309.4
2. $CH_3(CH_2)_3$ -	11.2	110.7	33.3	141.9	28.4	66.7
3. $CH_3(CH_2)_5$ -	6.9	57.2	19.8	83.8	18.7	36.8
4. $CH_3(CH_2)_9$ -	8.7	62.4	25.3	111.1	28.1	38.9

*1 Barrer = 10^{-10} cm^3 (STP) cm/cm^2 s cm Hg

Table 3. Ideal selectivity coefficients for APNB polynornornenes.

Polynorbornene **Pendant group (R)**	**H_2/N_2**	**O_2/N_2**	**He/N_2**	**CO_2/N_2**	**CH_4/N_2**	**CO_2/CH_4**	**H_2/CH_4**
1. CH_3 -	20.8	3.7	12.8	16.4	1.2	13.0	16.5
2. $CH_3(CH_2)_3$ -	9.9	3.0	5.9	12.6	2.5	4.9	3.9
3. $CH_3(CH_2)_5$ -	8.3	2.9	5.3	12.2	2.7	4.4	3.0
4. $CH_3(CH_2)_9$ -	7.2	2.9	4.5	12.8	3.2	3.9	2.2

Table 4. Properties of ROMP polynorbornenes.

Polynorbornene	r (g/cm^3)	FFV	T_g (^oC)	N_2	H_2	O_2	CO_2	CH_4	C_2H_6
						Barrer*			
No Side Chain									
5. PNB[a]	0.98	0.156	31	1.5	21	2.8	15.4	2.5	1.4
Fluorine-Containing Side Chains									
6. PFMNB[a]	1.586	0.165	169	17	166	50	200	13	6.6
7. POFPNB[a]	1.626	0.187	77	17	130	55	200	18	14
Silicone-Containing Side Chains									
8. PTMSNB[b]	0.92	0.200	113	7.2	140	30	89	17	7
9. PDSNB[b]	0.93	0.142[c]	24	3.7	73	16	67	8.5	10

[a] Measurements performed at 22±3°C and 50-500 Torr (ref 9.).
[b] Measurement performed at 22±1°C, 10-200 mm Hg, and the low-pressure side was about 10^{-3} mm Hg (ref 8.).
[c] Calculated by authors using Bondi method.
*1 Barrer = 10^{-10} cm^3 (STP) cm/cm^2 s cm Hg

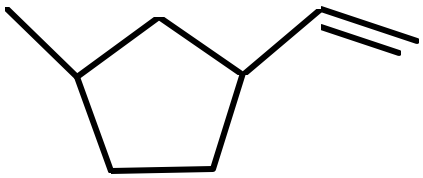

Figure 1. Repeat unit of ROMP polynorbornene polymerized by ring-opening metathesis.

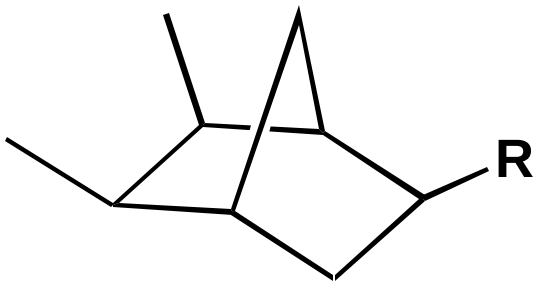

Figure 2. Repeat unit of addition polynorbornene (APNB) polymerized by using an organometallic complex as catalyst (prepared by BFGoodrich, R see Table 1).

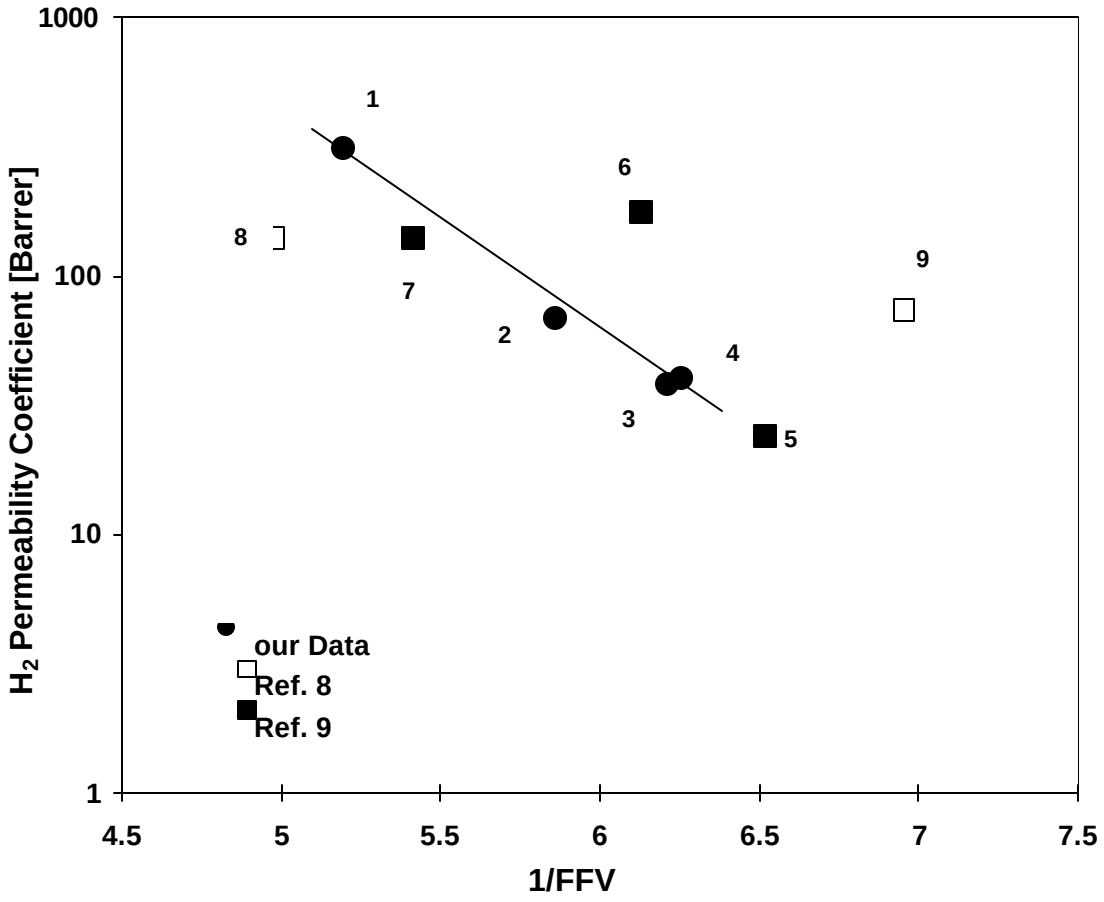

Figure 3. Correlation between inverse fractional free volume of APNB polynorbornenes and the permeability coefficient for H_2. Comparison with literature data (Table 1 and Table 4). (1 Barrer = 10^{-10} cm^3 (STP) cm/cm^2 s cm Hg).

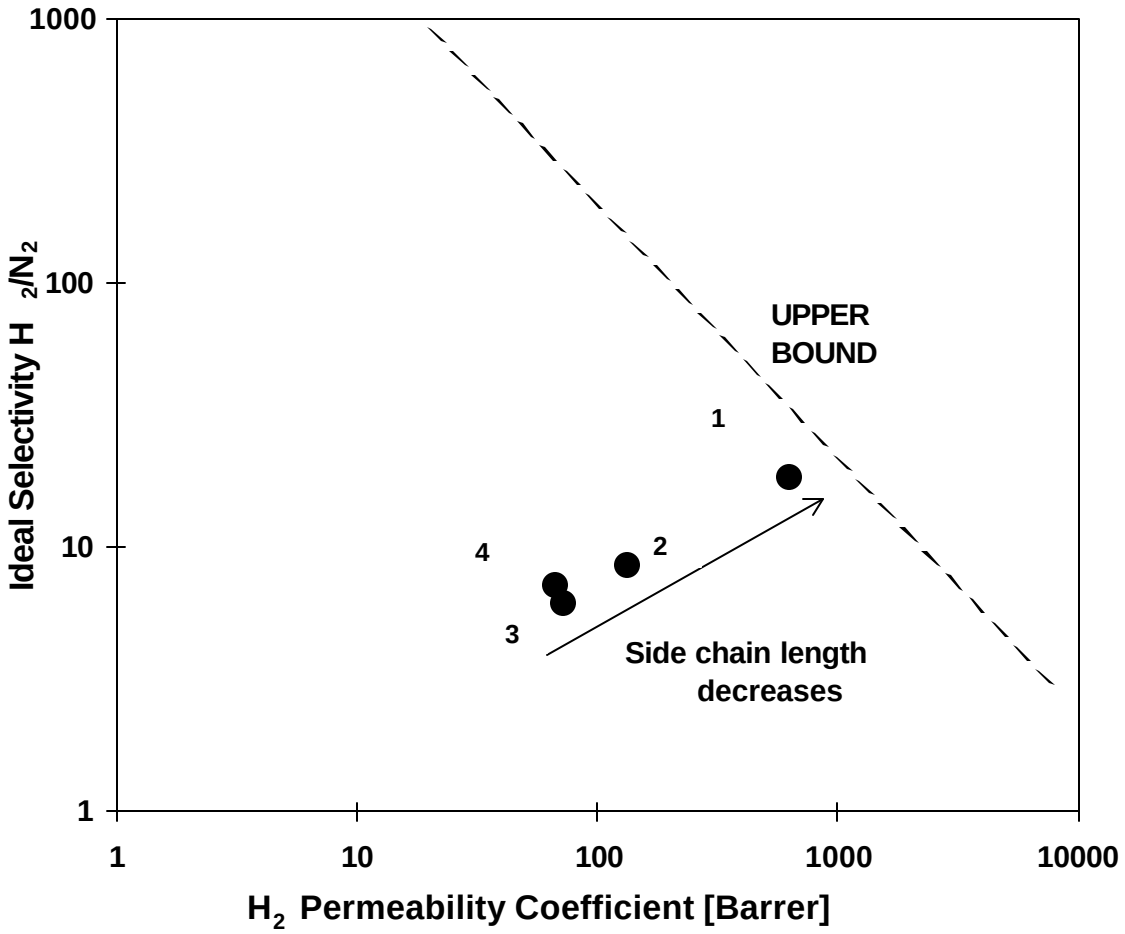

Figure 4. Relative position of our polynorbornenes in comparison with Robeson's upper bound.[22] Permeability and selectivity increase simultaneously with decreasing side group length. (1 Barrer = 10^{-10} cm^3 (STP) cm/cm^2 s cm Hg).

Figure 1. Repeat unit of ROMP polynorbornene polymerized by ring-opening metathesis.

Figure 2. Repeat unit of addition polynorbornene (APNB) polymerized by using an organometallic complex as catalyst (prepared by BFGoodrich, R see Table 1).

Figure 3. Correlation between inverse fractional free volume of APNB polynorbornenes and the permeability coefficient for H_2. Comparison with literature data (Table 1 and Table 4). (1 Barrer = 10^{-10} cm^3 (STP) cm/cm^2 s cm Hg).

Figure 4. Relative position of our polynorbornenes in comparison with Robeson's upper bound.[22] Permeability and selectivity increase simultaneously with decreasing side group length. (1 Barrer = 10^{-10} cm^3 (STP) cm/cm^2 s cm Hg).

Appendix D: Selective Removal of Methanol from Humid Air Streams using a Water Vapor-Purged Membrane Separator

Selective Removal of Methanol from Humid Air Streams using a Water Vapor-Purged Membrane Separator

Arto Klug[a], Peter H. Pfromm[b*], Mary E. Rezac[c], Peter Czermak[a]

[a]Institute of Biochemical Engineering and Membrane Technology, Department of Biotechnology, University of Applied Sciences Giessen, Giessen, Germany

[b]Institute of Paper Science and Technology, 500 10th Street, Atlanta, Georgia, 30318, U.S.A, phone: 404-894-5305, fax: 404-894-5752, e-mail peter.pfromm@ipst.edu

[c]School of Chemical Engineering, Georgia Institute of Technology, 778 Atlantic Drive, Atlanta, Georgia, 30332, U.S.A.

Abstract

Methanol is an unwanted byproduct of kraft pulping in the pulp and paper industry. More than 50 million tons of kraft pulp is produced in the U.S. per year, and methanol releases are on the order of pounds per ton of pulp produced. Methanol is released in low concentrations with humid air streams from many sources in a kraft pulp mill. Membrane vapor separation was tested for selective removal of low concentrations of methanol from a humid air stream. The separation studied here was driven by a water vapor purge stream on the permeate side of a poly(ether amide) block copolymer (PEBAX® 2533) membrane. The separation characteristics of the membrane were essentially unchanged comparing the water vapor purge mode and previous single component measurements. Modeling based on the experiments and for another possible target membrane material is discussed.

---

*To whom correspondence should be addressed

Introduction

Hazardous Air Pollutants (HAP's) such as methanol (the major HAP in kraft pulping) have become a focus for reduction of emissions from pulp and paper mills.[1,2] Methanol and a host of other organics are produced during the kraft pulping process and released downstream of the kraft digester since many downstream operations are open to the atmosphere. Closure of the various process steps to the atmosphere is generally not an acceptable solution, since the emissions would simply be shifted elsewhere and become intractable, for example in the wastewater treatment system or at the papermachine. Conventional HAP control would consist of the costly collection, transport, and centralized treatment of vent streams. As a potential alternative, we are here exploring treatment of vapor-phase HAP point sources in bleached kraft pulp mills (tank vents and washer hoods etc.) with a membrane separation process to selectively remove methanol (a surrogate of the HAP's in these streams). The streams targeted here consist mainly of air near ambient conditions with high relative humidity.

The potential of polymeric membranes to recover organic vapors from gas streams has been recognized.[3,4,5] We have chosen to evaluate the use of a water purge stream to (1) maintain a minimum methanol partial pressure on the permeate side of the membrane and, therefore, provide the maximum possible methanol driving force, and (2) eliminate the driving force for water transport and, thus, minimize water flux. Thus, through appropriate system design, the need to selectively separate methanol from water will be eliminated and the key separation requirement will be the selective removal methanol from air. If this can be successfully achieved, the industrial concern of complying with methanol emission regulations can be achieved.

This system design examined in this paper is the use of water vapor as a purge stream on the permeate side of a membrane separator to drive the methanol removal from the feed. This purge mode has been rarely explored. Nevertheless, it provides a mechanism by which the methanol can be selectively removed from the feed stream with minimal transport of water. Previous experimental evaluation of an air purge to facilitate the removal of carbon dioxide from air indicated that, under certain conditions, the use of a purge stream could greatly reduce the

required membrane area.[6] The use of a portion of the dry retentate stream as a permeate sweep for the dehydration of moist air has also been analyzed.[7] The permeabilities and selectivities in the work by Wang et al. are similar to ours (vapor/air selectivities of several hundred to several thousand, high permeabilities for vapors on the order of thousands of Barrers). In a situation of high permeability and high selectivity for the vapor to be removed, the main resistance to mass transfer may lie in the boundary layers and not in the membrane itself.[7] In reference 7, the purge stream was recognized to partially overcome concentration polarization in the permeate side fluid boundary layers of the membrane. The "internal purge" by a somewhat "leaky" membrane was seen as not as efficient as an external purge since the permeate space at the retentate end of the module (where an external purge would enter) is not well purged. The external purge also allows for greater control.

Our work examines a polymeric membrane for the recovery of dilute methanol from a nitrogen stream at high relative humidity while using a water vapor purge on the permeate side of the membrane. This external permeate purge is explored to address mass transfer issues and minimize the needed membrane area while producing an easily condensible permeate. One objective is to experimentally determine the selectivity and productivity of a thin film composite membrane for this process under realistic process conditions. Another objective is to evaluate the utility of the concept by modeling.

Principle of the process

The partial pressure driving force available for methanol removal in our industrial problem is small. The exact concentration of methanol varies in a kraft mill with values on the order of 1000 ppm (volume) or lower. This would usually favor carbon adsorption over a membrane system,[8] but the high level of water saturation complicates adsorption.

Figure 1 shows the concept. The permeate is condensed and a vacuum pump is used to exhaust a small amount of air permeating the membrane. It could also be considered to send the permeate stream to an existing stripper many of which operate at below atmospheric pressure.[9]

Many candidate membrane materials will likely be able to effectively block the permeation of air. However, the methanol/water selectivity will generally be low.[10] Therefore, if a partial vacuum on the permeate side would be used to drive the mass transfer, the high permeability of water will cause significant water transport along with the methanol removal. The permeate purge with water vapor will have advantages compared to a vacuum driven process at technical vacuum levels: permeate side mass transfer limitations are minimized, permeate condensation can be used to drive the process, and the needed membrane area will be reduced.

The commercial recovery of methanol from a humid air stream would be likely limited by the available pressure ratio (total feed pressure/total permeate pressure). Typical values for the feed gas would have a pressure of on the order of 5.3 psig with a methanol concentration of only 1000 ppm. An industrial vacuum system with a pressure of 0.1 atm might be reasonably assumed for this system (for example a single-stage dry vacuum pump). The pressure ratio of 13 limits the separation achievable. For this system, the maximum methanol concentration in the permeate would then be approximately 1.4 mole%.[8] The balance is a nearly equal ratio of water and air. However, if water vapor is used as a purge on the permeate side, the air content in the resultant permeate stream will be reduced. Further, depending on the purge flowrate, the membrane area required may also be reduced.

Experimental

Test system

The test system is shown in Figure 2. Descriptions of the feed, permeate, and analytical systems are provided. The permeation system was enclosed in a temperature controlled air bath (30°C), except for the liquid nitrogen traps.

Feed system

The feed was made with nitrogen evaporated from a liquid nitrogen dewar. A liquid mixture of methanol and water was injected into the gaseous nitrogen stream using a syringe pump. The liquid was evaporated using heating tapes. Complete evaporation was assured by maintaining the temperature in the liquid feed evaporation zone at twice the boiling point of

water. No liquid was found in the feed system when it was examined after several hours of experimentation. The absolute feed pressure in the feed system was always 5.3 ± 0.2 psig. The temperature at the membrane cell was maintained at 30 °C.

Permeate (purge) system

A permeate water vapor purge stream was set up by evaporating water under partial vacuum from a reservoir while heating the reservoir to counteract evaporative cooling. After passing through the test cell, the water vapor stream which now also contained the permeated components was condensed in liquid nitrogen traps. The condensate was later analyzed by gas chromatography. The pressure difference for water vapor flow was supplied by condensing vapors in the liquid nitrogen traps downstream of the membrane test cell. A rotary vane vacuum pump downstream of the cooling traps evacuated the nitrogen. The nitrogen permeation rate was measured with a soap film flowmeter at the vacuum pump exhaust (corrected for gas leaks in the permeate system). The methanol permeation rate was determined from the mass of methanol collected in the condensate over a given time period.

The system was typically operated at a total permeate pressure of 2.84 cmHg.

The permeate system was equipped with an absolute pressure transducer so that the permeation properties of pure gases could be determined to assure membrane integrity (constant volume/variable pressure method).

Stage Cut

The stage cut of a component i that is transported through the membrane is defined here as

$$SC = (m_{i,2}/m_{i,1})*100 \qquad (1)$$

where $m_{i,1}$ and $m_{i,2}$ represent the masses of component i in the stream from which the component is removed and the stream which receives the component, respectively.

Methanol was transported from the feed to the permeate, while some water was transported from the permeate to the feed. The stage cut, SC, for methanol was always lower

than 1.5%. The stage cut for water (transport from the permeate to the feed) was always less than 2.5%. The feed composition shall therefore be assumed to be constant.

Materials

The polymer was a commercial grade poly(ether amid) block copolymer (PEBAX® 2533, Elf Atochem). PEBAX® 2533 was determined elsewhere[10] to contain, on average, about 2.7 Nylon 12 units and about 27.8 polytetramethylene oxide units per repeat unit. Some properties of PEBAX® 2533 are listed in Table 1.

Commercial Anopore discs (Whatman) with a nominal pore size on the polymer-coated surface of 0.02 micrometer were employed.

Methanol and butanol were ACS grade (Fisher) and were used as received. Deionized water was used. Industrial grade nitrogen obtained from a dewar was used to prepare the feed stream and to perform nitrogen permeation measurements.

Membrane manufacture and characterization

Polymer/ceramic composite membranes were manufactured by one-sided dip coating of the ceramic support membranes in a polymer solution (1 wt% of PEBAX® 2533 in 1-butanol) at room temperature. The coated membranes were air-dried hanging coated face down at room temperature for two days. One membrane was used for all tests reported here. An average polymer layer thickness of 1.33 ± 0.06 micrometer was calculated by mass balance. The effective membrane area employed was 13.8 cm^2.

The perfection of the polymer layer was checked by observing the pressure-normalized nitrogen flux as a function of feed pressure (20 ± 2 °C; 0, 3, 6, and 9 psig; constant volume/variable pressure method). The nitrogen pressure-normalized flux was constant (as expected for solution-diffusion gas transport in absence of defects) within ± 2.1% of the absolute value.

The membrane integrity was periodically checked during the experiments by monitoring the flux of pure nitrogen. No change of properties was observed throughout the course of the experimental program.

Analytical

The methanol content of the condensate was determined by gas chromatography (HP5 capillary column, 35 m length).

Representation of permeation results

It is widely accepted to present gas and vapor membrane permeation results in units of Barrer (1 Barrer = $1*10^{-10}$ $cm^3_{(STP)}$ cm/cm^2 cmHg s). This is essentially a volume flow normalized by the membrane area, membrane thickness, and the driving force for permeation. In our case, "membrane thickness" refers to the thickness of the polymer layer on the ceramic support. Membrane thicknesses may become ambiguous if the polymer swells significantly. The significant sorption of water in PEBAX® 2533 at high water vapor partial pressures is the issue in our case.

No direct measure of polymer swelling was performed. Therefore, the "dry" thickness of the polymer layer, derived from the known density of the polymer and the mass of polymer deposited on the known superficial surface area of the ceramic support, has been used in the calculation of all permeabilities.

Data at every feed methanol concentration was obtained in at least three independent permeation runs. Each symbol in Figures 3 and 4 represents one run. An estimation of the accuracy of the results was obtained using Gauss' method of error propagation (indicated as error bars on the figures).[11]

Results and Discussion

The permeabilities of methanol, nitrogen and water through PEBAX® 2533 into a water vapor purge stream are shown in Figure 3 at three different feed methanol concentrations. The

feed relative humidity was held constant at 73%. The lines in Figure 3 and 4 are linear regressions.

In the range of methanol concentrations evaluated, the methanol permeability does not depend significantly on the feed concentration. A strong dependence of organic vapor permeabilities on the feed concentration is often found and has been observed for PEBAX® 2533 in single-component experiments.[10] This is due to the strong dependence of sorption in the polymer on the feed organic vapor partial pressure. However, due to the presence of significant amounts of a water in the polymer in our case, no significant change in permeability with additional methanol sorption is noted.

Actual selectivities, calculated by dividing the respective permeabilities measured in the mixture experiments, are shown in Figure 4. As expected, the methanol/water selectivity is not significant, while the methanol/nitrogen selectivity is quite high.

Comparing the permeabilities in Figure 3 with the permeabilities obtained by sorption and diffusion measurements[10] from Table 1, the results are reasonably consistent especially considering the uncertainty due to the unknown swollen membrane thickness in our experiments. For methanol and water, the mixture permeabilities are slightly lower than those calculated from sorption experiments. Our permeability values would increase towards the published single component permeation data if the true swollen (increased) membrane thickness would be used.

Modeling and Scaleup Estimate

Background and general assumptions

The modeling of membrane gas separation processes with permeate purging has been treated for example by Pan and Habgood,[12] Li and coworkers,[6] and recently by Coker and coworkers.[13] Typically, the purge stream was a small fraction (1-10%) of the residue stream. The permeate stream was discarded and the residue stream was the stream of value. Such analyses provide a good starting point for modeling our process. However, in our application, the permeate stream will require further processing and careful consideration must be placed on the composition.

In our study, simultaneous transport of highly permeable methanol present at low concentration in the feed, and of a low permeability, but high concentration air fraction is considered. The feed stream also has a significant water concentration (highly permeable). Our process reduces this three-component problem essentially to a two component problem (methanol and air) by purging the permeate side of the membrane with water vapor at a partial pressure equivalent to that in the feed. This avoids water vapor removal from the feed while making the best possible use of the small available methanol partial pressure driving force. The methanol is to be recovered in the permeate as a methanol/water vapor mixture with a minimum of non-condensable gas. The use of a water-vapor purge should also decrease permeate side gas phase mass-transfer resistences.[7]

The feed pressure is assumed somewhat above atmospheric pressure (5.3 psig) to allow for the pressure drop due to flow of the feed (Figure 5). We define as the goal of the process to remove 99% of the methanol from a feed stream of 1000 standard cubic feet per minute (28.3 $m^3_{(STP)}$/min, 30°C) containing 0.1034 cmHg methanol partial pressure (1000ppm (vol.)), a water partial pressure of 2.25 cmHg (~70% relative humidity, atmospheric conditions), and the balance nitrogen (surrogate for air). We assume constant values for the methanol and nitrogen permeabilities at 30°C (1780 Barrer and 4.2 Barrer, respectively) as determined in our experiments for PEBAX® 2533. The permeate purge outlet partial pressure of water is set at 2.25 cmHg. The permeate inlet pressure is adjusted to achieve the necessary outlet conditions. Under certain circumstances, some permeation of water from the purge to the feed stream may occur.

A single pass through a membrane module (effective membrane thickness 0.5 micrometers, PEBAX® 2533) with no recycle of any permeate to the feed is assumed. No mass transfer limitations on the feed or permeate side are considered.

Modeling

We use an ideal gas transport model where pressure drop is neglected in the feed and permeate. A schematic of the system and nomenclature is presented in Figure 5.

The water partial pressure is initially assumed to be constant and equal on both sides of the membrane. Under this assumption, there is no driving force for water transport. If the total pressure in the feed and retentate are equal, the material balances follow as

Air: $$y_{Air,F}\ F = y_{Air,R}\ R + y_{Air,C}\ C \qquad [2]$$

Methanol: $$y_{M,F}\ F = y_{M,R}\ R + y_{M,C}\ C \qquad [3]$$

where the $y_{i,j}$ represents the mole fraction of component i in stream j, and F,R, and C are the molar flows of the Feed, Retentate and Permeate streams, respectively. In our system, $y_{Air,F}$, $y_{M,F}$, F, and $(y_{M,R}\ R)$ are known. This allows determination of the amount of methanol transported from the feed side of the membrane to the permeate, Q_M:

$$Q_M = y_{M,F}F - y_{M,R}R \qquad [4]$$

The rate at which this transport occurs can be related to the available membrane area, A, and thickness, ℓ, the methanol driving force, Δp_M, and the permeability of the membrane material, $\overline{P}_M$:

$$Q_M = K\frac{A\,\overline{P}_M\,\Delta p_M}{\ell} \qquad [5]$$

Equation (5) can be rearranged to determine the membrane area required to treat the feed specified in Figure 5. The rate of transport of air from the feed to the permeate side of the membrane can be described via an equation analogous to equation (5).

In the analysis of equation (5), all values are known and assumed to be constant with the exception of the various partial pressure driving forces. Precise determination of these values can be obtained by numerical integration of the pressure and composition profiles along the length of the membrane.[13] To achieve our goals of understanding the influence of membrane permeabilities on the system performance and the relationship between the purge rate, membrane area required, and the composition of the permeate, we will use an approximate driving force (log-mean) for the calculations. This driving force is approximate and neglects the momentum balance. While pressure drop on the permeate side is certainly an important issue,

the proper design of membrane modules will only be considered for attractive membrane materials (see below).

The procedure used for solving these simultaneous equations is as follows:

1. Specify the water purge rate, U.
2. Make an initial guess for the air transported, Q_{Air} .
3. Calculate the mole fractions of the components in the permeate outlet, C, the partial pressures of the components in this stream and the average driving forces.
4. Calculate the area required for 99% methanol recovery based on equation (5).
5. For this membrane area, calculate the rate of nitrogen permeating the membrane and the resultant nitrogen mole fraction in the permeate outlet.
6. Compare the nitrogen mole fractions in steps 3 and 5. If the two are not equal, return to step 3 and continue to iterate until the change in the mole fraction divided by the actual mole fraction is $< 10^{-6}$.

For each purge rate, the minimum membrane area that is required to achieve the specified separation is calculated. The composition of the permeate that results from this combination of membrane area and purge flow rate is then determined.

Modeling for PEBAX® 2533

Plots of the predicted performance of a PEBAX® 2533 membrane to treat the gas stream specified in Figure 5 are presented in Figures 6 and 7. Figure 6 presents the relationship between the purge rate of water employed and the membrane area required to achieve the specified separation. At high purge rates, the permeating methanol is highly diluted creating the highest available driving force. This results in a minimum membrane area. As the purge rate is decreased, the driving force decreases (and required membrane area increases) until the methanol partial pressures in the feed and permeate are equal. At this point, no further increase in membrane area will cause additional transport. For the present system, at 99% methanol recovery, purge rates of less than about 27 mole/min will be insufficient to achieve the desired separation. Examination of Figure 6 also indicates that for a fixed membrane area, as the purge rate is increased, the methanol recovery is increased.

Each combination of membrane area and purge rate shown in Figure 6 will result in a membrane system capable of achieving the specified methanol recovery. However, because of the great variation in purge rate, the permeate composition for each system will be different. Figure 7(a) shows the mole fractions of water, air, and methanol in the permeate as a function of the water vapor purge rate for the PEBAX® 2533 membrane. The figure indicates that as the purge rate is increased, the methanol concentration in the permeate outlet first increases, reaches a maximum (at about 1.7 mol%) and then decreases until it approaches zero in the limit of high purge rates. Figure 7(b) examines the composition of the permeate streams as a function of the membrane area employed. Similar behavior is observed.

One may like to have the possibility of condensing the permeate stream (Figure 1). Another option is to condense partially or not at all and use the permeate stream in an existing steam stripper.[9] Any of these options will be greatly hindered by the presence of air in the permeate. Unfortunately, for all membrane area/purge rate conditions examined, the air mole fraction in the permeate is high.

Modeling for an optimized polymer membrane

To reduce air permeation, a high methanol/nitrogen selectivity is most important. Since our experiments showed that single component permeation tests predict the mixture permeation properties with water vapor purge quite well, we model the performance of another membrane material. The low reported nitrogen permeability (0.42 Barrer, we will use 0.5 Barrer to allow for presence of oxygen in air) and high vapor permeabilities (methanol 24,600 Barrer, water 1,750 Barrer) of butadiene-acrylonitrile rubber (poly(butadiene-acrylonitrile), 35%, BAR) would likely eliminate the problem of inert gas intrusion to the permeate almost completely.[14]

The simulation results for treating the gas stream as outlined in Figure 5 with a BAR membrane are presented in Figures 8 and 9. Because of the significantly higher methanol permeability of this material as compared to PEBAX® 2533, the membrane area required is reduced by nearly an order of magnitude. Air intrusion into the permeate is strongly reduced. As the membrane area is increased, the methanol concentration in the permeate is increased and reaches a maximum, steady value of approximately 4.0 mole%. Further increases in membrane

area result in a reduction in the water mole fraction of the permeate with a corresponding increase in the air mole fraction.

If the permeate stream is to be condensed, then a trade-off between increasing methanol content and increasing air content exists. Operation with a BAR membrane area of approximately 80 m^2 and a purge flow of 47 mole/min would result in a permeate with 2.5 mole percent methanol and less than 0.5 mole percent air. Ninety-nine percent recovery of the methanol occurs. This condition may be near the optimum. However, the precise optimum could only be predicted with the aid of cost functions. Assumptions would then also have to be made if the permeate would be condensed or sent to another treatment option such as the condensate stripper in the evaporator systems of pulp mills.[15]

We have neglected the transport of water from the permeate to the feed and have assumed that the water vapor flow rate at the permeate outlet is approximately equivalent to that at the purge inlet. For calculations based on BAR, these assumptions seem justified. In the case of the minimum purge rate at 99% methanol recovery, the total pressure at the permeate outlet is less than 15% higher than that of water. As the purge rate is increased to 1.5 times the minimum, this difference in pressure is rapidly reduced to less than 4%. Neglecting water transport in the case of the PEBAX® 2533 membranes is more problematic. In the limit of minimum purge rate and 99% methanol removal, the total pressure at the outlet is nearly 21 cmHg (over eight times that of the water). Clearly, this would require a significant increase in the water purge rate and pressure, resulting in a measurable transport of water from purge to feed. This rate could be calculated, but we have not done this because of the inferior performance of the PEBAX® 2533 membrane as compared to the predicted performance of BAR.

Comparison to a total pressure driven process (no purge)

If a BAR membrane were employed with a technical vacuum on the permeate side (2.25 cmHg), the total membrane area for 99% methanol recovery would be slightly more than 200 m^2. This calculation is a best case for the pressure driven process since it assumes that there are negligible mass transfer resistances in the gas phases on the feed and permeate sides. The

methanol and air mole fractions in this case would be approximately 0.036 and 0.017, respectively. Nearly identical compositions would result from operation of a purged membrane with 200 m^2 area and 30 mol/min purge. If the purge rate were increased, the membrane area and the composition of air in the permeate could be reduced, albeit at the expense of a reduction in the methanol mole fraction (see Figures 8 & 9). The purge could be used to overcome gas phase resistances and to reduce the membrane area for a given methanol recovery without significantly diluting the permeate.

Module engineering considerations

The main pressure difference for the permeate flow (the vapor pressure of water) is not high and care must be taken to minimize pressure drop. This could be envisioned by using a hollow fiber membrane module (feed on the bore side), or a specially designed spiral wound module (thick and/or asymmetric permeate spacers).

Conclusions

Methanol removal from humid air streams by membrane vapor permeation was investigated. The permeation process was driven by a water vapor purge on the permeate side of the membrane.

Permeation experiments were performed with a water vapor purge on the permeate side of the membrane to supply the driving force for methanol permeation. Under these conditions, the single component methanol, water, and air transport properties from diffusion and sorption measurements predicted the mixture transport properties well for the PEBAX® 2533 polymer. Further, for a nitrogen stream with 73 relative humidity and methanol concentrations ranging from 0.1 to 0.8 volume percent, the permeation properties were not a function of the methanol concentration. When pure methanol was evaluated, increases in partial pressure resulted in a marked increase in permeability. The relatively constant methanol permeability occurs in the current situation because the polymer is uniformly swollen with high levels of water and the additional sorption of methanol (over the range evaluated) does not significantly alter the polymer mobility.

In the design of a membrane system to recover methanol from humid air streams, nitrogen permeation is a serious issue for process scaleup since this is detrimental to condensing or other processing of the permeate. Our modeling shows that membranes with high methanol/air selectivity and high methanol permeability appear most advantageous for the process. When a water vapor purge is employed, the methanol/water selectivity is much less important. Finally, the use of a water vapor purge has been shown to reduce the air mole fraction in the permeate relative to the non-purged case.

Acknowledgements

This paper was prepared with the support of the U.S. Department of Energy (DOE) Cooperative Agreement No. DE-FC07-96ID13438. However, any opinions, findings, conclusions, or recommendations expressed herein are those of the author and do not necessarily reflect the views of DOE.

Symbols

A	membrane area, m^2
F, R, C, U	molar flow, mole/min, in feed, retentate, permeate side exit (water vapor plus permeated gases and vapors), and permeate side inlet (water vapor)
K	conversion factor, 0.268(s mol cm)/(min $cm^3_{(STP)}$ m)
P	total pressure, cmHg
$\overline{P}$	permeability, Barrer, 1 Barrer = $1*10^{-10}$ $cm^3_{(STP)}$ cm/cm^2 cmHg s
Q	trans-membrane molar flow rate, mol/min
SC	stage cut of a component that is transported through a membrane, %
ℓ	membrane thickness, m
m	mass flow, kg/s
p	partial pressure, cmHg
Δp	partial pressure difference, cmHg
y	mole fraction

Subscripts

F, R, C, U	feed, retentate, permeate side exit, and permeate side inlet (water vapor), respectively
M	methanol
W	water
i	component i
1	stream from which a component is removed
2	stream that receives a component

List of Figures

graph (a) and based on the membrane area and the corresponding minimum purge rate for graph (b). X indicates the limit of minimum purge flow which can still achieve 99% methanol recovery.

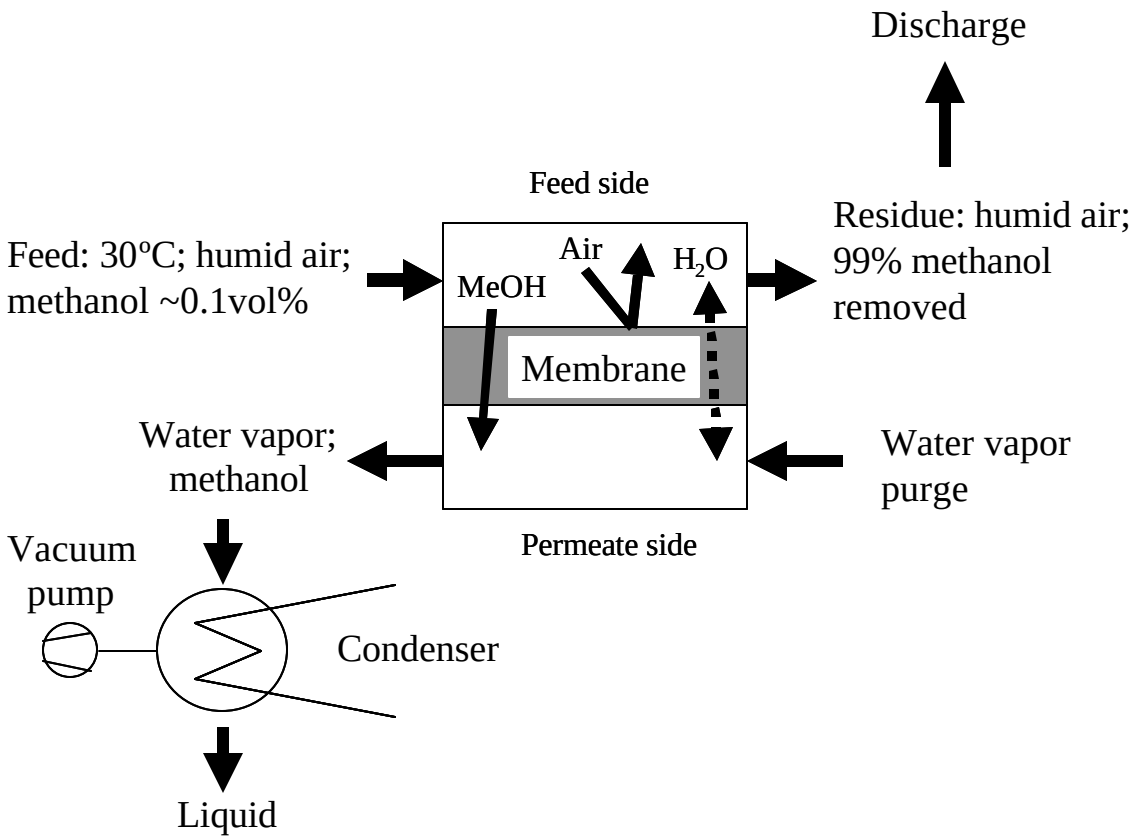

Figure 1: Concept of removal of methanol from a humid air stream with a water vapor purge on the permeate side of the membrane.

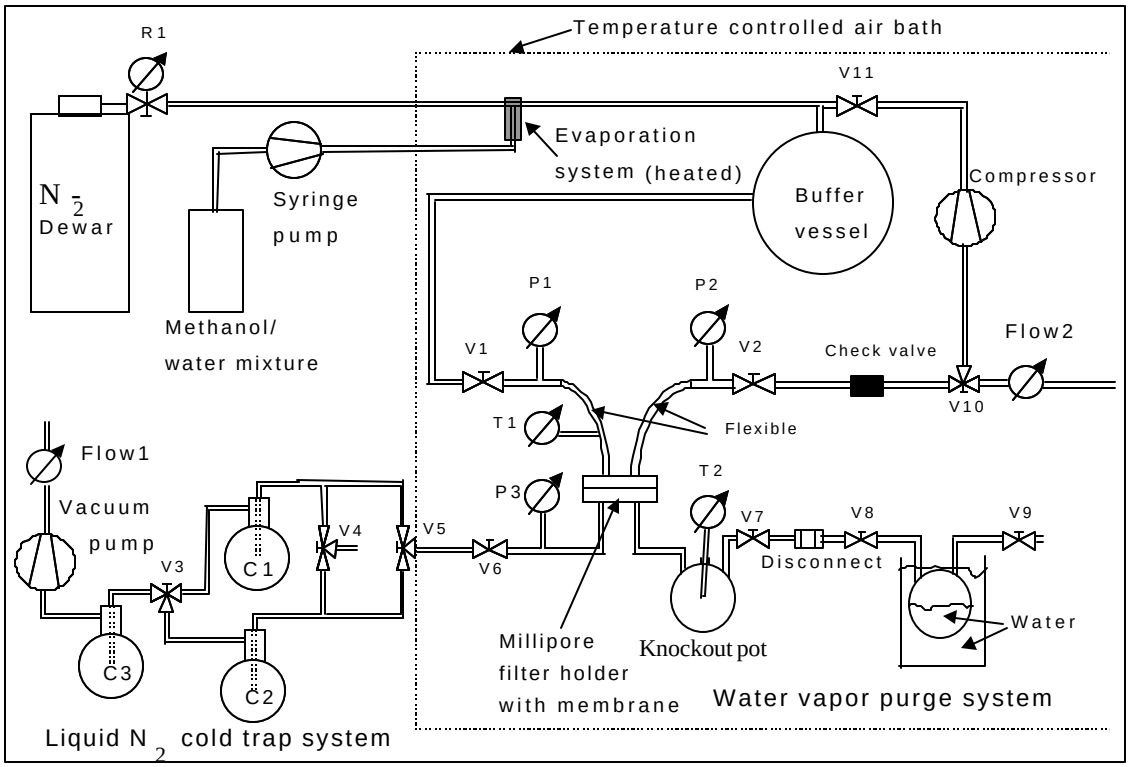

Figure 2: Laboratory system for removal of methanol from humid air streams using a water vapor purge (V: valve, P: pressure gauge, T: temperature gauge, R: regulator; C: cold trap, Flow 1: soap film flowmeter). The recirculation compressor was not used (V11 closed).

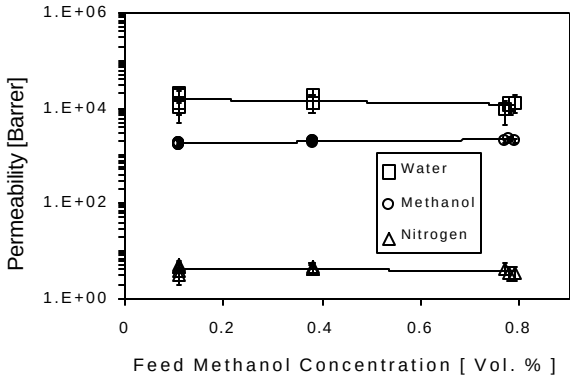

Figure 3: Permeabilities of PEBAX® 2533 at 30°C and at three different methanol concentrations. A water vapor purge was used on the permeate side of the membrane. Feed conditions: 2.18 ± 0.1 vol% H_2O (~73% relative humidity), methanol as indicated, balance nitrogen, 5.3 ± 0.2 psig, stage cut < 3% for each component.

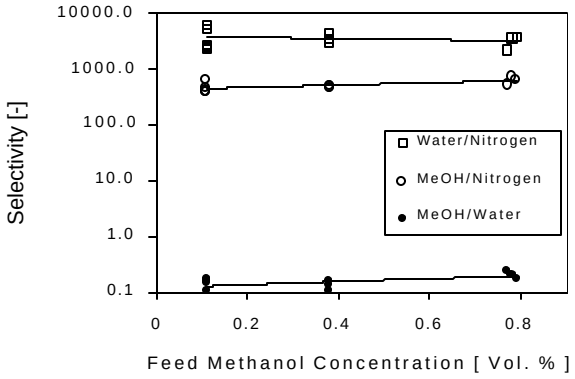

Figure 4: Mixture selectivities of PEBAX® 2533 at 30°C and at three different methanol concentrations. A water vapor purge was used on the permeate side of the membrane. Feed conditions: 2.18 ± 0.1 vol% H_2O (~73% relative humidity), methanol as indicated, balance nitrogen, 5.3 ± 0.2 psig, stage cut < 3% for each component.

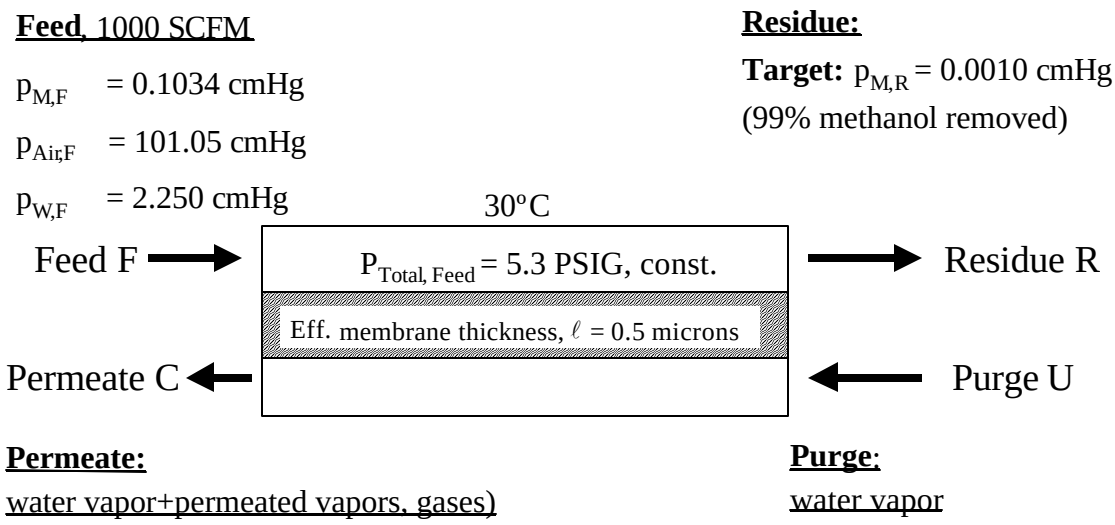

Figure 5: Process conditions and assumptions used for modeling.

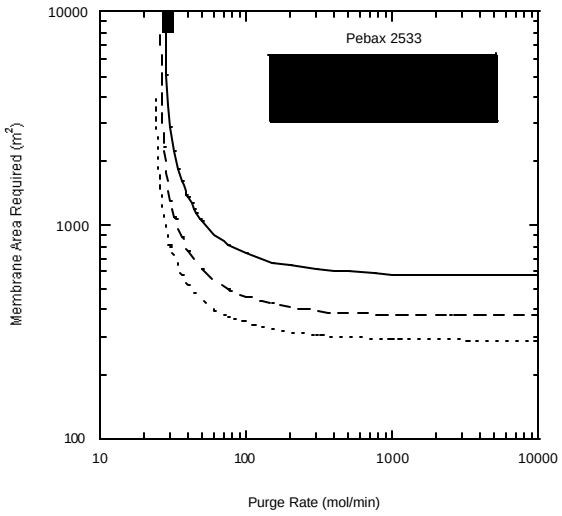

Figure 6: Relationship between the membrane area, A, required to achieve 99% methanol removal from the feed (Figure 5), and the permeate purge rate, U, of water (PEBAX® 2533 membrane, 0.5 microns thickness). X indicates the limit of minimum purge flow which can still achieve 99% methanol recovery.

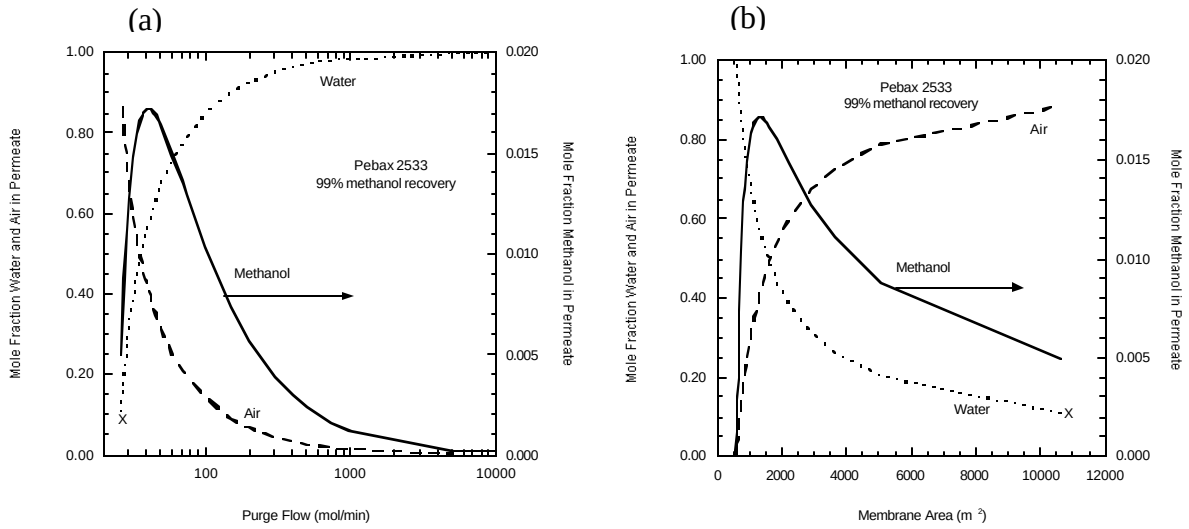

Figure 7: Predicted permeate composition for the system described in Figure 5 (99% methanol removal) as a function of purge rate, U (a) and membrane area, A (b) (PEBAX® 2533 membrane, properties as in Figures 3 and 4). The compositions were calculated based on the purge rate presented and the corresponding minimum membrane area shown in Figure 6 for graph (a) and the membrane area and based on the corresponding minimum purge rate for graph (b). X indicates the limit of minimum purge flow which can still achieve 99% methanol recovery.

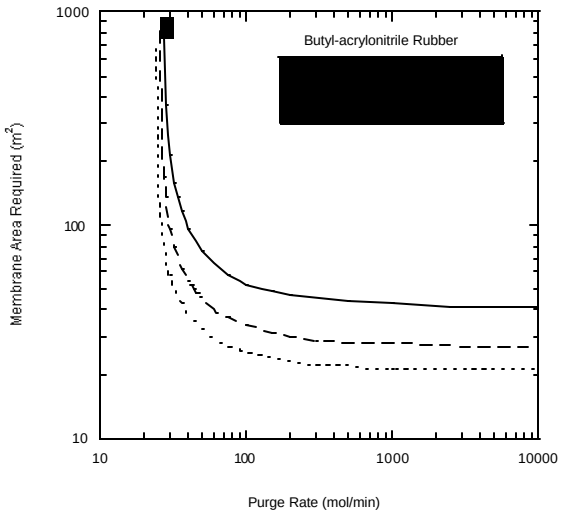

Figure 8: Relationship between the membrane area, A, required to achieve 99% methanol removal from the feed (Figure 5) and the permeate purge rate, U, of water (butyl-acrylonitrile rubber membrane, 0.5 microns thickness). X indicates the limit of minimum purge flow which can still achieve 99% methanol recovery.

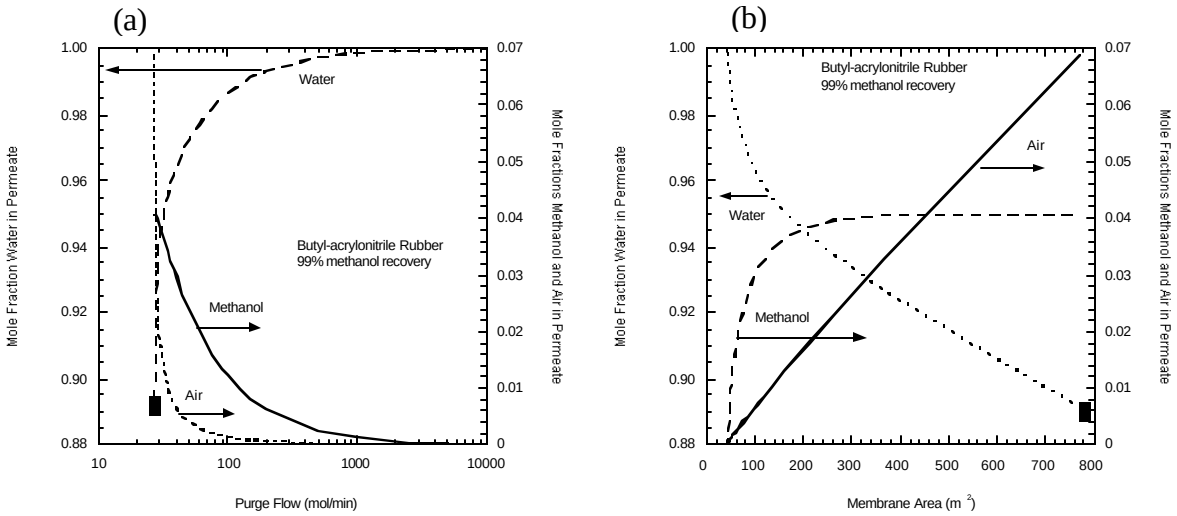

Figure 9: Predicted permeate composition for the system described in Figure 5 (99% methanol removal) as a function of purge rate, U (a) and membrane area, A (b) (butyl-acrylonitrile rubber membrane). The compositions were calculated based on the purge rate presented and the corresponding minimum membrane area shown in Figure 8 for graph (a) and based on the membrane area and the corresponding minimum purge rate for graph (b). X indicates the limit of minimum purge flow which can still achieve 99% methanol recovery.

Table 1: Some properties of PEBAX® 2533. All data from manufacturer's information unless indicated otherwise. All permeabilities at 30°C.

Density	1.01	g/cm^3
Glass transition temperature	-60	°C
Air permeability[10, a]	4.4	Barrer[d]
Methanol permeability[10, b]	8090	Barrer[d]
Water permeability[10, c]	25600	Barrer[d]
Melting point (ASTM D3481)	133.5	°C
Hardness (ASTM D2240)	25	Shore D

a: air pressure 73 cmHg
b: methanol activity 0.09
c: water activity 0.53
d: 1 Barrer = $1*10^{-10}$ $cm^3_{(STP)}$ cm/cmHg cm^2 s

References

(1) Vice, K.; Carroll, R. The cluster rule: a summary of phase I. TAPPI Journal 1998, 81(2), 91.

(2) Collection and Burning of Kraft Non-Condensable Gases. NCASI (National Council of the Paper Industry for Air and Stream Improvement, Inc., P.O. Box 13318, Research Triangle Park, NC, 27709-3318*)*, Technical Bulletin No. 469, **1985**.

(3) Baker, R. W.; Yoshioka, N.; Mohr, J. M.; Khan, A. J. Separation of Organic Vapors from Air. *Journal of Membrane Science* **1987**, *31(2-3)*, 259.

(4) Behling, R.-D.; Ohlrogge, K.; Peinemann, K.-V.; Kyburz, E. Separation of hydrocarbons from waste vapor streams. *AIChE Symp. Ser.* **1989**, *85(272)*, 68.

(5) Nitsche, V.; Ohlrogge, K.; Sturken, K. Separation of organic vapors by means of membranes. *Chemical Engineering Technology* **1998**, *21(12)*, 925.

(6) Li. K.; Acharya, D.R.; Hughes, R. Membrane Gas Separation with Permeate Purging, *Gas Sep. Purif*. **1990**, *4*, 81.

(7) Wang, K.L.; McCray, S.H.; Newbold, D.D.; Cussler, E.L.; Hollow Fiber Air Drying. *J. Membr. Sci.* **1992,** *72*, 231.

(8) Baker, R. W. *Membrane Technology and Applications*; McGraw Hill: New York, **2000**.

(9) Stripping of kraft foul condensates: literature review, operating experience, and field studies, NCASI (National Council of the Paper Industry for Air and Stream Improvement Inc.,

P.O. Box 13318, Research Triangle Park, NC, 27709-3318), Technical Bulletin No. 661, **1994**.

(10) Rezac, M. E.; John, T.; Pfromm, P. H. Effect of copolymer composition on the solubility and diffusivity of water and methanol in a series of polyether amides. *J. Appl. Polym. Sci.* **1997**, *65(10)*, 1983.

(11) Kreyszig, R. *Introductory mathematical statistics; principles and methods*; Wiley: New York, **1970**.

(12) Pan, C.Y.; Habgood, H.W. An Analysis of the Single-Stage Gaseous Permeation Process, *Ind. Eng. Chem. Fundam.* **1974,** *13(4),* 323.

(13) Coker, D.T.; Freeman, B.D.; Fleming, G.K. Modeling Multicomponent Gas Separation Using Hollow-fiber Membrane Contactors, *AIChE J.* **1998**, *44*, 1289.

(14) Rogers, C. E., Fels, M., Li, N. N. Separation by Permeation through Polymeric Membranes. In *Recent Developments in Separation Science, Volume II*, Li, N. N., Ed.; CRC Press: Cleveland, Ohio, 1972.

(15) Eckert, N.; Witkowski, J. P.; Wright, J. M. Production of liquid methanol from foul condensate stripping systems. *Proceedings*, 1998 TAPPI International Environmental Conference & Exhibit; Technical Association of the Pulp and Paper Industry (TAPPI): Atlanta, GA, **1998**; Part 2 (of 3), p. 513-520.